FLUORINATED RESPONSIVE LANTHANIDE COMPLEXES FOR MAGNETIC RESONANCE

ELENA DE-LUCA

How to cite:

DE-LUCA, ELENA (2010) FLUORINATED RESPONSIVE LANTHANIDE COMPLEXES FOR MAGNETIC RESONANCE. Doctoral thesis, Durham University.

Durham University

Department of Chemistry

FLUORINATED RESPONSIVE LANTHANIDE COMPLEXES FOR MAGNETIC RESONANCE

Elena De Luca

A thesis submitted for the degree of Doctor of Philosophy

2010

Abstract

A series of novel fluorinated lanthanide complexes has been synthesised for use as responsive probes for ^{19}F MRS and MRI. The careful positioning of the CF_3 group within 6.5 Å from the metal ion caused the fluorine longitudinal and transversal relaxation rates to be strongly enhanced. This allows faster MR signal acquisition, reducing the sample concentration and acquisition time required to obtain the desired signal intensity. The lanthanide ion also enhanced the chemical shift sensitivity of the fluorine nucleus to changes in the chemical environment. These characteristics have been exploited to develop responsive probes.

A series of pH reporters containing an aromatic mono-amide arm has been prepared and their pH sensitivity assessed. Deprotonation of the amide proton caused a large variation of the ^{19}F chemical shift. The pK_a of the probe was modulated by varying the substituents on the aromatic group and an optimal value of 7.1 was obtained with an *ortho* cyano substituent. The introduction of phosphinate pendant arms allowed narrower linewidths and faster longitudinal relaxation rates to be achieved.

The spectroscopic properties and the conformational isomerism of the same series of complexes have been analysed. In particular, their ^{19}F NMR chemical shift, relaxation properties and ^{1}H relaxivity characteristics were studied.

A series of complexes bearing different ester functional groups was prepared and their ability as reporters for enzymatic activity assessed. PLE and α-chymotripsin recognised the substrate and catalysed its transformation. Modification of the probe structure was revealed by variation of the relative signal intensity of the substrate and product fluorine resonances in the ^{19}F NMR spectrum.

Glycol chitosan conjugates with paramagnetic fluorinated complexes were prepared and their NMR properties assessed. *In vivo* MRI studies in animal models were undertaken and a selective uptake of the contrast agent in the tumour was observed with the Gd analogue.

Declaration

The work described herein was carried out in the Department of Chemistry, University of Durham between April 2007 and June 2010. All of the work is my own, except where specifically stated otherwise. No part has previously been submitted for a degree at this or any other university.

Statement of Copyright

Acknowledgements

I would like to thank my supervisor Prof. David Parker, for his constant help, support and precious advice and for showing great sensitivity when I needed it most.

Dr. Alan Kenwright for his advice and together with Catherine Hefferman and Ian McKeag for their precious assistance with NMR. Dr. Mike Jones, Lara Turner and Dr. Jackie Mosely for mass spectrometry analysis. Dr. Andrei Batsanov for crystal analysis. Judith Magee for elemental analysis and for some nice chats. Elizabeth Woods for her help. Dr. Ilya Kuprov and Naomi Hogg for the DFT calculations.

Dr. Ian Wilson at the Newcastle Magnetic Resonance Centre for the *in vivo* experiments.

Prof. Mauro Botta at the Universitá del Piemonte Orientale in Alessandria for the relaxivity measurements and for welcoming me in his lab for a week.

All the past and present members of CG27 for their friendship and for making the lab a great place to work. In particular I would like to thank Elisa for her constant support, Filip, Kanthi, Rachel Dickins, James, Ga-Lai, and Craig for their friendship and also Kirsten, Rachel, David, Anurag, Raman, Sashi, Peter, Brad, Roy, Liz and Robek. My friends in Durham for making this experience unforgettable, in particular Alessandra, Pierpaolo, David, Anne, Milena, Andrea, Andy, Daniela, Serena, Jaime, Jonathan, Margherita, Ali, Anuji, Jesus, Laura, Maykel and Rachel. My friends at home for their support in particular to Giulia who I miss tremendously, Rosa, Marta, Virna, Alice, Denis, Lory, Danilo and Pamela. My family for their support.

Ben for his love and support, for his patience and for learning Italian.

A very special thanks to my mum and dad, for their endless love and support and for their encouragement to come here.

For Mum and Dad

Contents

List of Abbreviations

15C5 - perfluoro-15-crown-5-ether
5-FC5 - fluorocytosine
5-FU - 5-fluorouracil
6-FPAL - 6-fluoropyridoxal
6-FPAM - 6-fluoropyridoxamine
6-FPOL - 2-fluoro-5-hydroxy-6-methyl-3,4-pyridinedimethanol
APTRA - o-aminophenol-*N*,*N*,O-triacetic acid
BAPTA - 1,2-bis(o-amino-phenoxy)ethane-*N,N,N’,N’*-tetraacetic acid
CA - contrast agent
CAP - mono-capped square-antiprismatic
CD - cytosine deaminase
CEST - chemical exchange saturation transfer
CHO - chinese hamster ovary
CSA - chemical shift anisotropy
CSI - chemical shift imaging
cyclen - 1,4,7,10-tetraazacyclododecane
d - doublet
DC - dendritic cells
DCE - dynamic contrast enhanced
DCM - dichloromethane
DD - dipole-dipole
dd - doublet of doublets
DFT - density functional theory
DHFU - 5,6-dihydrofluorouracil
DMAP - 4-(dimethylamino)pyridine
DMF - *N,N*-dimethylformamide
DMSO - dimethyl sulfoxide
DNA - deoxyribonucleic acid
DO3A - 1,4,7,10-cyclododecane-1,4,7-triacetic acid
DOTA - 1,4,7,10-cyclododecane-1,4,7,10-tetraacetic acid
DOTP - 1,4,7,10-tetraazacyclododecane-1,4,7,10-tetrakis(methylene phosphonate)
DTPA - diethylenetriaminepentaacetic acid
DTPA-BMA - 5,8-bis(carboxymethyl)-11-[2-(methylamino)-2-oxoethyl]-3-oxo-2,5,8,11-tetraazatridecan-13-oic acid
EDC - *N*-(3-dimethylaminopropyl)-*N′*-ethylcarbodiimide hydrochloride
EPR - enhanced permeability and retention
ESI/MS$^-$ - electrospray ionisation with negative ion detection
ESI/MS$^+$ - electrospray ionisation with positive ion detection
EXSY - exchange spectroscopy

F_2MeAla - D-L-2-amino-3,3-difluoro-2-methylpropanoic acid
FBAL - α-fluoro-β-alanine
FDG - fluorodeoxyglucose
F-DOTPME - 1,4,7,10-tetraazacyclododecane-1,4,7,10-tetrakis(methanephosphonic acid mono(2‘,2‘,2‘-trifluoroethyl)ester)
FNuc - fluorinated nucleosides/nucleotides
F-POSS - perfluorinated cubic silsesquioxane
FSB - (E,E)-1-fluoro-2,5-bis(3-hydroxycarbonyl-4-hydroxy)styryl-benzene
GPC - gel permeation chromatography
GS-MS - gas chromatography mass spectrometry
HDH - histidinol dehydrogenase
HFB - hexafluorobenzene
HPDO3A - 10-(2-hydroxypropyl)-1,4,7-tetraazacyclododecane-1,4,7-triacetic acid
HPLC - high performance liquid chromatography
ICP-MS - inductively coupled plasma mass spectrometry
IQ - indolequinone
LC-MS - liquid chromatography mass spectrometry
LIS - lanthanide induced shift
m - multiplet
MHC - major histocompatibility complex
MR - magnetic resonance
MRI - magnetic resonance imaging
MRS - magnetic resonance spectroscopy
MTT - 3-(4,5-dimethyl-2-thiazolyl)-2,5-diphenyl-2H-tetrazolium bromide
MW - molecular weight
MWCO - molecular weight cut off
NHS - *N*-hydroxysuccinimide
NIR - near infrared
NMM - *N*-methylmorpholine
NMR - nuclear magnetic resonance
NMRD - nuclear magnetic resonance dispersion
NOD – non-obese diabetic
NTR - homodimers nitroreductase
PBS - phosphate buffered saline
PEG - polyethylene glycol
PET - positron emission tomography
PFC - perfluorocarbon
PFOB - perfluorooctylbromide
PFONPG - 4-fluoro-2-nitrophenyl-β-D-galactopyranoside
PFP - phenyliodoacetamide
PFPE - perfluoropolyether
PLE - pig liver esterase
q – quartet

RF - radio frequency
RNA - ribonucleic acid
s - singlet
SBM - Solomon-Bloembergen-Morgan
t - triplet
TBTU - *O*-(benzotriazol-1-yl)-*N,N,N′,N′*-tetramethyluronium tetrafluoroborate
TFA - trifluoroacetic acid
tfm-Phe - trifluoromethyl-L-phenylalanine
THF - tetrahydrofurane
TPP - tetraphenyl iron(III)porphyrins
tri-BOC - *tert*-butoxycarbonyl
TSAP - twisted square-antiprismatic
UV - ultraviolet
Vis - visible
β-CD - poly-β-cyclodextrin

Chapter 1

Introduction

1.1 ^{19}F as a probe nucleus for magnetic resonance spectroscopy and imaging

Magnetic resonance imaging (MRI) is recognised as one of the most important diagnostic tools in clinical practice[1,2]. MRI is a non-invasive, radiation-free technique, with an excellent (sub-millimetre) spatial resolution. Conventional proton-based images offer detailed anatomic information for thorough analysis of physiological processes and tissue morphology. Additional information is provided with the use of contrast agents (CA). Traditionally, these are paramagnetic Gd(III) complexes[3] and super-paramagnetic iron oxide particles[4], which highlight different tissues of the body selectively, affecting the longitudinal or transverse relaxation time of the nearby water protons. Nevertheless, the intense background of the water signal causes insufficient discrimination between normal and tumour tissues and complicates the detection of metabolites other than water because of the relative signal intensity. Hence, heteronuclear magnetic resonance has been investigated[5]. The most promising nucleus is ^{19}F, which has a nuclear spin, $I = ½$, and a 100% natural abundance, being the only stable isotope of fluorine. The high NMR sensitivity of ^{19}F, 0.83 relative to ^{1}H, gives a strong NMR signal and the gyromagnetic ratio (γ) of 40.05 MHz/T (only 6 % lower than ^{1}H) allows spectral or image acquisition on the existing instrumentation used for ^{1}H NMR by appropriately tuning the RF coil.

Fluorine atoms are present in low concentration in the body, mostly in the form of solid salts in the bones and teeth. The transverse relaxation time, T_2, of endogenous fluorine is extremely short, causing the resulting signal to be below the NMR detection limit. When an exogenous fluorine-containing compound is administered, it can be monitored without interference from background signals[6]. The contrast is therefore a direct observation of the fluorine probe in which the signal to noise ratio is only due to the local concentration of the probe. Moreover, the proton MR image can be acquired together with the image reporting the ^{19}F-signal, identifying the spatial localisation of the probe, giving additional diagnostic information.

The ^{19}F chemical shift range covers more than 300 parts per million (ppm), compared to 10 ppm for protons, and shows a particular sensitivity to variations in the chemical microenvironment. These characteristics essentially guarantee chemical shift non-equivalence between different fluorinated signals and allow the examination of multiple agents simultaneously. Other than chemical shift and relative chemical shift changes, many parameters, as for proton NMR, can be interrogated, such as signal intensity (quantitative response), scalar coupling, chemical exchange, longitudinal relaxation rate, R_1, and transverse relaxation rate, R_2. These provide a pool of potential information but can also complicate the planning for an optimal experiment.

The potential of ^{19}F NMR has prompted the development of various fluorinated probes, aided also by the recent technological advancements in NMR instruments. Many common drugs contain a fluorine atom and are suitable to be investigated by magnetic resonance to follow metabolic and pharmacokinetic processes[7]. Fluorine can also be used to visualise anatomical characteristics when added as a simple tracking label, as in the case of angiography when the fluorinated probe is confined in the circulatory system[8], or it can be accurately placed in a ^{19}F-reporter agent designed to investigate various parameters of interest such as pH, gene activity, metal ion concentrations, oxygen tension, hypoxia, vascular flow and volume[9]. Finally bimodal ^{1}H/^{19}F imaging coils allow the use of dual probes.

Therefore, fluorine is an attractive nucleus for study in MR spectroscopy and imaging applications. Furthermore, there is a great deal of interest in ^{18}F-labeled probes used in Positron Emission Tomography (PET)[10,11], but they will not be considered here.

1.2 Fluorinated probes

There is a wide range of fluorinated molecules used in magnetic resonance with different applications. They can be divided in three categories:

- passive agents: which reveal anatomical properties without themselves experiencing any alteration;

- responsive agents: which undergo noticeable modification after interaction with the local environment;
- fluorinated drugs: whose metabolism and pharmacokinetics can be followed by NMR.

Each is considered in more detail below.

1.2.1 Passive agents

Passive agents are fluorinated molecules that give an indication of tissue or organ properties without any particular interaction, except for occupying a particular space or region *in vivo*, such as the lungs or blood vessels. Their spatial and temporal distributions are followed by means of their MR signal.

Examples of such inert fluorinated compounds are perfluorocarbons. They are biologically inert and present high gas solubility and a great ability in carrying oxygen and carbon dioxide. Due to these characteristics they have been accepted as synthetic blood substitutes in emulsion form. As liquids, they have been used to support respiration in mice and cats, as demonstrated in the famous experiment of Clark and Gollan, in which mice breathing oxygen-saturated liquid perfluorocarbon (4 hours at 18°C) survived for several weeks[12]. Partial liquid ventilation in animal models (pigs in this example) enabled the monitoring of lung filling extension, using ^{19}F MRI, and the evaluation of the regional oxygen partial pressure (pO_2) distribution, measuring the fluorine T_1 relaxation, thanks to the linear variation of the fluorine T_1 of perfluorocarbons with pO_2[13].

Due to the stress that can be induced by ventilation of liquid, inert fluorinated gases have also been studied, such as CF_4, C_2F_6 and SF_6. The last one in particular has been successfully used in rat models for lung imaging[14] (Fig. 1.1) and in subsequent work to measure lung volume during the entire respiratory cycle. This allowed the discrimination between healthy subjects and emphysema-induced rats which showed greater lung volume and reduced expiratory flow rate, in a similar manner to humans with obstructive pulmonary diseases[15]. Fluorinated gases present extremely short relaxation times (typically $T_1 = 5.9 \pm 0.2$ ms for SF_6) which require specialised instrumentation, so they have tended to be replaced by hyperpolarised gases such as xenon and helium despite their high cost of preparation.

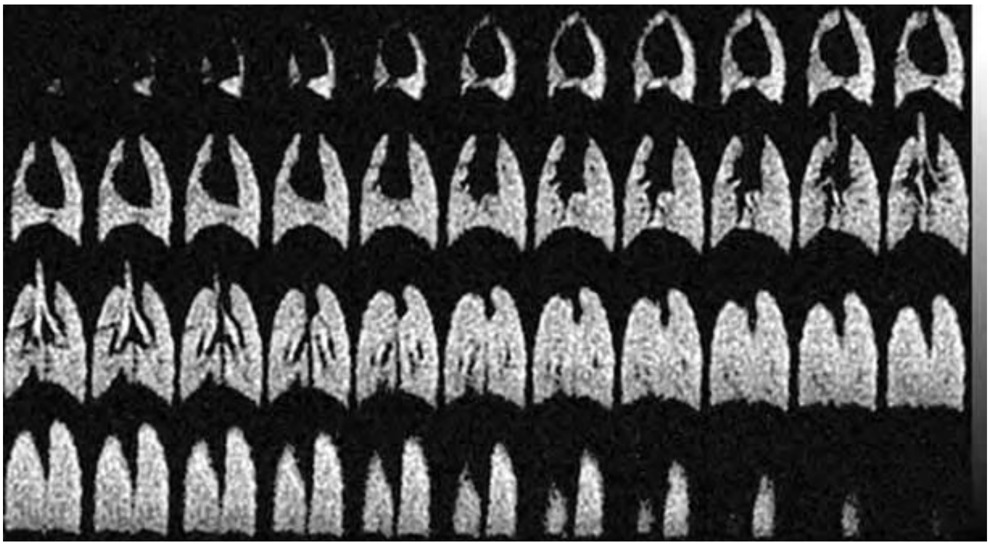

Fig. 1.1 ^{19}F MRI of SF_6 in the lungs of a large rat. Frames, from top left to bottom right are successive planes of the image from chest to back (Figure taken from reference [6]).

Perfluorooctylbromide (PFOB, **1**) and perfluorononane **2** have been applied as contrast agents for gastrointestinal imaging. In clinical trials, an improved definition of bowel MR images at 0.38, 1.0, 1.5 T has been observed upon ingestion of PFOB without image artefacts or side effects, and the efficacy was independent of pulse sequence and magnetic field strength[16]. Perfluorononane has been employed in mice to obtain a three-dimensional reconstruction of the entire GI tract at 282 MHz, based on the ^{19}F images of the intraluminal perfluorocarbon signal. Applying a frequency-selective sequence, the terminal CF_3 groups ($T_1 = 1692 \pm 132$ ms, $T_2 = 645 \pm 15$ ms *in vivo*) gave a strong positive contrast after saturation of the unwanted CF_2 resonances[17] (Fig. 1.2).

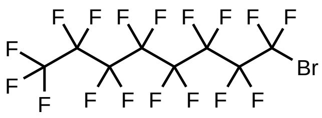

PFOB
1

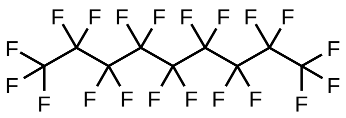

2

Intravenous emulsions of PFCs are retained for long periods (hours) in the vasculature and have been used both for angiography imaging[8] and to measure vascular volume and tumour blood volume[6].

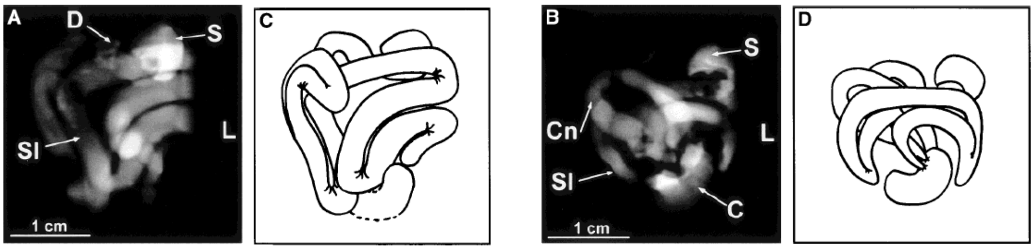

Fig. 1.2 ^{19}F-MR images at 282 MHz of the GI tract of a mouse obtained after 0.3 ml meals of perfluorononane administered every 30 min over 2.5 h. A) Acquired immediately after the last meal. B) obtained after a period of 1 h. C-D) Cartoons describing the intestine 3D- arrangement corresponding to A and B. L, left-hand side; S, stomach; D, duodenum; SI, small intestine; C, cecum; Cn, colon (Figure taken from reference [17]).

Recent interest has grown around the application of perfluorocarbons for MRI cell tracking. Conventionally, cell labelling employed super-paramagnetic iron oxide particles to produce negative contrast (darkening) in ^{1}H-based images. However, with this method it is often difficult to discriminate labelled cells from the background image. The use of fluorinated markers allows selective identification of the labelled cells (positive contrast, *i.e.* brightening) without endogenous background signal, and proton MR images acquired in the same imaging session provide anatomical localisation. Several examples have been recently published; Partlow *et al.* employed perfluorooctylbromide (PFOB) **1** and perfluoro-15-crown-5-ether (15C5) **3** nanoparticles as fluorinated tags for stem cells. These cells, harvested from human umbilical cord blood and grown under pro-endothelial conditions, promptly internalised the particles while maintaining their functionality. Six million *ex vivo* labelled cells were injected intravenously in tumour-bearing mice and allowed to migrate for 5 days, then localised by ^{19}F MRI (11.7 T research and 1.5 T clinic scanners) in the tumour vasculature. The homing ability of labelled cells to neovasculature is the sign of their maintained functionality *in vivo*[18].

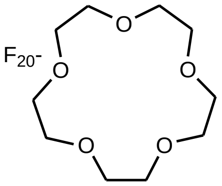

F_{20}-15C5
3

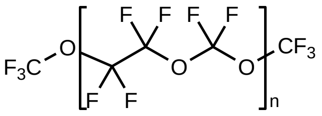

PFPE
4

Different publications have described the application of perfluoropolyether (PFPE) **4** to visualise a specific cell population. It has multiple signals in the ^{19}F NMR but *in vivo* only the OCF_2 resonance is observed, the others being below the detection limit. Ahrens' group showed the early homing of diabetogenic T cells to the pancreas in diabetic mice, an established model of type 1 diabetes. This is one of the earliest events in the pathogenesis course and is asymptomatic, because it occurs before the destruction of the insulin-producing β cells of the islet of Langerhans. Therefore, early detection of this lymphoid cell infiltration would be of great benefit. A computational algorithm provided cell counting showing that approximately 2% of transferred cells reached the pancreas after 48 hours[19] (Fig. 1.3).

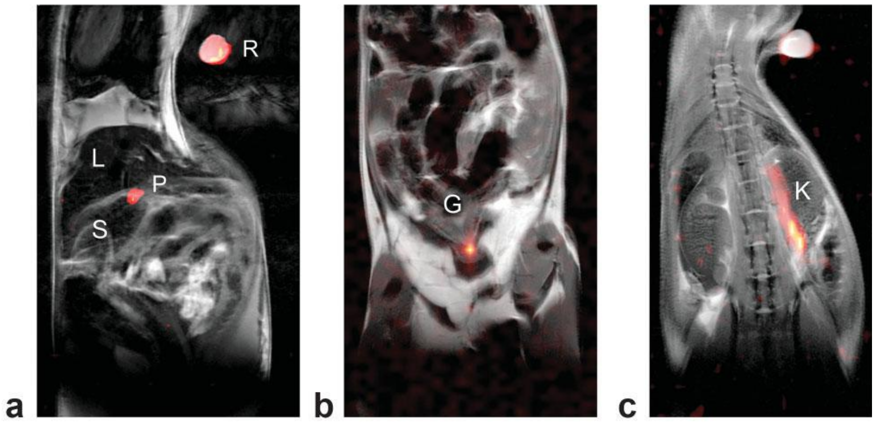

Fig. 1.3 *In vivo* MR images through the torso of a nonobese diabetic (NOD) mouse. a) Image of PFPE-labelled T cells transferred intraperitoneally (i.p.) 48 h prior. The image shows specific T cells (color) homing to the pancreas (P) (^{19}F reference capillary (R), spleen (S), liver (L)). b) Negative control: mouse received cell-free PFPE nanoparticles in PBS at an equivalent fluorine dose of labelled T cells. PFPE detected only near the gut (G). c) Negative control: mouse received activated, labelled MHC mismatched T cells. No detect signal in the pancreas. Cells can be seen near the kidney (K) (Figure taken from reference [19]).

Other studies utilised dendritic cells (DC) which have a central role in the immune response and offer a wide range of medical applications *i.e.* cancer therapy, autoimmunity and organ transplantation research. Mature human DC have been labelled *ex vivo* with PFPE and inoculated into mice. After 18 hours, 5% of the cells reached the lymph node region. As a control, immature DC have also been injected which weren't observed to leave the injection site[20]. PFPE has also been covalently conjugated to common fluorescent dyes to allow dual mode detection of labelled T cells. The MRI images can be successively confirmed by fluorescence microscopy on biopsied tissues. The linear correlation between the intracellular fluorescence and ^{19}F signal can be utilised to calibrate the *in vitro* cell loading of the MR agent[21]. A different example has been proposed by Maki *et al.* in which the linear cationic polymer (non perfluorinated) poly-L-lysine-CF_3 **5** has been linked through the amino group to fluorescein isothiocyanate. This allows the labelled stem cells of bone and cartilage to be detected via MRI and fluorescence imaging, following transplantation in the cranial bone of mice. The MR signal decreased with time and was visible for 7 days (single signal at δ_F = -59.3 ppm, 7 T)[22].

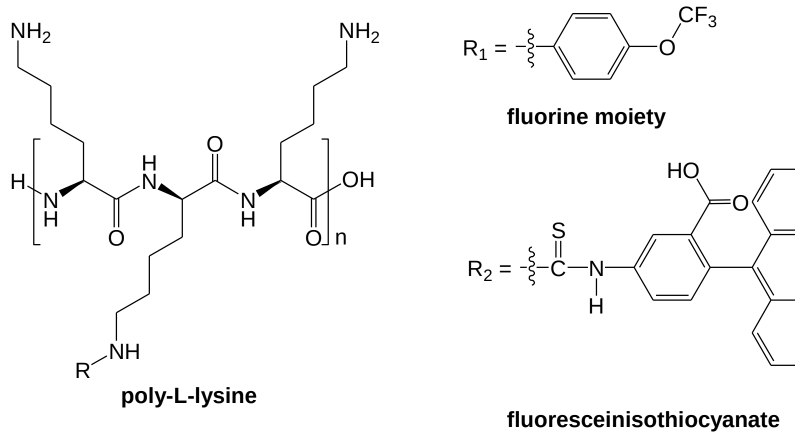

5

Perfluorocarbons are non-toxic compounds, chemically stable and well tolerated *in vivo*. Despite these advantages they present some drawbacks such as multiple resonances that reduce sensitivity and long longitudinal relaxation rates (T_1) which increase the time of image acquisition. In attempts to increase the signal intensity recent interest has grown around fluorinated polymers. They present the possibility of introducing a large number of fluorinated groups and also of functioning as delivery platforms for conjugated therapeutic agents. In fact, high molecular weight molecules can be passively targeted to the tumour periphery exploiting the enhanced permeability and retention (EPR) effect. Peng *et al.* synthesised block copolymers consisting of hydrophilic blocks of poly-acrylic acid and hydrophobic blocks of n-butyl acrylate copolymerised with partially fluorinated acrylate or methacrylate. They spontaneously formed micelles in water/DMF mixture, in which the fluorine was in the core of the particle and showed a single peak in ^{19}F NMR (2.5 wt%

polymer, 7 T, 310 K). The acrylate based polymers **6** were more stable after dialysis in water, had shorter T_1 (511 ms vs 676 ms for methacrylate) and gave better images compared to the methacrylate analogue, thanks to the greater chain flexibility[23]. T_2 is particularly influenced by local motion: if the fluorine nucleus is constrained, it shows a faster spin-spin relaxation compared to a less-static environment and this causes a signal broadening leading to loss of signal intensity. To increase the ^{19}F mobility, the same group prepared fluorinated polyelectrolytes **7**, in order to exploit the electrostatic repulsion between charged monomer units. They found longer T_2 values upon increasing charge density[24].

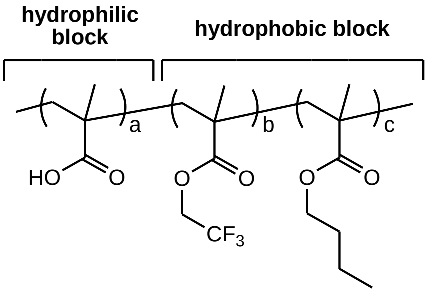

6

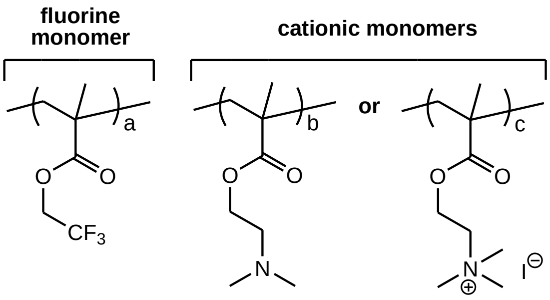

7

Hyperbranched polymers have also been studied. Du *et al.* prepared an example with a hydrophobic core and a copolymeric shell made of a fluorinated monomer and hydrophilic acrylic acid. They form micelles in water that have a single signal in the fluorine spectrum with linewidth of 130 Hz, T_1 of 500 ms and T_2 of 50 ms. A good signal is obtained but only after a long acquisition time (1 mg/ml, 13 hours, phantom imaging, 11.7 T)[25]. Hyperbranched fluorinated polymers can also be functionalised, as demonstrated in the work of Thurecht *et al.* where mannose has been conjugated to the polymer **8** and recognised by mannose-binding lectins which are important in the immune response. Good images of the parent non-functionalised polymer micelles were recorded in vivo in less than 10 minutes, with a concentration of 20 mg/ml (16.4 T, T_1 = 480 ms, T_2 = 88 ms)[26].

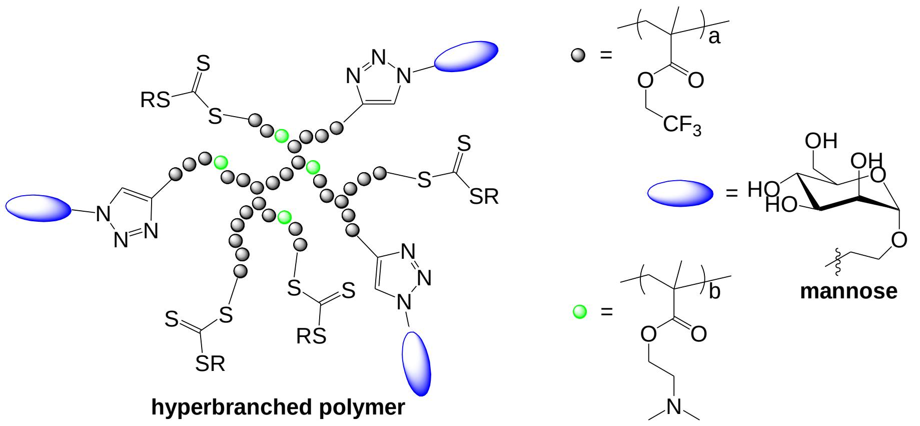

8

A different approach exploited bispherical symmetry to incorporate up to 27 fluorine atoms in a molecule **9** which contain one fluorine rich part that gives a single strong NMR signal, and a hydrophilic part which ensures the water solubility of the macromolecule (T_1 = 163 ms at 11.7 T)[27]. Preliminary work was performed with polylysines and dextrans modified with fluorinated groups such as trifluoroacetyl, yielding a single ^{19}F signal with good sensitivity[28].

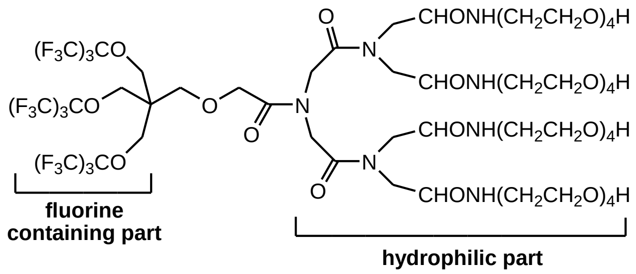

9

The fluorine nucleus can also be added as a simple label to different molecules, in order to make them visible in ^{19}F NMR and allow the tracking of the conjugate. One example is the labelling of biomolecules, as in the case of 4-perfluoro-tert-butyl-phenyliodoacetamide (PFP) **10**. This has been coupled to the sulfhydryl groups of actin. The sharp ^{19}F NMR signals of monomeric actin (located between δ_F = 13.5 and 13.8 ppm, 308 K, 470.5 MHz) gradually disappeared during the polymerization of the protein. The presence of nine equivalent fluorine atoms in the probe allows the detection of the labelled conjugate at low concentrations (1 µM for 1 h acquisition time) and can be potentially applied to track other biomolecules, such as antibodies[29].

One interesting application is the detection of β-amyloid plaques *in vivo*, using amyloidophilic compounds such as FSB **11**. The formation of senile plaques of amyloid β peptide is one of the earliest signs of Alzheimer's disease. Hence, an early diagnosis would allow preventive treatment of the patients before irreversible neurodegeneration. When FSB is administered intravenously in mice (20 mg/kg), it crosses the blood-brain barrier and targets the β-amyloid plaques with high specificity. The ^{19}F imaging results were successively confirmed by fluorescence experiments on brain sections of the sacrificed animals[30]. Modifications of the parent structure have also been proposed with addition of fluorine atoms on the central aromatic ring or CF_3 group on the lateral ones, producing stronger NMR signals and increased binding affinities but reduced solubility[31].

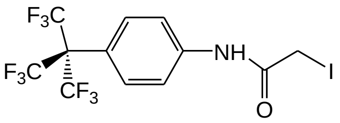

PFP
10

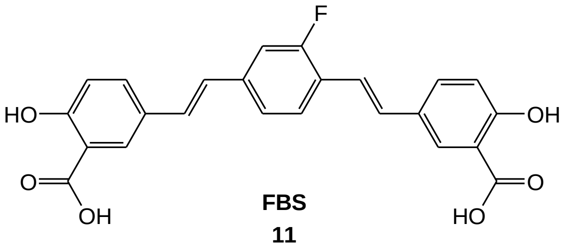

FBS
11

1.2.2 Responsive agents

Responsive agents are fluorinated probes precisely designed to respond through a change in ^{19}F chemical shift or signal intensity, to a particular parameter such as pH, enzyme and gene activity, hypoxia or ion concentration. The response can lead to an irreversible modification of the probe structure - as in the case of enzymes recognising the probe as a substrate. Alternatively, a reversible change may occur - as for metal ion binding or pH variation.

1.2.2.1 Gene transfection reporters

Gene therapy has emerged as a potential strategy for the treatment of various diseases, but its development has been hindered by the lack of a non-invasive method to prove the quality of transfection. ^{19}F NMR may be an effective technique for the detection of transgene expression in target tissues, as suggested in the study of gene-directed enzyme prodrug therapy, focussed on the cytosine deaminase (CD) gene.

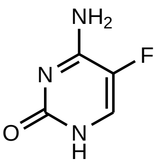

5-FC
12

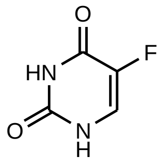

5-FU
13

CD is a microbial enzyme that transforms the low-toxicity pro-drug 5-fluorocytosine (5-FC) **12**, into the active chemotherapeutic agent 5-fluorouracil (5-FU) **13**. CD is not expressed in human cells; hence the selective localisation of the CD gene to the target tumour can impart local conversion of 5-FU production, reducing the toxicity related to its systemic administration. The enzyme-catalysed activation of transfected cells was revealed *in vivo* by a ^{19}F chemical shift change of about 1.5 ppm, proving the gene activity (δ_F = -48.5 ppm 5-FC, δ_F = -49.6 ppm 5-FU relative to NaF at 7 T), utilising human carcinoma xenografts tumour model in mice tranfected with yeast CD. The temporal profile of the fluorine spectrum obtained from the tumour (Fig. 1.4) was used to follow the metabolism of 5-FC and the presence of anabolism products such as FNuc, which is responsible for the antitumoral activity. Localised production of 5-FU in the tumour was confirmed by control spectra in muscle tissues, where only 5-FC was found[32].

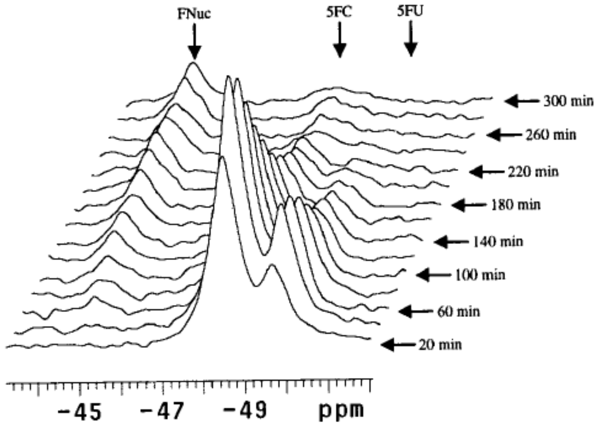

Fig. 1.4 ^{19}F NMR spectra over time monitoring the changes of 5-FC in a subcutaneous tumour expressing yeast CD. Start 20 min after i.p. administration of 1g/kg 5-FC. 20-min interval for each spectrum (Figure taken from reference [32]).

The most popular reporter gene employed to prove transfection efficacy is the bacterial LacZ gene that encodes the enzyme β-galactosidase. Mason and coworkers developed a fluorinated arylgalactopyranoside prototype (PFONPG) **14**, which acts as an effective substrate for the enzyme. 4-Fluoro-2-nitrophenyl-β-D-galactopyranoside has a single sharp ^{19}F NMR signal at δ_F = -42.7 ppm (relative to NaTFA), which is invariant to pH (in the range 1 to 11) and temperature (25-37°C). It is stable in blood but in the presence of the enzyme or transfected cells that express β-galactosidase, undergoes hydrolysis of the glycosidic bond causing the release of the phenolic product. Upon cleavage, a chemical shift difference of more than 3.6 ppm at pH 7.4 is observed in solution. The same behaviour is recorded also when applied to whole blood or prostate cancer cells. The signal of the released aglycone fluoro-nitrophenol exhibits a pH sensitive response in a range of 9.3 ppm with a pK_a of 6.85. This may prove to be useful in measuring the pH at the site of enzyme activity[33].

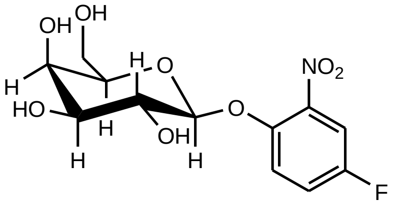

PFONPG
14

A series of analogues has been synthesised in order to reduce the high toxicity of the prototype, with differences in chemical shift between the substrate and the product from a minimum of 3.6 ppm at pH 7.4, ranging from 1.6 to 12.9 ppm depending on the pH, with pK_a values in the range 5.4-9.8 and different sensitivities to hydrolysis[34]. Introduction of CF_3 groups as a replacement for mono-fluoro substituents yielded a higher signal intensity (1.1 mg, 3 mmol against 2.87 mg, 9 mmol of PFONPG) but the chemical shift changes were smaller ($\Delta\delta_F$ = 1.1 ppm) and the aqueous solubility lower[35]. Further work based on the less toxic 2-fluoro-4-nitrophenol analogue (δ_F = -55 ppm) reported ^{19}F chemical shift imaging (CSI) studies of the β-galactosidase-catalysed reaction in transfected cancer cell lines, in which the conversion was detected by the decrease of the substrate image intensity and the concurrent increase of the product signal (4-6 ppm chemical shift difference)[36]. The same experiment was also performed on prostate tumour xenografts in mice, after intratumoral injection of 50 μl solution of the substrate (3.9

mg in water/DMSO, 4.7 T), with positive results obtained with ^{19}F MRS but insufficient signal intensity for in vivo ^{19}F CSI[37].

1.2.2.2 pH indicators

Because of the exquisite sensitivity of the ^{19}F NMR chemical shift towards changes in the microenvironment, many fluorinated pH indicators have been exploited. When the exchange between protonated and non-protonated forms is fast on the NMR time scale, a single ^{19}F signal is observed. Under slow-exchange conditions, the acid and base forms produce two distinct signals that can be detected at the same time. Fluorinated amino acids were one of the first examples of fluorinated pH probes; they have been employed successfully for pH measurement of intracellular compartments. For example, human peripheral blood lymphocytes have been investigated with D-L-2-amino-3,3-difluoro-2-methylpropanoic acid (F_2MeAla) **15**. The fluorinated amino acid is internalised in the cells, with greater efficiency if administered in the liphophilic methyl ester form that is hydrolysed by endogenous esterases to the desired free acid. The chemical shift difference between the diastereotopic fluorines varies with pH. The fluorine signal appears as a quartet and the centre-line separation is pH sensitive due to the protonation equilibrium of the α-amino group ($pK_a = 7.3$). This permits the measurement of the intracellular pH at 25-30°C. When incubated with blood lymphocytes, two sets of signals appear, showing the presence of intra- and extra-cellular species, after equilibration through the membrane. Spectra were recorded at different values of external pH, demonstrating the presence of a regulatory mechanism in the lymphocytes that maintains the internal pH constant: with external pH values from 6.8 to 7.4 the internal pH was kept at 7.17 ± 0.06 while, outside this interval, it started changing accordingly to the ambient values. This system can lead to complex spectra, due to overlapping of intra- and extra-cellular resonances from both ester and acid species, and the splitting of the peaks produces an internal reference but also reduces signal intensity. Furthermore, a small chemical shift range is observed (≤ 2 ppm)[38].

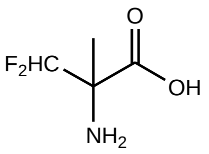

(D-L)-F$_2$MeAla
15

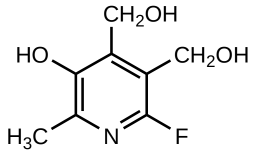

6-FPOL
16

Better sensitivity to pH is expressed by fluorinated derivatives of vitamin B$_6$, such as 6-FPOL (2-fluoro-5-hydroxy-6-methyl-3,4-pyridinedimethanol) **16**. It presents a single ^{19}F signal (linewidth = 20 Hz at 282.3 MHz) with a chemical shift change between protonated and deprotonated forms of 9.8 ppm, that is independent of the presence of metal ions or variation in temperature (27-45°C). The basic pK$_a$ of 8.2 can be exploited for interrogating alkaline conditions, but is too high for analysis of the normal physiological environment (6.5-7.5). Upon addition to whole blood, two resonances were observed immediately, reporting the intra- (i) and extra-cellular (e) species which corresponded to $pH_i = 7.19$ and $pH_e = 7.45$ ($T_{1i} = 0.87$ s, $T_{1e} = 1.21$ s). The rapid cell uptake probably exploits the natural transport of the vitamin[39].

Perfused rat hearts have been used as whole organ model for investigating alkalosis conditions. The addition of 6-FPOL to the perfusate (3.6 mM), gave rise to two resonances at $\delta_F = -10.6$ ppm (linewidth = 160 Hz) and $\delta_F = -11.5$ ppm (linewidth = 120 Hz) representing $pH_i = 7.11$ and $pH_e = 7.60$ at 376 MHz. NaTFA was used as internal standard. Induced metabolic alkalosis and acidosis didn't show significant change of pH_i, while during respiratory alkalosis, an increase of pH_e was accompanied by a simultaneous rise in pH_i, which returned to normal values under physiological conditions[40]. The deprotonation equilibrium of the phenolic group in position 3 is responsible for the pH sensitivity of the probe. Therefore, introduction of electron withdrawing or donating groups in the *meta* and/or *para* positions could shift the pK$_a$ to the range of interest. A series of analogues has been synthesised, each presenting a single resonance and shifts ranging between 7.4 and 12.1 ppm. The 4-aminomethyl derivative, 6-FPAM **17**, maintained the positive characteristics of the parent molecule 6-FPOL, but possessed a more suitable pK$_a$ of 7.05 and a greater chemical shift difference between intra- and extracellular resonances ($\Delta\delta_F =$ 2.2 ppm) compared to 6-FPOL ($\Delta\delta_F = 1.1$ ppm) thereby improving resolution. An internal reference has been provided by introducing a CF$_3$ group in the structure **18** which produced an additional signal insensitive to pH, but the increased liphophilicity of this analogue relegated the probe to the extracellular compartment[41].

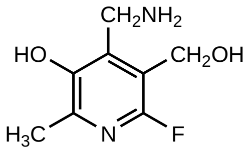

6-FPAM
17

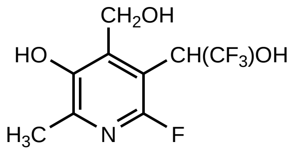

CF_3 analogue
18

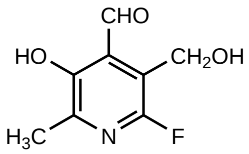

6-FPAL
19

In order to exploit the enhanced vascular retention and tissue targeting imparted by polymeric carriers, conjugation of the pH indicator with polyaminodextran, polylysine and albumin has been attempted. The polymers have been attached through the aldehyde group in position 4 of the 6-FPAL **19** analogue, to obtain a macromolecule that exhibits a single ^{19}F signal in each case, with a chemical shift sensitivity of 10.3-10.9 ppm and a more acidic pK_a range (5.9-6.8). Thus, the polymer didn't disturb the pH sensitivity of the probe, but caused line broadening (55 Hz compared to 22 Hz of 6-FPAL, 282.3 MHz) and when analysed in whole blood only the extracellular peak was detected, indicating a lack of cell penetration[42].

Another class of pH indicators is represented by fluoro-substituted aniline derivatives. The presence of a fluorine atom in the aromatic ring lowers the pK_a of the amino group. A series of analogues has been explored, obtaining single resonances with good sensitivity (acid-base difference 5-15 ppm) and a range of pK_a between 1 and 6. Further modification produced the candidate molecule *N,N*-(methyl-2-carboxyisopropyl)-4-fluoroaniline **20**, which retained a considerable chemical shift change of 12 ppm and a pK_a of 6.8, suitable for *in vivo* evaluations. Line broadening due to chemical exchange between conjugated acid and base was observed around the aniline pK_a value[43]. Similar probes have been based on *N*-ethylaminophenol **21**, these show chemical shift changes of 11 ppm and pK_a values of about 6.8. Introduction of a second fluorine whose shift is insensitive to pH variations acts as internal chemical shift reference[44].

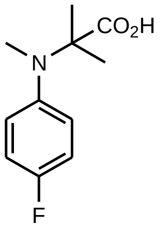

20

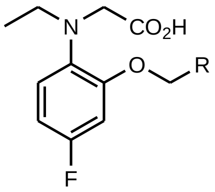

General structure

21

An interesting approach is represented by the use of pH sensitive fluorinated nanosized particles that can accumulate in solid tumours through exploiting the EPR effect. PEGylated nanogels have been utilised for monitoring pH values between 6.5 and 7.0, typical of tumour tissues, with a particular on-off regulation of the ^{19}F signal. The probe is composed of a pH sensitive polyamine gel core cross-linked with CF_3-containing groups, and an external shell formed by PEG chains carrying an acetal group for conjugating ligands of interest (Fig. 1.5).

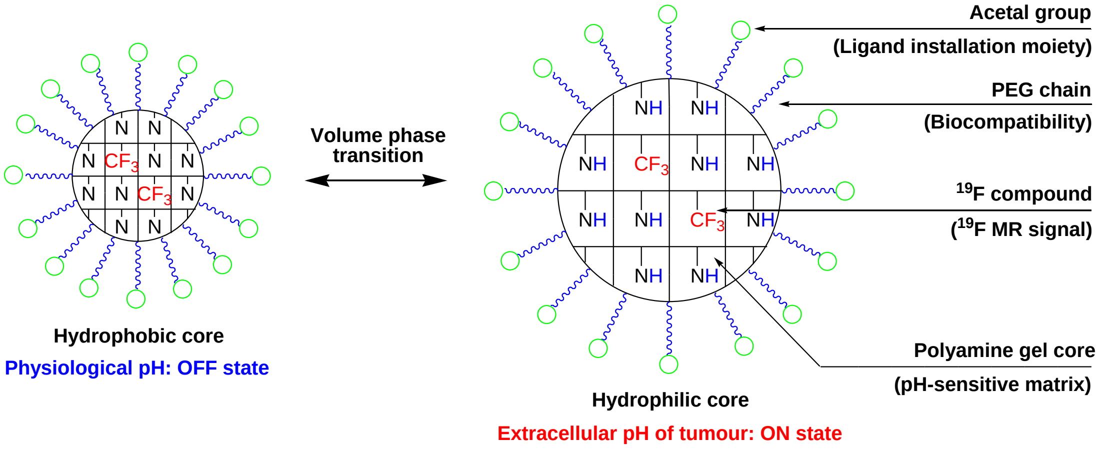

Fig. 1.5 Schematic representation of the pH sensitive PEGylated nanogels.

The internal matrix can undergo variation in size (swelling/shrinking) according to the environmental pH, due to the protonation-deprotonation process of the amino groups. At physiological pH the amino groups are deprotonated; inside the hydrophobic (solid-state) gel core the fluorine compounds suffer limited molecular motion which causes line broadening (short T_2, <1 ms) of the ^{19}F signal, resulting in it not being visible in the spectrum: this corresponds to the ‘off-state’. When the pH reaches 6.5 protonation occurs, corresponding to an increase in particle volume and in the fluorine motion, whose resonance now appears as a clear peak in the MR spectrum (T_2 = 56.8 ms, T_1 = 280 ms, 470 MHz): this corresponds to the 'on-state'. These nanoparticles have potential application *in vivo*, but the lower field scanners used in the clinic may lead to insufficient signal intensity, and addition of a ^{19}F reference is required[45,46].

1.2.2.3 Metal ion probes

Metal ions are involved in several physiological processes; therefore the development of responsive probes for their selective detection can help in understanding their key role. Calcium is of particular significance and has been measured in mouse thymocytes and perfused ferret hearts using fluorinated derivatives of BAPTA, in particular 4- and 5- substituted **22**.

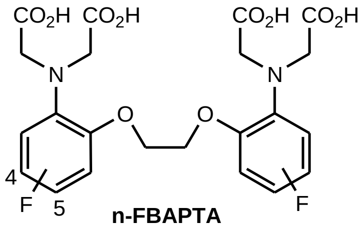

n-FBAPTA

22

Upon binding of divalent cations, a change in the ^{19}F chemical shift occurs. 5-FBAPTA exhibits a slow exchange between free and bound forms on the NMR time scale ($\delta_{F(free)}$ ~2 ppm, $\delta_{F(bound)}$ ~8 ppm from a 6-fluorotryptophan external reference, 188 MHz, pH 7.1, 37ºC); hence, in the presence of non-saturating concentrations of Ca^{2+} (0.33 mol equivalents), they appear as two separate resonances in the ^{19}F spectrum and their area can be used to calculate the calcium concentration. In contrast, in the case of 4-FBAPTA the two forms ($\delta_{F(free)}$ ~1 ppm, $\delta_{F(bound)}$ ~2 ppm) are in fast exchange, giving a single peak with a chemical shift which is a function of their relative proportions, thus indicating the Ca^{2+} concentration. In both cases the resulting signals are broadened when the two forms co-exist compared to the all-free or all-bound resonances: a proof of the chemical exchange. The 5-substituted probe presents a small chemical shift δ_F <0.2 ppm in the presence of Mg^{2+} up to 10 mM and δ_F <0.1 ppm in the pH range 6.9-7.3; hence, intracellular variation of Mg^{2+} concentration and pH will not disturb the evaluation of the amount of calcium by the chelator. The tetraacetoxymethyl ester derivatives have been used for cell studies because they easily penetrate the membranes and are hydrolysed by esterases to release the free probe: after loading thymocytes with 1 mM 5-FBAPTA, two resonances emerged in the ^{19}F NMR spectrum indicating a $[Ca^{2+}]_i$ of 250 nM. These agents can also bind other divalent metal ions such as Zn^{2+}, Fe^{2+} and Mn^{2+} giving for each chelate a characteristic chemical shift, allowing diverse metals to be detected without interference. The ^{19}F chemical shifts of the saturated complexes (equimolar solution of M^{2+}) have been measured at 94.1 and 188.3 MHz at 37ºC utilising 6-fluorotryptophan as reference, reporting in the case of 5-FBAPTA: Zn^{2+} $\delta_F = 5.6$ ppm, Ca^{2+} $\delta_F = 7.8$ ppm, Fe^{2+} $\delta_F = 28.5$ ppm. Mn^{2+} causes excessive line broadening, while the low affinity for Mg^{2+} does not allow the saturation of the chelate to be achieved[47].

5-FBAPTA has been utilised to measure the changes of $[Ca^{2+}]_i$ during the cardiac cycle in perfused ferret hearts by means of the ^{19}F peak ratio. The administration of the ester form caused a drop in the pressure, due to the induced increase of the buffer capacity for calcium in the cytosol. This effect has been proved by addition of $ZnCl_2$ to the medium: Zn^{2+} has a higher affinity for the probe and displaces the calcium, restoring the pressure. Though the heart appeared to be perturbed by the indicator, the calcium modifications can be promptly recorded. In the same experiment, α−fluorocitrate **23** has been employed for estimating the magnesium levels, by means of the chemical shift change that occurs upon binding. Only the (+)-enantiomer can be used, due to the high toxicity of the (-)-isomer[48]. Similar behaviour to 5-FBAPTA was observed for the fluorinated magnesium chelator APTRA **24**. The 5-substituted isomer is in the slow exchange regime on the NMR time scale and appears as two resonances in the NMR spectrum, while the 4-substituted isomer exhibits fast exchange which results in a single peak. After infusion in rat hearts, both analogues induce a pressure fall[49].

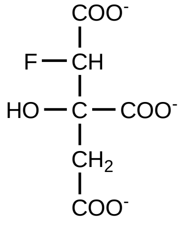

α-fluorocitrate
23

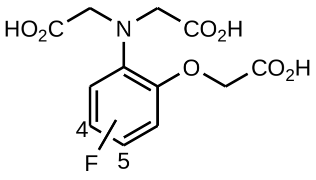

n-FAPTRA
24

A peculiar example of fluorinated chelators are fluoro crown ethers **25** and fluoro cryptands **26**, in which the C-F bond is directed toward the metal coordination site acting as a σ-donor bond. In the presence of divalent cations stable complexes formed showing a characteristic chemical shift up to 18.2 ppm from the ligand signal. For crown ethers, the metal-ion exchange is fast on the NMR time scale, while it is slow for the cryptands[50].

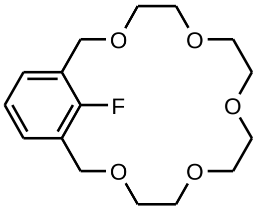

F-crown ether

25

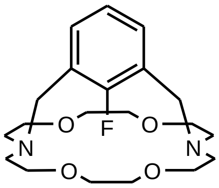

F-cryptand

26

1.2.2.4 pO_2 and hypoxia reporters

A key diagnostic marker in cancer treatment is pO_2 (oxygen partial pressure), giving knowledge of the oxygenation level of diseased tissues. Hypoxic tumour cells are recognised to be more resistant to both radiotherapy and chemotherapy. Low levels of oxygenation also influence other aspects, such as angiogenesis, tumour invasion and metastasis. This information is therefore important in the evaluation of therapeutic planning, as hypoxic tumours are less responsive to treatment and often more aggressive. Mason and coworkers exploited the linear correlation between pO_2 and the relaxation rate, R_1, exhibited by perfluorocarbons to measure tissue oxygenation *in vivo*. One problem with perfluorocarbons is the presence of multiple resonances which hampers the ease of acquisition and lowers the S/N ratio. Symmetric PFCs that appear as one major ^{19}F signal are preferred, as occurs for hexafluorobenzene (HFB) **27** and perfluoro-15-crown-5-ether (15C5) **3**, which are two of the most commonly used agents. HFB proved to be particularly sensitive to changes in pO_2, and relatively insensitive to temperature variations which would compromise the accuracy of the measurements. These characteristics made it a better candidate than 15C5, which was less sensitive and more affected by temperature fluctuations.

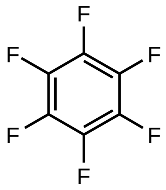

HFB
27

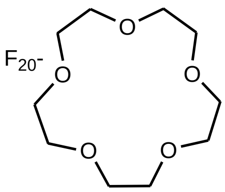

F_{20}-15C5
3

After intratumoral injection (i.t.) of 20µl HFB in a prostatic carcinoma in rat model, an HFB signal was observed in the same central or peripheral region where it was administered, indicating the absence of redistribution, which allowed the interrogation of the same area of interest for several hours. Basal values obtained during breathing of 66% oxygen were 4.0 ± 1.5 torr and 48.8 ± 2.6 torr for the internal and external tumour region respectively. The increase to 100% of the inhaled oxygen produced a large variation in the peripheral area of up to 61.9 torr, which returned to basal values after restoration of the oxygen level to 66%; the internal part of the tumour was only slightly perturbed. Previous studies employed the less invasive intravenous administration of HFB using a much higher infusion volume of 16 ml (compared to 20µl i.t.). Comparative pO_2 values were obtained after 7 days of infusion for detection of external tumour regions; while the detection of central regions required administration of HFB at the beginning of the tumour growth, in order to be sequestered in the central area which after 17 days of development became necrotic and no more vascularised. In contrast, i.t. injection allows immediate evaluation of the area of interest[51].

A different class of hypoxia markers are fluorinated nitroimidazoles: they are bioreductive agents which undergo 1-electron reduction by intracellular reductases generating reactive intermediates. Under physiological oxygen levels, the intermediates are re-oxidised and excreted from the cells, whereas in the presence of a hypoxic environment, they covalently bind to cellular elements. Their presence in the cells is therefore an indication of hypoxia. SR-4554 **28**, for example, has been evaluated in a mouse tumour model (carcinosarcoma) that closely resembles the characteristics of human tumours, with the purpose of validating the quality of this hypoxia marker prior to clinical studies. Because there is no detectable difference between the parent molecule and its metabolites, the retention is evaluated by means of the ratio between the fluorine signal at an early time point, which corresponds to the parent molecule, and the same signal at a later point which corresponds to residual parent molecules plus the trapped products[52]. A different approach has been recently reported using a ^{19}F-labelled indolequinone derivative (IQ-F) **29**. Upon reduction in hypoxic cells by the intracellular reductases, the probe releases nonafluoro-*tert*-butyl alcohol which can be detected in the ^{19}F NMR spectrum as a new signal, shifted by ~5 ppm from the resonance of the parent structure[53].

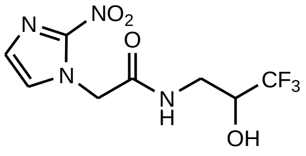

SR 4554
28

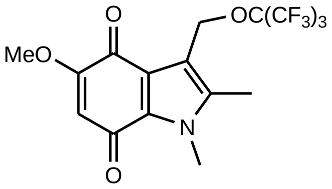

IQ-F
29

1.2.2.5 Protein studies

Fluorinated probes have been used for studying various macromolecules such as proteins, DNA/RNA and enzymes, for understanding the way biological molecules interact with one another or for investigating their structures and conformational changes[54]. Jackson *et al.* developed a method for site-specific genetic incorporation of the fluorinated amino acid trifluoromethyl-L-phenylalanine (tfm-Phe) **30** into *E. Coli* proteins and used the resulting ^{19}F NMR signal to characterise the protein structure and monitor its reactivity.

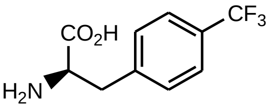

Tfm-Phe
30

Tfm-Phe was introduced at different positions in the active interface between the two homodimers nitroreductase (NTR) and histidinol dehydrogenase (HDH), and the chemical shift of the ^{19}F signal was observed upon binding of substrate and inhibitor at the active site[9].

A singular approach has been recently reported for detection and imaging of specific proteins by means of nanoprobes with an on/off type of signal. The probe is composed of monomers consisting of ligands with the ability of targeting a specific protein, in this case human carbonic anhydrase, and forming aggregates of about 200-500 nm. The ligand also contains the fluorine moiety. When the probe is in the aggregate form the fluorine signal is largely broadened and is not visible in the spectrum. Upon addition of the protein, the probe disassembles and the ^{19}F signal appears (Fig. 1.6)[55].

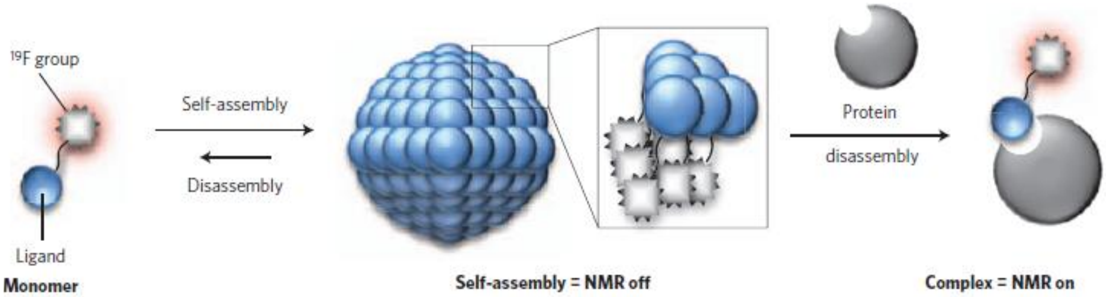

Fig. 1.6 Schematic representation of the on/off mechanism for the protein probe (Figure taken from reference [55]).

1.2.2.6 Enzyme reporters

Several applications of fluorinated probes exploited a series of enzymes in pro-drug therapy or as means to release the active form of the probe as was discussed previously. However, enzymes may also be the object of study themselves, monitoring the presence of certain enzymes in cells or determining the kinetic parameters for new substrates. Carboxylesterases have been the focus of the study of Mendz *et al.* in which simple fluorinated compounds such as ethyl fluoroacetate and diethyl fluoromalonate have been used to measure the enzyme activity in erythrocytes and to confirm the presence of the enzyme in several strains of the bacterium *Helicobacter pylori*[56].

Nanoprobes formed by perfluorinated cubic silsesquioxane (F-POSS **31**) immobilised onto silica particles have been applied to examine the action of alkaline phosphatase. The F-POSS were linked to the silica nanoparticles by a phosphordiamidate bond that is recognised by the enzyme. The impaired rotation of the linked F-POSS caused a large broadening of the fluorine MR signal, which is therefore not observable. Upon addition of the enzyme, the fluorinated cubic silsesquioxanes are released by the enzymatic reaction and the ^{19}F MR signal is restored. The enzymatic activity is hence monitored by an increase in the signal intensity[57].

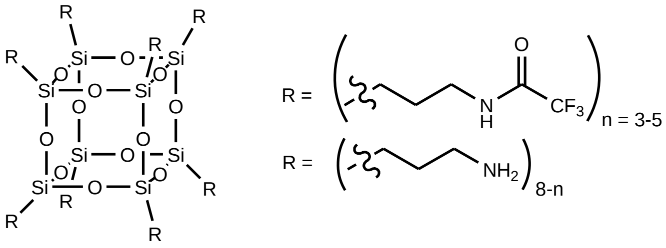

F-POSS
31

1.2.3 Fluorinated pharmaceuticals

There are several drugs containing a fluorine atom or a fluorinated group, which range from psychoactive compounds (*e.g.* fluoxetine) to anti-inflammatory agents (*e.g.* niflumic acid). They are good candidates to be studied by ^{19}F MRS and MRI, allowing a deeper understanding of pharmacokinetics, metabolism processes and effectiveness of drug targeting. These aspects are important for drug design and are essential aspects of preclinical trials.

A classic fluorinated drug is 5-fluorouracil (5-FU) **13,** a chemotherapeutic compound, whose range of doses between efficacy and toxicity is very tight and thought to be related to pharmacokinetics.

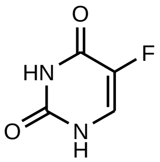

5-FU
13

The cytostatic activity is expressed *in vivo* by conversion of 5-FU to fluoronucleotides that bind irreversibly an essential enzyme for DNA replication, thymidylate synthase, and are incorporated in DNA and RNA as substitutes for the natural nucleotides. Competitive catabolic transformation to DHFU (5,6-dihydrofluorouracil) and FBAL (α-fluoro-β-alanine) occurs in the liver, reducing the bioavailability of 5-FU. From here, there is clearly an interest in understanding the details of the different anabolic and catabolic pathways in order to enhance the therapeutic efficacy. Brix *et al.* integrated the investigation of pharmacokinetics aspects by dynamic ^{18}F PET with the analysis of metabolic processes by ^{19}F NMR, confirming the liver as the major site of metabolism, based on selective 5-FU and FBAL shift images[58]. ^{19}F MR spectroscopy also supported the development of several pro-drugs, conceived to reduce 5-FU toxicity and its liver intensive extraction by exploiting the higher enzymatic level in tumours in order to improve targeting.

2-Fluorodeoxyglucose (FDG) **32** is a glucose analogue utilised in PET (Positron Emission Tomography, ^{18}F) as an imaging agent to assess the metabolic activity of tumours and metastases. Being a glucose analogue, it enters highly metabolically active cells, such as those of tumours, brain and heart, exploiting their glucose transporters. Here, it is converted to FDG-6-phosphate which is not recognised as a substrate for phosphohexose isomerase. Hence, it doesn't undergo further metabolism, accumulating inside the cells. PET provides information about regional uptake with great sensitivity, but cannot differentiate between different metabolic products. For this purpose, a valuable method is ^{19}F NMR, as demonstrated by the study of 2-FDG metabolism in rat brain, in which ^{19}F MRS spectra and their temporal profile have been recorded, showing four metabolites, two of which have been recognised as FDG-6-phosphate and 2-fluoro-2-deoxy-6-phosphogluconate (the other two were not identified), proving the more extensive metabolism of FDG, which goes beyond the phosphorylation[59].

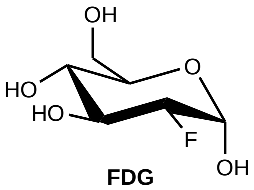

FDG
32

One of the earliest applications of ^{19}F NMR *in vivo* was the study of gaseous fluorinated anaesthetics such as halothane, enflurane and isoflurane to understand their anaesthesia mechanisms. Of particular interest was their site of action, brain residence time and metabolite toxicity. They exhibit a short transverse relaxation time T_2 (T_1 = 1.0 s, T_2 = 3.6 ms at 2.0 T for halothane), which makes imaging approaches more difficult. Even so, maps of the local distribution of halothane were achieved in rabbit brains, showing the selective concentration of anaesthetic in the cerebral cortex, rather than deeper brain regions[60].

Clinical applications of ^{19}F MRS have been reported for studying psychotropic drugs and antibiotics. Fluvoxamine **33** is used to treat various psychiatric conditions and its elimination from the human brain has been examined on subjects under clinical treatment: no direct correlation was found between plasma and cerebral $t_{1/2}$ (14-26 hours and 58 hours respectively) of fluvoxamine and these values were not related to age[61].

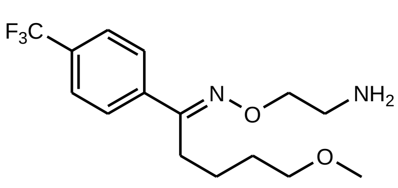

Fluvoxamine
33

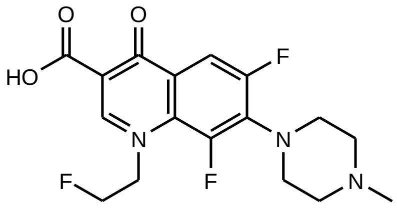

Fleroxacin
34

After oral administration of fleroxacin **34**, a fluorinated antibiotic, healthy volunteer subjects have been studied for 24 hours, acquiring successive MR spectra of liver and calf muscles combined with HPLC analysis of plasma. Various pharmacokinetics parameters have been successfully measured (*e.g.* C_{max} = 53 μmol/l plasma, 250 μmol/l liver and 60 μmol/l muscle). These studies confirm the potential of ^{19}F MRS and MRI for observing non-invasively the fate of fluorinated drugs *in vivo*[62].

1.3 Paramagnetic NMR

The lanthanides series presents distinctive characteristics in the periodic table, since the first and last trivalent ions, La^{3+} and Lu^{3+}, are diamagnetic while all the others show paramagnetic properties thanks to the unpaired 4f electrons. These are shielded by 5s and 5p electrons and thus are not accessible for interacting with ligands to form covalent bonds. Therefore, the complexes are formed predominantly through electrostatic interactions. All the Ln^{3+} ions have similar chemical behaviour and differences are mainly related to the contraction of ionic radius along the series.

Different lanthanide complexes of the same ligand are almost isostructural but each of them presents peculiar NMR properties. When a Ln^{3+} ion interacts with an NMR active nucleus, the presence of the unpaired 4f electrons causes increased relaxation, broadening and sometimes shift to a different frequency of the resonance of the nucleus. While Gd^{3+} has an isotropic distribution of its unpaired electrons and hence cannot produce a dipolar shift, the other ions possess an anisotropic distribution. Therefore, they can generate a dipolar lanthanide induced shift (LIS) in solution, often called the pseudocontact shift, a property that renders them useful as shift agents to obtain structural information.

1.3.1 Chemical shift

The paramagnetic shift for a nucleus of a ligand that coordinates to a Ln ion is the sum of three terms:

$$\Delta = \Delta_d + \Delta_c + \Delta_p \qquad (1)$$

Δ_d is the diamagnetic shift, usually insignificant except for nuclei directly coordinated to the Ln cation and derives from inductive and electrical field effects and conformational changes. It can be determined from the induced shift of diamagnetic La^{3+} and Lu^{3+} complexes. The term Δ_c is the contact shift (Fermi contact), resulting from the through-bond transmission of the spin density of the unpaired electrons from the 4f orbital of Ln^{3+} to the nucleus in study. The effect decreases rapidly with the number of bonds, allowing the identification of the ligand nuclei directly bonded to the metal. It is described by the following equation:

$$\Delta_c = < S_Z > F = < S_Z > \frac{-A}{\hbar \gamma_I B_0} 10^6 \qquad (2)$$

where B_0 is the magnetic field strength, $<S_z>$ the calculated spin expectation value for a paramagnetic ion (Table 1.1), $A/\hbar$ the hyperfine coupling constant (rad/s) and γ_I the gyromagnetic ratio of the observed nucleus. The Ln unpaired spin density can be transferred to the nucleus of the ligand by direct spin delocalisation through weak covalent bonding using the 6s metal orbital or through spin polarisation from 4f orbitals.

The term Δ_p is the pseudocontact or dipolar shift, which derives from the local magnetic field induced through space by the magnetic moment anisotropy of the lanthanide ion in the nucleus under study. If the principal magnetic axes are used as the coordinate system, Δ_p can be expressed by the following equation:

$$\Delta_p = \frac{C_J \mu_B{}^2}{60k^2T^2}\left[\frac{\langle r^2\rangle A(3\cos^2\theta - 1)}{r^3} + \frac{\langle r^2\rangle A'\sin^2\theta\cos 2\varphi}{r^3}\right] \qquad (3)$$

where μ_B is the Bohr magneton, k the Boltzmann constant, C_J the Bleaney's constant characteristic of the Ln ion (Table 1.1), and $<r^2>A$ and $<r^2>A'$ are ligand field coefficients that remain constant along the lanthanide series for isostructural complexes. r, θ and φ are the spherical coordinates which describe the position of the nucleus under study in the coordinate system with the Ln ion at its centre. The equation can be simplified to:

$$\Delta_p = D_1\frac{3\cos^2\theta - 1}{r^3} + D_2\frac{\sin^2\theta\cos 2\varphi}{r^3} \qquad (4)$$

In the case of systems with axial symmetry the second term of equation (4) is zero. It is clear then, excluding the few nuclei directly coordinated to the metal, that for all the other nuclei only the dipolar shift contributes to the observed shift because unpaired electrons are shielded by the 5s and 5p valence electrons. Therefore, they are not available for covalent interaction with the ligand, but only for through space interactions[63].

Table 1.1 NMR parameters for paramagnetic lanthanide ions.

Ln	$^{2S+1}L_J$	**C_J** [a]	**$<S_Z>$** [b]	**μ_{eff}** [c]	**^{1}Hshift/aqua** [d]	**$\Delta\omega_{1/2}$** [e]	**T_{1e}** [f]
Ce	$^2F_{5/2}$	-6.3	-0.98	2.56	---	---	0.9
Pr	$^3H_4$	-11.0	-2.97	3.62	0.27	5.6	0.57
Nd	$^4I_{9/2}$	-4.2	-4.49	3.68	0.32	4.0	1.15
Pm	$^5I_4$	2.0	4.01	---	---	---	---
Sm	$^6H_{5/2}$	-0.7	0.06	1.55-1.65	---	4.4	0.45
Eu	$^7F_0$	4.0	10.7	3.40-3.51	---	5.0	0.09
Gd	$^8S_{7/2}$	0	31.5	7.94	3.01	Broad	10^4-10^5
Tb	$^7F_6$	-86	31.8	9.7	-10.53	96	2.03
Dy	$^6H_{15/2}$	-100	28.5	10.6	-6.95	200	2.99
Ho	$^5I_8$	-39	22.6	10.6	-4.88	50	1.94
Er	$^4I_{15/2}$	33	15.4	9.6	3.83	50	2.38
Tm	$^3H_6$	53	8.21	7.6	9.29	65	3.69
Yb	$^2F_{7/2}$	22	2.59	4.5	2.52	12	1.37

[a] Normalised to 100 for Dy[64]; [b] Calculated values[65]; [c] [64]; [d] Values in ppm[65]; [e] Half-height widths of ^{1}H methyl resonance of 2-picoline in Ln[tris(dipivaloylmethane)$_3$ adduct, values in Hz[65], [f] 10^{-13}s[64].

There have been many applications illustrating the use of paramagnetic complexes as shift reagents, for example, to simplify the interpretation of the NMR spectra of many biomolecules such as proteins and nucleic acids. Sherry and coworkers have studied the shift variation of the ^{1}H and ^{31}P resonances in the complex $TmDOTP^{5-}$ **35** as a function of temperature, pH and Ca^{2+} concentration. ^{1}H and ^{31}P chemical shifts were found to change linearly with temperature ranging from 20 to 50°C ($\Delta\delta$ ~25 ppm for ^{1}H and $\Delta\delta$ ~60 ppm for ^{31}P, 7 T) as well as with pH over the range 6-8 ($\Delta\delta$ ~5 ppm for ^{1}H and $\Delta\delta$ ~25 ppm for ^{31}P, 7 T). The temperature dependence showed little sensitivity to variations in pH or calcium concentrations up to 5.3 mM, allowing precise temperature measurements at similar Ca^{2+} concentrations to those encountered *in vivo*. The probe can also be applied to monitor simultaneously temperature and pH using multiple resonances, but only in extracellular compartments, as it cannot enter cells[66].

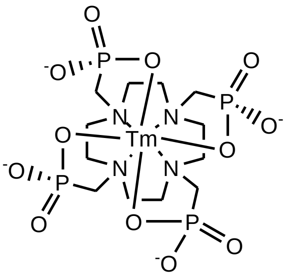

TmDOTP^{5-}

35

1.3.2 Relaxation phenomena

When a ligand coordinates a paramagnetic lanthanide ion, it experiences an enhancement of both the longitudinal ($R_1 = 1/T_1$) and the transverse relaxation rates ($R_2 = 1/T_2$). The ability of paramagnetic complexes to increase the relaxation rates of nearby nuclei is often termed its relaxivity (r_i). Strictly, relaxivity is the increment of the observed relaxation rate per unit probe concentration and has the units of a second order rate constant, typically expressed as $mM^{-1}s^{-1}$. Most often, this is discussed in ^{1}H MR, by examining the effect of a paramagnetic complex (mainly Gd^{3+}) on the relaxation rate of bulk water: *i.e.* an intermolecular effect. The relaxation effect has contributions from the inner sphere and outer sphere. The second term is often small and is normally neglected in structural studies with Ln^{3+}, but in some Gd^{3+} complexes it can contribute to the same extent as the inner sphere to the total relaxivity. The measured relaxation rate ($R_{iobs,}$ i = 1,2) is the sum of a diamagnetic contribution R_{id} (determined with La^{3+}, Lu^{3+} and Y^{3+} complexes) and a paramagnetic contribution R_{iM}:

$$R_{iobs} = R_{id} + R_{iM} \qquad (5)$$

$$R_{iobs} = R_{id} + r_i[Gd] \qquad (6)$$

R_{iM} represents the interaction of the magnetic field that is generated by the unpaired electrons of the lanthanide ion with the nuclear spin of the nucleus under study. This electron-nuclear interaction is controlled by electron spin relaxation, molecular tumbling and chemical exchange. The overall relaxation rates are described as the sum of contributions from the contact R_{icon} (also termed scalar or hyperfine), dipolar R_{idip} and Curie $R_{i\chi}$ mechanisms:

$$R_{iM} = R_{icon} + R_{idip} + R_{i\chi} \qquad (7)$$

The contact contribution is negligible for all lanthanide(III) ions except Gd^{3+}, and is relevant only for directly bound nuclei. The dipolar contribution is a through-space interaction that originates from the fluctuations of the electronic magnetic field. For Ln ions, other than Gd^{3+}, with short electronic relaxation times ($T_{1e} = T_{2e} \approx 10^{-13} – 10^{-12}$ s, Table 1.1), the dipolar contribution can be described by the simplified Solomon-Bloembergen equation as:

$$R_{1dip} = R_{2dip} = \frac{4}{3}\left(\frac{\mu_0}{4\pi}\right)^2 \frac{\gamma_I^2 \mu_{eff}^2}{r^6} T_{1e} \qquad (8)$$

where $\mu_0/4\pi$ is the magnetic permeability of a vacuum, μ_{eff} is the effective magnetic moment of the Ln^{3+} ion (Table 1.1) and r is the Ln-nucleus distance. In the case of Gd^{3+} this simplification cannot be applied because of the relatively long electronic relaxation times ($T_{1e} > 2 \times 10^{-7}$ s at fields higher than 200 MHz). The Curie or susceptibility contribution is another dipolar effect developing from the nuclear spin interaction with the electronic spin thermal average and depends on the rotational motion of the complex. It is given by equations 9 and 10:

$$R_{1\chi} = \frac{6}{5}\left(\frac{\mu_0}{4\pi}\right)^2 \frac{\gamma_I^2 B_0^2 \mu_{eff}^4}{(3kT)^2 r^6}\left(\frac{\tau_R}{1+\omega_I^2\tau_R^2}\right) \qquad (9)$$

$$R_{2\chi} = \frac{1}{5}\left(\frac{\mu_0}{4\pi}\right)^2 \frac{\gamma_I^2 B_0^2 \mu_{eff}^4}{(3kT)^2 r^6}\left(4\tau_r + \frac{3\tau_R}{1+\omega_I^2\tau_R^2}\right) \qquad (10)$$

where τ_R is the rotational tumbling time of the complex and ω_I the Larmor frequency of the nucleus. The dipolar contribution in lanthanide complexes, other than Gd, influences to the same extent both the transverse and longitudinal relaxation rates; conversely the Curie effect on the transverse relaxation rate, $R_{2\chi}$, is larger than that over the longitudinal relaxation $R_{1\chi}$. This is particularly evident in the case of macromolecules with a long τ_R[63].

Knowing τ_R, equations 9 and 10 can be adopted to calculate the relative distances between the lanthanide ion and the ligand nuclei using rate data obtained at different fields. An example has been reported by Aime *et al.* using tetraaza-macrocyclic phosphinate complexes of Yb^{3+} **36**.

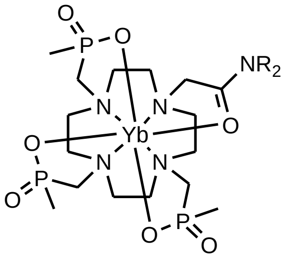

36

The R_1 values of the ^{31}P resonances have been measured (at 2.1, 6.3 and 9.4 T) and plotted against the square of the field B_0, resulting in a linear correlation. The slopes of the graphs gave the distances between the metal and the phosphorus nuclei[67].

In clinical practice, different complexes based on Gd^{3+} are commonly used as contrast agents in MRI, exploiting its ability to decrease the bulk water relaxation time which enhances the contrast in T_1 weighted images. Examples include GdDTPA, GdDOTA, GdDTPA-BMA and GdHPDO3A[3].

1.4 Requirements for use of fluorinated probes in magnetic resonance

As discussed in the previous paragraphs, ^{19}F-containing probes for magnetic resonance applications offer a very interesting tool for biological studies. The absence of an endogenous background, the high sensitivity to even small changes in the chemical environment or in the probe geometry render this a potential class of agents for future MRS and MRI analysis. During recent years, some progress has been made[6,68], however important issues are still hindering the widespread usage of these agents.

1.4.1 Problems with current probes

The main drawback in the use of ^{19}F magnetic resonance is the low sensitivity, a problem common to all the NMR techniques. This is related to the slow longitudinal relaxation rate R_1 of the fluorine nucleus. This is particularly problematic for CF_3 groups, for which R_1 values are about 0.3 to 1 s^{-1}. To obtain sufficient signal intensity, multiple scans are therefore required, increasing significantly the acquisition time of the experiment. Before a successive scan can be undertaken in magnetic resonance spectroscopy, it is necessary that the nucleus under study reaches complete relaxation, a condition that is normally ensured by allowing a delay time between scans of 3 to 5 times the T_1. It is, therefore, evident how having a long longitudinal relaxation time can affect the practicability of these MRS analyses where each scan takes 3 to 6 seconds, especially in the case of potential future clinical applications for which fast analysis is necessary. Furthermore, it has to be considered that the signal to noise ratio varies with the square root of the number of scans acquired, hence a great number of repetitions are required even for small enhancements of signal intensity.

To achieve adequate sensitivities, a high local concentration of fluorine is essential. This results in the need for high concentrations of a fluorinated probe (*e.g.* about 20-50 mM), raising concerns for solubility and toxicity problems.

The ample chemical shift range of ^{19}F containing species have not been exploited to its maximum, with chemical shift differences in the majority of cases being too small to be employed in chemical shift imaging protocols. Interpretation of the spectra can also present some difficulties because of the large J coupling between proximate protons and the fluorine nucleus.

A faster relaxation of the ^{19}F nucleus of at least one order of magnitude is consequently desired to allow rapid acquisition of magnetic resonance data, bearing in mind the need to have acceptable line broadening (proportional to R_2) to prevent signal loss. Essential requirements for a fluorinated probe to be applied *in vivo* are also high kinetic stability, increased fluorine chemical shift non equivalence and the possibility to be detected in the 0.1-0.5 mM range.

1.4.2 Possible solution: use of proximate lanthanide(III) ions

One way to satisfy these requirements is to place a fluorine atom, for example a CF_3 group, close in space (within 7 Å) to an open shell paramagnetic ion and within the McConnell cone (Fig. 1.7), described as $3\cos^2\theta{-}1/r^3$ in equation (3), in a kinetically stable paramagnetic lanthanide complex or conjugate, that is responsive to the parameters of interest.

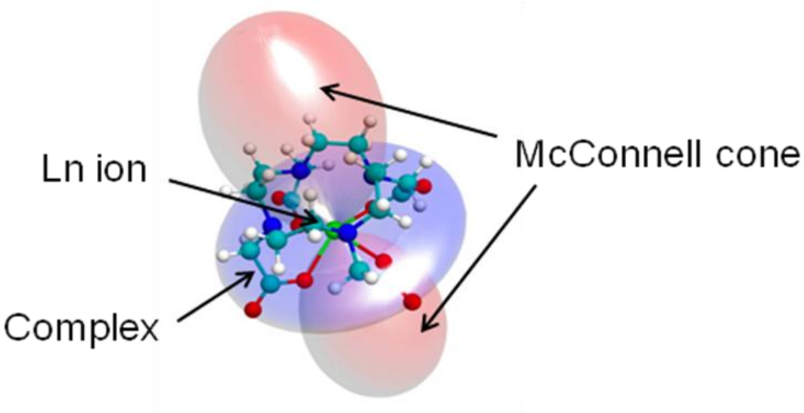

Fig. 1.7 Schematic representation of the McConnell cone originated by the paramagnetic ions at the centre of the complex.

As described in paragraphs 1.3.1 and 1.3.2, the proximity of a nucleus, fluorine in this case, to the lanthanide ion results in two main effects: enhancement of R_1 and R_2 thanks to the contribution of the dipolar and Curie mechanisms, and amplification of fluorine chemical shift non-equivalence because of the pseudocontact shift or dipolar lanthanide induced shift (LIS).

The consequences of these effects on the fluorinated moiety of the ligand impart improved performances to the NMR probe. The reduced T_1 value permits the acquisition of a larger number of scans in a shorter time, resulting in increased signal intensity. The signal to noise ratio is consequently augmented with the possibility of obtaining sufficient signal intensity using lower probe concentrations, with benefits also for solubility and toxicity.

Additionally, the increased chemical shift non-equivalence of the fluorine resonances amplifies the sensitivity of the probes to changes in the microenvironment and consequently to very minor variations of the complex structure, leading to improved chemical shift-based images.

These considerations represent the rationale of the recent work that has been carried out in our laboratory with interesting results[69]. Using probes with CF_3 groups in which the fluorine nuclei are between 6 and 7 Å from the lanthanide ion, the enhancement of R_1 was found to be greater than two orders of magnitude for complexes of Dy^{3+}, Tb^{3+} and Ho^{3+}. The parallel increase of R_2 has to be carefully considered: it can be advantageously used in T_2-weighted images, on the other hand it also produces larger linewidths, that renders signal detection more difficult. Hence, a balance between the benefits of improved relaxation and the broadening effect has to be preserved.

By varying the lanthanide ion for a series of complexes of the same ligand, different information can be obtained exploiting the peculiar characteristics of each metal: Dy, Tm, Tb, Ho and Er are moderate relaxation enhancers, Eu and Yb do not affect relaxation significantly but introduce a large dipolar shift. Analogous Gd complexes can serve as possible ^1H MRI contrast agents that have similar biodistribution and chemical properties.

1.5 Fluorinated paramagnetic probes

Although there has been great interest in the use of lanthanides as shift reagents and relaxation enhancers for simplifying interpretation of spectra or obtaining structural information, much less has been reported about the shift and relaxation effects on fluorine NMR parameters. Lately, new interest has grown around ^{19}F MRS/MRI reporters, thanks to the recent development of more sensitive instrumentation and dual probes design, and examples of different paramagnetic fluorinated probes have been reported.

1.5.1 Previous studies of ^{19}F NMR in lanthanide systems

The earliest reported examples of studies regarding ^{19}F NMR shifts of paramagnetic complexes includes the work of Yatsunyk and Walker focusing on the fluorine chemical shift of paramagnetic tetraphenyl iron(III)porphyrins (TPP) **37** derivatives.

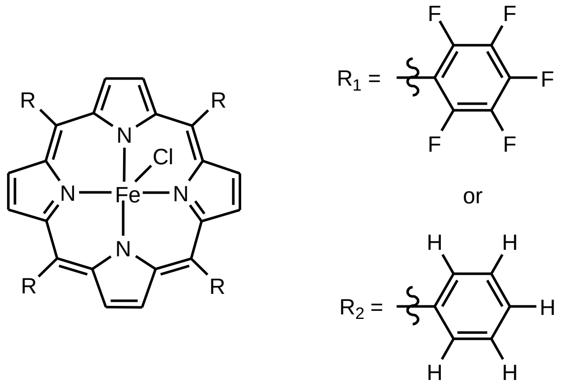

TPP

37

They compared the ^{19}F shifts of different fluorophenyl complexes with the ^{1}H shift of their non-fluorinated analogues, with the purpose of determining the contributions responsible for the large shift observed for the *ortho*-fluorine resonance and for the smaller shift, also of the same sign, for the *meta* and *para* resonances. They found a direct correlation between the *o*-fluorine shift and the spin density present at the *meso*-carbon to which the phenyl rings were attached; however, discrimination between the possibilities of ligand-centred dipolar shift and a through space contact shift resulting from an overlap of the electron cloud of the *o*-fluorine and the porphyrin ring π system was not established[70].

A reversible signal regulation of ^{19}F NMR has been reported using ferrocene complexes as switching modules. The probe is formed by a POSS scaffold (cubic silsesquioxanes) to which are linked the fluorine reporter in form of trifluoroacetyl groups and the ferrocene moiety **38**. When the ferrocene is oxidised, its paramagnetic character enhances the relaxation of the nearby fluorine nuclei causing line broadening and a consequent reduction in their signal intensity, whereas after reduction the signal is recovered[71].

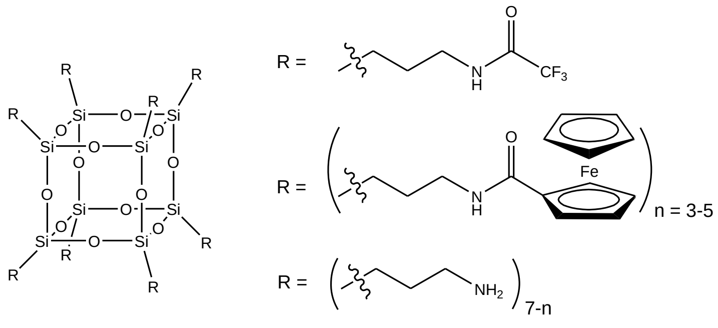

F-POSS

38

Sherry and coworkers examined the ^{19}F NMR spectra for a series of lanthanide complexes of F-DOTPME **39**, a trifluoroethyl ester derivative of macrocyclic phosphonate, and observed that they exist in solution as a mixture of diastereomers. Thanks to the sensitivity of fluorine to minor structural changes, assignment of several of the shifted fluorine resonances to specific diastereomers was undertaken. Addition of cationic detergents altered the shift and population of the isomers in favour of the Δ-SSSS isomer, while the neutral polyethylene glycol (PEG) influenced the shift of some stereoisomers but not their population[72].

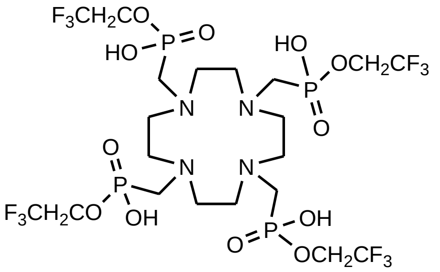

F-DOTPME

39

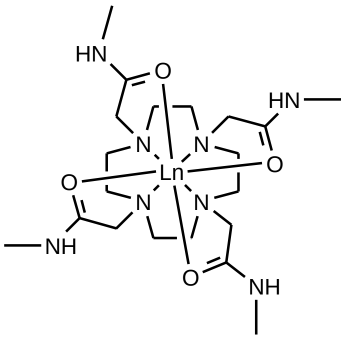

40

The temperature and pH dependence of the longitudinal relaxation rate of ^{19}F nuclei in a fluorinated counter ion such as $CF_3SO_3^-$, has been measured, as a means of studying the local hydration sphere and the dynamics of water, prototropic and anion exchange in paramagnetic complexes **40**[73,74]. In particular, T_1 was found to be constant (~75 ms, 235.3 MHz) in the pH range 8 to 2, while a noticeable increase was observed at lower pH values, when the distance between the lanthanide ion and fluorine increased, as displacement of the triflate by other anions (sulfate, phosphate, chloride) took place. This example offers further proof of the paramagnetic effect on relaxation when the fluorine nucleus remains close to the metal. Trifluoromethylsulfonate has been studied also as a potential extracellular fluorinated probe *in vivo*, when administered with the ^{1}H MRI T_1 relaxation agent $[GdDTPA]^{2-}$. The aim was to enhance the fluorine relaxation in order to obtain faster acquisition of ^{19}F MR images. The fluorinated anion was administered in a brain abscess of an animal model and images were recorded before and after the injection of $[GdDTPA]^{2-}$ in less than 5 minutes[75]. This approach is of limited use, as the Gd complex and the anion will repel each other, inhibiting the close encounter that is required for enhanced relaxation and can be used only upon simultaneous injection in the same compartment.

Furthermore, the temperature dependence of the fluorine longitudinal relaxation rate of ternary adducts between paramagnetic complexes and reversibly bound anions, such as trifluoromethyl-L-lactate **41**, has been studied, showing the highest rate (R_1 ~100 s^{-1}, 7 T) at lower temperatures (300 K compared to 330 K of ^1H values for L-lactate)[76]. The replacement of the two bound water molecules with the substrate allowed the fluorine atoms to be sufficiently close to the metal to experience the paramagnetic R_1 enhancement[77].

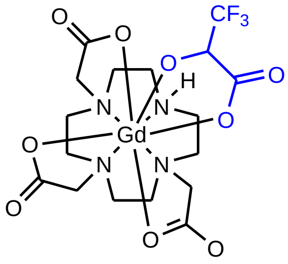

41

Recently, a Gd based paramagnetic probe for protease activity **42** has been examined *in vitro*. It contains a Gd^{3+} complex, a ^{19}F containing group and a peptidic linker, which is recognised as substrate by caspase-3, a marker enzyme for apoptosis. The compound shows a weak signal due to the relaxation enhancement of the paramagnetic metal on the fluorine atom, which causes a shortening of the fluorine T_2 and therefore broadening of the resonance. Upon enzymatic cleavage of the peptide, the paramagnetic effect is reduced and the signal intensity increases[78]. This system exhibits some limitations: first, even after enzymatic hydrolysis the signal experiences partial intermolecular paramagnetic broadening because of the Gd complex in solution which hampers its total recovery, and second, the position of the fluorinated moiety on the cleavage product results in a fluorine signal which presents the usual problematic slow T_1 value, common to all the diamagnetic probes.

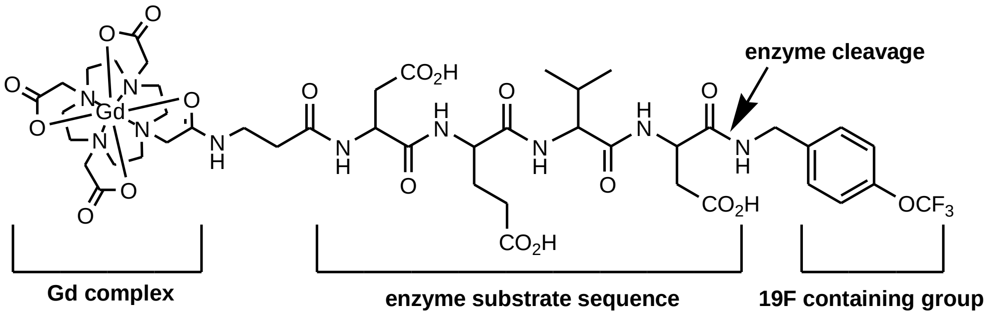

42

One of the problems that affects the use of MRI probes *in vivo* is the need to determine their local concentration, otherwise the observed reporter signal can be ascribed either to variation of the parameter of interest or to changes in the probe concentration. To tackle this issue, different ratiometric methods can be exploited. Recently, a Gd/^{19}F ratiometric attempt for pH mapping has been discussed. The probe is composed of a poly-β-cyclodextrin (β-CD) carrier to which a pH probe and a fluorine reporter molecule are bound through the appended adamantane moiety, which ensures strong binding to the β-CD cavity (Fig. 1.8). The pH probe is a Gd complex which exhibits pH sensitive relaxivity in the range 6 to 9; the binding with a macromolecule causes the increase of the rotational correlation time which yields a higher relaxivity for the adduct, particularly at acidic pH and in a 1 T magnetic field. The relaxation enhancement produced by the pH probe can be normalised with the fluorine signal that is proportional to the concentration, obtaining the relaxivity values that are now only proportional to pH. The fluorine containing molecules are sufficiently far from the Gd so as to avoid signal broadening. This work presents an interesting proof of principle but presents many drawbacks for *in vivo* applications. The cage of the Gd complex requires modifications to avoid the easy replacement of the two bound water molecules by oxoanions, which would impede the pH response, also the binding affinities of the fluorine containing group and of the complex for the β-CD are not suitable to ensure sufficient stability of the conjugate *in vivo*. In addition, the ratio of the three components has been assumed from their affinity constants, but more precise adduct characterisation would be required[79].

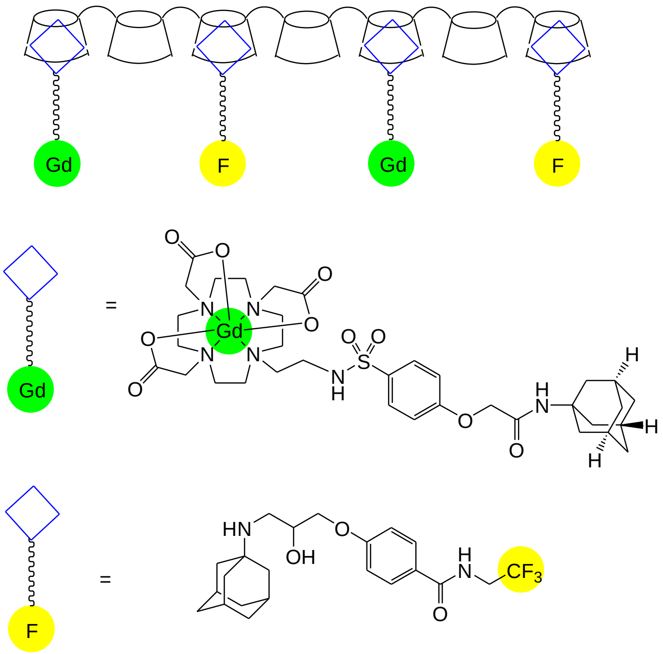

Fig. 1.8 Schematic representation of the poly-β-cyclodextrin pH probe.

A different carrier has been exploited by Langereis *et al.*, who used a temperature sensitive liposome containing within its the inner core a chemical shift agent [Tm(hpdo3a)(H_2O)] (65 mM) for ^{1}H lipoCEST detection and a fluorinated compound NH_4PF_6 (50 mM) as a probe for ^{19}F MRI. At temperature values lower than the melting temperature of the membrane T_m (~311 K), the CEST effect is visualised while the fluorine signal is not observable because of the broadening induced by the concentrated paramagnetic agent. When the T_m is reached, the liposome releases the encapsulated molecules causing a decrease of the CEST signal and a parallel increase of the ^{19}F peak. This work shows promising future applications as a means for localised therapy or imaging in the tissue of interest using focused ultrasound to induce local hyperthermia, but improvements are needed to increase fluorine sensitivity[80].

Perfluorocarbon nanoparticles, stabilised by a lipid-surfactant monolayer surrounding the internal liquid core, have been discussed in previous paragraphs as fluorinated probes with different applications. Recently, the addition of Gd chelates in the external lipid monolayer of the particles has been considered as a mean of increasing the ^{19}F signal intensity. At first, the introduction of Gd complexes on the surface of the probes has been only exploited for common ^{1}H relaxation enhancement for allowing dual detection of the nanoparticle via ^{1}H and ^{19}F NMR[81].

Lately, the relaxation enhancement produced by the paramagnetic ion on the fluorine nuclei of the perfluorocarbon core has been exploited, in order to obtain a decrease of the ^{19}F T_1 to achieve better fluorine signal intensity. The best compromise between increased R_1 and smaller R_2 was reached at 1.5 T (R_1 = 4.2 s^{-1}, R_2 = 16 s^{-1}). The particles have been targeted to fibrin clots by addition of anti-fibrin antibodies to the formulation. One limitation of this approach is that only nuclei in sufficient proximity to the lanthanide cation are affected by the paramagnetic effect, which varies with distance as r^{-6}; therefore the process is limited by the diffusion of the fluorine nuclei within the range of action of the metal. Furthermore, the chelating agent DTPA used in these studies can undergo metal dissociation *in vivo* and should be therefore substituted with a more stable analogue[82].

1.5.2 Our previous work and aims

The main aim of this work was the development of practicable ^{19}F probes for magnetic resonance spectroscopy and imaging, with the potential to report for pH (as described in Chapter 2) and enzyme activity (Chapter 4), by an observable change in chemical shift or signal intensity. Previous work in Durham has established the ability of fluorinated macrocyclic ligands based on tetraazacyclododecane to form stable lanthanide complexes. They present faster relaxation rates and increased chemical shift sensitivity of the fluorinated moiety with respect to the diamagnetic analogues[69]. Cyclen-based complexes of lanthanides ions are well known to be kinetically inert and thermodynamically stable and several analogues are currently commercially available as contrast agents for ^{1}H MRI (Gd). The introduction of a CF_3 group in their structure allows the probe to be visualised by ^{19}F NMR and the careful positioning of this label, within the range of action of the paramagnetic effect of the metal ion, imparts improved relaxation and chemical shift sensitivity (see section 1.4.2).

Therefore, this work focussed on the synthesis and characterisation of novel stable fluorinated lanthanide complexes that can report changes in pH and enzyme activity. Their NMR properties and structural dynamics have been also investigated (Chapter 3). Furthermore, and with the aim of further increasing signal intensity, we set out to prepare and characterise a chitosan-based conjugate which combines faster relaxation rates with a higher local fluorine concentration (Chapter 5).

References

[1] S. Aime, M. Botta, M. Fasano, E. Terreno, *Chem. Soc. Rev.*, **1998**, *27*, 19.

[2] K. M. Brindle, *Br. J. Radiol.*, **2003**, *76*, S111.

[3] P. Caravan, J. J. Ellison, T. J. McMurry, R. B. Lauffer, *Chem. Rev.*, **1999**, *99*, 2293.

[4] C. Corot, P. Robert, J. M. Idee, M. Port, *Adv. Drug Deliver. Rev.*, **2006**, *58*, 1471.

[5] M. Stubbs, L. Rodrigues, F. A. Howe, J. Wang, K. S. Jeong, R. L. Veech, J. R. Griffiths, *Cancer Res.*, **1994**, *54*, 4011.

[6] J. X. Yu, V. D. Kodibagkar, W. N. Cui, R. P. Mason, *Curr. Med. Chem.*, **2005**, *12*, 819.

[7] K. Kitamura, A. A. Omran, S. Takegami, R. Tanaka, T. Kitade, *Anal. Bioanal. Chem.*, **2007**, *387*, 2843.

[8] A. M. Neubauer, S. D. Caruthers, F. D. Hockett, T. Cyrus, J. D. Robertson, J. S. Allen, T. D. Williams, R. W. Fuhrhop, G. M. Lanza, S. A. Wickline, *J. Cardiov. Magn. Reson.*, **2007**, *9*, 565.

[9] J. C. Jackson, J. T. Hammill, R. A. Mehl, *J. Am. Chem. Soc.*, **2007**, *129*, 1160.

[10] M. J. Adam, D. S. Wilbur, *Chem. Soc. Rev.*, **2005**, *34*, 153.

[11] O. Couturier, A. Luxen, J. F. Chatal, J. P. Vuillez, P. Rigo, R. Hustinx, *Eur. J. Nucl. Med. Mol. Imaging*, **2004**, *31*, 1182.

[12] L. C. Clark, F. Gollan, *Science*, **1966**, *152*, 1755.

[13] C. P. Heussel, A. Scholz, M. Schmittner, S. Laukemper-Ostendorf, W. G. Schreiber, S. Ley, M. Quintel, N. Weiler, M. Thelen, H. U. Kauczor, *Invest. Radiol.*, **2003**, *38*, 635.

[14] D. O. Kuethe, A. Caprihan, E. Fukushima, R. A. Waggoner, *Magn. Reson. Med.*, **1998**, *39*, 85.

[15] D. O. Kuethe, V. C. Behr, S. Begay, *Magn. Reson. Med.*, **2002**, *48*, 547.

[16] R. F. Mattrey, M. A. Trambert, J. J. Brown, S. W. Young, J. N. Bruneton, G. E. Wesbey, Z. N. Balsara, *Radiology*, **1994**, *191*, 841.

[17] R. Schwarz, M. Schuurmans, J. Seelig, B. Kunnecke, *Magn. Reson. Med.*, **1999**, *41*, 80.

[18] K. C. Partlow, J. J. Chen, J. A. Brant, A. M. Neubauer, T. E. Meyerrose, M. H. Creer, J. A. Nolta, S. D. Caruthers, G. M. Lanza, S. A. Wickline, *Faseb J.*, **2007**, *21*, 1647.

[19] M. Srinivas, P. A. Morel, L. A. Ernst, D. H. Laidlaw, E. T. Ahrens, *Magn. Reson. Med.*, **2007**, *58*, 725.

[20] B. M. Helfer, A. Balducci, A. D. Nelson, J. M. Janjic, R. R. Gil, P. Kalinski, I. J. M. De Vries, E. T. Ahrens, R. B. Mailliard, *Cytotherapy*, **2010**, *12*, 238.

[21] J. M. Janjic, M. Srinivas, D. K. K. Kadayakkara, E. T. Ahrens, *J. Am. Chem. Soc.*, **2008**, *130*, 2832.

[22] J. Maki, C. Masuda, S. Morikawa, M. Morita, T. Inubushi, Y. Matsusue, H. Taguchi, I. Tooyama, *Biomaterials*, **2007**, *28*, 434.

[23] H. Peng, I. Blakey, B. Dargaville, F. Rasoul, S. Rose, A. K. Whittaker, *Biomacromolecules*, **2009**, *10*, 374.

[24] L. Nurmi, H. Peng, J. Seppälä, D. M. Haddleton, I. Blakey, A. K. Whittaker, *Polym. Chem.*, **2010**.

[25] W. J. Du, A. M. Nystrom, L. Zhang, K. T. Powell, Y. L. Li, C. Cheng, S. A. Wickline, K. L. Wooley, *Biomacromolecules*, **2008**, *9*, 2826.

[26] K. J. Thurecht, I. Blakey, H. Peng, O. Squires, S. Hsu, C. Alexander, A. K. Whittaker, *J. Am. Chem. Soc.*, **2010**, *132*, 5336.

[27] Z. X. Jiang, X. Liu, E. K. Jeong, Y. B. Yu, *Angew. Chem.-Int. Edit.*, **2009**, *48*, 4755.

[28] V. D. Mehta, P. V. Kulkarni, R. P. Mason, E. E. Babcock, A. Constantinescu, P. P. Antich, *Bioorg. Med. Chem. Lett.*, **1992**, *2*, 527.

[29] H. R. Kalbitzer, G. Rohr, E. Nowak, R. S. Goody, W. Kuhn, H. Zimmermann, *NMR Biomed.*, **1992**, *5*, 347.

[30] M. Higuchi, N. Iwata, Y. Matsuba, K. Sato, K. Sasamoto, T. C. Saido, *Nat. Neurosci.*, **2005**, *8*, 527.

[31] D. P. Flaherty, S. M. Walsh, T. Kiyota, Y. Dong, T. Ikezu, J. L. Vennerstrom, *J. Med. Chem.*, **2007**, *50*, 4986.

[32] L. D. Stegman, A. Rehemtulla, B. Beattie, E. Kievit, T. S. Lawrence, R. G. Blasberg, J. G. Tjuvajev, B. D. Ross, *Proc. Natl. Acad. Sci. U. S. A.*, **1999**, *96*, 9821.

[33] W. N. Cui, P. Otten, Y. M. Li, K. S. Koeneman, J. X. Yu, R. P. Mason, *Magn. Reson. Med.*, **2004**, *51*, 616.

[34] J. X. Yu, P. Otten, Z. Y. Ma, W. N. Cui, L. Liu, R. P. Mason, *Bioconjugate Chem.*, **2004**, *15*, 1334.

[35] J. X. Yu, L. Liu, V. D. Kodibagkar, W. N. Cui, R. P. Mason, *Bioorg. Med. Chem.*, **2006**, *14*, 326.

[36] V. D. Kodibagkar, J. X. Yu, L. Liu, H. P. Hetherington, R. P. Mason, *Magn. Reson. Imaging*, **2006**, *24*, 959.

[37] L. Liu, V. D. Kodibagkar, J. X. Yu, R. P. Mason, *Faseb J.*, **2007**, *21*, 2014.

[38] C. Deutsch, J. S. Taylor, D. F. Wilson, *Proc. Natl. Acad. Sci. U. S. A.-Biol.*, **1982**, *79*, 7944.

[39] V. D. Mehta, P. V. Kulkarni, R. P. Mason, A. Constantinescu, S. Aravind, N. Goomer, P. P. Antich, *FEBS Lett.*, **1994**, *349*, 234.

[40] S. Hunjan, R. P. Mason, V. D. Mehta, P. V. Kulkarni, S. Aravind, V. Arora, P. P. Antich, *Magn. Reson. Med.*, **1998**, *39*, 551.

[41] S. He, R. P. Mason, S. Hunjan, V. D. Mehta, V. Arora, R. Katipally, P. V. Kulkarni, P. P. Antich, *Bioorg. Med. Chem.*, **1998**, *6*, 1631.

[42] V. D. Mehta, A. Sivasubramanian, P. V. Kulkarni, R. P. Mason, P. P. Antich, *Bioconjugate Chem.*, **1996**, *7*, 536.

[43] C. J. Deutsch, J. S. Taylor, *Biophys. J.*, **1989**, *55*, 799.

[44] C. K. Rhee, L. A. Levy, R. E. London, *Bioconjugate Chem.*, **1995**, *6*, 77.

[45] M. Oishi, S. Sumitani, Y. Nagasaki, *Bioconjugate Chem.*, **2007**, *18*, 1379.

[46] M. Oishi, S. Sumitani, T. K. Bronich, A. V. Kabanov, M. D. Boska, Y. Nagasaki, *Chem. Lett.*, **2009**, *38*, 128.

[47] G. A. Smith, R. T. Hesketh, J. C. Metcalfe, J. Feeney, P. G. Morris, *Proc. Natl. Acad. Sci. U. S. A.-Bio.*, **1983**, *80*, 7178.

[48] H. L. Kirschenlohr, J. C. Metcalfe, P. G. Morris, G. C. Rodrigo, G. A. Smith, *Proc. Natl. Acad. Sci. U. S. A.*, **1988**, *85*, 9017.

[49] E. Murphy, C. Steenbergen, L. A. Levy, B. Raju, R. E. London, *J. Biol. Chem.*, **1989**, *264*, 5622.

[50] H. Plenio, R. Diodone, *J. Am. Chem. Soc.*, **1996**, *118*, 356.

[51] R. P. Mason, W. Rodbumrung, P. P. Antich, *NMR Biomed.*, **1996**, *9*, 125.

[52] B. M. Seddon, R. J. Maxwell, D. J. Honess, R. Grimshaw, F. Raynaud, G. M. Tozer, P. Workman, *Clin. Cancer Res.*, **2002**, *8*, 2323.

[53] K. Tanabe, H. Harada, M. Narazaki, K. Tanaka, K. Inafuku, H. Komatsu, T. Ito, H. Yamada, Y. Chujo, T. Matsuda, M. Hiraoka, S. Nishimoto, *J. Am. Chem. Soc.*, **2009**, *131*, 15982.

[54] S. L. Cobb, C. D. Murphy, *J. Fluor. Chem.*, **2009**, *130*, 132.

[55] Y. Takaoka, T. Sakamoto, S. Tsukiji, M. Narazaki, T. Matsuda, H. Tochio, M. Shirakawa, I. Hamachi, *Nat. Chem.*, **2009**, *1*, 557.

[56] G. L. Mendz, T. N. Lim, S. L. Hazell, *Arch. Biochem. Biophys.*, **1993**, *305*, 252.

[57] K. Tanaka, N. Kitamura, K. Naka, Y. Chujo, *Chem. Commun.*, **2008**, 6176.

[58] G. Brix, M. E. Bellemann, U. Haberkorn, L. Gerlach, W. J. Lorenz, *Nucl. Med. Biol.*, **1996**, *23*, 897.

[59] T. Nakada, I. L. Kwee, C. B. Conboy, *J. Neurochem.*, **1986**, *46*, 198.

[60] P. N. Venkatasubramanian, Y. J. Shen, A. M. Wyrwicz, *Biochim. Biophys. Acta-Gen. Subj.*, **1995**, *1245*, 262.

[61] W. L. Strauss, M. E. Layton, S. R. Dager, *Am. J. Psychiat.*, **1998**, *155*, 380.

[62] P. Jynge, T. Skjetne, I. Gribbestad, C. H. Kleinbloesem, H. F. W. Hoogkamer, O. Antonsen, O. E. Bakoy, K. M. Furuheim, O. G. Nilsen, *Clin. Pharm. Ther.*, **1990**, *48*, 481.

[63] A. Sigel, H. Sigel, *The Lanthanides and Their Interrelations with Biosystems Vol. 40*, Chapter 14, Marcel Dekker, University of Basel, Switzerland, **2003**.

[64] E. Bovens, PhD thesis, Delft University of Technology **2001**.

[65] J. A. G. Williams, PhD thesis, University of Durham (Durham), **1995**.

[66] C. S. Zuo, K. R. Metz, Y. Sun, A. D. Sherry, *J. Magn. Reson.*, **1998**, *133*, 53.

[67] S. Aime, M. Botta, D. Parker, J. A. G. Williams, *J. Chem. Soc.-Dalton Trans.*, **1995**, 2259.

[68] Y. G. Gakh, A. A. Gakh, A. M. Gronenborn, *Magn. Reson. Chem.*, **2000**, *38*, 551.

[69] P. K. Senanayake, A. M. Kenwright, D. Parker, S. K. van der Hoorn, *Chem. Commun.*, **2007**, 2923.

[70] L. Yatsunyk, F. A. Walker, *Inorg. Chim. Acta*, **2002**, *337*, 266.

[71] K. Tanaka, N. Kitamura, Y. Takahashi, Y. Chujo, *Bioorg. Med. Chem.*, **2009**, *17*, 3818.

[72] W. D. Kim, G. E. Kiefer, J. Huskens, A. D. Sherry, *Inorg. Chem.*, **1997**, *36*, 4128.

[73] S. Aime, A. Barge, M. Botta, D. Parker, A. S. DeSousa, *J. Am. Chem. Soc.*, **1997**, *119*, 4767.

[74] S. Aime, A. Barge, J. I. Bruce, M. Botta, J. A. K. Howard, J. M. Moloney, D. Parker, A. S. de Sousa, M. Woods, *J. Am. Chem. Soc.*, **1999**, *121*, 5762.

[75] H. Lee, R. R. Price, G. E. Holburn, C. L. Partain, M. D. Adams, W. P. Cacheris, *JMRI-J. Magn. Reson. Imaging*, **1994**, *4*, 609.

[76] E. Terreno, M. Botta, P. Boniforte, C. Bracco, L. Milone, B. Mondino, F. Uggeri, S. Aime, *Chem. Eur. J.*, **2005**, *11*, 5531.

[77] E. Terreno, M. Botta, W. Dastru, S. Aime, *Contrast Media Mol. Imaging*, **2006**, *1*, 101.

[78] S. Mizukami, R. Takikawa, F. Sugihara, Y. Hori, H. Tochio, M. Walchli, M. Shirakawa, K. Kikuchi, *J. Am. Chem. Soc.*, **2008**, *130*, 794.

[79] E. Gianolio, R. Napolitano, F. Fedeli, F. Arena, S. Aime, *Chem. Commun.*, **2009**, 6044.

[80] S. Langereis, J. Keupp, J. L. J. van Velthoven, I. H. C. de Roos, D. Burdinski, J. A. Pikkemaat, H. Grull, *J. Am. Chem. Soc.*, **2009**, *131*, 1380.

[81] A. M. Morawski, P. M. Winter, X. Yu, R. W. Fuhrhop, M. J. Scott, F. Hockett, J. D. Robertson, P. J. Gaffney, G. M. Lanza, S. A. Wickline, *Magn. Reson. Med.*, **2004**, *52*, 1255.

[82] A. M. Neubauer, J. Myerson, S. D. Caruthers, F. D. Hockett, P. M. Winter, J. J. Chen, P. J. Gaffney, J. D. Robertson, G. M. Lanza, S. A. Wickline, *Magn. Reson. Med.*, **2008**, *60*, 1066.

Chapter 2

Fluorinated responsive probes: pH studies

2.1 Introduction

As previously discussed (Chapter 1), the careful positioning of a fluorine nucleus within 7Å of the paramagnetic ion in a stable lanthanide complex, causes the fluorine longitudinal and transversal relaxation rates to be strongly enhanced[1,2]. This allows faster MR signal acquisition, reducing the sample concentration and acquisition time required to obtain the desired signal intensity. The lanthanide ion also enhances the chemical shift sensitivity of the fluorine nucleus to changes in the chemical environment. This characteristic can be exploited to develop responsive probes able to report various parameters of interest such as pH, enzyme activity or gene expression. A variation of the parameter under study will result in an observable change of ^{19}F chemical shift or signal intensity of the probe.

With this in mind, we have synthesised a series of lanthanide complexes with the purpose of developing pH reporters to be employed in ^{19}F magnetic resonance spectroscopy and imaging.

2.2 DO3A-based complexes

The lanthanide complexes under study are based on tetra-substituted 1,4,7,10-tetraazacyclododecane. In particular, DO3A (1,4,7,10-cyclododecane-1,4,7-triacetate) mono-amide derivatives (Fig. 2.1) were chosen because of the good kinetic and thermodynamic stability of their lanthanide complexes with respect to metal dissociation, making them safe systems for *in vivo* application. The presence of an *ortho*-trifluoromethyl group on the aromatic ring of the amide arm allows the complex to be visualised by ^{19}F NMR, and its proximity to the paramagnetic ion ensures fast relaxation. The amide functionality provides the pH sensitive moiety. Normally, its deprotonation equilibrium gives rise to a pK_a value higher than 9.5, not suitable for physiological measurements. However, this value can be modulated by introducing appropriate substituents on the aromatic ring, able to influence the amide proton acidity. Hence, a series of complexes bearing different functional groups in the *para* or *ortho* position of the aromatic ring has been synthesised and the pH dependence of their NMR properties assessed.

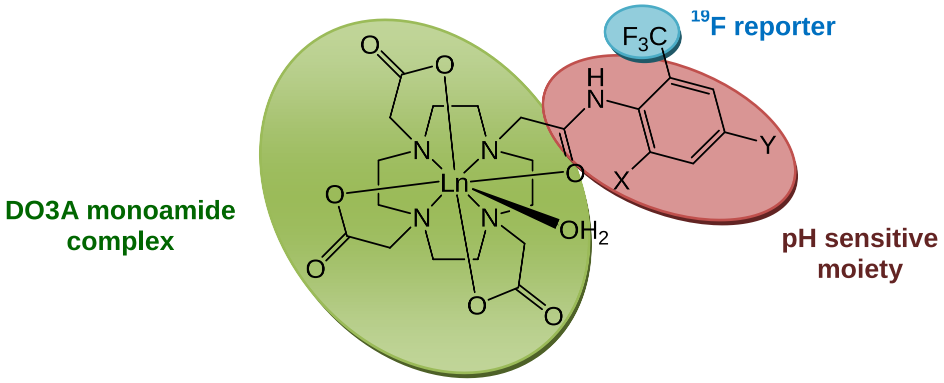

Fig. 2.1 Schematic representation of the pH probe general structure.

A direct comparison can be made with *ortho* and *para*-substituted phenols - a similar system that has been extensively studied. pK_a values in the presence of different substituents have been reported[3,4] and form the reference for our studies.

The lanthanide induced shift effect increases the sensitivity of the ^{19}F chemical shift to changes in the chemical environment; therefore, the deprotonation process should lead to an observable variation due to the presence of two different forms, protonated and non-protonated.

The ideal NMR probe for pH analysis *in vivo* should possess the following features:

- significant observable change,
- pK_a value centred at 7,
- observable change in the range 6 to 8,
- narrow linewidths.

This chapter outlines the studies that we performed towards the achievement of these goals.

2.2.1 Synthesis

The general synthetic scheme for the preparation of DO3A ligands involved the mono-alkylation of the tri-protected cyclen with the appropriate fluorinated α-chloroamide, as illustrated in Scheme 2.1. The tris(*tert*-butylacetate) compound **1** was prepared under mild basic conditions ($NaHCO_3$) at room temperature. Stronger bases and heating were found to give a majority of the tetra-substituted analogue. The desired product was isolated by recrystallisation from hot toluene, with better yields compared to purification using column chromatography over silica gel (MeOH in DCM), than had been previously reported.

The α-chloroamide arm was prepared by acylation with chloroacetyl chloride of the *para*- or *ortho*-substituted trifluoromethylaniline, using only slightly different conditions according to the nature of the substituents.

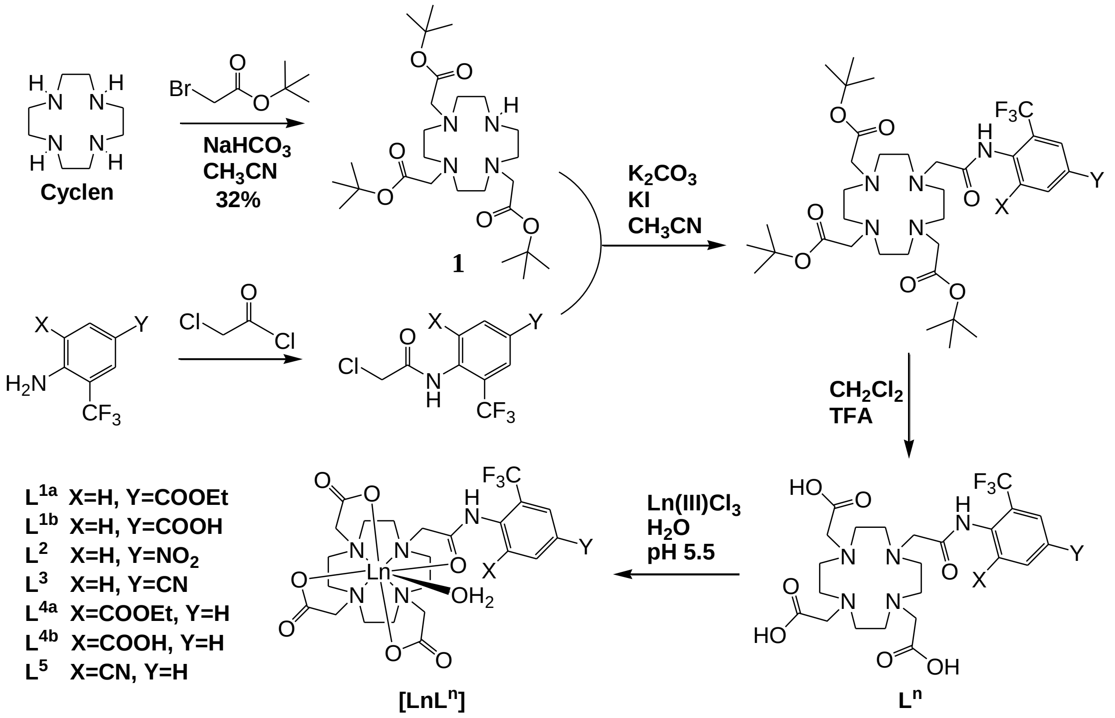

Scheme 2.1 General synthetic procedure for mono-amide DO3A derivatives.

A preliminary step (Scheme 2.2) was required for the formation of the two ethyl ester derivatives from the commercially available acid or nitrile precursors. In each case, esterification proceeded using sulfuric acid in ethanol. The ethyl derivative was preferred over the methyl ester because it showed greater stability and ease of preparation.

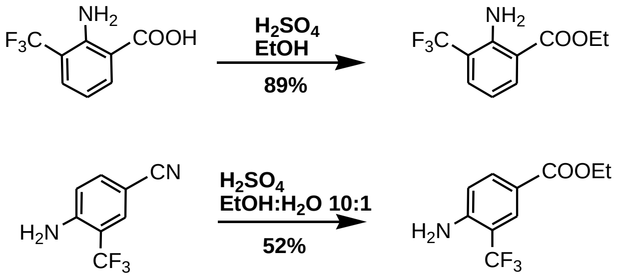

Scheme 2.2 Esterification step from the commercially available precursors.

The purification steps involved careful neutralisation of the sulfuric acid by addition of a stoichiometric amount of K_2CO_3 in water. The products were then acylated with chloroacetyl chloride in dichloromethane with triethylamine to obtain the desired α-haloamide. The same reaction was performed for the *para*-nitro and cyano derivatives in tetrahydrofuran, using DMAP as an acyl transfer catalyst. Harsher conditions were required in the case of the *ortho*-cyano arm; NaH in DMF was used to increase the nucleophilicity of the amino group.

The alkylation of the tri-ester **1** with the given α-chloroamide was performed under basic conditions using KI as a catalyst. Treatment with trifluoroacetic acid in dichloromethane resulted in removal of the *tert*-butyl protecting groups, to give the ligand as its trifluoroacetate salt. Anion exchange chromatography afforded the hydrochloride salt, which ensured the water solubility of the compound. Reaction of the ligand in water at pH 5.5 with a slight excess of the appropriate lanthanide chloride salt yielded the final complex. The unreacted excess metal ion was removed by precipitation as the hydroxyl salt at pH 10, while the NaCl contaminating the sample after pH adjustment was eliminated by extraction of the complex into 20% MeOH in dichloromethane or by dialysis to yield the clean complex. Ligand and complex homogeneity was confirmed by reverse phase HPLC.

During treatment with TFA of the *ortho*-cyano ligand $\mathbf{L^5}$, the formation of small amounts of a primary amide by-product was observed, as confirmed by mass spectrometry analysis. In order to avoid formation of this side product the same reaction was attempted under different reaction conditions. Lower temperature (0°C), alternative acids such as formic acid and varying reaction times were attempted, but none were particularly successful. The best compromise between complete ligand deprotection and minimum amide formation was found using the standard conditions, *i.e.* TFA in dichloromethane at room temperature overnight. The partial hydrolysis of the nitrile group is probably assisted by the presence of the amide functionality in the *ortho* position, as suggested by the lack of any side-product formation for the *para*-cyano analogue, where this phenomenon cannot occur.

The acid ligands, $\mathbf{L^{1b}}$ and $\mathbf{L^{4b}}$, were prepared by hydrolysis of the respective ethyl ester analogues, as illustrated in Scheme 2.3.

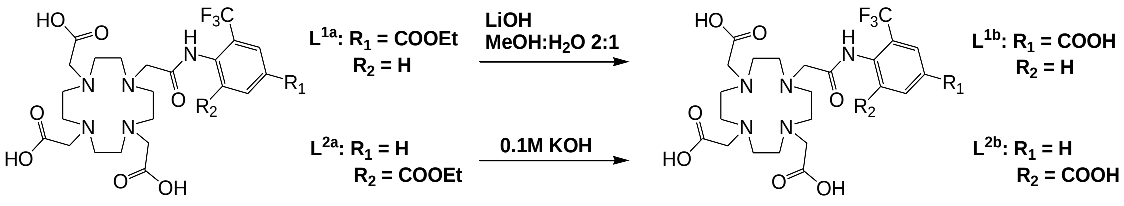

Scheme 2.3 Synthesis of $\mathbf{L^{1b}}$ and $\mathbf{L^{4b}}$ by hydrolysis of their ethyl ester precursors.

The *para* carboxylic acid derivative $\mathbf{L^{1b}}$, was obtained using 0.1 M KOH over 48 hours at 50°C. The *ortho* acid derivative $\mathbf{L^{4b}}$, required the use of LiOH in a water/methanol mixture at room temperature for two days. The product was obtained after extraction of the desired ligand with ethyl acetate from the water layer at pH 4. Formation of the Ln(III) complex was undertaken at pH 6 using the appropriate $LnCl_3$ salt. Partial hydrolysis occurred during the complexation reaction of the ester ligand $\mathbf{L^{1a}}$ resulting in a mixture of ester and acid form. Isolation of the ester was achieved performing the reaction at room temperature or leaving the mixture in ethanol with 1% of acetyl chloride for one week, while the acid form could be obtained by hydrolysis at room temperature at pH 10 (KOH) over one week. The *ortho* ester analogue proved to be more stable during the complexation reaction; therefore, no hydrolysis occurred. The acid $\mathbf{[LnL^{4b}]}$ was obtained by leaving $\mathbf{[LnL^{4a}]}$ in a solution of KOH at pH 10 for one week at room temperature.

The glucosamide complex $\mathbf{[HoL^{13}]}$ was prepared starting from the *para* acid derivative $\mathbf{[HoL^{1b}]}$ as illustrated in Scheme 2.4. The acid group was activated with *N*-methylmorpholine and TBTU in DMF and then reacted with the free glucosamine, obtained from the commercially available hydrochloride salt, after treatment with anion exchange resin.

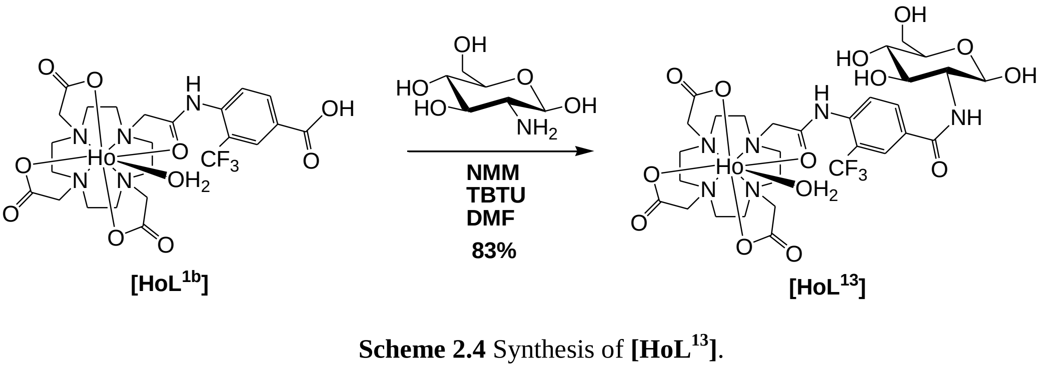

Scheme 2.4 Synthesis of $\mathbf{[HoL^{13}]}$.

2.2.2 pH Dependent spectroscopic behaviour

The first complexes to be studied as pH reporters were the dysprosium complexes of $\mathbf{L^{1a}}$ and $\mathbf{L^{1b}}$, which contained respectively an ethyl ester and a carboxylic acid group in the *para* position of the aromatic ring. Amide deprotonation occurred under basic conditions and was reflected in each case in a change in the chemical shift of the CF_3 group. Between pH 6 and 10.5, this varied from -64.3 ppm to -17.7 ppm for $\mathbf{[DyL^{1a}]}$, and from -65.0 ppm to -24.8 ppm in the case of $\mathbf{[DyL^{1b}]}$. Therefore, the deprotonation process produced a large chemical shift variation, reaching a maximum difference between the protonated and deprotonated forms of 46.6 ppm for the ester complex and 40.2 ppm for the acid. The acid-base equilibrium is fast on the NMR time scale, hence only one signal is observed in the fluorine spectrum. The chemical shift corresponds to the weighted average of the individual chemical shifts of the acid and its conjugate base, as illustrated in Scheme 2.5.

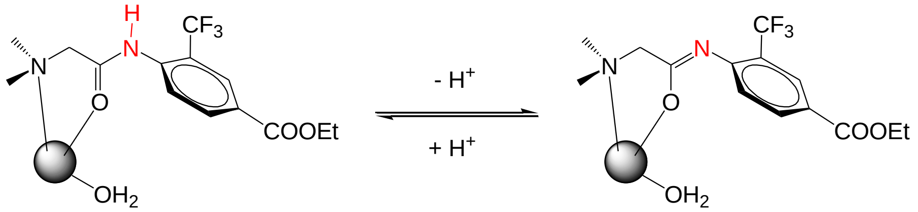

Scheme 2.5 Acid-base equilibrium between the protonated and deprotonated form in $\mathbf{[LnL^{1a}]}$.

The pH dependence of the ^{19}F chemical shift of $\mathbf{[DyL^{1a}]}$ and $\mathbf{[DyL^{1b}]}$ can be clearly observed in the pH titration curve (Fig. 2.2), performed using a dilute (~1mM) solution of the complex in 0.1 M NaCl at 295 K and 188 MHz. The aqueous solution of NaCl was employed in order to maintain a constant ionic strength. A coaxial insert containing D_2O was used to lock the instrument.

The resulting plots show the continuous chemical shift change as a function of pH, following a typical acid-base equilibrium profile. The least-squares fitting of the experimental data resulted in a pK_a of 8.80 ± 0.03 for $\mathbf{[DyL^{1a}]}$ and 9.61 ± 0.04 for $\mathbf{[DyL^{1b}]}$. These values reflect the different electron withdrawing nature of the two substituents.

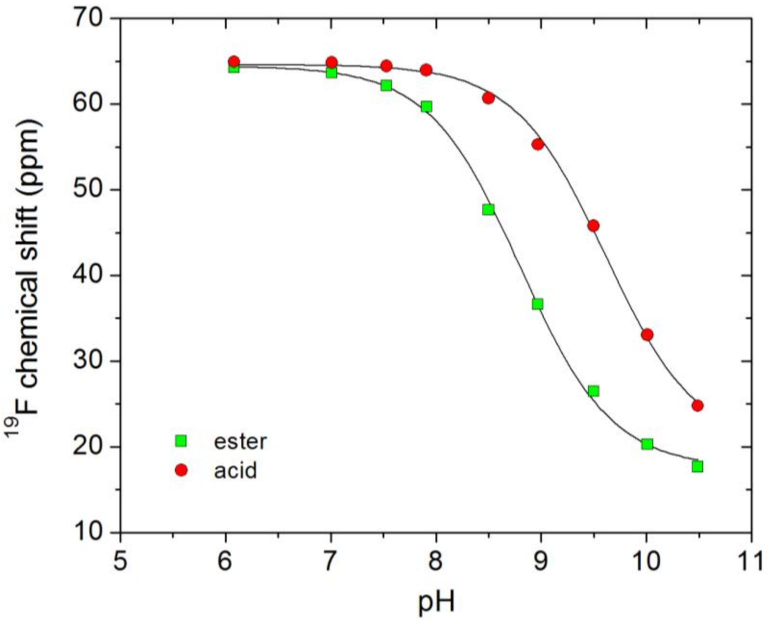

Fig. 2.2 pH titration curve of a solution (~1mM) of the ester **[DyL^{1a}]** and the acid **[DyL^{1b}]** (0.1 M NaCl in H_2O, 295 K, 188 MHz, D_2O lock) showing the fit (line) to the data. **[DyL^{1a}]**: pK_a = 8.80 ± 0.03, $\Delta\delta_F$ = 46.6 ppm; **[DyL^{1a}]**: pK_a = 9.61 ± 0.04, $\Delta\delta_F$ = 40.2 ppm.

The electron withdrawing ability of different substituents can be quantified with the Hammett constant, σ, based on the ionisation of substituted benzoic acids[5]. The ethyl ester is a strong electron withdrawing group, consistent with a value of σ_{para} = 0.45. The acid group instead for pH values >4 is in the deprotonated form and possesses a value of σ_{para} = 0.00. Hence, the different protonation constant of **L^{1a}** and **L^{1b}** is related to the stability of the deprotonated amide form in each case: the ester group allows a more effective delocalisation of negative charge in the conjugate base compared to the negatively charged carboxylate group. This is confirmed by the lack of ^{19}F chemical shift variation observed in the case of *para* electron-donating groups such as NH_2 (σ_{para} = -0.66) or OH (σ_{para} = -0.37) over the pH range 3.5 to 9, consistent with a pK_a >9.5[2].

The variation of linewidth of the ^{19}F resonances for **[DyL^{1a}]** and **[DyL^{1b}]** with pH was also recorded (Fig. 2.3). The linewidth (in Hz) is defined as the width of the peak at half-height, $v_{1/2}$ or $\omega_{1/2}$. It can be directly related to the transverse relaxation rate, R_2 (equation 11).

$$R_2 = \pi \times \omega_{1/2} \qquad (11)$$

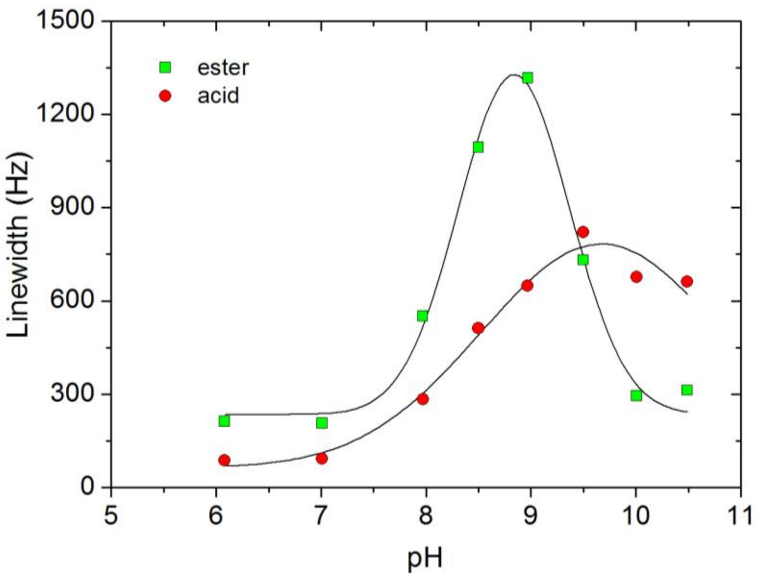

Fig. 2.3 Linewidth profiles for **[DyL^{1a}]** and **[DyL^{1b}]** (295 K, 188 MHz).

The profile showed a maximum at the pH corresponding to the pK$_a$, which decreased at more acidic or basic values and was similar for each complex. This exchange broadening is probably caused by the chemical exchange between the protonated amide and its conjugate base. For the dysprosium complexes, the maximum broadening reached 1300 Hz for the ethyl ester and 800 Hz for the acid. However, by using different lanthanide ions it was possible to obtain much smaller linewidth values. In the case of the holmium complexes, for example, the maximum linewidths were 197 Hz and 131 Hz for the ester and the acid respectively, considerably less than the values for the Dy complexes.

A pH titration, using the same conditions as for the Dy complexes, was performed for **[HoL^{1a}]** and **[HoL^{1b}]** (Fig. 2.4). The same pH-dependent behaviour was observed, showing that the homologous complexes possessed similar pK$_a$ values. The maximum difference between protonated and non-protonated forms, in this case, was about 15 ppm for the ester and 11 ppm for the acid. These values were lower than for the dysprosium complexes ($\Delta\delta_F$ = 46.6 ppm (ester) and 40.2 ppm (acid)), but this is still a large variation over two units of pH. Therefore, holmium complexes seemed to be better candidates for comparing the different pH probes. They show good shift variation with pH and exhibit narrower linewidths.

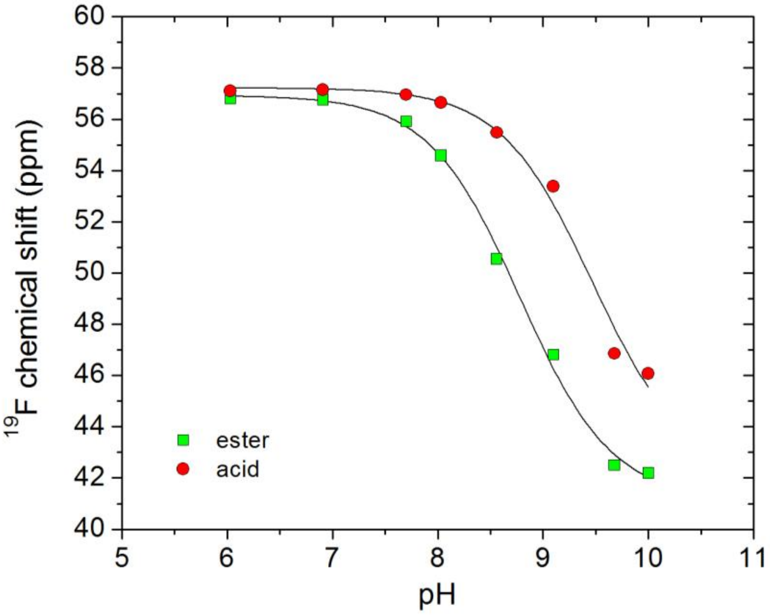

Fig. 2.4 pH titration curve of **[HoL^{1a}]** and **[HoL^{1b}]** (0.1 M NaCl in H_2O, 295 K, 188 MHz, D_2O lock) showing the fit (line) to the data. **[HoL^{1a}]**: $pK_a = 8.78 \pm 0.06$, $\Delta\delta_F = 14.6$ ppm; **[HoL^{1b}]**: $pK_a = 9.46 \pm 0.11$, $\Delta\delta_F = 11.0$ ppm.

A titration curve over the same pH range was also undertaken for **[TbL^{1b}]** monitoring the process using luminescence emission. No significant change was observed in spectral form as a function of pH, probably because of the known low sensitivity of the terbium emission to the chemical environment. The complex was also employed to measure the hydration number (q value) in both a basic (pH 11) and acidic regime (pH 5). Lifetime data were consistent with the presence of one water molecule directly coordinated to the metal, as expected for DO3A mono-amide complexes[6]. The q value was obtained by analysis of the radiative rate constants associated with depopulation of the lanthanide excited state. Values were measured in both H_2O and D_2O, allowing computation of q according to equation 12 for the terbium complexes[6],

$$q_{Tb} = 5 \times (k_{H_2O} - k_{D_2O} - 0.06) \qquad (12)$$

where k_{H_2O} and k_{D_2O} are the reciprocals of the luminescence lifetimes of each complex, τ_{H_2O} and τ_{D_2O}, respectively. Lifetimes and calculated q values are reported in Table 2.1.

Table 2.1 Measured lifetimes (± 10%) and calculated hydration numbers (± 20%) for **[TbL^{1b}]**.

pH	τ_{H_2O}	τ_{D_2O}	**q**
11	2.01 ms	3.29 ms	0.67
5	1.95 ms	3.25 ms	0.73

The glucosamide derivative **[HoL^{13}]**, with an amide substituent in the *para* position, exhibited a similar pH-shift variation (Fig. 2.5). The electron withdrawing ability of a secondary amide group is comparable to that of an alkyl ester and is reflected in the similar pK$_a$ values of 8.98 ± 0.02 for **[HoL^{13}]** and 8.78 ± 0.06 for **[HoL^{1a}]**.

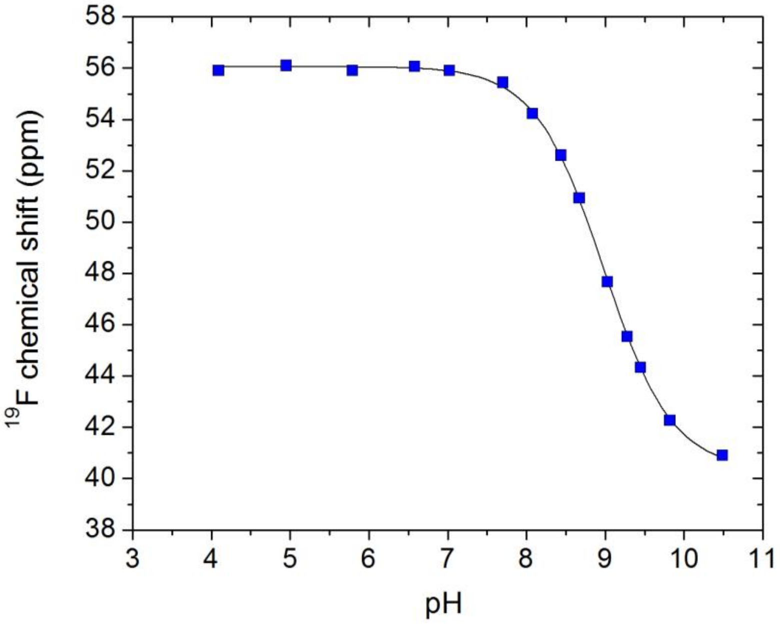

Fig. 2.5 pH titration curve of **[HoL^{13}]** (0.1 M NaCl in H_2O, 295 K, 188 MHz, D_2O lock) showing the fit (line) to the data. pK$_a$ = 8.98 ± 0.02, $\Delta\delta_F$ = 15.0 ppm.

The chemical shift difference for the acid/conjugate base was 15 ppm. The linewidth values were slightly less than those observed for **[HoL^{1a}]** and followed the same trend (Fig. 2.6), reaching a maximum at the pK$_a$.

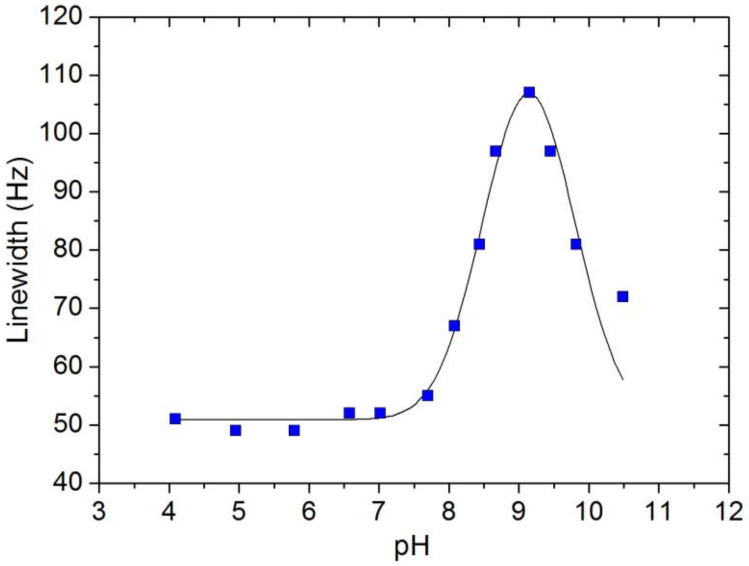

Fig. 2.6 Linewidth profile for **[HoL^{13}]** (295 K, 188 MHz).

Each of the Ln(III) complexes of **L^{1a}**, **L^{1b}** and **L^{13}** display a large ^{19}F chemical shift variation with pH, with differing linewidths according to the metal used. However, their pK$_a$ values were too high to allow pH measurements under physiological conditions. More electron withdrawing substituents were therefore chosen to further increase the acidity of the amide hydrogen.

The nitro functionality is one of the most electron-withdrawing groups (σ_{para} = 0.78) and has been introduced in the *para* position on the aromatic ring to give **L^{2}**. The pH dependence of the ^{19}F chemical shift of **[HoL^{2}]** is shown (Fig. 2.7). The titration was performed as before at 295 K, 188 MHz, in 0.1 M NaCl with a D_2O coaxial insert to lock the instrument. The pH dependence showed the acid-base equilibrium profile was shifted towards more acidic pH values compared to the previous examples. The fitting of the experimental data resulted in a pK$_a$ of 7.77 ± 0.02. This lower value reflects the influence of the increased electron withdrawing effect of the nitro group. In the case of *para* nitrophenol the pK$_a$ is 7.15. The complex maintained a large chemical shift variation of 18 ppm between the acid and its conjugate base.

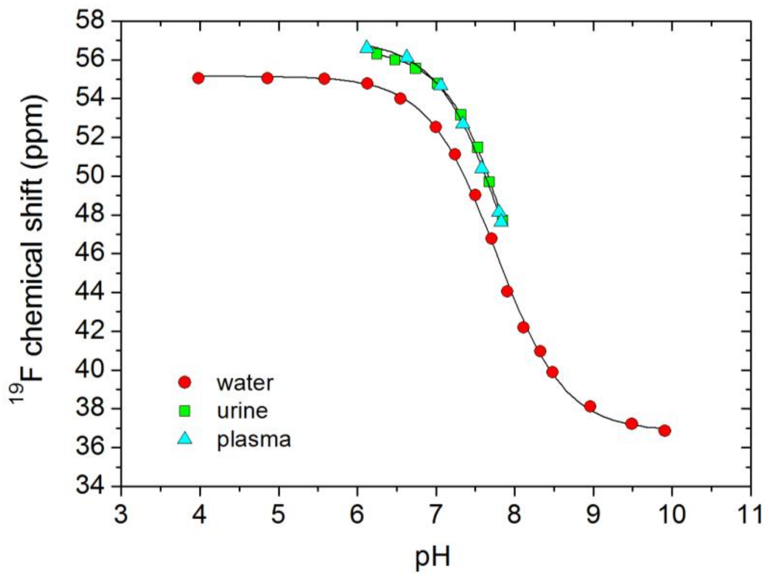

Fig. 2.7 pH titration curve of **[HoL^2]** in 0.1 M NaCl in H_2O, mouse urine and mouse plasma (295 K, 188 MHz, D_2O lock) showing the fit (line) to the data. pK_a = 7.77 ± 0.02, $\Delta\delta_F$ = 18.2 ppm.

To assess the effect of biological fluids on the pH response of the probe, the same experiment was undertaken in mouse urine and mouse plasma, over the physiologically relevant pH range 6-8 (Fig. 2.7). Mouse urine allowed the presence of various anionic species to be evaluated, while mouse plasma allowed the study of possible interaction of the complex with proteins. In each case, the complex maintained its behaviour without evidence of any interaction with proteins or anions, consistent with the suitability of the complex as a responsive pH probe for use *in vivo*. Indeed, the pH of a sample undergoing analysis can be directly obtained from the observed chemical shift of the probe by referring to the calibration curve.

Compared to the ester and acid analogues, **[HoL^2]** showed a different profile for the linewidth variation as a function of pH (Fig. 2.8). In the conjugate base an abrupt increase of the linewidth by a factor of 8 was observed, compared to the protonated amide. To explain this behaviour, a variable temperature experiment was carried out between 278 and 328 K, at both pH 5 and pH 8.5 at 470 MHz (urine sample with D_2O insert).

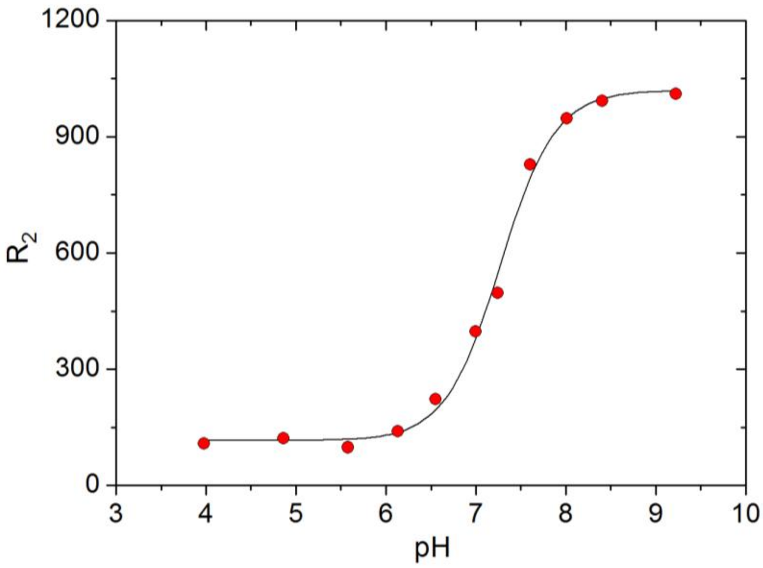

Fig. 2.8 R_2 variation as a function of pH for **[HoL^2]** (295 K, 188 MHz).

A linear variation of the ^{19}F chemical shift with the inverse of the second power of the absolute temperature in Kelvin was observed (as expected from equation 3[7]) (Fig. 2.9). At higher temperatures, the linewidth of the deprotonated form decreased noticeably, with a thermal contribution to the narrowing of the resonances which was greater than what it would be expected according to equation 10[7], while it was normal for the protonated form. Values for the linewidth of the protonated form were as expected.

$$\Delta_p = \frac{C_J \mu_B{}^2}{60k^2T^2}\left[\frac{\langle r^2\rangle A(3\cos^2\theta - 1)}{r^3} + \frac{\langle r^2\rangle A'\sin^2\theta\cos 2\varphi}{r^3}\right] \qquad (3)$$

$$R_{2\chi} = \frac{1}{5}\left(\frac{\mu_0}{4\pi}\right)^2 \frac{\gamma_I^2 B_0^2 \mu_{eff}^4}{(3kT)^2 r^6}\left(4\tau_r + \frac{3\tau_r}{1+\omega_I^2\tau_r^2}\right) \qquad (10)$$

This behaviour suggested the presence of a unique conformational exchange process for the deprotonated complex, that was giving rise to additional exchange broadening.

Two possible processes were considered: lanthanide ion re-coordination from oxygen to nitrogen and *cis-trans* isomerization around the C=N double bond. On the basis of DFT calculations performed by Dr. Ilya Kuprov (Oxford University), the first hypothesis can be excluded. To simplify the process yttrium and lanthanum were used as the metal ions in the DFT calculations with very similar results. The Y^{3+} ion has an ionic radius that is within 0.02 Å of Ho^{3+} and the structures of complexes with other lanthanides are likely to be identical.

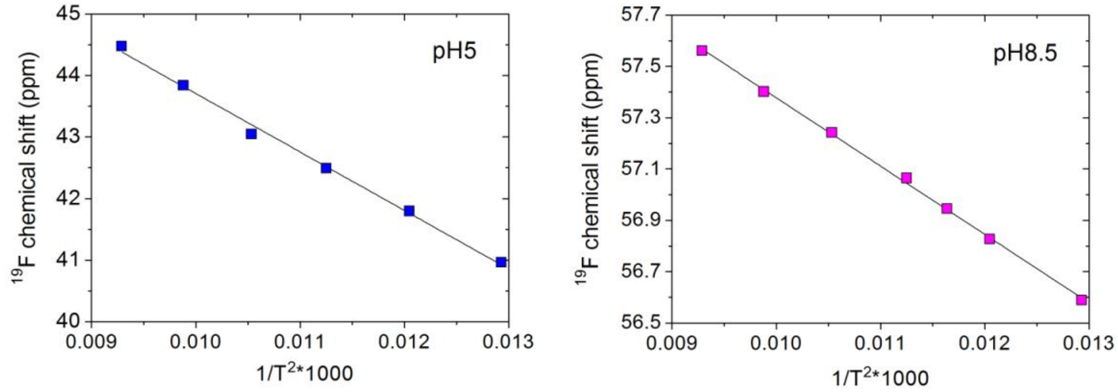

Fig. 2.9 Linear variation of the observed ^{19}F shift of **[HoL^{2}]** as a function of T^{-2} from 278 K to 328 K at pH 5 and 8.5.

The calculations on **[LaL^{2}]**, showed an energy difference of 62 kJ/mol between the two coordination isomers in favour of the oxygen-bound isomer. A smaller energy difference of only 18 kJ/mol was calculated between the *cis* and *trans* isomers, making this second process a more probable explanation (Scheme 2.6).

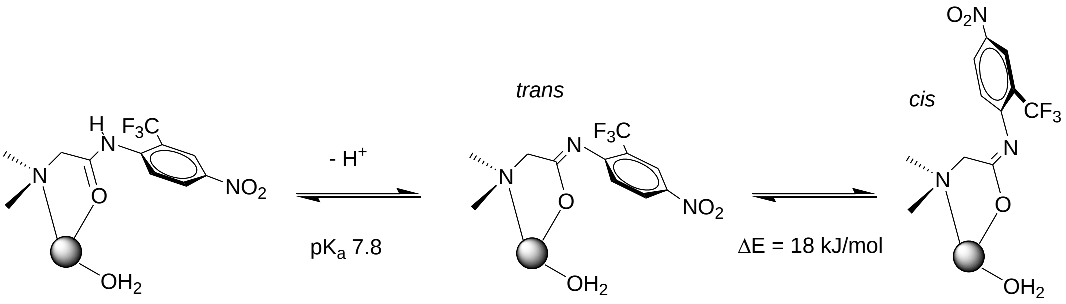

Scheme 2.6 Acid-base equilibrium between the protonated and non-protonated form in **[LaL^{2}]** showing the conformational exchange between *cis/trans* amide forms in the deprotonated species.

The forward and backward calculated activation energies for the *cis-trans* isomerization are 27 and 45 kJ/mol respectively and are consistent with the observed exchange broadening in the ^{19}F NMR spectra. The bulky CF_3 group favours those structures that direct this group away from the amide oxygen, as illustrated in the following calculated structures for the yttrium analogue.

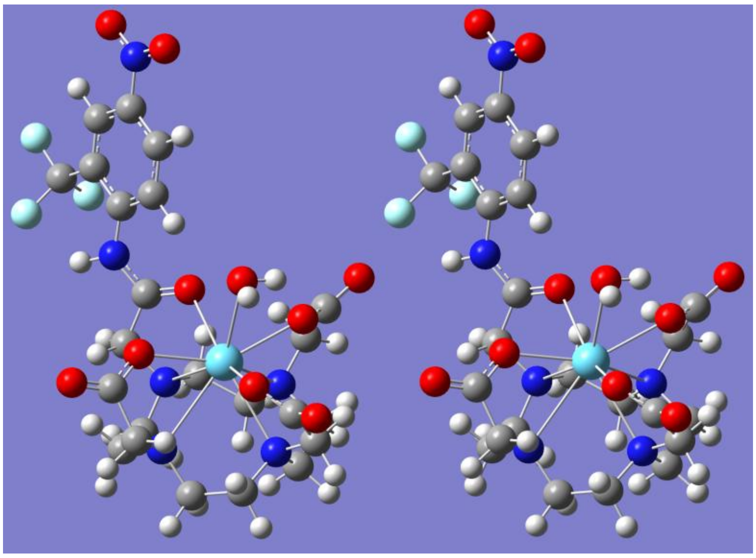

Fig. 2.10 DFT calculated structure of **[YL^{2}H]**.

a)

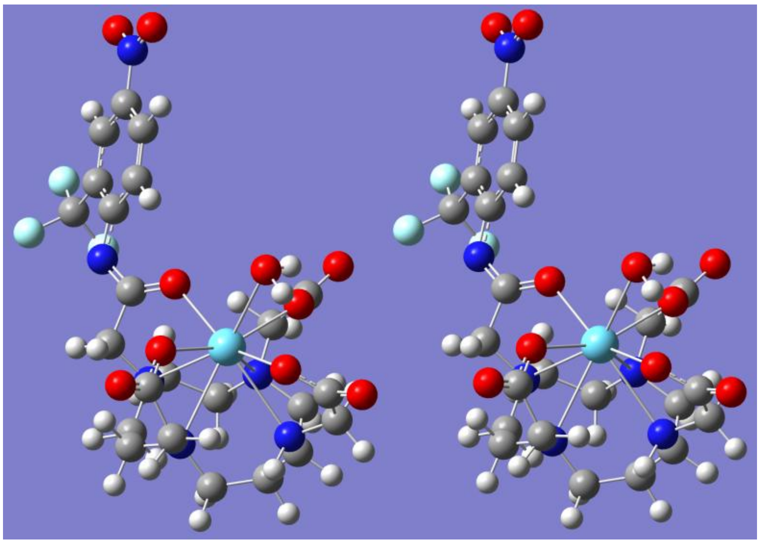

b)

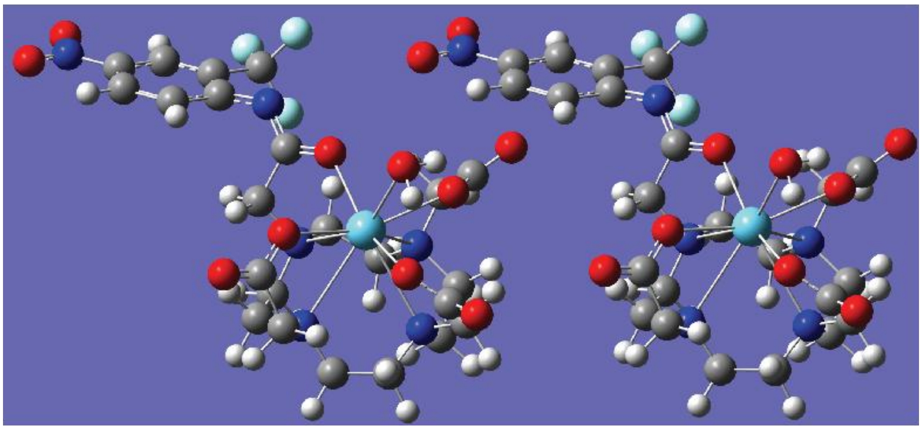

Fig. 2.11 DFT calculated structures of the two isomers of **[YL^2]$^-$**. a) *cis* form. b) *trans* form.

The fluorine chemical shift of **[HoL^2]** was examined over different complex concentrations and in different NMR solvents. The shift was independent of the complex concentration over one order of magnitude (mM), while it varied according to the solvent used: with respect to the chemical shift in D_2O, the fluorine resonance shifts to higher frequency by 2.9 ppm in deuteriated methanol and by 10.7 ppm in DMF-d_7. In this latter case the peak broadened significantly, most likely due to a slow exchange of DMF molecules coordinated to the metal. The chemical shift variation followed the trend in solvent polarity and can most simply be rationalised in terms of the qualitatively effect of changing the axial donor from D_2O to CD_3OD or DMF[8].

A very similar pH profile was observed for the *p*-cyano complex. The pH/δ_F titration curve for **[HoL^3]** is reported below (Fig. 2.12).

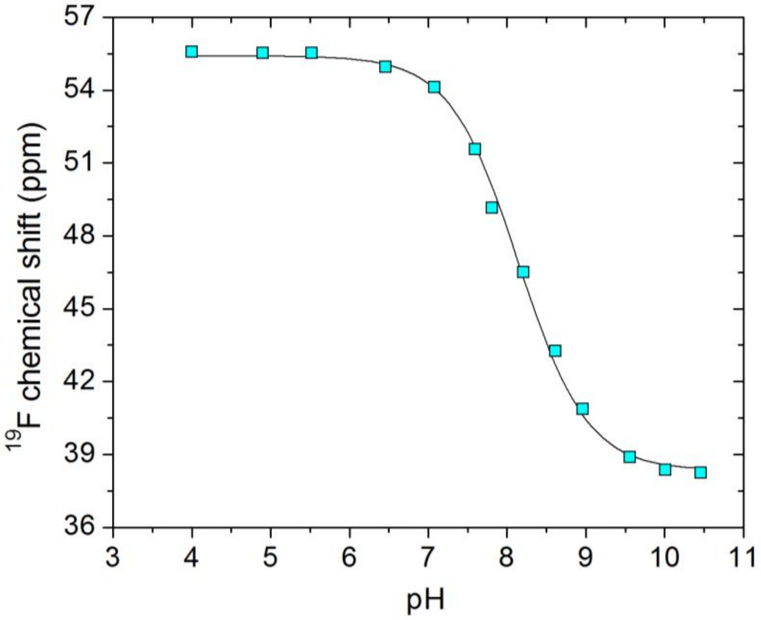

Fig. 2.12 pH titration curve of **[HoL^3]** (0.1 M NaCl in H_2O, 295 K, 188 MHz, D_2O lock) showing the fit (line) to the data. $pK_a = 8.15 \pm 0.03$, $\Delta\delta_F = 17.3$ ppm.

The pH-shift profile shows a variation over two units of pH with a difference of 17.0 ppm between protonated and non-protonated forms. The *para* cyanophenol has a pK_a of 7.95. The *p*-CN group has a significant electron withdrawing ability, with $\sigma_{para} = 0.66$. The fitting of the data by a non-linear least squares iterative analysis resulted in a pK_a of 8.15 ± 0.03. These values are comparable to those obtained for the nitro analogue ($\Delta\delta_F = 18.0$ ppm, $pK_a = 7.77 \pm 0.02$). However, in the latter case the pH dependence of the linewidth was complex. As previously described, the linewidth of the nitro compound increases dramatically at basic pH due to the conformational exchange process present in the deprotonated form. In the case of **[HoL^3]**, the linewidth increased around the pK$_a$ value and decreased further (Fig. 2.13), as expected for a chemical exchange process between the amide and its conjugate base, as noted for the *para* ester, acid and amide analogues.

A comparison of the R$_2$ profiles for the *para* nitro **[HoL^2]** and *para* cyano **[HoL^3]** complexes is reported in Fig. 2.13. The remarkable decrease of linewith is evident in the case of the cyano complex **[HoL^3]**, in particular at basic pH values. This implies that the conformational exchange process occurring in the *p*-NO$_2$ system **[HoL^2]** was not present here. Such a difference in behaviour is surprising, considering the similar electron-withdrawing ability of these two functional groups (σ_{para} = 0.45 nitro, 0.66 cyano). Each substituent can delocalise the negative charge in the deprotonated amide form, as revealed by the similar pK$_a$ values. The line broadening, as well as the lower pK$_a$ for **[HoL^2]**, is probably related to a slightly greater conjugative stabilising effect of the *para*-nitro group. This could enhance the stabilisation of the *cis* stereoisomer, leading to the increased linewidth. The *p*-cyano system **[HoL^3]** therefore, represents an improvement compared to the nitro analogue.

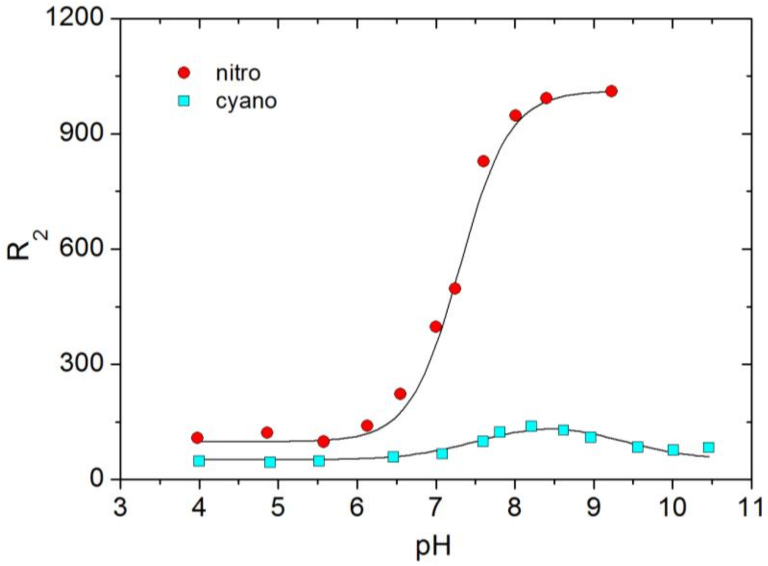

Fig. 2.13 Comparison of R$_2$ variation with pH for the *p*-nitro **[HoL^2]** and the *p*-cyano **[HoL^3]** (295 K, 188 MHz).

The series of *para*-substituted complexes discussed so far allowed the pK_a to be decreased up to a value of 7.77 in the nitro analogue. The introduction of additional CN or NO_2 groups into the structure was not pursued because of the likely reduced solubility of the final complex and the synthetic accessibility of such systems. Based on the analysis of the pK_a values of the *ortho* and *para*-substituted phenols[3,4], subsequent work investigated the effect of the presence of *ortho* substituents in the ligand structure.

The first example was the *ortho* ethyl ester $\mathbf{L^{4a}}$. Its lanthanide complexes appeared in the fluorine spectrum as two resonances of equal intensity (instead of only one as seen for the *para*-analogues) but with very different chemical shifts. The separation between the two signals varied from 20 to 55 ppm according to the metal ion. As will be discussed in Chapter 3, the two resonances probably correspond to two isomers resulting from the rotation of the aromatic ring on the amide arm around the C-N bond. The two rotamers are characterised by very different positions of the CF_3 group with respect to the pseudocontact shift field created by the paramagnetic ion (Scheme 2.7).

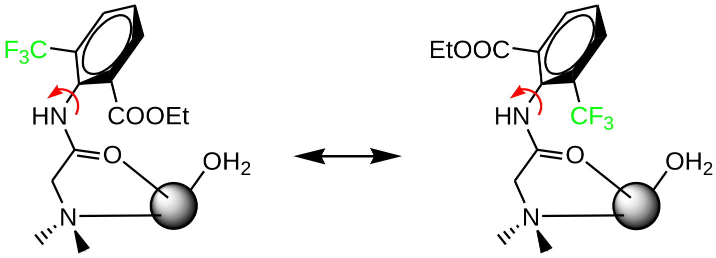

Scheme 2.7 Schematic representation of the two isomers of **[LnL^{4a}]** arising from the rotation of the aromatic ring around the CN bond.

For each complex, the two resonances exhibit a slightly different pH dependence, as illustrated in the pH titrations undertaken for **[HoL^{4a}]** and **[TmL^{4a}]** in 0.1 M NaCl at 295 K and 188 MHz (Fig. 2.14). The different lanthanide complexes of the same ligand $\mathbf{L^{4a}}$ maintained similar protonation constants (as previously observed for the different complexes of $\mathbf{L^{1a}}$), with values of 8.65 ± 0.02 for **[HoL^{4a}]** and 8.61 ± 0.02 for **[TmL^{4a}]**, analogous to 8.78 ± 0.06 and 8.80 ± 0.03 for the *para* ester **[HoL^{1a}]** and **[DyL^{1a}]** complexes. The opposite shifting effect observed for the two metals, as well as the different size of the chemical shift non-equivalence, is related to the sign and magnitude of the Bleaney constants (see Table 1.1 of section 1.3.1). These are -

39 for Ho^{3+} and +56 for Tm^{3+} (relative to -100 for Dy). The pK_a is lower than expected, in comparison to the value of 10.2 for the phenol analogue[4].

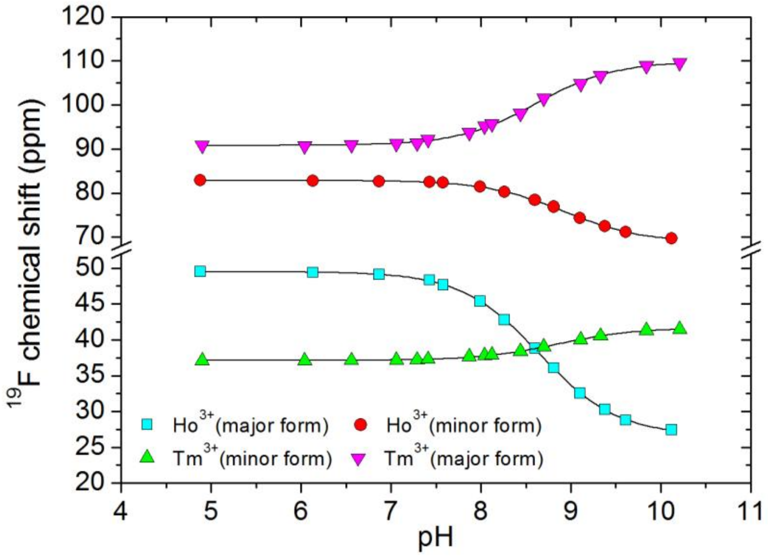

Fig. 2.14 pH titration curve for **[HoL^{4a}]** and **[TmL^{4a}]** (0.1 M NaCl in H_2O, 295 K, 188 MHz, D_2O lock) showing the fit (line) to the data. **[HoL^{4a}]** major: $pK_a = 8.65 \pm 0.02$, $\Delta\delta_F = 22.9$ ppm; **[TmL^{4a}]** major: $pK_a = 8.61 \pm 0.02$, $\Delta\delta_F = 19.1$ ppm.

A summary of the main features obtained from the pH titration is shown in Table 2.2.

Table 2.2 Summary of data obtained from the pH titration of **[HoL^{4a}]** and **[TmL^{4a}]**.

complex (isomer)	δ_F acidic form (ppm)	δ_F basic form (ppm)	$\Delta\delta_F$ (ppm)	pK_a
Ho major	- 49.5	- 26.6	22.9	8.65 ± 0.02
Ho minor	- 82.8	- 68.8	14.0	8.93 ± 0.02
Tm minor	- 37.1	- 41.7	4.6	8.84 ± 0.05
Tm major	- 90.8	- 109.9	19.1	8.61 ± 0.02

[HoL^{4a}] exhibits a chemical shift variation of ~23 ppm for the major isomer over 2.5 units of pH, larger than that obtained for the *para* analogue (15 ppm over 2 units of pH). The linewidth profile for each isomer (Fig. 2.15) follows the normal pattern of increased broadening around the pK_a value, as observed for **[HoL^{1a}]**. The latter possess intermediate linewidth values compared to those of the major and minor isomers of **[HoL^{4a}]** (maximum linewidth for **[HoL^{1a}]** is 197 Hz, 211 Hz for the major form of the *ortho* complex **[HoL^{4a}]** and 156 Hz for the minor form).

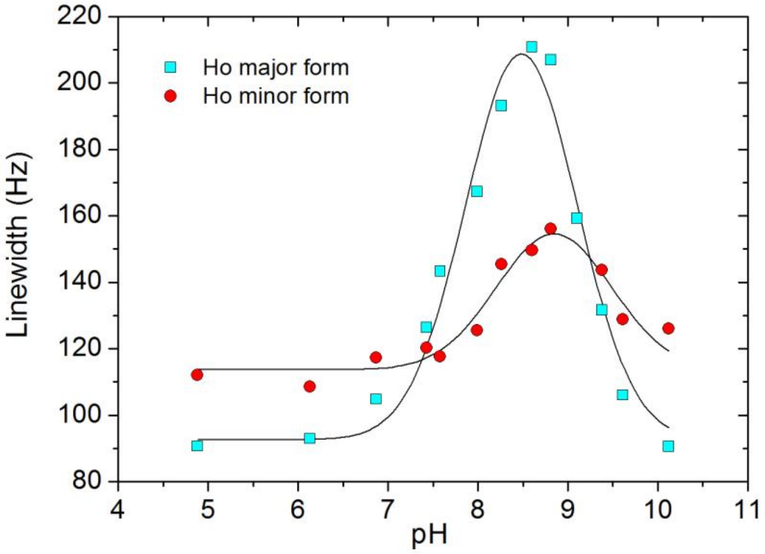

Fig. 2.15 Linewidth variation as a function of pH for **[HoL^{4a}]** (295 K, 188 MHz).

With the *ortho* acid lanthanide complexes **[LnL^{4b}]**, two resonances were observed with a large chemical shift difference, corresponding to two rotameric forms. The signals have similar chemical shifts to the corresponding *ortho* ester complexes **[LnL^{4a}]**, but in a 3:1 ratio and with larger linewidths.

The pH profile for each isomer was also undertaken for the analogous thulium complex (Fig. 2.16).

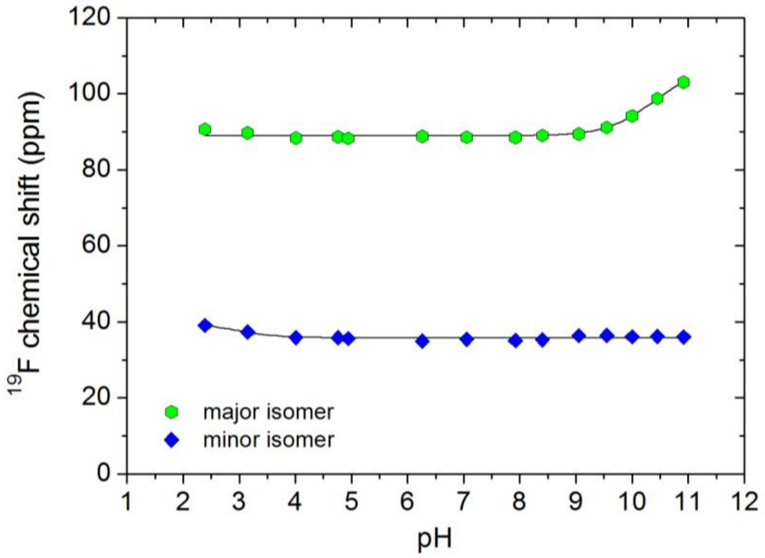

Fig. 2.16 pH titration curve for **[TmL^{4b}]** (0.1 M NaCl in H_2O, 295 K, 188 MHz, D_2O lock) showing the fit (line) to the data. Major: $pK_a = 10.40 \pm 0.09$, $\Delta\delta_F = 14.0$ ppm.

The amide pK_a of 10.40 ± 0.09 in this case was apparent only for the major isomer and was higher than the values of 9.61 and 9.46 for the *para*-substituted analogues **[DyL^{1a}]** and **[HoL^{1a}]**. At pH values lower than 4, the acid protonation started to be visible.

The *ortho* ester and acid series of complexes introduce an interesting approach to pH measurement compared to the previous examples. The *para*-substituted compounds **[LnL^{1a}]** appear in the fluorine spectrum as one observed resonance. The observed chemical shift has to be referenced to a standard before accurate pH measurement is possible. In the case of the *ortho* analogues **[LnL^{4a}]**, two resonances in the ^{19}F NMR spectrum occur, which exhibit differing sensitivity to pH. This allows pH measurement simply by measuring the shift difference between the two isomers. This method is advantageous because it does not require any chemical shift reference. The plot of the difference between the two isomers is reported for **[HoL^{4a}]** (Fig. 2.17). It varies from 33.3 ppm at acidic pH to 42.3 ppm in basic conditions. The same variation ranged from 53.7 to 68.1 ppm for **[TmL^{4a}]** and 51.5 to 67.0 ppm for **[TmL^{4b}]**.

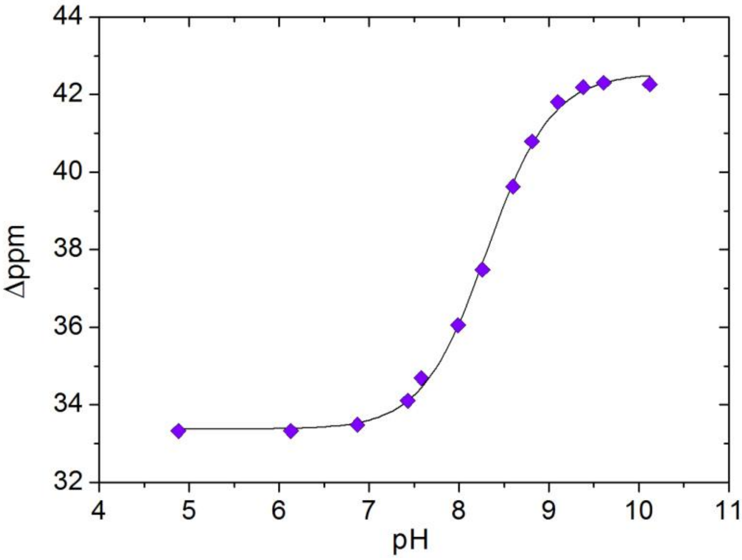

Fig. 2.17 Chemical shift difference between the two isomers of **[HoL^{4a}]** with pH (295K, 188 MHz) showing the fit (line) to the data. $pK_a = 8.31 \pm 0.02$.

Ligand **L^5** was investigated after observing the behaviour of the previous complexes. The introduction of the cyano functionality in the *ortho* position was proposed to increase the acidity of the amide hydrogen, based on its high electron withdrawing ability and on pK_a values of about 7.0 for analogous systems.

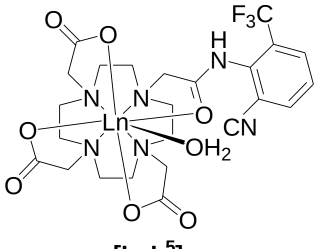

[LnL⁵]

A pH titration was performed in 0.1 M NaCl in water for **[HoL^5]** (Fig. 2.18).

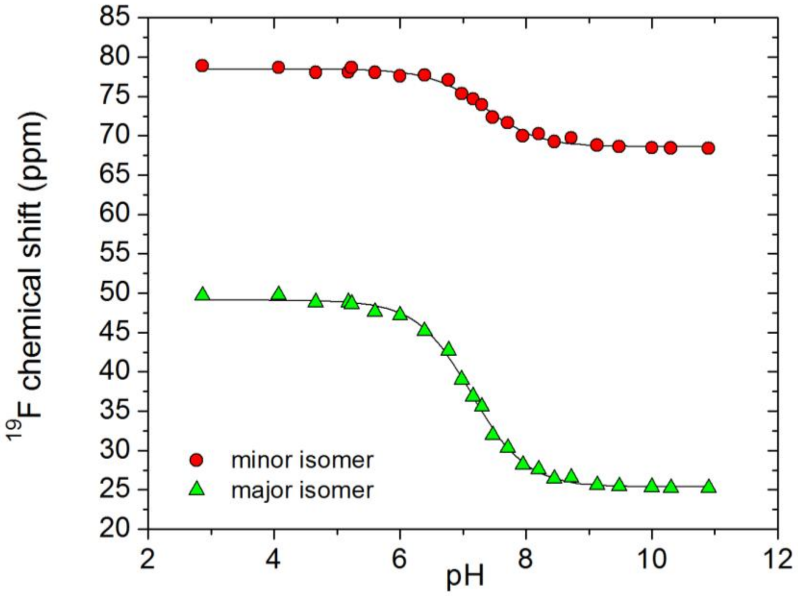

Fig. 2.18 pH titration curve of **[HoL^5]** (0.1 M NaCl in H_2O, 295 K, 188 MHz, D_2O lock) showing the fit (line) to the data. $pK_a = 7.13 \pm 0.02$, $\Delta\delta_F = 24.5$ ppm and 10.5 ppm.

The complex **[HoL^5]** had a pK_a of 7.13 ± 0.02. This is centred in the optimal region for physiological pH measurements, with a chemical shift difference between the protonated amide and its conjugated base of 24.5 ppm for the major isomer and 10.5 ppm for the minor. The working pH range was 6 to 8. The lower pK_a is probably due to the additional inductive σ-polarisation effect exerted by the *ortho*-cyano group. The compound also gave rise to two distinct isomers in the fluorine spectrum, with a large pH variation of chemical shift ranging from 29.2 to 43.2 ppm. When plotted against the pH (Fig. 2.19), the difference in chemical shift of the two isomers allowed an internally referenced calibration curve to be created for measurement of pH.

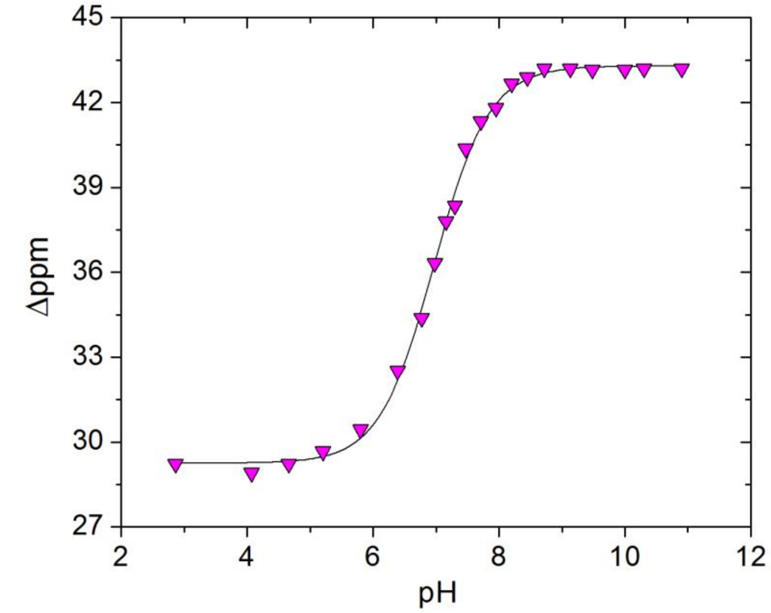

Fig. 2.19 Chemical shift difference between the two isomers of **[HoL^5]** with pH (295K, 188 MHz) showing the fit (line) to the data. pK_a = 6.97 ± 0.02.

The same study was also performed in mouse urine and plasma to assess the effect of anionic species and proteins in solution on the pH responsiveness of **[HoL^5]** (Fig. 2.20). No variations were observed in the pH behaviour of the probe; such characteristics favour possible future *in vivo* experiments.

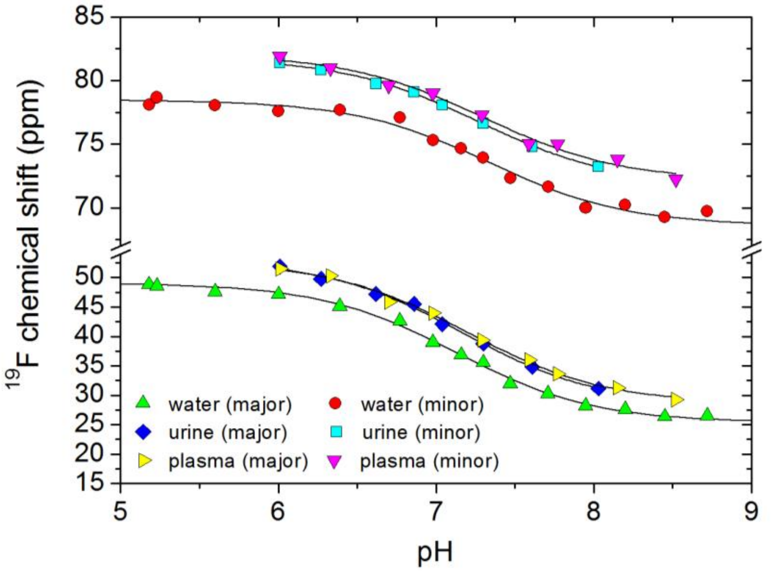

Fig. 2.20 pH titration of **[HoL^5]** in 0.1 M NaCl in H_2O, mouse urine and mouse plasma (295 K, 188 MHz, D_2O lock).

The linewidth variation at different pH values exhibited a peculiar profile. Under basic conditions, **[HoL^5]** showed two sharp fluorine signals that broadened when reaching neutral pH corresponding to the pK$_a$ value. Under acidic conditions however, instead of exhibiting reduced linewidths, the two signals broadened again, up to a value of $\omega_{1/2}$ = 800 Hz. This characteristic was independent of the metal ion used. The fluorine resonances are actually formed by two pairs of overlapping peaks corresponding to four diastereoisomers. These isomers may be ascribed to rotation of the aromatic ring around the C-N bond and to cyclen ring inversion and concurrent acetate group rotation. Further work has investigated this stereochemical complexity in an effort to explain these processes and will be discussed later in Chapter 3.

Chemical exchange broadening may be reduced by structural modification aimed at suppressing these dynamic processes. One possible solution could be the substitution of the carboxylate pendant arms with more rigid donors such as phosphinate arms, as will be discussed in the next section.

A summary of the principal features for the series of ligands presented in this section are listed in the table below:

Table 2.3 Summary of pH data for complexes of ligands **L^1-L^5** and **L^{13}**.

Complex	**$\Delta\delta_F$ (ppm)** [a]	**pK$_a$**	**Phenols pK$_a$**
[HoL^{1a}] *p*-ester	46.6	8.78 ± 0.06	8.34 [c]
[HoL^{1b}] *p*-acid	40.2	9.46 ± 0.11	/
[HoL^{13}] *p*-amide	15.0	8.98 ± 0.06	/
[HoL^2] *p*-nitro	17.2	7.77 ± 0.02	7.15 [b]
[HoL^3] *p*-cyano	17.3	8.15 ± 0.03	7.95 [b]
[HoL^{4a}] *o*-ester	22.9	8.65 ± 0.02	10.2 [c]
[TmL^{4b}] *o*-acid	14.0	10.40 ± 0.09	/
[HoL^5] *o*-cyano	24.5	7.13 ± 0.02	7.0 [c]

[a] Major isomer only; [b] 3; [c] 4.

2.3 DOTP-based complexes

The *ortho* cyano holmium complex **[HoL^5]** proved to be the best ^{19}F NMR pH probe of the series under study (section 2.2.2). It has a pK$_a$ of 7.13 centred in the range of interest and observable over two units of pH with a variation in shift of nearly 25 ppm. In addition, the presence of two isomers with different sensitivity to the pH allows measurements of pH to be made without the need for chemical shift reference. In an attempt to minimise the broadening of the resonances at acidic pH, the phosphinate analogues of the corresponding DO3A monoamide complexes (DOTP) were prepared (Fig. 2.21).

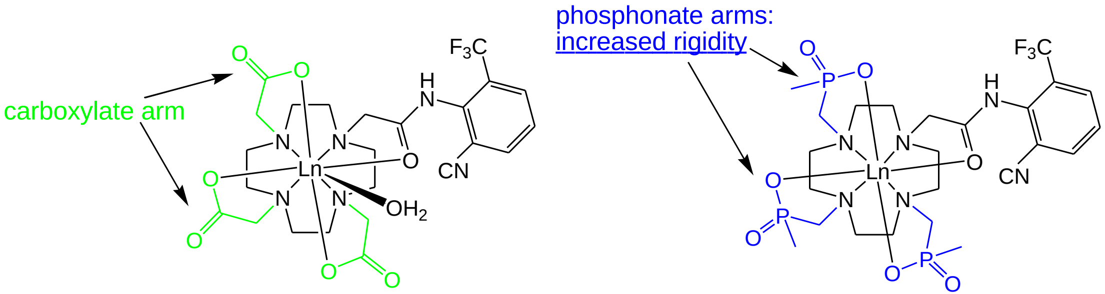

[LnL^5] [LnL^6]

Fig. 2.21 DO3A monoamide complex **[LnL^5]** vs DOTP monoamide complex **[LnL^6]**.

Lanthanide complexes of tri and tetraphosphinate[9,10] ligands maintain the high kinetic stability as seen for their carboxylate analogues with respect to metal dissociation, which makes them suitable for *in vivo* studies. Upon complexation, the three phosphinate pendant arms form a more rigid cage around the metal compared to the carboxylate analogues. In particular, the more bulky phosphinate moiety suppresses cooperative arm rotation about the principal axis and also favours the formation of one major isomeric species, at least with P-Me and P-Bn phosphinates[11]. The enhanced rigidity may then reduce the linewidth of the fluorine signals.

2.3.1 Synthesis

In this case, mono-alkylation of the macrocycle was undertaken by reaction of a 10 fold excess of cyclen with one equivalent of the α-chloroamide in the presence of K_2CO_3 in acetonitrile (Scheme 2.8). A homogeneous product was obtained after a series of consecutive washes partitioning between water, dichloromethane and chloroform in order to eliminate the excess cyclen and any impurities formed during the reaction. A different strategy previously attempted involved the reaction of the α-haloamide with the tri-BOC (*tert*-butoxycarbonyl) protected cyclen, and successive TFA deprotection to yield the desired monoamide. This procedure was unsuccessful. This was tentatively attributed to the higher steric hindrance around the ring nitrogen caused by the presence of the tri-BOC substituents. Reaction of the mono-substituted cyclen with paraformaldehyde and diethoxymethylphosphine in dry tetrahydrofuran, yielded the desired tri-ester in low yield (19%). Hydrolysis of the ester groups was achieved using a solution of KOD (0.1 M) over one week at room temperature. The lanthanide complex **[HoL^6]** was prepared by reaction of **L^6** with $HoCl_3$ in water at 50°C. The product was purified by dialysis.

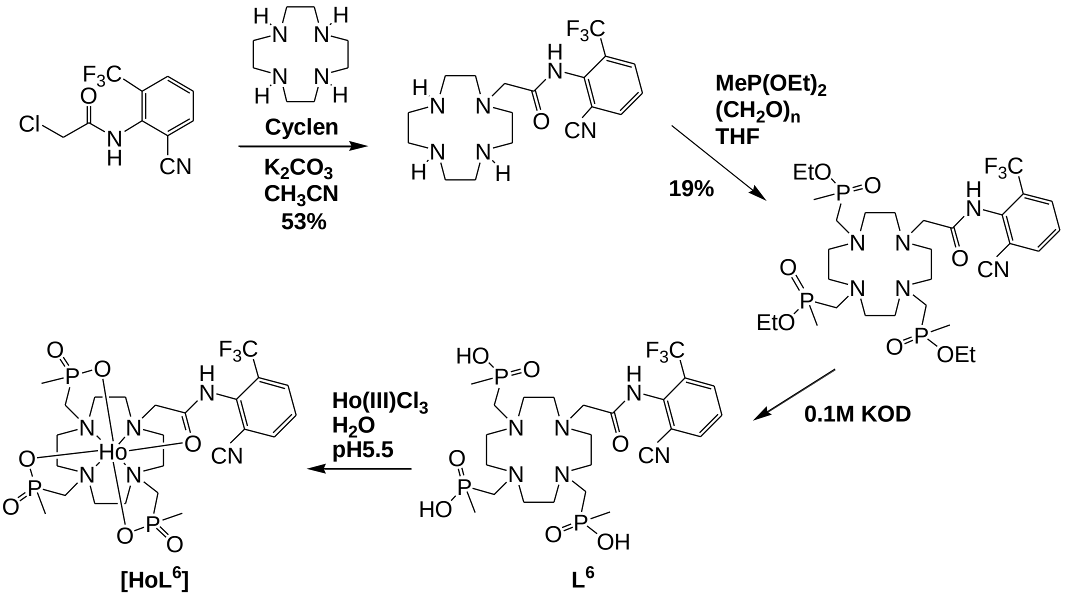

Scheme 2.8 Synthetic scheme for **[HoL^6]**.

2.3.2 pH Dependent spectroscopic behaviour

In the ^{19}F NMR spectrum of **[HoL^6]** three main resonances were observed in the ratio 1:2.7:3.1 at -46.8, -59.6 and -95.5 ppm (pH 6.8). The resonance at δ_F = -59.6 ppm was observed close to the shift of the ligand itself (δ_F = -61.6 ppm). Further studies, that will be discussed in Chapter 3, suggest that the signal may be actually formed by two pairs of overlapping resonances, in a similar fashion as for the carboxylate analogue. These four resonances may be attributed to four diastereoisomers related by restricted rotation around the aryl C-N bond, as well as the Δ(δδδδ) and Λ(λλλλ) isomers associated with cyclen ring inversion and acetate pendant arm rotation. A pH titration for **[HoL^6]** was undertaken in 0.1 M NaCl at 295 K and 188 MHz (Fig. 2.22). The unshifted resonance remained at the same position over the whole pH range, while the other two peaks showed very similar pH dependence to that observed for **[HoL^5]**. The same pK$_a$ value of 7.09 ± 0.02 was estimated (7.13 ± 0.02 for **[HoL^5]**). This offers additional proof that the pK$_a$ is associated with amide NH deprotonation and not to any other structural feature, such as coordinated water. The chemical shift difference between the protonated and non-protonated forms was greater than for the carboxylate analogue: Δδ$_F$ was 36.3 and 20.0 ppm for the two isomers of **[HoL^6]** compared to 24.5 and 10.5 ppm for **[HoL^5]**.

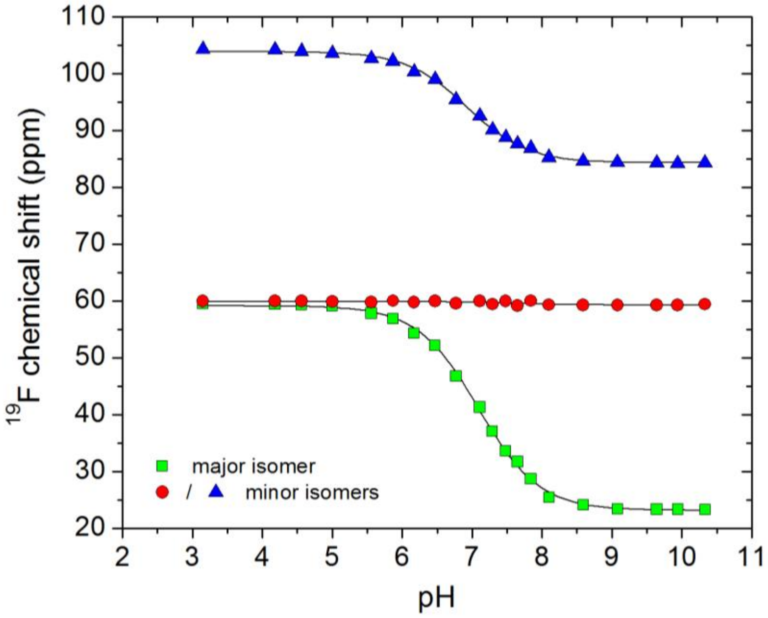

Fig. 2.22 pH titration of [**HoL^6**] (0.1 M NaCl in H$_2$O, 295 K, 188 MHz, D$_2$O lock) showing the fit (line) to the data. pK$_a$ = 7.09 ± 0.02, Δδ$_F$ = 36.3 ppm and 24.5 ppm.

The variation of δ$_F$ with pH for **[HoL^6]** was also undertaken in mouse plasma (Fig. 2.23). No change in the pH dependence of δ$_F$ was observed, auguring well for future *in vivo* studies.

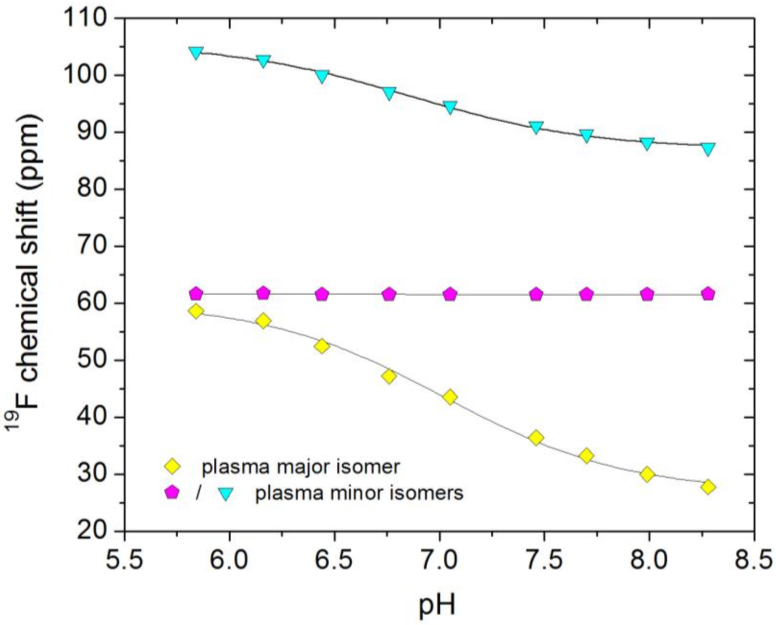

Fig. 2.23 pH titration of **[HoL^6]** in mouse plasma (295 K, 188 MHz, D_2O lock) showing the fit (line) to the data.

The linewidth variation of **[HoL^6]** followed the same trend as observed for the carboxylate analogue **[HoL^5]**, but with much narrower resonances, reaching a maximum of only ~230 Hz, compared to over 800 Hz for **[HoL^5]**.

2.4 Tetra-substituted cyclen

A different tetra-substituted complex **[HoL^7]** was prepared, containing four identical fluorinated arms as substituents on the cyclen nitrogens. The 12 fluorine atoms were introduced with the purpose of increasing the signal intensity in the ^{19}F NMR spectrum. The compound was considered to undergo four consecutive deprotonation equilibria, resulting in a wider pH variation of δ_F with pH.

2.4.1 Synthesis

The ligand **L^7** was prepared by reacting one equivalent of cyclen with five equivalents of the CF_3-labelled *para*-ethyl α-chloroamide ester, under the same conditions used for the DO3A analogues (Scheme 2.9). The purification procedure required two successive separations by columns chromatography over silica gel to obtain the product, and proceeded in very low yield (9%). Attempts to prepare the *ortho*-ester analogue were unsuccessful, probably due to steric congestion.

Complexation was performed in acetonitrile with the triflate salt of the lanthanide ion and the product was obtained after precipitation in diethyl ether and anion exchange to give the chloride salt.

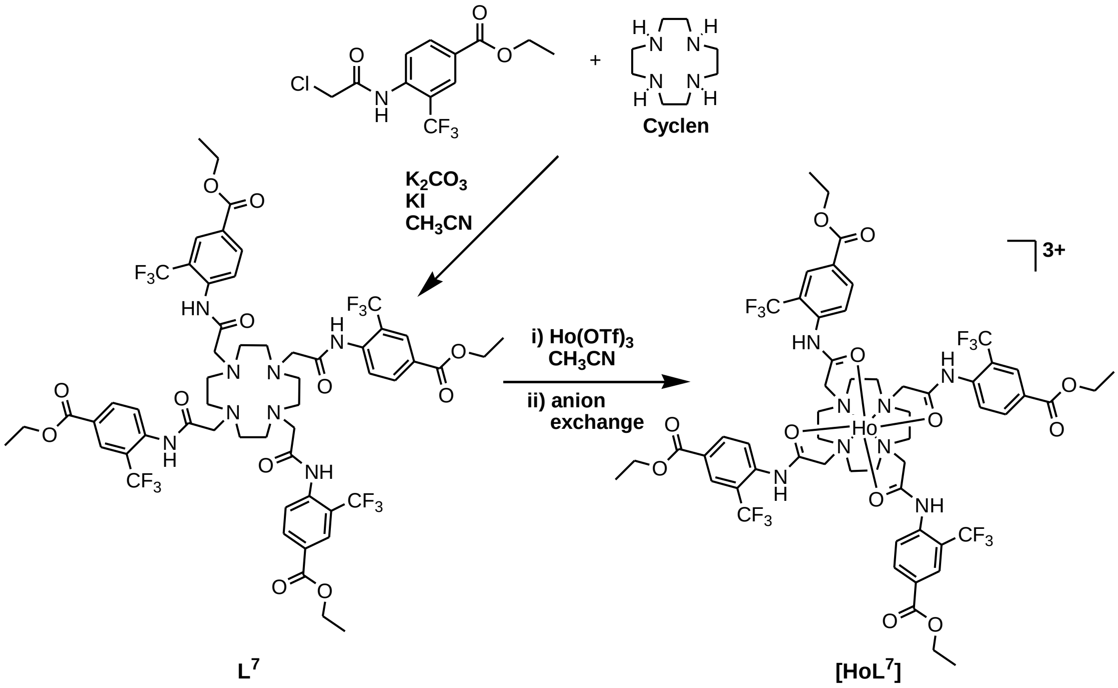

Scheme 2.9 Synthetic scheme for **$[HoL^7]^{3+}Cl_3$**.

2.4.2 pH Dependent spectroscopic behaviour

A pH titration of **$[HoL^7]^{3+}$** was performed in a solution of MeOH/H_2O 4:1 at 295 K and 188 MHz, using a D_2O capillary to lock the instrument (Fig. 2.24). The complex was not soluble in water due to the increased liphophilicity of the structure with four trifluoromethyl and four ethyl ester groups.

A single ^{19}F resonance was observed consistent with the C_4 symmetry of the complex. The δ_F/pH profile showed a ^{19}F chemical shift variation of about 20 ppm, over a range of more than 3 pH units centred at 8.7. This agrees with the hypothesis of extending the pH range by the presence of consecutive pK_a equilibria. No pK_a determination was possible, as the presence of two closely spaced protonation equilibria inhibits an accurate estimate from being made. In addition, after deprotonation of the first amide, the compound loses the C_4 symmetry, resulting in multiple resonances in the fluorine spectrum.

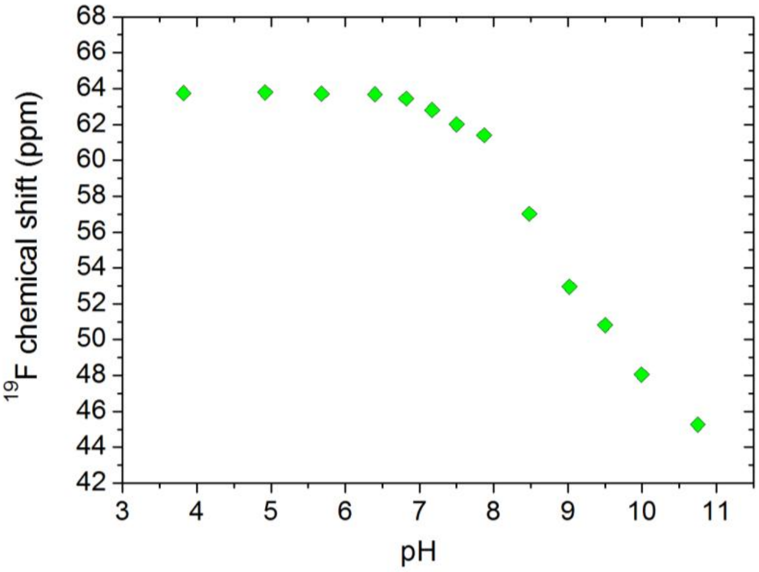

Fig. 2.24 pH titration curve of **[HoL^7]** (MeOH/H_2O 4:1, 295 K, 188 MHz, D_2O lock) showing only the major resonance. $\Delta\delta_F$ = 18.0 ppm.

A further consideration was to hydrolyse the complex fully to allow examination of the tetracarboxylate derivative. This compound should have improved solubility with respect to the ester precursor. Unfortunately, the hydrolysis, attempted in a solution of MeOH and water at pH 11 over a period of four weeks, was not successful, and was accompanied by decomplexation of the Ln^{3+} ion, with formation of $Ln(OH)_3$.

2.5 Conclusions

The purpose of this study was to develop a pH responsive probe to be used in ^{19}F MRS/MRI. The series of lanthanide complexes discussed, allowed the evaluation of the effect that different substituents of the aromatic ring have over the NH protonation constant of the amide group. The results were comparable to those obtained for analogous systems reported in the literature (see Table 2.3).

The tetra-substituted **[HoL^7]** did not possess the pK_a and solubility properties desired but it was useful because it highlighted the limitations of the system. In fact, a constant symmetry needs to be maintained for both acidic and basic forms in order to avoid the formation of multiple ^{19}F resonances. In addition, the introduction of liphophilic groups into the structure has to be carefully evaluated to preserve the water solubility of the compound.

The complexes based on DO3A-monoamide ligands and their phosphinate analogues are kinetically and thermodynamically stable, sufficiently soluble in water and can be safely used for *in vivo* applications. This was also confirmed by toxicity studies performed on **[HoL^2]**, which was tested on two cell lines, NIH 3T3 and CHO cells, with an incubation time of 24 hours. No toxicity was found up to 150 μM (IC_{50} > 150 μM). The absence of toxicity may be due to the fact that the complex is not internalised by the cell under these conditions.

From the first series, **L^1-L^5** and **L^{13}**, the best candidate was **L^5**. **[HoL^5]** showed a pK_a of 7.13 with a shift variation of nearly 25 ppm over two units of pH. Furthermore, the presence of two isomers with different pH sensitivity allows the pH to be measured without need of chemical shift reference.

Substitution of the carboxylate pendant arms with the corresponding phosphinate analogues, as in **L^6**, led to a 4 times improvement of the linewidth, while maintaining the pK_a value. **[HoL^6]** therefore, represents the best pH reporter within the series under study thanks to a pK_a of 7.09, with a variation of the fluorine chemical shift of more than 36 ppm over nearly three pH units, spanning the normal range of physiological and pathological pH conditions. The presence of two independent resonances allows an internal calibration, without the need for external referencing. Finally, the reduced linewidths enhance its suitability for chemical shift imaging (CSI) studies *in vivo*.

References

[1] P. K. Senanayake, A. M. Kenwright, D. Parker, S. K. van der Hoorn, *Chem. Commun.*, **2007**, 2923.

[2] A. M. Kenwright, I. Kuprov, E. De Luca, D. Parker, S. U. Pandya, P. K. Senanayake, D. G. Smith, *Chem. Commun.*, **2008**, 2514.

[3] M. D. Liptak, K. C. Gross, P. G. Seybold, S. Feldgus, G. C. Shields, *J. Am. Chem. Soc.*, **2002**, *124*, 6421.

[4] S. Bawa, M. L. Cote, P. Dubois, R. A. Lalancette, H. W. Thompson, *Acta Crystallogr. Sect. B-Struct. Sci.*, **2004**, *60*, 438.

[5] D. H. McDaniel, H. C. Brown, *J. Org. Chem.*, **1958**, *23*, 420.

[6] A. Beeby, I. M. Clarkson, R. S. Dickins, S. Faulkner, D. Parker, L. Royle, A. S. de Sousa, J. A. G. Williams, M. Woods, *J. Chem. Soc.-Perkin Trans. 2*, **1999**, 493.

[7] A. Sigel, H. Sigel, *The Lanthanides and Their Interrelations with Biosystems Vol. 40*, Chapter 14, Marcel Dekker, University of Basel, Switzerland, **2003**.

[8] R. S. Dickins, D. Parker, J. I. Bruce, D. J. Tozer, *Dalton Trans.*, **2003**, 1264.

[9] S. Aime, A. S. Batsanov, M. Botta, J. A. K. Howard, D. Parker, K. Senanayake, J. A. G. Williams, *Inorg. Chem.*, **1994**, *33*, 4696.

[10] S. Aime, A. S. Batsanov, M. Botta, R. S. Dickins, S. Faulkner, C. E. Foster, A. Harrison, J. A. K. Howard, J. M. Moloney, T. J. Norman, D. Parker, L. Royle, J. A. G. Williams, *J. Chem. Soc. Dalton Trans.*, **1997**, 3623.

[11] S. Aime, M. Botta, D. Parker, J. A. G. Williams, *J. Chem. Soc. Dalton Trans.*, **1995**, 2259.

Chapter 3

NMR characterisation of exchange phenomena and relaxation behaviour

3.1 Introduction

A series of lanthanide complexes has been described in Chapter 2, based on mono-amide derivatives of DO3A, **L^1-L^5** and DOTP, **L^6** and their characteristics as pH reporters for ^{19}F NMR analysis discussed. Here, we report the spectroscopic properties of the same series of complexes, in particular their ^{19}F NMR shift and relaxation properties, as well as ^{1}H relaxivity studies on the Gd^{3+} analogues.

3.2 Spectroscopic properties and conformational analysis

The ^{19}F NMR spectra of various lanthanide ion complexes of ligands **L^1-L^6** have been recorded and their peculiar characteristics will be discussed here.

3.2.1 *p*-Substituted systems

The Ho, Tb, Er, Dy and Tm complexes of the *para*-substituted systems **L^1-L^3** (Fig. 3.1) showed similar characteristics. Upon dissolution of the complex in water, one main species was observed (>60%) by both ^{19}F and ^{1}H NMR spectroscopy (pD 5.4, 295 K). Other minor species (up to eight) were observed, whose proportion varied according to the nature of the lanthanide ion. The relative isomeric composition did not change with time, while changes in the ^{19}F spectrum were evident at different pH values (Fig. 3.2).

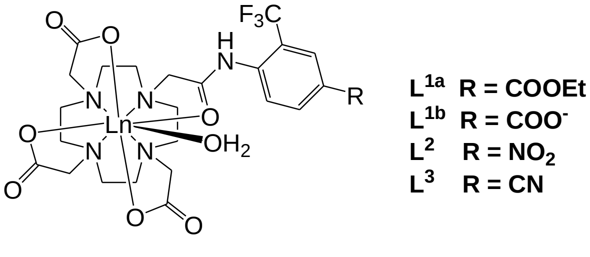

Fig. 3.1 General structure of the *para*-substituted complexes.

Indeed, as described in the previous chapter, the deprotonation equilibrium of the amide proton in this series of complexes, gives rise to two species: the protonated form and its conjugate base. These are in fast exchange on the NMR time scale. Therefore, they appear as a single signal corresponding to the weighted average of the chemical shifts of the two forms. At different pH values, the population of these two forms changes, and is reflected by a variation of the chemical shift.

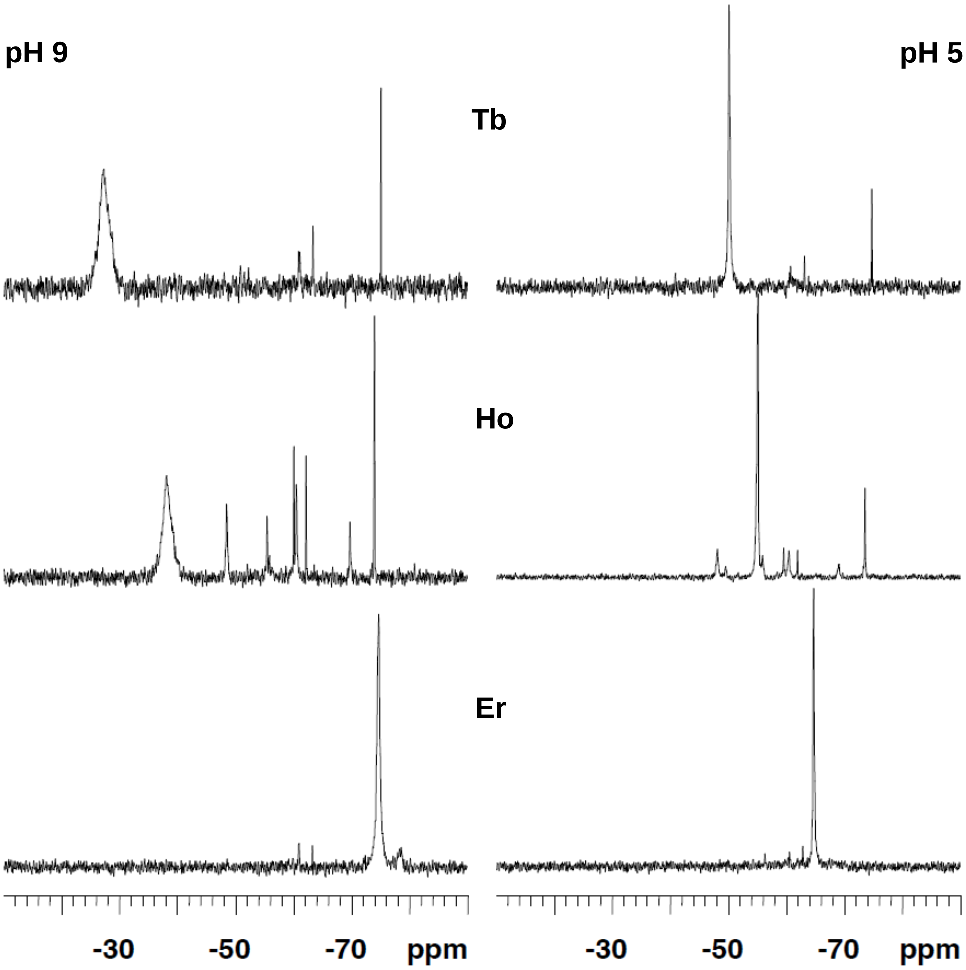

Fig. 3.2 ^{19}F NMR spectra for **[LnL^2]** (H_2O with D_2O insert, 295 K, 376 MHz). Left: pH 9 for Tb (upper), Ho (centre), Er (lower). Right: pH 5 in the same order. The differences in chemical shift, linewidth and number of species for the various lanthanide complexes of the same ligand, are evident at pH 5 and 9.

Furthermore, the linewidth of the fluorine resonance also varied with pH, reaching a maximum at pH values corresponding to the pK_a of the amide proton and decreasing at higher or lower values. This line broadening phenomenon is associated with chemical exchange between the protonated and non-protonated forms. For the *p*-

nitro complexes, **[LnL^2]**, the linewidth variation with pH exhibited an unusual dependence, reaching a maximum in basic conditions. This behaviour, already explained in chapter 2, is probably due to a conformational exchange process associated with the *cis-trans* isomerisation around the C-N double bond. This produces line broadening selectively at basic pH.

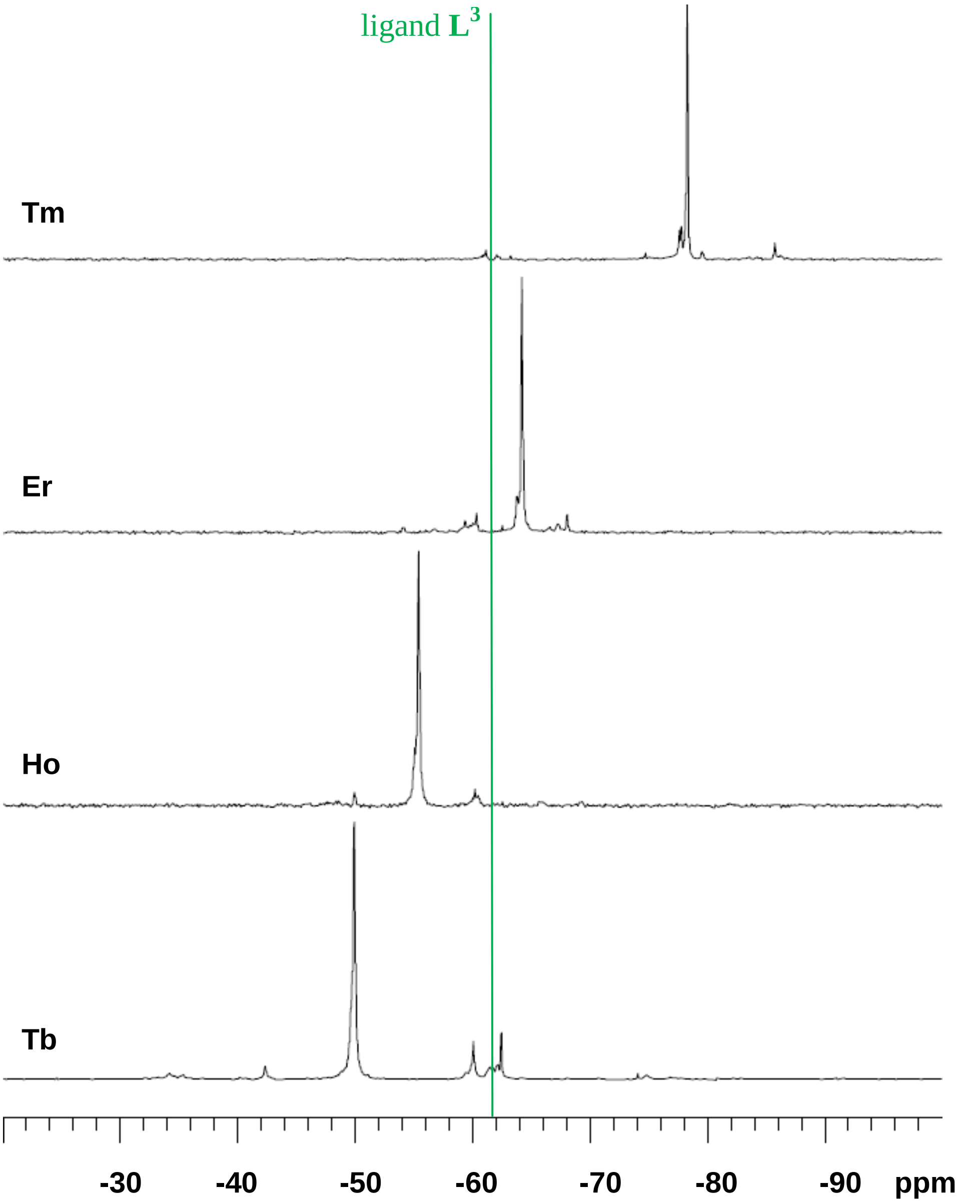

Fig. 3.3 ^{19}F NMR spectra for **[LnL^3]** (H_2O with D_2O insert, 295 K, 376 MHz) illustrating the difference in chemical shift for each lanthanide complex of **L^3**. For each metal $\Delta\delta_F$ is proportional to the Bleaney constant C_J (Ho -39, Tb -86, Tm +53, Er +33), relative to the chemical shift of the ligand δ_F = -61.9 ppm, or the diamagnetic Y^{3+} complex at -62.0 ppm.

For each complex, the chemical shift and linewidth changed according to the nature of the metal ion used (Fig. 3.2 and 3.3). The observed dipolar shift is related to the sign and magnitude of the Bleaney constant C_J (see section 1.3.1), which is a characteristic of each lanthanide ion. For example, Ho and Tb exhibit negative values of -39 and -86 respectively, while Tm and Er possess positive values of +53 and +33, relative to -100 for Dy.[1] Therefore, the fluorine resonance of Ho or Tb complexes are shifted to higher frequency, while Tm and Er analogues move to lower frequency, with respect to the chemical shift of the diamagnetic ligand (Fig. 3.3), or its diamagnetic complex with Y^{3+}.

The Gd analogue, prepared for **L**$^{\mathbf{1b}}$, appeared in the ^{19}F spectrum as a very broad signal (1325 Hz, 295 K, 188 MHz) with a chemical shift very similar to that of the ligand ($\delta_{F\,=}$ -61.6 ppm). This is expected as the Gd^{3+} ion induces fast relaxation of the CF_3 resonance, but causes no dipolar shift (C_J = 0)[1].

3.2.2 *o*-Substituted systems

Very different behaviour was observed for the complexes of the *ortho*-substituted ligands, **L**$^{\mathbf{4a}}$, **L**$^{\mathbf{4b}}$ and **L**$^{\mathbf{5}}$ (Fig. 3.4).

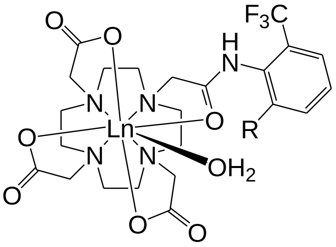

L^{4a} R = COOEt
L^{4b} R = COO$^-$
L^{5} R = CN

Fig. 3.4 General structure of the *ortho*-substituted series of complexes.

In the ^{1}H and ^{19}F spectra of each lanthanide complex, two major species were observed. These were in 1:1 ratio for **[LnL**$^{\mathbf{4a}}$**]** and **[LnL**$^{\mathbf{5}}$**]** and 3:1 ratio for **[LnL**$^{\mathbf{4b}}$**]**, with very different chemical shifts. For the **[LnL**$^{\mathbf{4a}}$**]** series for example, the two fluorine resonances were separated by 49.7 ppm for Tb, 33.4 ppm for Ho, 20.0 ppm for Er and 53.6 ppm for Tm. For the *ortho*-carboxylate series of complexes **[LnL**$^{\mathbf{4b}}$**]**, the two signals had very similar fluorine chemical shifts to the ester analogues, but exhibited larger linewidths. For the *ortho*-cyano complexes **[LnL**$^{\mathbf{5}}$**]**, under certain conditions of pH and according to the nature of the lanthanide used, one or two other resonances were observed. Their proportion and chemical shift varied for different lanthanides and for each *ortho*-substituent. As will be explained in section 3.2.2.1, there are indeed four species in solution for the lanthanide complexes of $\mathbf{L^{4a}}$, $\mathbf{L^{4b}}$ and $\mathbf{L^{5}}$, but in most cases they were not resolved, so that only two resonances are noted. Different experiments were undertaken in order to explain this behaviour and identify the nature of the major species observed. Initially, the coordination environment around the Ln ion in each of the three series of complexes was interrogated. The europium emission spectra for both the ester and acid complexes were recorded at pH values between 5 and 8. They were identical in each case, as shown (Fig. 3.5, pH 7).

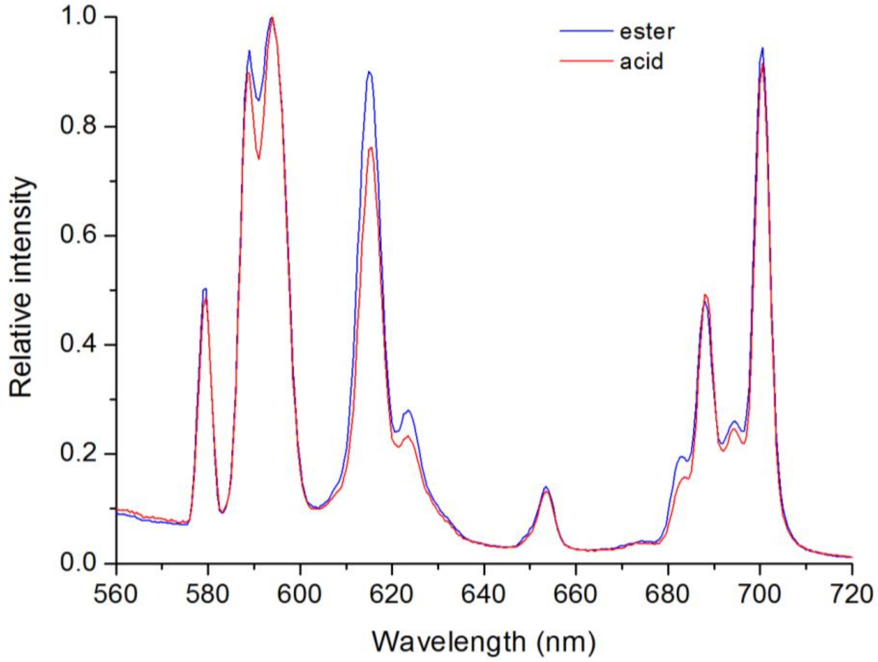

Fig. 3.5 Emission spectrum of the ethyl ester **[EuL^{4a}]** (blue) and the carboxylate **[EuL^{4b}]** (red) (H_2O, 295 K, pH 7).

The metal hydration state (q value) was also assessed for the europium and terbium complexes of ligands $\mathbf{L^{4a}}$, $\mathbf{L^{4b}}$ and $\mathbf{L^{5}}$ by measuring the radiative lifetime of the lanthanide excited state, k, in H_2O and D_2O. The q values were calculated using equation 11 for Tb(III) and equation 12 for Eu(III).[2]

$$q_{Tb} = 5 \times (k_{H_2O} - k_{D_2O} - 0.06) \qquad (12)$$

$$q_{Eu} = 1.2 \times (k_{H_2O} - k_{D_2O} - 0.25 - 0.075n) \qquad (13)$$

where k_{H_2O} and k_{D_2O} are the reciprocals of the luminescence lifetimes of each complex, τ_{H_2O} and τ_{D_2O} respectively, and n is the number of carbonyl-bound amide NH oscillators. Lifetimes and calculated q values are reported in Table 3.1.

Table 3.1 Measured lifetimes (± 10%) and calculated hydration numbers (± 20%) for Eu and Tb complexes of **L^{4a}**, **L^{4b}** and **L^{5}**.

Complex	τ_{H_2O} **(ms)**	τ_{D_2O} **(ms)**	***q***
[EuL^{4a}]	0.54	1.87	1.2
[TbL^{4a}]	1.99	3.41	0.8
[EuL^{4b}]	0.59	1.67	0.9
[TbL^{4b}]	2.47	3.70	0.4
[TbL^{5}]	1.90	2.99	0.7

The results are consistent with the presence of one water molecule directly bound to the metal centre in each case (except for **[TbL^{4b}]**), consistent with the behaviour of published mono-amide DO3A derivatives[2] and as observed for the *para*-substituted analogues. The identical Eu(III) emission spectra for the ester and acid complexes and the very similar hydration state observed, suggests that the same metal coordination environment is adopted in solution in each case. This strongly suggests that direct coordination of the carboxylate group to the lanthanide ion for **[LnL^{4b}]** is not occurring.

The observation of two major species in slow exchange on the NMR timescale suggested the presence of two isomers. Hence, a series of variable temperature ^{19}F NMR experiments were performed in order to seek evidence for the presence of a dynamic exchange process between the two species.

The fluorine spectrum of **[TmL^{4a}]** was recorded at pH 5 over the temperature range 283 K to 323 K (470 MHz). The two resonances (δ_F = -38.0 ppm and δ_F = -91.6 ppm at 293 K) shifted very slightly towards each other as the temperature increased and showed an increased linewidth passing from $\omega_{1/2}$ ~ 70 Hz at 293 K to $\omega_{1/2}$ ~ 600 Hz at 323 K. Only a small change in chemical shift (less than 5 ppm) was observed and no coalescence phenomenon was noted in the temperature range under study.

The same experiment was carried out for **[TmL^{4b}]** at pH 5 (D_2O insert, 470 MHz). The two ^{19}F resonances (δ_F = -37.0 ppm and δ_F = -90.0 ppm at 293 K) shifted and broadened with increasing temperature. In this case, a coalescence phenomenon was observed, with a single major resonance formed at 320 K at δ_F = -84.0 ppm ($\omega_{1/2}$ = 1800 Hz). This behaviour is consistent with the presence of a dynamic exchange between the two species for **[TmL^{4b}]**, with an activation energy of the order of 50 kJmol^{-1} ($\Delta\nu$ = 24,500 Hz), based on an Eyring analysis^3. The Eyring equation is expressed as:

$$k_r = \frac{k_b T}{h} e^{-\frac{\Delta G^{\#}}{RT}} \qquad (14)$$

where k_b is Boltzmann's constant, h Planck's constant and R the gas constant. Equation 14 can be rewritten as:

$$\Delta G^{\#} = RT\left[\ln\left(\frac{k_b T}{h}\right) - \ln(k_r)\right] \qquad (15)$$

or

$$\Delta G^{\#} = RT\left[23.760 + \ln\left(\frac{T}{k_r}\right)\right] \qquad (16)$$

Knowing the rate constant k_r for the dynamic exchange and the temperature of coalescence T_c, it is possible to estimate the activation energy $\Delta G^{\#}$ for the process. The rate constant k_r at the coalescence temperature is expressed as:

$$k_r = \frac{\pi \Delta \nu}{\sqrt{2}} \qquad (17)$$

where $\Delta\nu$ is the separation in Hz of the two peaks in the slow exchange regime, *i.e.* at lower temperature.

The same behaviour was also noted in ^{1}H and ^{19}F NMR variable temperature experiments using **[EuL^{4b}]** between 278 and 323 K at pH 5 and 470 MHz. In each case, a coalescence phenomenon was observed. In the ^{19}F NMR spectrum, a single resonance was observed at δ_F = -61 ppm ($\omega_{1/2}$ = 900 Hz) at 310 K, becoming narrower at higher temperature ($\omega_{1/2}$ = 460 Hz at 323 K).

In the case of the *ortho*-cyano system **L^5**, variable temperature experiments were performed with the dysprosium and yttrium complexes between 278 and 323 K (D_2O insert, 470 MHz). For **[DyL^5]**, the two signals (δ_F = -60 ppm and δ_F = -111 ppm at pH 5, δ_F = 0 ppm and δ_F = -80 ppm at pH 9, 293 K) shifted and broadened at higher temperatures, both at pH 5 and 9, but no coalescence was observed.

Different behaviour was found for **[YL^5]**. Its ^{19}F NMR spectrum at room temperature (293 K) showed a single broad resonance at pH 5 (δ_F = -61.6 ppm, $\omega_{1/2}$ = 126 Hz, 376 MHz), that resolved into two broad resonances at pH 9 (δ_F = -61.6 ppm, $\omega_{1/2}$ ~ 560 MHz and δ_F = -62.8 ppm, $\omega_{1/2}$ ~ 560 MHz, 376 MHz). In the basic sample, the two signals coalesced at higher temperature (310 K) to form a single resonance (δ_F = -62.0 ppm, $\omega_{1/2}$ ~ 250 Hz), that narrowed on increasing the temperature ($\omega_{1/2}$ ~ 110 Hz at 323 K). At lower temperatures, the two signals resolved and sharpened (Fig. 3.6). The activation energy, calculated with the Eyring analysis, in this case is of the order of 60 kJmol^{-1}, higher than for the acid compound.

The Y^{3+} ion has a very similar ionic radius to Ho^{3+}, [4] and its complexes are frequently isostructural. The isostructural nature of the various lanthanide complexes of the same ligand and the common coordination environment that characterises each case, allows us to extend consideration of the dynamic process observed for **[YL^5]** to the paramagnetic complexes in which the coalescence phenomenon was not apparent. In these cases, the fluorine resonances are significantly separated in Hz (large $\Delta\nu$), therefore a higher temperature is required to observe the coalescence phenomenon. In particular for the complexes of the *ortho* cyano and ester ligands, **L^5** and **L^{4a}**, where the activation energy is higher, the temperature required to observe a coalescence phenomenon is probably out of the observable range. As expressed in equation 14 in fact, the rate constant k_r and the coalescence temperature T_c are directly proportional, and k_r is related to the chemical shift difference $\Delta\nu$ between the resonances of the two species in exchange. Therefore, for larger $\Delta\nu$ values, it is necessary to reach higher temperatures to observe the coalescence process.

In order to explain the observed exchange phenomena, the rotation of the phenyl ring around the C-N bond was considered. This varies the CNCC dihedral angle, resulting in a repositioning of the CF_3 group with respect to the metal centre. To address the likelihood of this hypothesis, DFT calculations on these systems were performed by Ilya Kuprov and Naomi Hogg at the University of Durham.

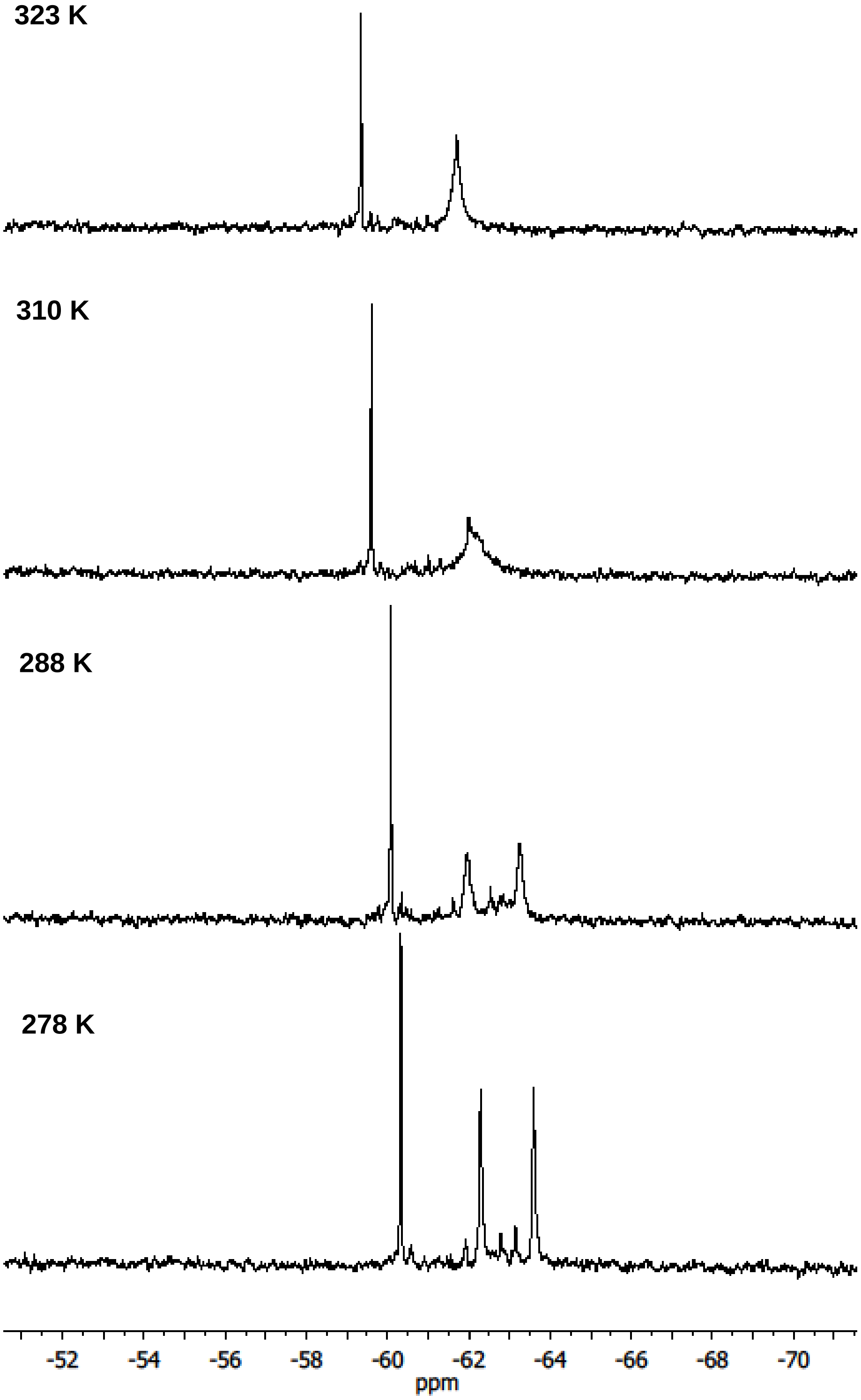

Fig. 3.6 ^{19}F NMR variable temperature of **[YL^5]** (D$_2$O insert, pH 9, 470 MHz). From the bottom: 278, 288, 310 and 323 K. A coalescence phenomenum is visible at ~310 K.

A relaxed potential energy scan was undertaken with respect to the CCNC dihedral angle for the Y(III) complex of ligands **L^{4a}**, **L^{4b}** and **L^{5}**. Indeed, two distinctive minima were identified, characterised by very different positions of the CF_3 group relative to the lanthanide ion (Fig. 3.7), and separated by an energy barrier of more than 20 kJmol^{-1}. If the metal-water-oxygen vector is taken as the principal axis, the CF_3 groups for each isomer are oriented at angles of -114° and +44°, which would result in opposite pseudocontact shifts. The direction and size of the observed chemical shift of the fluorine signals agrees well with the calculated theoretical values.

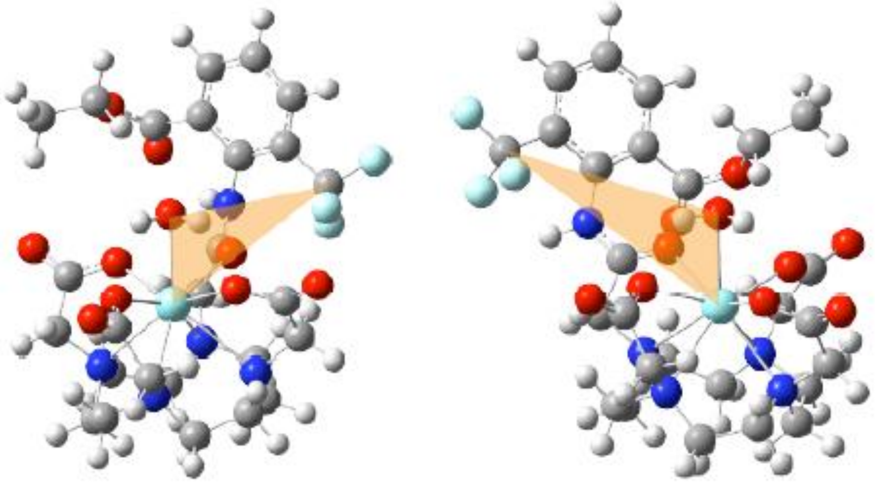

Major $\phi = -114°$ Minor $\phi = +44°$

Fig. 3.7 DFT calculated structures showing the two low-energy isomers of **[LnL^{4a}]** associated with the rotation of the phenyl ring around the C-N bond.

3.2.2.1 In depth stereochemical analysis

As previously mentioned (section 3.2.2), the ^{19}F NMR spectra of the *ortho* cyano complexes, **[LnL^{5}]**, often exhibited one or two resonances in addition to the two major species. This was particularly clear in the fluorine spectrum of **[TmL^{5}]** at pH 9 were four major resonances were observed at δ_F = -39.9, -41.2, -63.9 and -109.0 ppm. They appeared as two sets of paired resonances of equal intensity (Fig. 3.8).

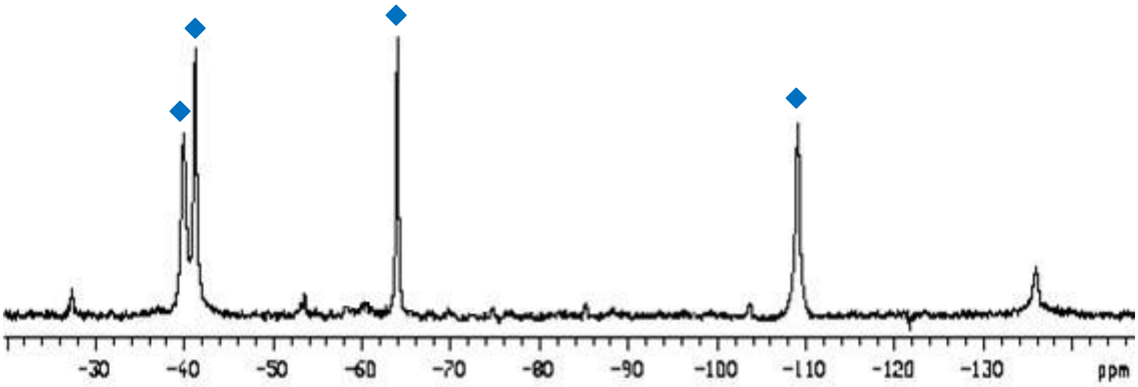

Fig. 3.8 ^{19}F NMR spectrum of **[TmL^5]** (H_2O, D_2O insert, pH 9, 470 MHz), showing the presence of four major species (◆).

A ^{19}F EXSY experiment performed on **[TmL^5]** (470 MHz) confirmed the occurrence of chemical exchange between at least two exchange sites. The clear presence of four fluorine resonances in slow exchange suggested that additional dynamic processes, to those discussed in the previous section, had to be considered to explain the observed behaviour. Normally, for DO3A mono-amide systems, the main coordination geometry adopted in solution is mono-capped square-antiprismatic (CAP), consisting of two enantiomeric species Δ/λλλλ and Λ/δδδδ present in a 50:50 ratio, that are indistinguishable by NMR. The two isomers can interconvert by inversion of configuration of the macrocyclic ring (λ/δ) and concurrent (but independent) rotation of the acetate arms (Λ/Δ) (Fig. 3.9).[5,6]

The introduction of an *ortho*-substituent on the aromatic ring slows down the rate of rotation around the C-N bond, and renders the mono-amide arm a chiral element. Thus, the CF_3 group can be positioned at different angles with respect to the metal centre. This increases the number of observable diastereoisomers present in solution. Therefore, it is postulated that the four species observed are: Δ/λλλλ-CF_3 up; Δ/λλλλ-CF_3 down; Λ/δδδδ-CF_3 up and Λ/δδδδ-CF_3 down. As noted above, the rate of interconversion is slower for the *ortho*-cyano **[LnL^5]** and *ortho*-ester **[LnL^{4a}]** series of complexes, and is faster for the carboxylate analogue **[LnL^{4b}]**. Furthermore, the activation energy differs for the protonated amide and its conjugate base, and varies for each series of complexes.

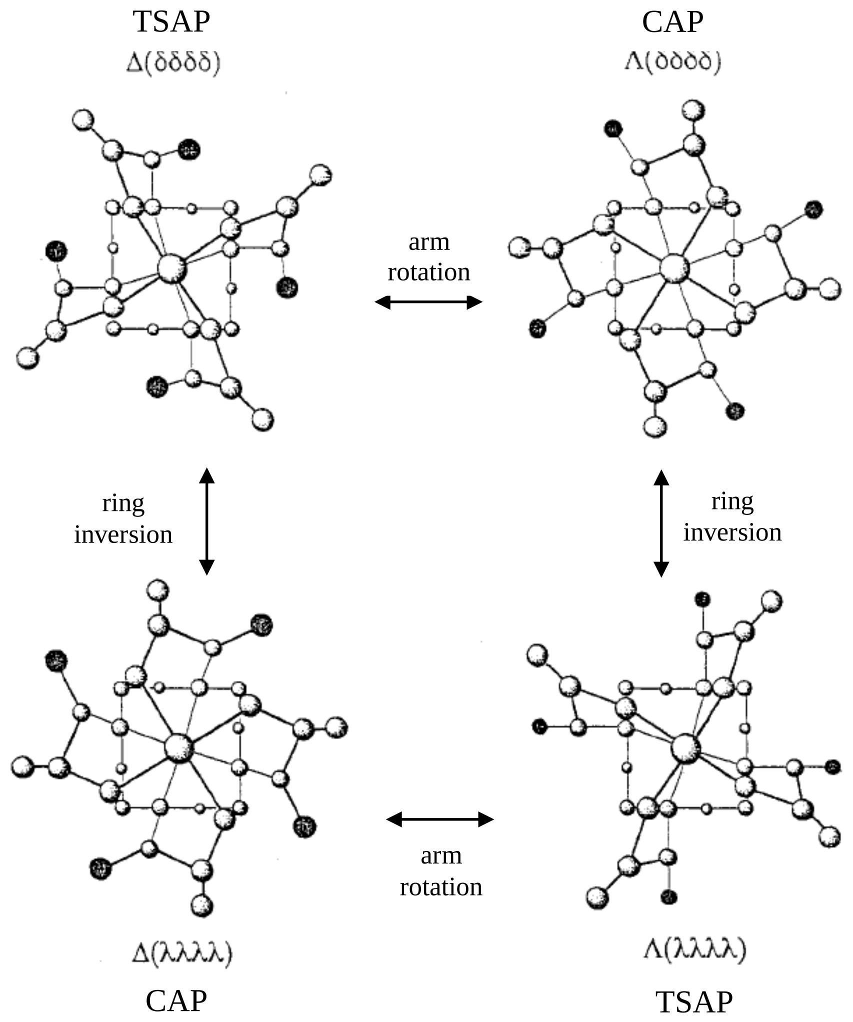

Fig. 3.9 Schematic representation of the two coordination geometry adopted in DOTA complexes: mono-capped square-antiprismatic (CAP) and twisted square-antiprismatic (TSAP) and their interconvertion processes. The DO3A mono-amide complexes normally adopt the CAP configuration (Figure taken from reference [6]).

As noted for the *para*-isomers, the isomeric composition of all the *ortho*-substituted systems did not vary with time. Also, a characteristic pH dependent variation of the ^{19}F chemical shift and of the observed linewidth for each resonance was found, as previously described in Chapter 2. The linewidth variation with pH was different in the case of the cyano complexes, **[LnL^5]**. An increase in $\omega_{1/2}$ was observed not only around pH values corresponding to the pK_a due to the chemical exchange between protonated and non-protonated form, but also in an acidic environment. At pH 5, the line broadening was independent of the Ln(III) ion ($\omega_{1/2} \approx 500$ Hz for Tb, Dy, Ho, Er, Tm at 9.4 T) and for a given metal was independent of the applied field ($\omega_{1/2} \approx$ 550 Hz at both 4.7 and 9.4 T for Tb). The activation energy for the dynamic exchange between two conformers is different for the protonated amide and its conjugate base, the latter probably inhibiting slightly more the rotation of the ring around the C-N bond due to the effect of increased π-conjugation (Fig. 3.10). This hypothesis is consistent with the observed behaviour in the ^{19}F NMR spectra for the **[YL^5]** at basic and acidic pH. As described in section 3.2.2, at pH 5 it appears as a single signal, which resolves to two broad peaks at pH 9.

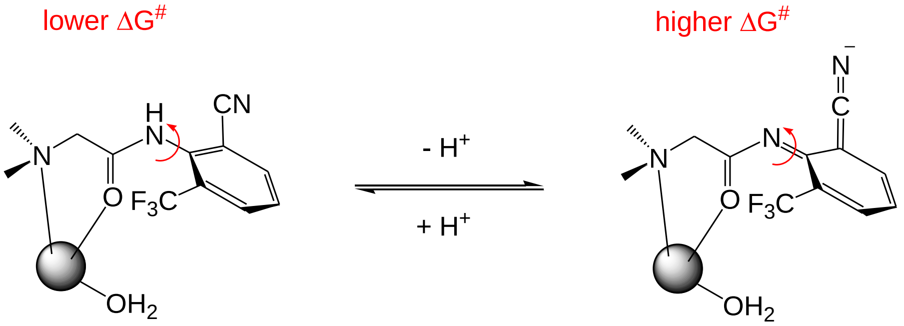

Fig. 3.10 Schematic representation of the effect of π-conjugation in the deprotonated form. This may inhibit the rotation around the C-N bound, leading to different activation energy for the protonated (left) and deprotonated form (right) in **[LnL^5]**.

3.2.3 *o*-Substituted phosphinate analogue: a system of added complexity

The replacement of the carboxylate groups by phosphinates, adds three supplementary chiral centres in the complex, as each P can have an S or R configuration (Fig. 3.11). In theory, 32 isomers are possible[7,8] (because of Δ/Λ, δ/λ and R/S permutations). In practice, one main favoured species was observed in the original investigations of such systems[7,8]. This corresponds to a pair of enantiomers with a twisted square-antiprism geometry (TSAP), Δ/δδδδ or Λ/λλλλ, with the same configuration at each phosphorus centre, *i.e.* enantiomeric RRR/Λ/λλλλ and SSS/Δ/δδδδ isomers were the preferred species[7,8].

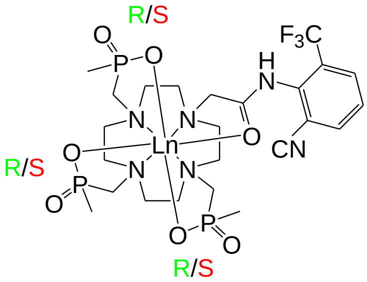

Fig. 3.11 General structure for *ortho*-substituted phopsphinate complexes **[LnL^6]**.

The presence of the second substituent in the *ortho* position on the aromatic ring, introduces a chiral element. The slower rate of rotation of the aryl ring around the C-N bond leads to two isomeric species, as observed for the *ortho* substituted DO3A analogues. Therefore, if the stereogeniticy at P is the same for a given isomer, the four most likely diasteroisomers will be: RRR/Λ/λλλλ-CF_3 up; RRR/Λ/λλλλ-CF_3 down; SSS/Δ/δδδδ-CF_3 up and SSS/Δ/δδδδ-CF_3 down. These diastereoisomers are likely to be present in different relative ratios. Furthermore, the presence of the bulky phosphorus groups, serves to reduce the rate of cooperative arm rotation interchange[9] (Δ/Λ). This may result in sharper resonances.

The observed ^{19}F NMR spectra, for each **[LnL^6]** complex, appeared as four main resonances: two overlapped (often non resolved) with chemical shift very close to that of the protonated ligand (δ_F = - 61.6 ppm). The other two species had large dipolar shifts. **[HoL^6]** for example, at pH 6.8 showed three main resonances at -46.8, -59.6 and -95.5 ppm in the ratio 1:2.7:3.1.

The isomeric composition did not change with time (up to 48 h) in this case and the characteristic pH dependence of chemical shift and linewidth, already described in chapter 2, was observed for the two more shifted resonances, while the peak at -59.6 ppm showed only very small shift changes. Overall, the resonances appeared much sharper than those of the carboxylate analogues, reducing from $\omega_{1/2}$ ~ 800 Hz to $\omega_{1/2}$ ~ 230 Hz (188 MHz for **[HoL^5]** vs **[HoL^6]**).

Variable temperature ^{19}F NMR experiments were performed on **[HoL^6]** at pH 5 and 9 between 278 and 323 K. The two most shifted resonances moved towards each other as the temperature increased, and became slightly narrower at higher temperatures in each case; no coalescence phenomenon was observed in the temperature range under study. It is likely that the activation energy associated with this dynamic exchange process is high and observation of coalescence is beyond the range of temperatures under study, as explained in the previous section (3.2.2).

The hydration state of the phosphinate complex **[TbL^6]** was measured (Table 3.2), using equation 12 (page 84). The q value was 0.02 so that no water molecules are directly coordinated to the metal, as expected for such phosphinate derivatives[2], in which the bulky side arms inhibits approach of a water molecule to the metal centre.

Table 3.2 Measured lifetimes (± 10%) and calculated hydration numbers (± 20%) for **[TbL^6]**.

Complex	τ_{H_2O} (ms)	τ_{D_2O} (ms)	q
[TbL^5]	3.28	4.03	0.02

3.3 ^{19}F relaxation model for Ln(III) complexes and relaxation properties

The relaxation process of a ^{19}F nucleus in a non-viscous solution of a paramagnetic molecule is regulated by five principal mechanisms: chemical shift anisotropy (CSA), inter-nuclear dipole-dipole (DD) interaction, electron-nucleus contact interaction, electron-nucleus dipole-dipole interaction and a special case of the latter one named Curie relaxation.

To describe the ^{19}F relaxation in the specific case of the lanthanide complexes here reported, some simplifications can be introduced. The CSA contribution for a trifluoromethyl group is generally small, and the inter-nuclear dipole-dipole (DD) interaction is negligible compared to the larger electron-nuclear interactions. Together they cannot account for more than 1 Hz, for relaxation rates that are normally of the order of 100 Hz, and therefore they can be neglected. The electron-nucleus contact interaction is not significant on the basis of DFT models which showed an expected value of zero for fluorine nuclei over 5 Å from the metal[10]. The other two mechanisms, electron-nucleus dipole-dipole interaction (equations 18-19) and Curie relaxation (equations 20-21), contribute considerably and are respectively described as follows[11,12] (a simplified version has been presented in Chapter 1):

$$R_1 = \frac{2}{15}\left(\frac{\mu_0}{4\pi}\right)^2 \frac{\gamma_F^2 g_e^2 \mu_B^2 S(S+1)}{r^6}\left(\frac{3\tau_{R+e}}{1+\omega_F^2\tau_{R+e}^2}+\frac{7\tau_{R+e}}{1+\omega_e^2\tau_{R+e}^2}\right) \qquad (18)$$

$$R_2 = \frac{1}{15}\left(\frac{\mu_0}{4\pi}\right)^2 \frac{\gamma_F^2 g_e^2 \mu_B^2 S(S+1)}{r^6}\left(4\tau_{R+e}\frac{3\tau_{R+e}}{1+\omega_F^2\tau_{R+e}^2}+\frac{13\tau_{R+e}}{1+\omega_e^2\tau_{R+e}^2}\right) \qquad (19)$$

$$R_1 = \frac{2}{5}\left(\frac{\mu_0}{4\pi}\right)^2 \frac{\omega_F^2 g_e^4 S^2(S+1)^2}{(3kT)^2 r^6}\frac{3\tau_R}{1+\omega_F^2\tau_R^2} \qquad (20)$$

$$R_2 = \frac{1}{5}\left(\frac{\mu_0}{4\pi}\right)^2 \frac{\omega_F^2 g_e^4 S^2 (S+1)^2}{(3kT)^2 r^6}\left(4\tau_R + \frac{3\tau_R}{1+\omega_F^2\tau_R^2}\right) \qquad (21)$$

where $\tau_{R+e} = (\tau_R^{-1} + T_{1e}^{-1})$ and $T_{1e} = T_{2e}$, τ_R is the rotational correlation time, $T_{1,2}$ the electronic relaxation rates, ω_F the fluorine Larmor frequency, γ_F the fluorine gyromagnetic ratio, μ_B the Bohr magneton, k the Boltzmann constant, g_e the electron g-factor (or Landé factor), $\mu_0/4\pi$ the magnetic permeability of a vacuum, S(S+1) the total electron angular momentum and r is the Ln-fluorine distance.

The combination of these two mechanisms gives the following equations that describe the total relaxation rates:

$$R_1 = \frac{2}{15}\left(\frac{\mu_0}{4\pi}\right)^2 \frac{\gamma_F^2 \mu_{eff}^2}{r^6}\left(\frac{7\tau_{R+e}}{1+\omega_e^2\tau_{R+e}^2} + \frac{3\tau_{R+e}}{1+\omega_F^2\tau_{R+e}^2}\right) + \frac{2}{5}\left(\frac{\mu_0}{4\pi}\right)^2 \frac{\omega_F^2 \mu_{eff}^4}{(3kT)^2 r^6}\frac{3\tau_R}{1+\omega_F^2\tau_R^2} \qquad (22)$$

$$\begin{aligned} R_2 = {} & \frac{1}{15}\left(\frac{\mu_0}{4\pi}\right)^2 \frac{\gamma_F^2 \mu_{eff}^2}{r^6}\left(4\tau_{R+e} + \frac{3\tau_{R+e}}{1+\omega_e^2\tau_{R+e}^2} + \frac{13\tau_{R+e}}{1+\omega_F^2\tau_{R+e}^2}\right) \\ & + \frac{1}{5}\left(\frac{\mu_0}{4\pi}\right)^2 \frac{\omega_F^2 \mu_{eff}^4}{(3kT)^2 r^6}\left(4\tau_R + \frac{3\tau_R}{1+\omega_F^2\tau_R^2}\right) \end{aligned} \qquad (23)$$

where $\mu_{eff}^2 = g_e^2 \mu_B^2 \langle S^2 \rangle$ is the effective magnetic moment of the Ln^{3+} ion and ω_e is the electron Larmor frequency.

Volumetric plots have been produced based on these equations, calculating the ^{19}F longitudinal and transversal relaxation rates R_1 and R_2 as a function of the applied magnetic field (B_0), the rotational correlation time (τ_R) and the distance between the fluorine nucleus and the paramagnetic centre (r). Values of μ_{eff} = 10.0 and T_{1e} = 0.20 ps were used for an idealised complex (Fig. 3.12).

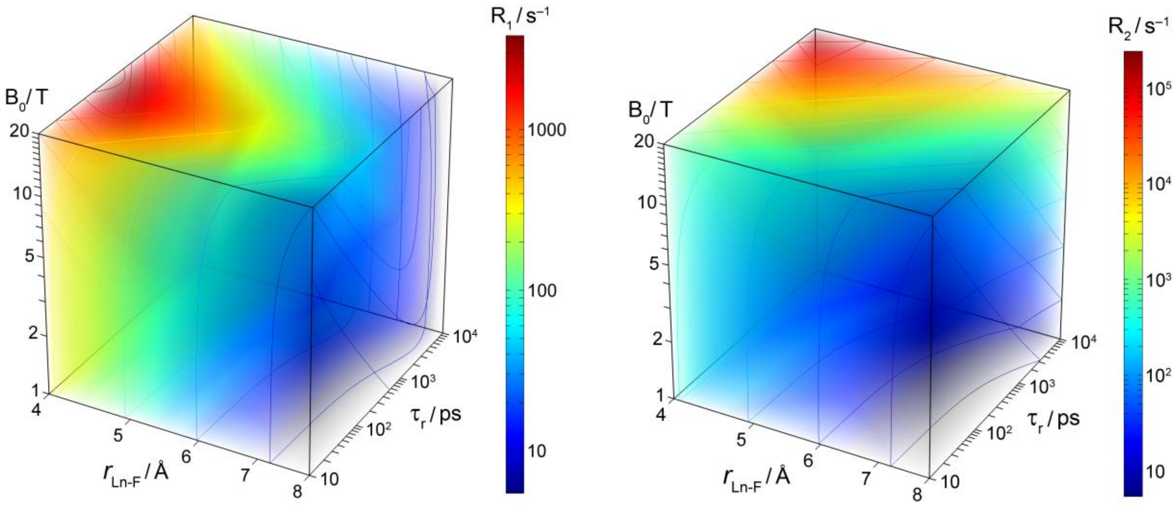

a) b)

Fig. 3.12 Volumetric plots showing a) R_1 and b) R_2 as a function of the applied magnetic field B_0, the rotational correlation time τ_R, and the distance from the lanthanide ion r, for a idealised complex with $\mu_{eff} = 10.0$ and $T_{1e} = 0.20$ ps.

The plots visualise the rapid decrease of R_1 and R_2 with the distance from the Ln(III), as expected from the r^{-6} dependence expressed in equations 22 and 23; R_2 rises with the increase of the correlation time and the field applied.

The correlation between the longitudinal relaxation rate and the ^{19}F-Ln distance expressed in equation 21, allows the latter parameter to be readily calculated by fitting R_1 values recorded at different magnetic fields to the equation[10]. For this purpose ^{19}F longitudinal relaxation times for selected complexes of ligands $\mathbf{L^1}$-$\mathbf{L^5}$ were recorded at four different magnetic fields using the inversion recovery technique (1 mM, D_2O, pD 5.4, 295 K). The large number of data collected allowed a direct global fit to equation 22 to be performed, without any further simplifications. Values of μ_{eff} and τ_R reported in the literature are estimated using the coordinated water protons of Gd complexes, *i.e.* an intermolecular effect. In contrast, in our case there is an intramolecular interaction between the lanthanide ion and the fluorine nuclei. Hence, we calculated μ_{eff} and τ_R directly from the experimental data using a global fitting procedure. Because of the small difference in ionic radius over the series of lanthanide metals under study (Tb, Ho, Er, Tm), r and τ_R were considered global variables, thus the same in each case. The value of μ_{eff} instead was allowed to vary for each lanthanide. The μ_{eff} values estimated from the calculations are listed in Table 3.3, as well as the values reported in the literature. When using the literature values of μ_{eff}, the error in the calculations of the distance r and the correlation time τ_R is smaller, but the measurement may be affected by the approximations used. On the contrary, by allowing calculation of μ_{eff}, the error increases because of the larger number of variables in the computation.

Table 3.3 μ_{eff} values reported in literature and measured from experimental data.

Ln(III)	**Literature**[1]	**Estimated**
Tb	9.7	9.8 ± 1.8
Dy	10.6	10.6 ± 1.9
Ho	10.6	10.4 ± 1.9
Er	9.6	9.1 ± 1.6
Tm	7.6	7.6 ± 1.4

An example of the analysis is reported for the Tb, Ho, Er and Tm complexes of $\mathbf{L^{4a}}$. The experimental R_1 values are reported in Table 3.4 for the two isomers in 1:1 ratio, present in the ^{19}F NMR spectrum (see section 3.2.2).

Table 3.4 ^{19}F Longitudinal relaxation rates (Hz) for $\mathbf{[LnL^{4a}]}$ (295K, pD 5.4, D_2O).

$\mathbf{[LnL^{4a}]}$	**4.7 T**	**9.4 T**	**11.7 T**	**16.5 T**
Tb	149	250	323	565
	100	147	179	192
Ho	91	233	333	588
	71	137	172	313
Er	59	152	20.5	313
	45	88	110	161
Tm	53	100	135	294
	37	56	68	152

The global least square fitting of the data is reported below (Fig. 3.13).

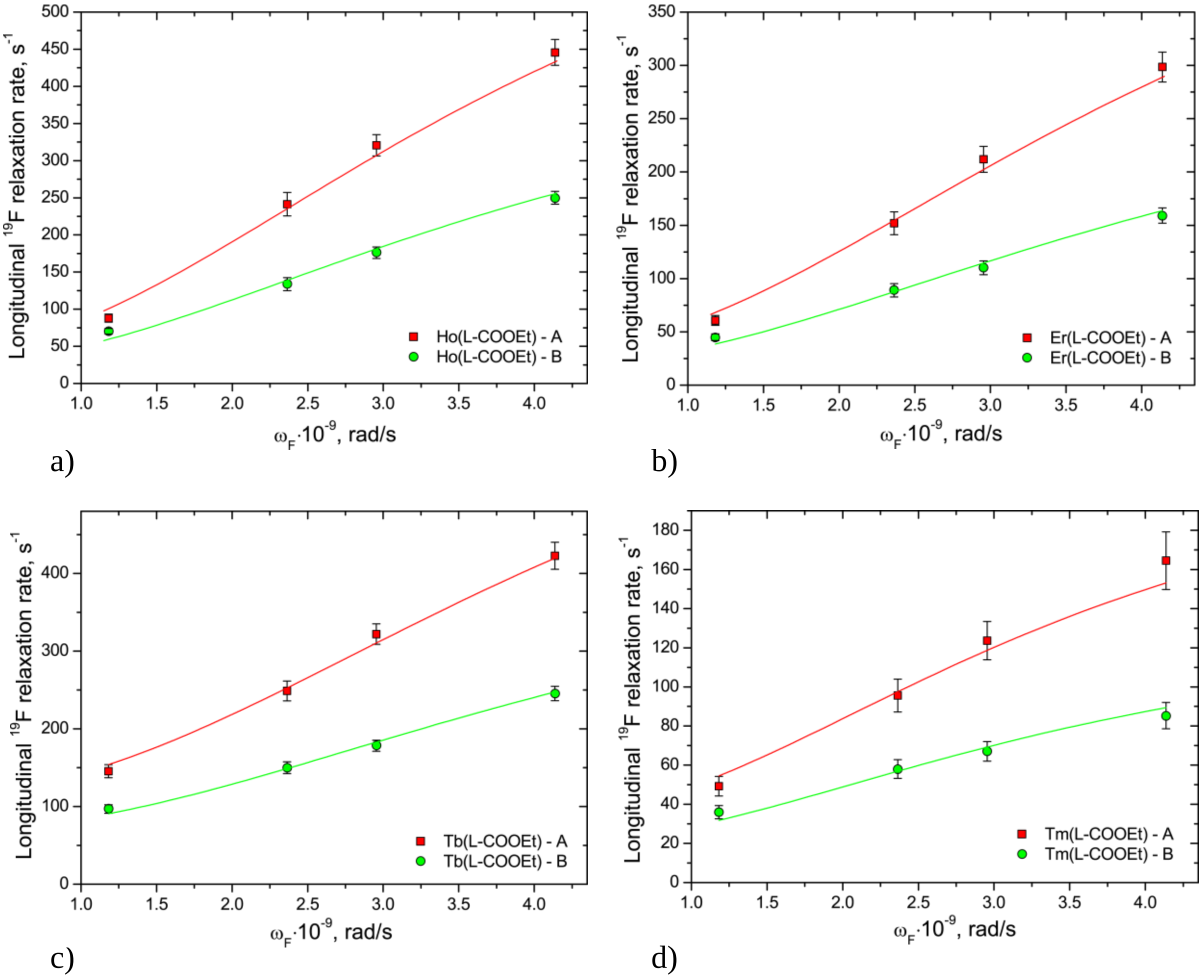

a) b) c) d)

Fig. 3.13 R_1 of the two isomers of **[LnL^{4a}]** as a function of ω_F (4.7, 9.4, 11.7, 16.5 T, D_2O, 1mM, 295 K), showing the global least squares fit (line). a) Ho, b) Er, c) Tb, d) Tm.

The analyses were performed by Dr. Ilya Kuprov at the University of Durham. The r values obtained for the two isomers were 5.7 ± 0.1 Å and 6.3 ± 0.2 Å with τ_R = 270 ± 10 ps. The DFT calculated structures (section 3.2.2) resulted in values of 5.6 Å and 6.2 Å, with an estimated τ_R = 300 ps. Based on the calculated distances of 5.7 and 6.3 Å, a volumetric plot is reported to describe the R_1 variation as a function of μ_{eff} and B_0, using a τ_R = 250 ps and a τ_e = 0.2 ps (Fig. 3.14). The plot shows a noticeable increase of the longitudinal relaxation rate at higher fields for Ho and Er complexes and a smaller change for Tm. Hence, to achieve fast relaxation (R_1) without excessive line broadening (R_2) within the distance range of 5.7 to 6.3 Å, Tb and Dy complexes seem to be the metals of choice for lower magnetic field analyses between 3 and 7 T. Ho and Er look more promising in the medium strength range, 7 to 11.5 T, as for higher fields line broadening intervenes. At fields higher than 11.5 T, Tm seems to be the metal of choice.

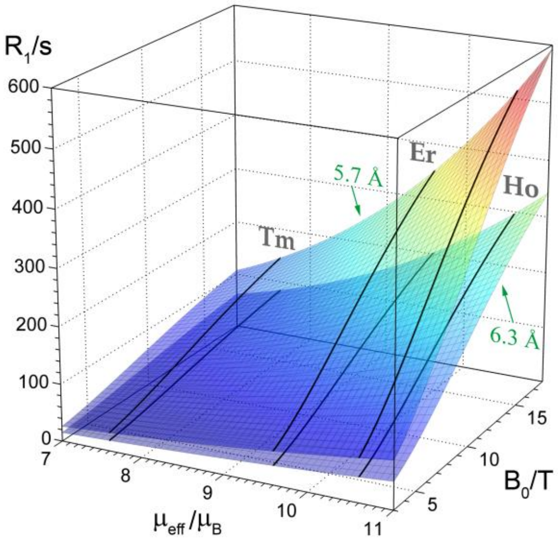

Fig. 3.14 Volumetric plot showing the variation of R_1 as a function of the applied magnetic field B_0, the effective magnetic moment μ_{eff} for r = 5.7 and 6.3 Å. τ_R = 250 ps, τ_e = 0.2 ps.

The calculated Ln-F distances are supported also by independent crystallographic measurements (for crystallographic details see appendix B). The crystal structure of the trisubstituted *para*-ethyl ligand **4** has been obtained (Fig. 3.15). Thanks to the sodium cation positioned at the centre of the macrocycle, which is coordinated to the oxygen and the nitrogen atoms, the macrocycle assumes the same conformation as in the corresponding lanthanide complexes. In the X-ray structure, the CF_3 group is distorted by libration about one of the three fluorine atoms, resulting in partial occupancy of two sites (occupied as 80:20). The nearest distances of the Na^+ ion to the fluorines in the partially occupied sites were 6.05 and 6.14 Å. The ionic radio for the eight coordinated Na^+ ion is 1.32 Å, slightly larger than the value of 1.21 Å for the nine coordinated Ho^{3+} and Y^{3+} [4]. The smaller minimum distances obtained with the sodium ion are consistent with its larger size. This supports the values calculated by fitting of R_1 values to equation 22 and with the computed DFT structures.

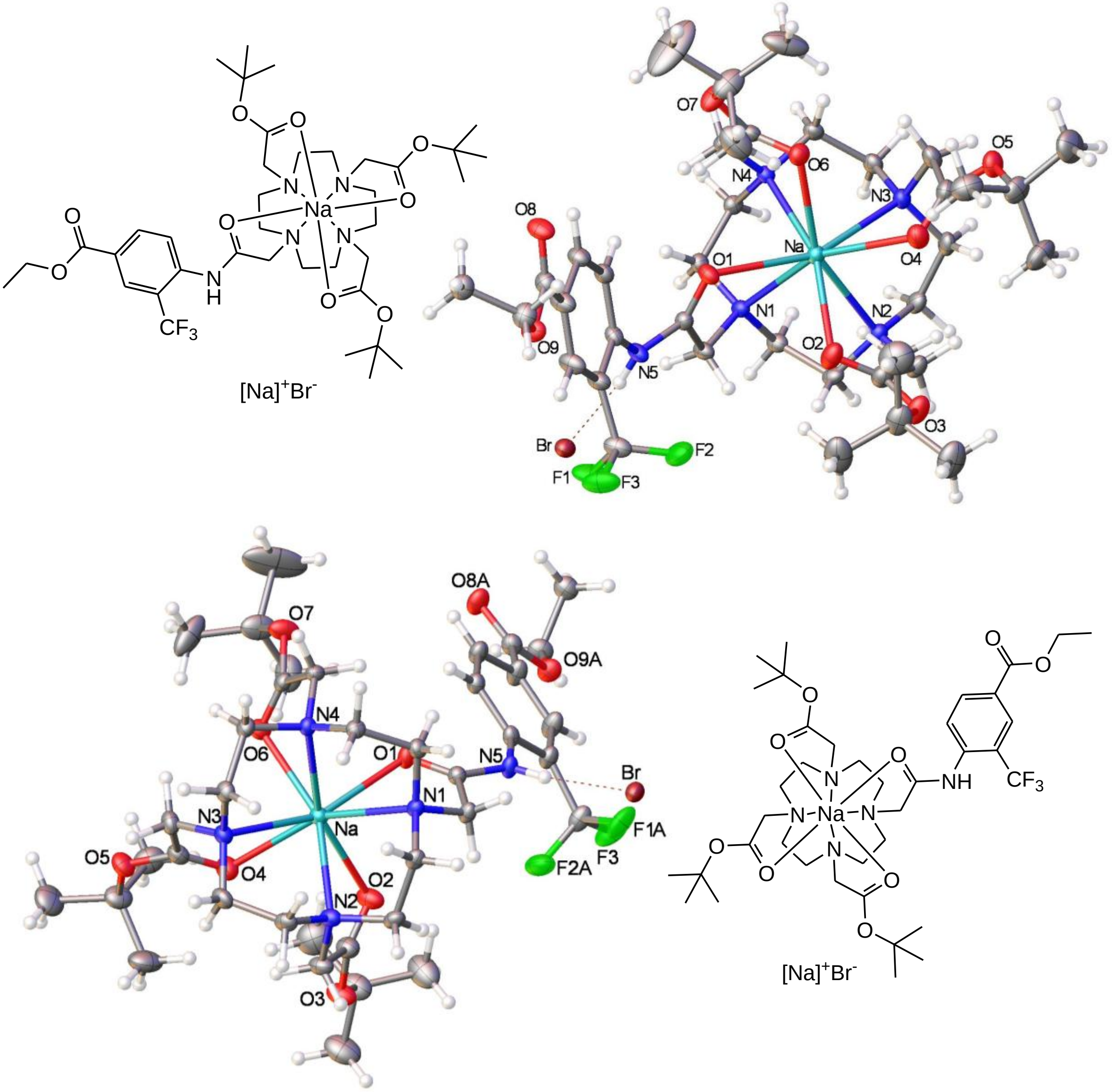

Fig. 3.15 Crystal structure of the trisubstituted *para*-ethyl ligand **4**, containing an octadentate Na^+ ion with bromide as the counter ion, hydrogen-bonded to the amide proton. The two structures are the same molecule seen from above and below (for crystallographic details see appendix B).

The experimental relaxation rates and chemical shift data for selected lanthanide complexes of ligands $\mathbf{L^1}$-$\mathbf{L^6}$ are reported below (Table 3.5-3.12). As expected from the presence of the μ_{eff}^2 and μ_{eff}^4 terms in equations 22 and 23, the relaxation rates follow the order Dy>Tb>Ho>Er>Tm.

For the *para*-substituted complexes **[LnL^1]-[LnL^3]** the longitudinal relaxation rates for a given lanthanide were very similar in each case (Table 3.5-3.6). As discussed in chapter 2, the chemical shift and the linewidth changed with pH. Here, we note also that T_1 varies with pH, following the change in the linewidth. In general, for larger values of $\omega_{1/2}$, smaller values of T_1 are observed and vice versa.

Table 3.5 Longitudinal relaxation times (T_1/s) and chemical shifts (ppm) for **[LnL^{1a}]**.

[LnL^{1a}]	**Tb**	**Dy**	**Ho**	**Er**	**Tm**
δ_F (ppm)	- 49.3	- 53.8	- 48.8	- 62.4	- 78.1
188 MHz	0.014	0.011	0.018	0.034	0.039
376 MHz	0.0080	0.0073	0.0083	0.015	0.022
470 MHz	0.0067	0.0052	0.0063	/	0.018
658 MHz	0.0052	0.0038	0.0042	/	0.014

Table 3.6 Longitudinal relaxation times (T_1/s) and chemical shifts (ppm) for **[LnL^{1b}]**.

[LnL^{1a}]	**Tb**	**Dy**	**Ho**	**Er**	**Tm**
δ_F (ppm)	- 51.2	- 62.3	- 54.6	- 62.0	- 79.9
188 MHz	0.014	0.012	0.020	0.034	0.035
376 MHz	0.0080	0.0066	0.0075	0.015	0.020
470 MHz	0.0066	0.0053	0.0065	/	0.017
658 MHz	0.0050	0.0039	0.0046	/	0.013

Table 3.7 Longitudinal relaxation times (T_1/s), chemical shifts (ppm) and linewidths ($\omega_{1/2}$/Hz) for **[LnL^2]** at pH 5 and 9.

Tb		**δ_F (ppm)**	**$\omega_{1/2}$ (Hz)**	**T_1 (s)**
188 MHz	pH 9	- 26.4	366	0.013
	pH 5	- 50.2	73	/
376 MHz	pH 9	- 26.7	513	0.0076
	pH 5	- 50.0	128	/
Dy		**δ_F (ppm)**	**$\omega_{1/2}$ (Hz)**	**T_1 (s)**
188 MHz	pH 9	- 59.0	700	0.012
	pH 5	- 65.5	74	/
Ho		**δ_F (ppm)**	**$\omega_{1/2}$ (Hz)**	**T_1 (s)**
188 MHz	pH 9	- 38.1	340	0.019
	pH 5	- 55.0	31	0.025
376 MHz	pH 9	- 41.0	403	0.011
	pH 5	- 56.8	73	0.010
Er		**δ_F (ppm)**	**$\omega_{1/2}$ (Hz)**	**T_1 (s)**
188 MHz	pH 9	- 73.8	118	0.030
	pH 5	- 64.7	63	/
376 MHz	pH 9	- 74.6	277	0.014
	pH 5	- 64.8	74	/
Tm		**δ_F (ppm)**	**$\omega_{1/2}$ (Hz)**	**T_1 (s)**
188 MHz	pH 9	- 90.0	277	0.026
	pH 5	- 77.5	45	0.057
376 MHz	pH 9	- 89.6	442	0.017
	pH 5	- 77.8	43	0.033

Table 3.8 Longitudinal relaxation times (T_1/s), chemical shifts (ppm) and linewidths ($\omega_{1/2}$/Hz) for **[LnL^3]** at pH 5 and 9.

Tb		**δ_F (ppm)**	**$\omega_{1/2}$ (Hz)**	**T_1 (s)**
188 MHz	pH 9	- 33.1	190	0.012
	pH 5	- 50.1	60	0.016
376 MHz	pH 9	- 32.9	480	0.0072
	pH 5	- 50.0	130	0.0096
Ho		**δ_F (ppm)**	**$\omega_{1/2}$ (Hz)**	**T_1 (s)**
188 MHz	pH 9	- 42.5	125	0.020
	pH 5	- 55.4	45	0.024
376 MHz	pH 9	- 42.4	332	0.0084
	pH 5	- 55.4	72	0.011
Er		**δ_F (ppm)**	**$\omega_{1/2}$ (Hz)**	**T_1 (s)**
188 MHz	pH 9	- 72.2	95	0.029
	pH 5	- 64.1	39	0.040
376 MHz	pH 9	- 72.3	130	0.014
	pH 5	- 64.2	52	0.018
Tm		**δ_F (ppm)**	**$\omega_{1/2}$ (Hz)**	**T_1 (s)**
188 MHz	pH 9	- 87.6	99	0.028
	pH 5	- 78.2	36	0.058
376 MHz	pH 9	- 87.8	153	0.017
	pH 5	- 78.2	41	0.034

The *ortho*-substituted complexes of **L^{4a}** and **L^5** showed different relaxation rates for the two isomers (Table 3.9-3.11), consistent with their different position with respect to the metal centre, as previously discussed. In the case of the *ortho*-acid analogue **[LnL^{4b}]** the two isomers possess similar values of R_1 (Table 3.10), evident in particular at lower fields, consistent with the presence of a lower energy dynamic exchange process between the two species in solution that have been already described (section 3.2.2, page 86).

Table 3.9 Longitudinal relaxation times (T_1/s), chemical shifts (ppm) and linewidths ($\omega_{1/2}$/Hz) for **[LnL^{4a}]** at pH 5 and 9.

Tb		**δ_F (ppm)**	**$\omega_{1/2}$ (Hz)**	**T_1 (s)**
188 MHz	pH 9	- 19.6/- 81.5	203/148	0.010/0.0068
	pH 5	- 39.3/- 89.0	89/125	0.010/0.0067
376 MHz	pH 9	- 19.7/- 81.5	598/284	0.0067/0.0039
	pH 5	- 39.3/- 88.9	120/182	0.0068/0.0040
470 MHz	pH 5	//	175/385	0.0056/0.0031
658 MHz	pH5	//	/	0.0034/0.0018
Ho		**δ_F (ppm)**	**$\omega_{1/2}$ (Hz)**	**T_1 (s)**
188 MHz	pH 9	- 32.0/- 72.8	332/320	0.015/0.010
	pH 5	- 46.8/- 80.8	260/262	0.014/0.011
376 MHz	pH 9	- 31.7/- 73.2	326/268	0.0077/0.0042
	pH 5	- 47.1/- 80.5	104/162	0.0073/0.0043
470 MHz	pH 5	//	175/385	0.0057/0.0026
658 MHz	pH5	//	/ /588	0.0032/0.0017
Er		**δ_F (ppm)**	**$\omega_{1/2}$ (Hz)**	**T_1 (s)**
188 MHz	pH 9	- 49.5/- 75.8	105/95	0.016/0.022
	pH 5	- 46.4/- 66.6	93/69	0.017/0.022
376 MHz	pH 9	- 49.5/- 75.8	164/169	0.0064/0.012
	pH 5	- 46.4/- 66.7	133/86	0.0066/0.011
470 MHz	pH 5	//	213/110	0.0057/0.0026
658 MHz	pH5	//	313/162	0.0032/0.0062
Tm		**δ_F (ppm)**	**$\omega_{1/2}$ (Hz)**	**T_1 (s)**
188 MHz	pH 9	- 38.8/- 101.6	116/128	0.015/0.021
	pH 5	- 36.8/- 90.4	87/70	0.019/0.027
376 MHz	pH 9	- 38.7/- 101.7	156/306	0.0078/0.014
	pH 5	- 36.8/- 90.4	109/76	0.010/0.018
470 MHz	pH 5	//	135/68	0.0074/0.015
658 MHz	pH5	//	/ /147	0.0035/0.0077

Table 3.10 Longitudinal relaxation times (T_1/s), chemical shifts (ppm) and linewidths ($\omega_{1/2}$/Hz) for **[LnL^{4b}]** at pH 5 and 9.

Tb		**δ_F (ppm)**	**$\omega_{1/2}$ (Hz)**	**T_1 (s)**
188 MHz	pH 5	- 42.1/- 89.8	/	0.0099/0.012
376 MHz	pH 5	- 41.1/- 89.2	485/622	0.0060/0.0063
470 MHz	pH 5	//	/	0.0042/0.0037
658 MHz	pH5	//	/	0.0036/0.0031
Ho		**δ_F (ppm)**	**$\omega_{1/2}$ (Hz)**	**T_1 (s)**
188 MHz	pH 9	- 45.3/- 79.3	371/392	0.015/0.014
	pH 5	- 46.4/- 79.3	377/530	0.015/0.016
376 MHz	pH 9	- 45.4/- 79.1	404/655	0.0071/0.0072
	pH 5	- 47.1/- 80.5	/	0.0071/0.0070
470 MHz	pH 5	//	/	0.0045/0.0040
658 MHz	pH5	//	/	0.0036/0.0029
Er		**δ_F (ppm)**	**$\omega_{1/2}$ (Hz)**	**T_1 (s)**
188 MHz	pH 9	- 45.7/ - 67.1	460/258	0.026/0.027
	pH 5	- 45.9/- 66.6	542/263	0.026/0.026
376 MHz	pH 9	- 46.0/- 67.1	572/293	0.011/0.011
	pH 5	- 45.9/- 66.6	565/250	0.011/0.012
470 MHz	pH 5	//	/	0.0071/0.0080
658 MHz	pH5	//	/	0.0047/0.0054
Tm		**δ_F (ppm)**	**$\omega_{1/2}$ (Hz)**	**T_1 (s)**
188 MHz	pH 9	- 35.4/- 89.3	220/280	0.029/0.031
	pH 5	- 35.4/- 88.9	425/351	0.039/0.034
376 MHz	pH 9	- 36.0/- 89.5	389/303	0.018/0.018
	pH 5	- 36.1/- 89.0	435/275	0.017/0.018
470 MHz	pH 5	//	/	0.004/0.0091
658 MHz	pH5	//	/	0.0016/0.0063

The values in brackets for **[LnL^5]**, refer to data for the third and fourth species when present (Table 3.11). One of the species exhibits longer longitudinal relaxation times and a smaller pseudocontact shift compared to the other species. This is probably related to the particular position of the CF_3 group in this isomer with respect to the lanthanide ion.

Table 3.11 Longitudinal relaxation times (T_1/s), chemical shifts (ppm) and linewidths ($\omega_{1/2}$/Hz) for **[LnL^5]** at pH 5 and 9.

Tb		**δ_F (ppm)**	**$\omega_{1/2}$ (Hz)**	**T_1 (s)**
188 MHz	pH 9	- 3.9/- 73.1 (- 68.4)	192/232 (173)	0.0091/0.0081 (0.0071)
	pH 5	- 40.6/- 84.6 (- 57.4)	670/505 (82)	0.0091/0.0090 (0.047)
376 MHz	pH 9	- 4.0/- 73.1 (- 68.3)	240/270 (216)	0.0077/0.0037 (0.0035)
	pH 5	- 40.5/- 84.6 (- 57.5)	631/560 (140)	0.0061/0.0052 (0.028)
Dy		**δ_F (ppm)**	**$\omega_{1/2}$ (Hz)**	**T_1 (s)**
188 MHz	pH 9	2.5/- 76.0 (- 63.1/- 77.8)	281/272 (178/92)	0.0085/0.0079 (0.0051/0.024)
	pH 5	- 59.3/- 109.9 (- 78.0)	465/515 (98)	0.0089/0.0078 (0.043)
376 MHz	pH 9	3.3/- 75.5 (- 63.0/- 78.0)	351/334 (258/151)	0.0055/0.0039 (0.0027/0.021)
	pH 5	- 59.3/- 110.1 (- 78.3)	536/578 (157)	0.0053/0.0045 (0.022)
Ho		**δ_F (ppm)**	**$\omega_{1/2}$ (Hz)**	**T_1 (s)**
188 MHz	pH 9	- 25.6/- 68.8	196/212	0.013/0.012
	pH 5	- 48.8/- 78.1 (- 61.0)	745/419 (93)	0.013/0.013 (0.061)
376 MHz	pH 9	- 26.9/- 69.3 (- 61.1)	310/302 (102)	0.0077/0.0042 (0.027)
	pH 5	- 49.5/- 78.9 (- 61.8)	562/513 (167)	0.0065/0.0061 (0.027)
Er		**δ_F (ppm)**	**$\omega_{1/2}$ (Hz)**	**T_1 (s)**
188 MHz	pH 9	- 53.1/- 81.5 (- 58.3)	281/190 (74)	0.016/0.019 (0.097)
	pH 5	- 49.6/- 67.6 (- 58.2)	423/453 (94)	0.023/0.023 (0.098)

376 MHz	pH 9	- 53.2/- 81.5 (- 53.7/- 58.2)	422/210 (489/95)	0.0084/0.0096 (0.0076/0.043)
	pH 5	- 49.5/- 67.4 (- 58.1)	420/387 (91)	0.010/0.011 (0.044)
Tm		**δ_F (ppm)**	**$\omega_{1/2}$ (Hz)**	**T_1 (s)**
188 MHz	pH 9	- 39.9/- 109.0 (- 41.2/- 63.9)	417/195 (118/101)	0.014/0.012 (0.013/0.14)
	pH 5	- 39.0/- 88.1 (- 63.7)	444/419 (99)	0.022/0.024 (0.12)
376 MHz	pH 9	- 39.9/- 109.0 (- 41.2/- 63.9)	238/208 (149/103)	0.0073/0.0092 (0.0057/0.071)
	pH 5	- 38.9/- 88.2 (- 63.7)	405/468 (131)	0.013/0.015 (0.058)

For the phosphinate complexes **[LnL^6]**, faster longitudinal relaxation rates and smaller linewidths were generally observed, but with differences among the isomers in solution (Table 3.12). Different behaviours for each isomer was already observed for **[LnL^5]**. Also for **[LnL^6]** we observe a resonance with a relatively slow relaxation time, only slightly shifted from the ligand position, as for **[LnL^5]**.

The substitution of the carboxylate arms with the bulky phosphinate analogues, results in the inhibition of the cooperative arm rotation rigidifying the system and therefore reducing the linewidth associated with this exchange process. The faster longitudinal relaxation rate can be attributed to a shorter distance between the CF_3 group and the metal, in this series of complexes, consistent with the more compact structure for this eight coordinate (q = 0) system.

Table 3.12 Longitudinal relaxation times (T_1/s), chemical shifts (ppm) and linewidths ($\omega_{1/2}$/Hz) for **[LnL^6]** at pH 5 and 9.

Tb		**δ_F (ppm)**	**$\omega_{1/2}$ (Hz)**	**T_1 (s)**
188 MHz	pH 9	- 62.3/- 90.6	87/75	0.31/0.0076
	pH 5	- 52.1/- 62.7/- 98.5	149/160/77	0.012/0.50/0.0060
376 MHz	pH 9	- 62.4/- 90.5	71/142	0.41/0.0042
	pH 5	- 52.3/- 62.7/- 98.4	366/281/131	0.0077/0.38/0.0038
Ho		**δ_F (ppm)**	**$\omega_{1/2}$ (Hz)**	**T_1 (s)**
188 MHz	pH 9	- 26.3/- 62.0/- 87.3	102/111/87	0.0090/0.39/0.0071
	pH 5	- 61.6/- 62.4/- 106.4	101/99/83	0.019/0.038/0.0075
376 MHz	pH 9	- 26.4/- 62.1/- 62.3/- 87.2	253/231/283/185	0.0046/0.32/0.22/0.0039
	pH 5	- 61.7/- 62.4/- 106.3	595/218/170	0.0056/0.064/0.0041
Tm		**δ_F (ppm)**	**$\omega_{1/2}$ (Hz)**	**T_1 (s)**
188 MHz	pH 9	-16.5/- 62.3/- 133.6	82/45/102	0.0064/1.07/0.030
	pH 5	- 1.2/- 62.3/- 106.4	73/127/61	0.0077/0.54/0.026
376 MHz	pH 9	-16.5/- 62.4/- 134.5	145/52/397	0.0036/0.23/0.012
	pH 5	- 1.0/- 62.4/- 106.9	170/232/184	0.0047/0.27/0.015

3.4 ^{1}H NMR relaxation studies of Gd complexes

The gadolinium complexes of the ligands discussed in this work can be used as conventional contrast agents for proton MRI, thanks to their ability to increase the relaxation rate of the water protons. Hence, the proton relaxation properties of some examples have been studied.

The capability of a contrast agent to enhance the water proton relaxation rates is called relaxivity (r_1), when referred to a unit concentration of the agent. The observed relaxation rate (R_{1obs}) of the water protons in the presence of a Gd complex is the sum of diamagnetic R_{1d} and paramagnetic contributions R_{1p}:

$$R_{1obs} = R_{1d} + R_{1p} \qquad (24)$$

The paramagnetic contribution is proportional to the concentration of the paramagnetic species in solution (Equation 25) and is formed by contributions from inner sphere water molecules R_1^{is}, which are directly coordinated to the metal, the second sphere water molecules R_1^{ss}, which form interactions through hydrogen bonding, and the outer sphere R_1^{os}, which form a layer of diffusing water molecules around the complex (Equation 26):

$$R_{1obs} = R_{1d} + r_1[Gd] \qquad (25)$$

$$R_{1obs} = R_{1d} + R_1^{is} + R_1^{ss} + R_1^{os} \qquad (26)$$

The inner sphere contribution is given by equation 27:

$$R_{1p}^{is} = \frac{Cq}{55.5}\left(\frac{1}{T_{1m}^{H} + \tau_m}\right) \qquad (27)$$

where C is the concentration in mM of the Gd complex, q is the number of bound water molecules, τ_m is the water residence lifetime at the Gd and T_{1m}^{H} is the longitudinal relaxation time of the coordinated water protons[13]. The latter is described by the following equation:

$$\frac{1}{T_{1m}^{H}} = \frac{2}{15}\left(\frac{\mu_0}{4\pi}\right)^2 \frac{\gamma_H^2 g^2 \mu_B^2 S(S+1)}{r_{GdH}^6}\left(\frac{3\tau_{c1}}{1+\omega_H^2\tau_{c1}^2} + \frac{7\tau_{c2}}{1+\omega_s^2\tau_{c2}^2}\right) \qquad (28)$$

where γ_H is the gyromagnetic ratio for proton, g the electron g-factor, μ_B the Bohr magneton, S the electron spin magnetic number, r_{GdH} the distance between Gd and the inner sphere water proton, ω_H and ω_S the Larmor frequency for the proton and the electron, and τ_{ci} (i = 1, 2) the correlational times relative to the electron-proton dipolar coupling[13]. The latter can be modulated by the rotational correlation time τ_R, the residence lifetime of the water on the metal ion τ_m and the electronic relaxation times T_{ie} (i = 1,2).

$$\frac{1}{\tau_{ci}} = \frac{1}{\tau_R} + \frac{1}{T_{ie}} + \frac{1}{\tau_m} \qquad (29)$$

For Gd complexes, T_{1e} and T_{2e} are interpreted in terms of the zero field splitting interaction (ZFS) as described in equation 30 and 31, which are known as the Bloembergen-Morgan theory of paramagnetic electron-spin relaxation.

$$\left(\frac{1}{T_{1e}}\right)^{ZFS} = \frac{2\Delta^2\tau_v\{4S(S+1)-3\}}{50}\left(\frac{1}{1+\omega_s^2\tau_v^2} + \frac{4}{1+4\omega_s^2\tau_v^2}\right) \qquad (30)$$

$$\left(\frac{1}{T_{2e}}\right)^{ZFS} = \frac{\Delta^2\tau_v\{4S(S+1)-3\}}{50}\left(3+\frac{5}{1+\omega_s^2\tau_v^2} + \frac{2}{1+4\omega_s^2\tau_v^2}\right) \qquad (31)$$

where Δ^2 is the mean-square zero field splitting energy and τ_v is the correlation time for the ZFS modulation.

The outer sphere term describes the contribution of the diffusion of water molecules near the paramagnetic complex. It is described by the Freed model and for small paramagnetic complexes can be expressed in the simplified form:

$$R_{1p}^{os} = C^{os}\left(\frac{1}{aD}\right)\left[7J(\omega_S) + 3J(\omega_H)\right] \qquad (32)$$

where C^{os} is a constant (5.8 x 10^{-13} $s^{-2}M^{-1}$), a is the minimum distance between the water molecules and the metal, D the diffusion coefficient and the dependence on the electronic relaxation times is expressed as $J(\omega_i)$ which is the non-Lorentzian spectral density function.

For low molecular weight Gd complexes of the type reported herein, the most significant contribution is the inner sphere mechanism[13].

Proton relaxation analysis of **[GdL^{4a}]** and of **[GdL^{4b}]** were performed at the University of Piemonte Orientale in Alessandria, and the fitting to the experimental data was undertaken by Professor Mauro Botta. The relaxivity was recorded as a function of pH, over the range 2.5 to 11.5, and did not show any appreciable variation for each complex, confirming the high stability with respect to metal dissociation of mono-amide DO3A analogues. The relaxivity profile as a function of the applied magnetic field strength was recorded between 0.01 and 70 MHz, allowing computation of the rotational correlation times τ_R. The shape of the curve is consistent with fast values of τ_R in each case. Variable temperature ^{17}O NMR R_{2p} studies recorded at 9.4 T, allowed an estimate of water exchange lifetimes τ_m to be made, by fitting the temperature dependence to a classical Swift-Connick approximation[14]. The fast water exchange rate is consistent with the decrease of relaxivity with increasing temperature. The plots and the extrapolated data for **[GdL^{4a}]** and **[GdL^{4b}]** are reported below (Fig. 3.16 and 3.17, Table 3.13).

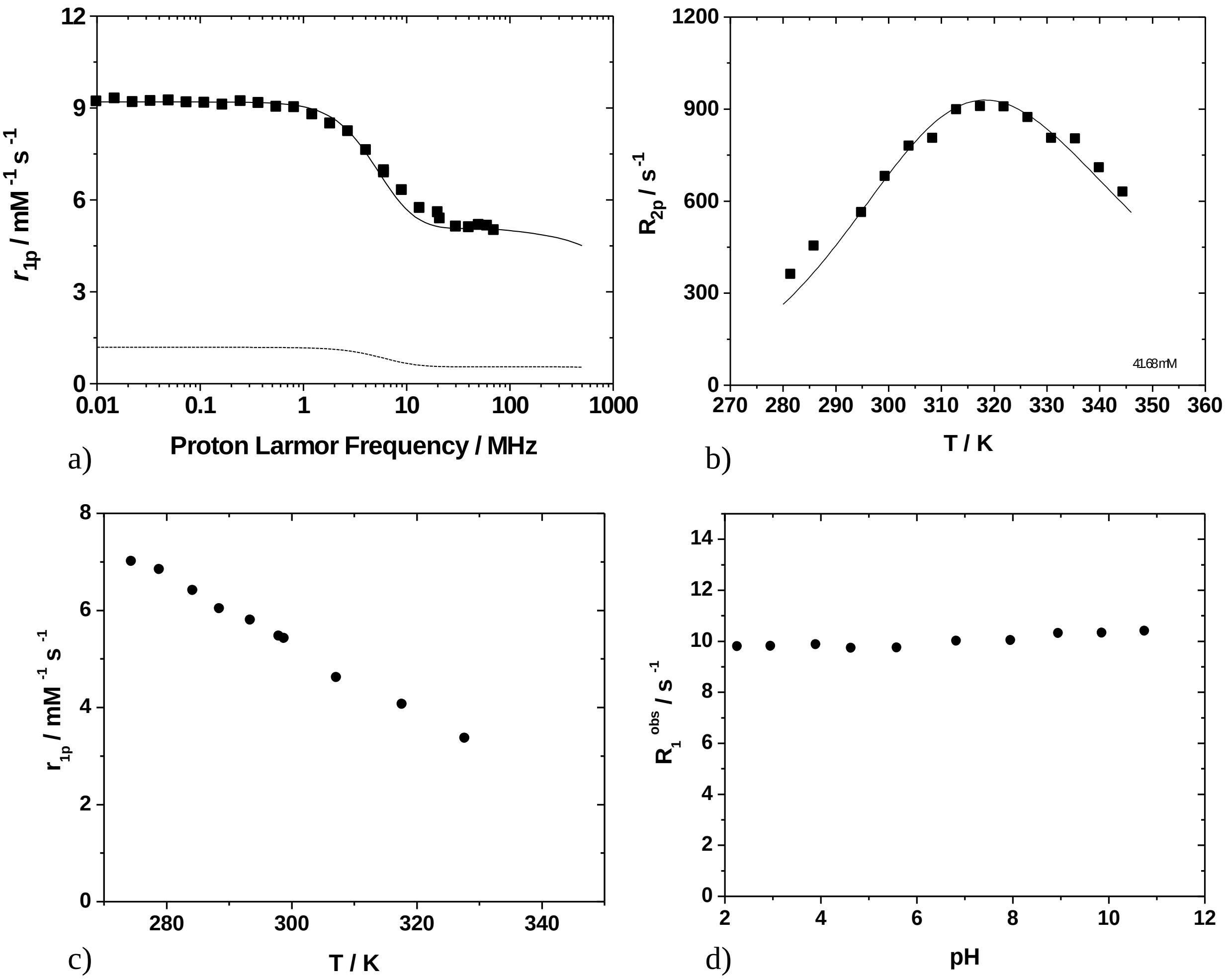

Fig. 3.16 Relaxivity studies for **[GdL^{4a}]** a) 1/T_1 NMRD profile. b) Variable temperature ^{17}O NMR R_{2p}. c) Relaxivity as function of temperature. d) Relaxivity as function of pH.

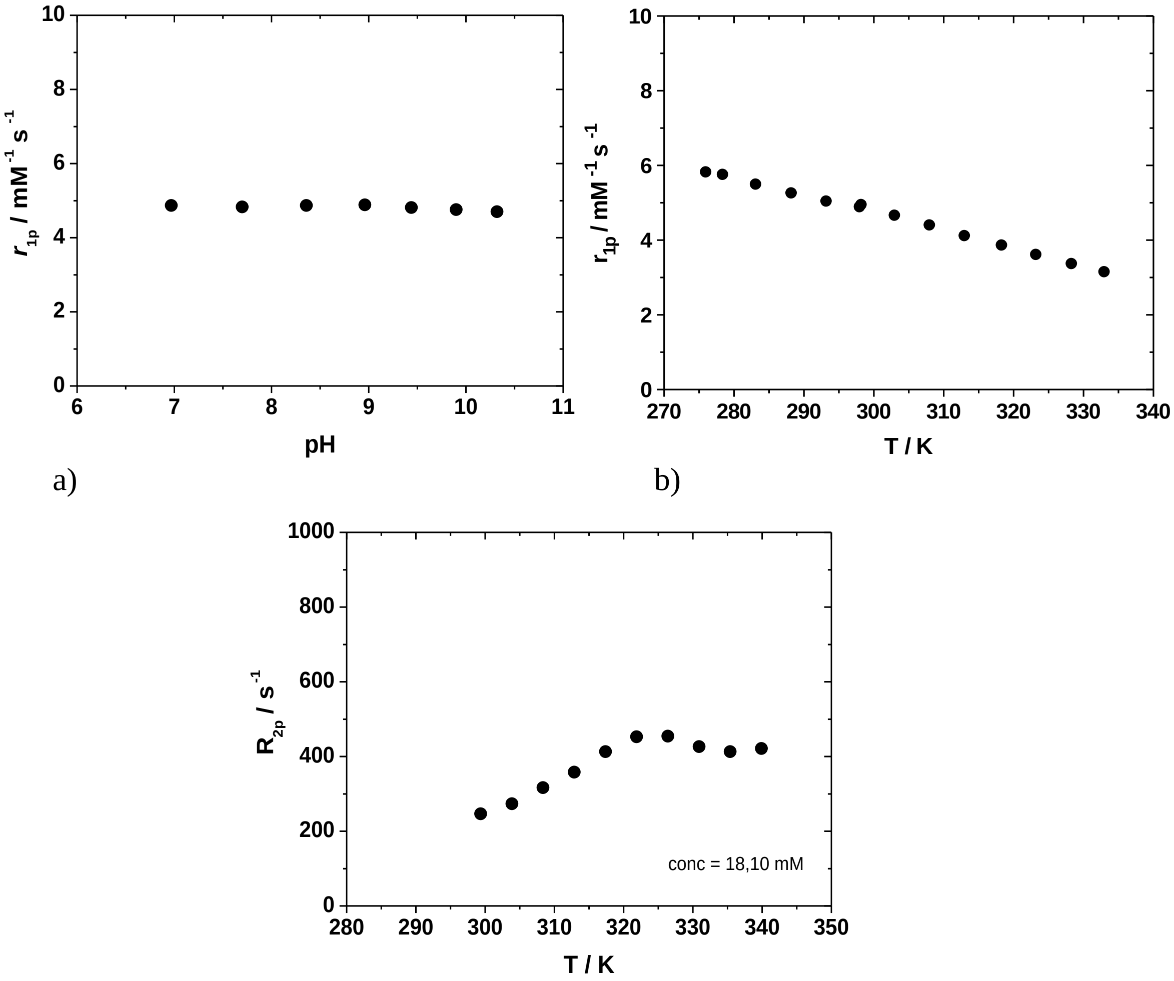

a)

b)

c)

Fig. 3.17 Relaxivity studies for **[GdL^{4b}]** a) Relaxivity as function of pH. b) Relaxivity as a function of temperature. c) Variable temperature ^{17}O NMR R_{2p}.

Small differences were observed in the parameters obtained for the *ortho* ethyl ester and the carboxylate complexes. The τ_R value and the relaxivity of the ester analogue were slightly higher than for the acid. These changes suggest a small variation in the second sphere of hydration.

Table 3.13 Relaxation parameters of **[GdL^{4a}]** and **[GdL^{4b}]** (298 K) obtained from analysis of VT ^{1}H relaxivity, ^{17}O NMR and fitting of NMRD profiles[a].

Parameter	**[GdL^{4a}]**	**[GdL^{4b}]$^{-}$**
r_{1p} (mM^{-1} s^{-1})	5.40	4.95
τ_m (μs)	0.57	0.93
τ_R (ps)	81	81
τ_v (ps)	15	13
$\Delta^2 \times 10^{19}$ (s^{-2})	6.3	6.3
q	1	1
q”	2	2

[a] The Gd-H distance for the coordinated water molecule r, and the outer sphere water molecules a, were fixed to 3.0 and 4.0 Å and the relative diffusion coefficient D to 2.24×10^{-5} cm^2 s^{-1} (298 K).

Probably, this is related to different ability of the amide NH to form hydrogen bonds to nearby water molecules in the case of the ester **[GdL^{4a}]** or the acid complexes **[GdL^{4b}]**. The presence of the substituent in *ortho*-position is likely to influence the hydrogen bond formation, by acting as competitive acceptors. The oxygen of the C=O group in the ester complex **[GdL^{4a}]**, can form a six membered ring by hydrogen bonding with the amide proton. The same can happen for the carboxylate analogue **[GdL^{4b}]**, with a stronger interaction due to its negative charge. Hence, in the latter case the amide proton is already involved in hydrogen bonding with the carboxylate anion, therefore suppressing its interaction with second sphere water molecules (Fig. 3.18).

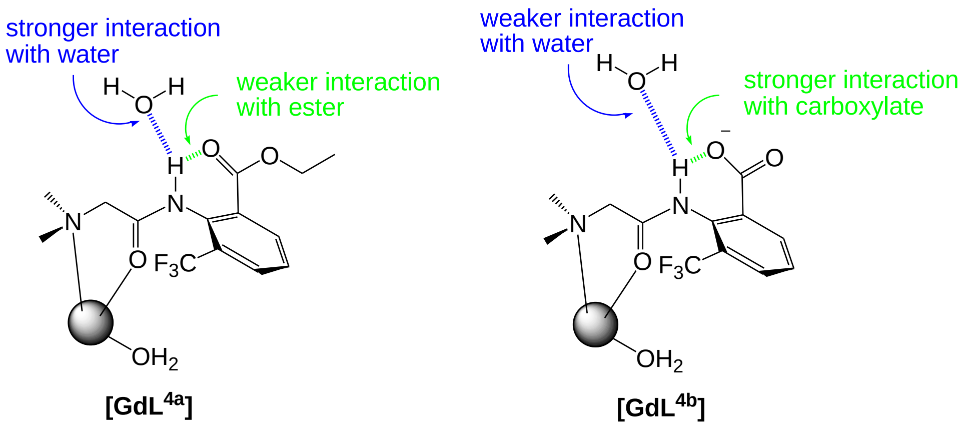

Fig. 3.18 Schematic representation of the different interaction of the amidic proton with the second sphere water molecules in **[GdL^{4a}]** and **[GdL^{4b}]**.

3.5 Conclusions

The spectroscopic and relaxation properties of a series of fluorinated lanthanide complexes have been discussed, as well as their conformational exchange processes. The distance of the CF_3 group with respect to the lanthanide ion has been calculated to be between 5.7 and 6.3 Å. This has been confirmed by DFT calculations and by single crystal X-ray diffraction. The proximity of the fluorine to the lanthanide ion allows an increase of the longitudinal relaxation rate R_1 leading to faster signal acquisition, but a balance is needed with the parallel increase of R_2 which causes line broadening. Between 5.7 and 6.3 Å, Tb and Dy complexes are most favourable at lower magnetic fields (3 to 7 T), while Er and Ho seem to have fast relaxation with 'reasonable' linewidths in the range 7 to 11.5 T. Above 11.5 T, the resonances broaden considerably. Tm complexes can be used at higher fields (>11.5 T) without excessive line broadening.

The substitution of the carboxylate pendant arms with phosphinate analogues, led to narrower linewidths because of increased rigidity of the structure. A faster longitudinal relaxation rate was also found due to the shorter distance of the CF_3 group to the metal ion.

The relaxivity analysis of the Gd complexes of $\mathbf{L^{4a}}$ and $\mathbf{L^{4b}}$, showed small changes in the second sphere of hydration due to a competitive hydrogen bonding mechanism in the case of the carboxylate.

References

[1] E. Bovens, PhD thesis, Delft University of Technology, **2001**.

[2] A. Beeby, I. M. Clarkson, R. S. Dickins, S. Faulkner, D. Parker, L. Royle, A. S. de Sousa, J. A. G. Williams, M. Woods, *J. Chem. Soc. Perkin Trans. 2*, **1999**, 493.

[3] K. D. Zimmer, R. Shoemaker, R. R. Ruminski, *Inorg. Chim. Acta*, **2006**, *359*, 1478.

[4] R. D. Shannon, *Acta Crystallogr. A*, **1976**, *32*, 751.

[5] P. Caravan, J. J. Ellison, T. J. McMurry, R. B. Lauffer, *Chem. Rev.*, **1999**, *99*, 2293.

[6] D. Parker, R. S. Dickins, H. Puschmann, C. Crossland, J. A. K. Howard, *Chem. Rev.*, **2002**, *102*, 1977.

[7] S. Aime, M. Botta, D. Parker, J. A. G. Williams, *J. Chem. Soc. Dalton Trans*, **1995**, 2259.

[8] S. Aime, M. Botta, R. S. Dickins, C. L. Maupin, D. Parker, J. P. Riehl, J. A. G. Williams, *J. Chem. Soc. Dalton Trans.*, **1998**, *0*, 881.

[9] S. Aime, A. S. Batsanov, M. Botta, J. A. K. Howard, D. Parker, K. Senanayake, J. A. G. Williams, *Inorg. Chem.*, **1994**, *33*, 4696.

[10] K. H. Chalmers, E. De Luca, N. H. M. Hogg, A. M. Kenwright, I. Kuprov, D. Parker, M. Botta, J. I. Wilson, A. M. Blamire, *Chem. Eur. J.*, **2010**, *16*, 134.

[11] I. Bertini, F. Capozzi, C. Luchinat, G. Nicastro, Z. Xia, *J. Phys. Chem.*, **1993**, *97*, 6351.

[12] I. Bertini, C. Luchinat, G. Parigi, *Prog. Nucl. Mag. Res. Sp.*, **2002**, *40*, 249.

[13] A. Sigel, H. Sigel, *The Lanthanides and Their Interrelations with Biosystems Vol. 40*, Chapter 14, Marcel Dekker, University of Basel, Switzerland, **2003**.

[14] T. J. Swift, R. E. Connick, *J. Chem. Phys.*, **1962**, *37*, 307.

Chapter 4

Enzyme reporters

4.1 Introduction

The enhanced sensitivity of the fluorine nucleus to changes in the microenvironment, produced by its proximity to a lanthanide ion in a stable complex (see Chapter 1), is exploited here to prepare responsive probes that can report enzyme activity. The introduction in the complex structure of a particular functional group that can be recognised as a substrate by the enzyme, can lead to the modification of the probe structure after enzyme catalysed transformation. This modification can be signalled by variation of the chemical shift or of the relative signal intensity of the fluorine resonance in the ^{19}F NMR spectrum.

4.2 Synthesis

A series of DO3A mono-amide complexes has been synthesised, bearing different ester groups in the *para* or *ortho* positions on the aromatic ring. The complexes **[HoL^{1a}]** and **[HoL^{4a}]** were prepared according to the procedure described in Chapter 2, where an ethyl ester group is introduced at the beginning of the synthetic route. Alternatively, the synthesis of the other complexes described here followed the scheme shown below (Scheme 4.1), where the ester group was introduced in the final stage, by reacting the *para* or *ortho* acid complexes, **[HoL^{1b}]** and **[HoL^{4b}]**, with the appropriate alkyl halide. The different substituted esters were obtained by an S_N2 reaction, using the commercially available chloro- or bromo-methyl derivative, in DMSO, using K_2CO_3 as base.

In each case, the reaction did not reach completion, leaving ~20% of unreacted starting acid complex. The presence of a small amount of by-product was also observed, caused by concomitant alkylation at the amide nitrogen, as confirmed by mass spectral analysis. Different conditions were attempted in order to limit the formation of the bialkylated product, but without complete success. Purification of the desired material was possible with reverse phase HPLC.

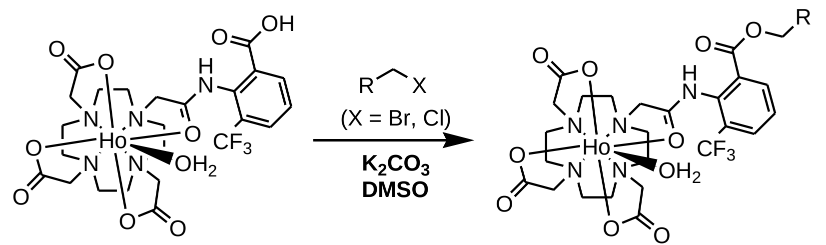

[HoL^{4b}]

L^8 R = $OCOCH_3$
L^9 R = $OCOCH_2CH_2CH_3$
L^{10} R = $OCOOCH_2CH_3$
L^{11} R = $PhOCOCH_3$
L^{12} *para* R = $PhOCOCH_3$

Scheme 4.1 General synthetic scheme for the preparation of **L^8-L^{12}**.

In the case of **[HoL^{10}]**, the reactive α-chloroester **66** was previously prepared by reaction of chloromethyl chloroformate with ethanol in dichloromethane and pyridine, to give a colourless liquid[1]. Subsequent reaction followed the general procedure discussed above, using DMSO-d_6 as solvent to allow direct NMR analysis (Scheme 4.2). The reaction was followed by ^{19}F NMR and mass spectrometry which confirmed the formation of the product. The α-chloromethyl ester itself was stable over two days in deuterated DMSO, but after isolation and dissolution in water, it hydrolysed rapidly, leaving only starting material. Attempt to perform the analogous reaction using 1-chloroethyl ethyl carbonate was unsuccessful, possibly because of the steric hindrance created by the presence of the methyl group next to the chlorine.

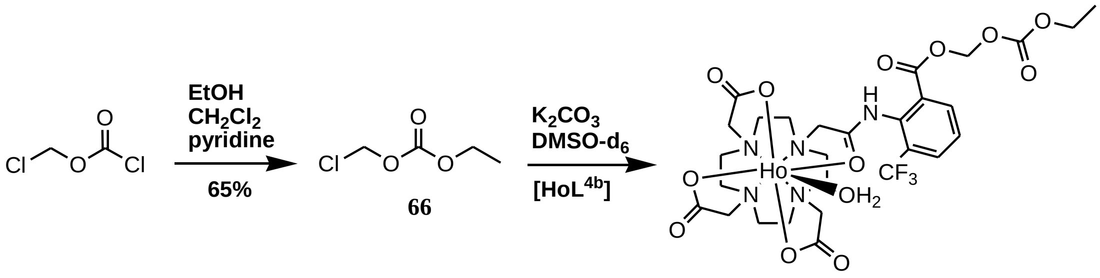

[HoL^{10}]

Scheme 4.2 Synthesis of **[HoL^{10}]**.

4.3 Enzyme studies

The carboxyester moiety was introduced into the complex structure with the purpose of being used as an enzyme substrate. Esterases should recognise this functional group and catalyse its hydrolysis to yield the corresponding carboxylic acid. Owing to the ability of the lanthanide ion to amplify the chemical shift variation associated with changes in the chemical environment, it was hypothesised that we would be able to differentiate the two species readily. Their difference in chemical shift should be as great as possible to facilitate monitoring of the reaction. The fast fluorine longitudinal relaxation rate allowed an increase in signal intensity by reducing the spectral acquisition time. Analysis at higher magnetic fields, leads to a parallel increase of the transverse relaxation time, characterised by line broadening. The best compromise was found using holmium complexes at a magnetic field of 4.7 or 9.4 T, under conditions that allow a fast relaxation with a reasonable linewidth, with respect to the other lanthanide ions considered, *i.e.* Tb, Er, Tm and Dy.

The first compound analysed was **[HoL^{1a}]**, which contains a simple ethyl ester in the *para* position of the aromatic ring. It shows a single ^{19}F peak in the NMR spectrum with a δ_F = -56.3 ppm (linewidth ~102 Hz) at pH 7.4. The corresponding acid form appears at δ_F = -57.1 ppm (linewidth ~56 Hz), giving a chemical shift difference of 0.8 ppm. Upon enzymatic hydrolysis, we should observe the acid peak appearing in the spectrum with a concomitant reduction in the intensity of the corresponding ester peak. Although physiological conditions were maintained to ensure optimal enzyme activity, better separation between the two species can be observed by measuring the spectrum at higher pH values. A maximum chemical shift non-equivalence of 6.5 ppm was noted at pH 9 (Fig. 4.1). Therefore, NMR analyses could be performed at this higher pH, where appropriate.

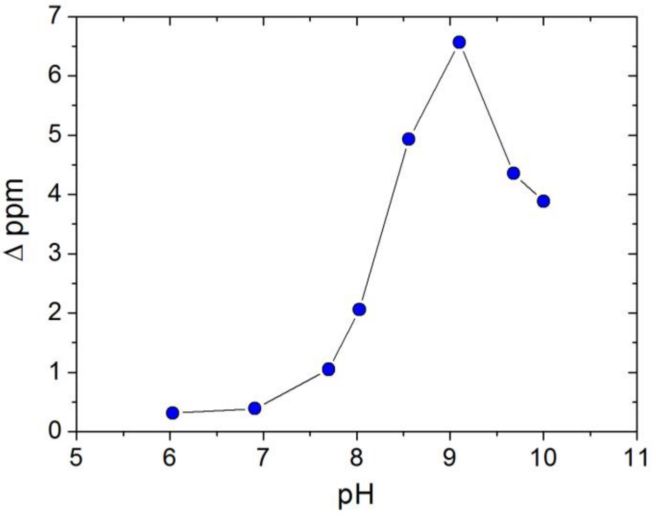

Fig. 4.1 Chemical shift difference between the fluorine resonances of **[HoL^{1a}]** and **[HoL^{1b}]** as a function of pH.

The enzymes selected for our studies were pig liver esterase (PLE) and α-chymotrypsin. These are common esterases that catalyse hydrolysis of various ester groups to yield the corresponding carboxylic acids. For each enzyme, the same experiment was performed using 10 μmoles of **[HoL^{1a}]** dissolved in 0.8 ml of PBS solution at pH 7.4. To half of the sample was added the lyophilised enzyme (5 mg, 75 units), while the other half was used as a control. The two samples were kept at 25°C and ^{19}F NMR spectra (188 MHz) were recorded at regular intervals. To lock the NMR instrument a coaxial insert containing D_2O was used. The sample containing the enzyme showed, as expected, a decrease in the signal intensity of the ester resonance, while a new signal corresponding to the carboxylic acid formed (Fig. 4.2). The control sample remained unchanged over the length of the experiment, confirming the enzymatic catalysis of hydrolysis and, therefore, the recognition of the complex as a substrate. The reaction proceeded to a limit when 50% of the ester had been hydrolysed. The same behaviour was observed either using PLE or α-chymotrypsin. The process, however, occurred over a period of more than one week; hence it was far too slow for a possible application. Performing the same experiment at 37°C gave similar results, with a doubling of reaction rate.

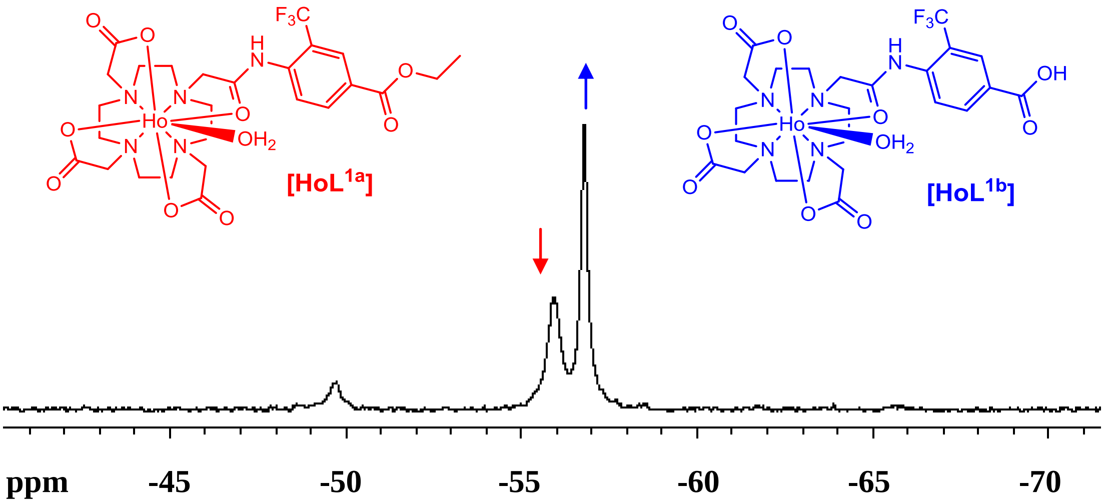

Fig. 4.2 ^{19}F NMR spectrum of **[HoL^{1a}]** after addition of PLE (25°C, 188 MHz, PBS, pH 7.4, D_2O insert) showing the presence of the corresponding acid **[HoL^{1b}]** produced by enzymatic hydrolysis.

The second compound analysed was **[HoL^{4a}]**, the *ortho* analogue of the previous example, which was prepared to evaluate the effect that a different position of the substituent on the aromatic ring may have on the enzyme activity. The ^{19}F NMR spectrum of the complex showed the presence of two resonances in 1:1 ratio with a large chemical shift difference of more than 30 ppm. This separation was ascribed to the presence in solution of two isomeric structures, bearing the CF_3 group in different positions with respect to the metal centre. As discussed in Chapter 3, these isomers correspond to rotamers, attributed to the restricted rotation of the aromatic ring around the CN bond.

The corresponding acid form **[HoL^{4b}]**, appeared in the spectrum as two different ^{19}F signals but in 1:3 ratio, with similar δ_F values to the ester but with larger linewidths. The chemical shift difference between the acid and the ester resonances was ~2 ppm for the major resonance, but the significant linewidth of the acid signal, 377 Hz (major) and 530 Hz (minor), somewhat inhibited spectral discrimination. It was possible to monitor enzymatic hydrolysis by following the change in the ratio and the linewidth of the two resonances. The same experiment described above was performed for **[HoL^{4a}]** using PLE and α-chymotrypsin at 25ºC. Surprisingly, no hydrolysis was observed in either case. Even after incubation at 37ºC, no signs of hydrolysis were visible. A possible explanation is that the ester carbonyl group in the *ortho* position is more sterically crowded compared to the *para* isomer, thus inhibiting approach to the enzymatic active site. A control experiment was carried out without enzyme leaving the sample in a KOH solution at pH 10 heating at 50°C, over one week. The chemical hydrolysis was observed through the variation of the signal intensity of the ^{19}F resonances, passing from a 1:1 ratio to a 1:3 ratio.

Following these observations, it was decided to introduce a small spacer between the aromatic ring and the ester group, in order to make the ester carbonyl group more exposed and facilitate its contact with the enzyme active site. The *ortho* position was maintained to exploit the greater chemical shift difference between the two fluorine resonances.

For example, **[HoL^{8}]** contains a simple acetoxymethyl group linked to the acid. These esters are known to be good substrates for intracellular esterases, and have been used over many years to mask negatively charged compounds; once inside the cells such compounds are readily hydrolysed[2] (Scheme 4.3).

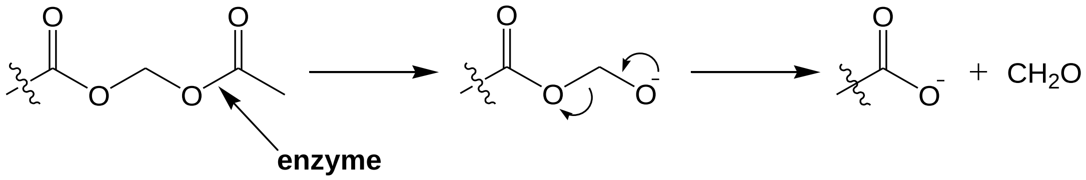

Scheme 4.3 Mechanism of cleavage of the acetoxymetyl group upon enzymatic hydrolysis.

The complex **[HoL^8]** showed the presence of more than one isomer in the ^{19}F NMR spectrum. One main signal was observed at δ_F = -47.4 ppm, with another resonance at δ_F = -55.2 ppm in the ratio 2.4 to 1. The presence of a bulkier group may have modified the geometry of the complex, resulting in two resonances closer to each other and in different proportion with respect to the ethyl ester. The acid complex peaks were at δ_F = -49.2 ppm and δ_F = -82.2 ppm in 3:1 ratio, giving a chemical shift difference of 1.8 ppm between the main signal of the two species. Transformation of **[HoL^8]** was undertaken using PLE, monitoring spectral changes at 376 MHz and 25°C. A decrease in ^{19}F signals of the ester was observed with a parallel increase in intensity of resonances corresponding to the acid (Fig. 4.3). The enzymatic nature of the catalysis was confirmed by the absence of change in the control, lacking the enzyme. Hence, the introduction of a methylene bridge facilitates formation of the enzyme-substrate complex. The enzymatic hydrolysis did not proceed to completion, but reached a limit (~50% conversion) after ~40 h (at 37°C), after which no further hydrolysis was observed. Complete cleavage was reached after three weeks, when chemical hydrolysis intervened. The kinetics of this reaction offered a slightly improvement compared to **[HoL^{1a}]**, especially when performed at 37°C, but was still too slow for practical application.

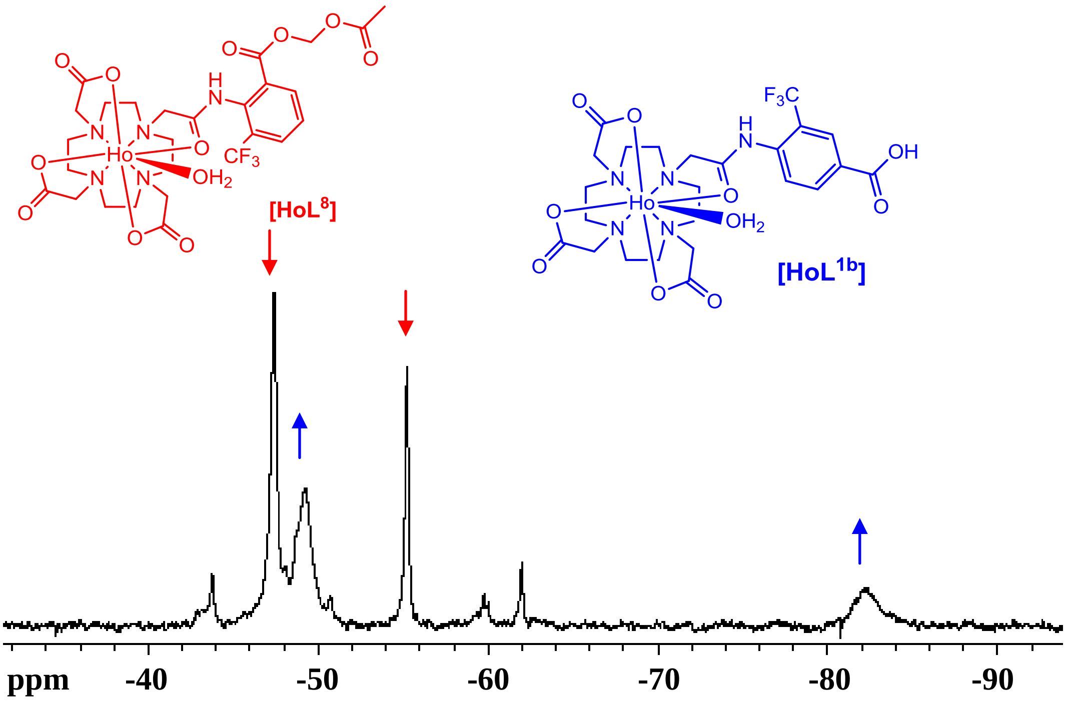

Fig. 4.3 ^{19}F NMR spectrum of **[HoL^8]** after addition of PLE (25°C, 376 MHz, PBS, pH 7.4, D$_2$O insert) showing the presence of the corresponding acid **[HoL^{1b}]** produced by enzymatic hydrolysis.

Two other substrate variations were considered. First, in the compound **[HoL^9]**, a propyl group was introduced instead of a methyl group, in an attempt to enhance the affinity of the substrate for the enzyme active site. Compared to **[HoL^8]**, no improvement was observed in the rate of reaction, upon incubation of the complex with PLE, either at 25 or 37°C. Second, in **[HoL^{10}]** a methyl ethyl carbonate ester[1] was introduced. This is a more labile group, which was investigated with the purpose of accelerating the enzyme cleavage. Unfortunately, the compound was unstable in water, therefore inhibiting enzyme experiments.

Another example of a cleavable spacer incorporates a 'self immolative' benzyl group, linked in the *para* position to the inverted ester[3], which in our case corresponded to an acetoxy group, **[HoL^{11}]**.

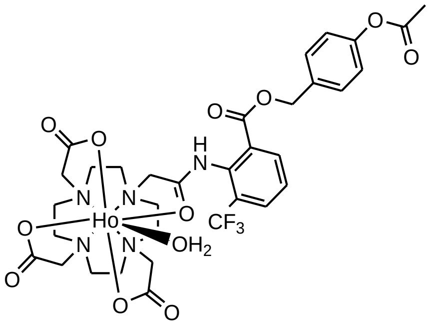

[HoL^{11}]

Upon enzymatic deacetylation, the linker spontaneously decomposes, releasing the free acid (Scheme 4.4).

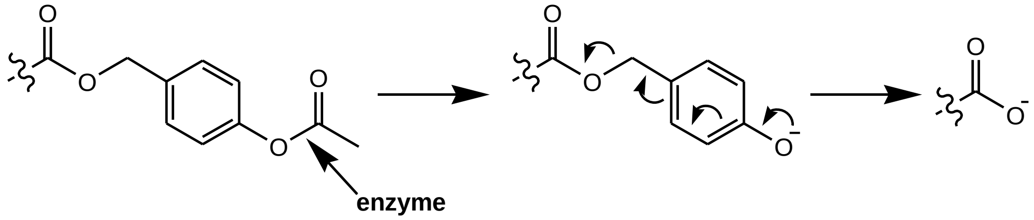

Scheme 4.4 Cleavage mechanism of the self-immolative spacer upon enzymatic hydrolysis in **[HoL^{11}]**.

This type of linker is often used as a pro-drug for different pharmaceuticals, in order to reduce their toxicity and to improve the control of their release *in vivo*. They are also used to link multiple drugs together for delivery of synergic therapies[4]. Previous published examples employed a variety of analogues of the linker, mostly incorporating an amino or amide group at one or both ends of the linker[5,6] Recently, the use of ester groups on either side of the spacer has been reported[3] (Fig. 4.4).

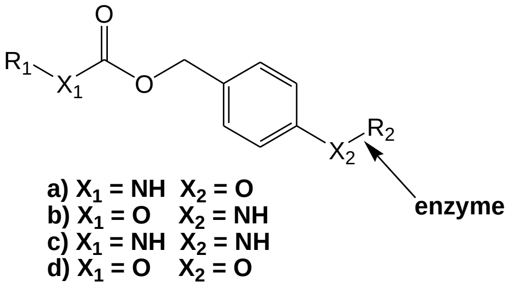

Fig. 4.4 Different self-immolative spacers. a) [5]. b) [6]. c) [4]. d) [3].

The ester **[HoL^{11}]** was stable in water and the ^{19}F NMR spectrum revealed a main signal at -47.1 ppm and two minor resonances at -48.5 and -49.8 ppm in 4.4:1:1 ratio. In the presence of PLE, a variation in the signal intensity of the fluorine resonances was observed. The minor peak at δ_F = -49.8 ppm disappeared completely within 29 h, accompanied over the same time interval by a slightly slower decrease in the signal intensity of the major species. This reached a maximum value, after which no further hydrolysis was noted up to 9 days (25°C). When performing the same experiment at 37°C the first transformation occurred in less than 2 h, and the limiting spectrum was obtained by 50 h. The resulting spectrum did not correspond to that expected for the acid product **[HoL^{4b}]**. Mass spectral and LC-MS analyses indicated that the enzymatic hydrolysis did not produce the acid compound as expected, but an intermediate phenol in which only the acetoxy group had been cleaved, as indicated in Scheme 4.5. The acetoxy group was therefore recognised and hydrolysed by the enzyme, but the remaining part of the linker did not fragment via the expected self-immolative cleavage.

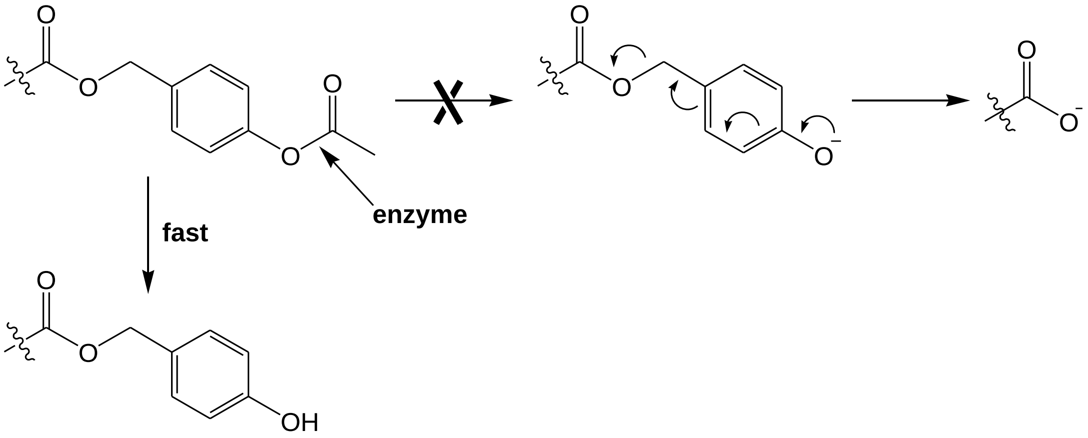

Scheme 4.5 Cleavage mechanism for **[HoL^{11}]** showing the phenolic intermediate produced after incubation with PLE or α-chymotripsin.

The same behaviour was observed with α-chymotrypsin at 25°C, but with different kinetic profiles. In this case the minor peak at -49.8 ppm, disappeared within 120 h and the major peak at -47.1 ppm decreased slowly, reaching a plateau after 170 h with a higher level of transformation (10% more than with PLE), as illustrated in Fig. 4.5.

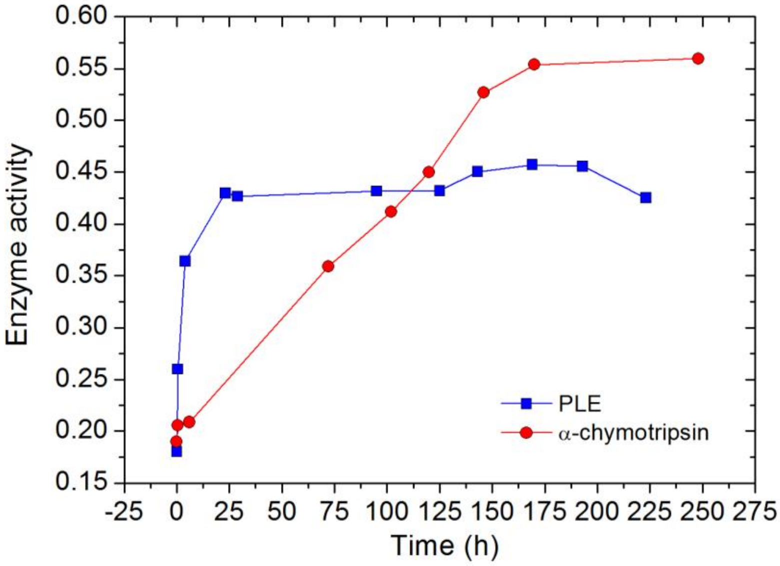

Fig. 4.5 Enzyme activity profile for **[HoL^{11}]** with PLE and α-chymotripsin. The activity is reported as the ratio of the intensity of the invariant peak at δ_F = -48.5 ppm to the intensity of the major peak at δ_F = -47.1 ppm .

The same self-immolative linker was also introduced in the *para* ester position, yielding **[HoL^{12}]**, to study any possible variation on enzymatic kinetics. The fluorine spectrum of **[HoL^{12}]** showed a major resonance at -50.8 ppm and minor signals at -48.9, -49.4 and -52.0 ppm, in the ratio 2.6:1.7:1.2:1 respectively. A decrease of the signal intensity for the peaks at δ_F = -49.4 and -52.0 ppm was observed within 22 h. Also, in this case, the spectrum did not correspond to the acid product expected (**[HoL^{1b}]** single signal at δ_F = -57.1 ppm). LC-MS data confirmed the presence of the phenolic intermediate, as had occurred with **[HoL^{11}]**.

A control experiment has been undertaken for both **[HoL^{11}]** and **[HoL^{12}]** leaving the two complexes stirring in a solution of KOH at pH 10 for two weeks. The ^{19}F NMR was then recorded. In each case, only the corresponding carboxylic acid product was observed, as proof that, under conditions of chemical hydrolysis, the linker undergoes the expected cleavage. The failure of these self immolative linkers to undergo complete cleavage under the experimental conditions, may be related to product inhibition of enzyme activity induced by the intermediate phenol.

4.4 Conclusions

The preliminary studies presented in this chapter have allowed the proof of principle to be established. The feasibility of following an enzymatic reaction using ^{19}F NMR has been assessed, by examining the change in signal intensity of the resonances of paramagnetic fluorinated complexes.

The series examined proved the need for careful design of probe structure, as small changes in the structure led to large variations in the enzyme response, as observed for the *para* and *ortho* ethyl esters **[HoL^{1a}]** and **[HoL^{4a}]**. The first underwent catalytic hydrolysis by the esterases, while the *ortho* analogue was too sterically hindered to be a good substrate. Improvements were noted with the introduction of a cleavable linker, which presumably allows easier access to the enzyme active site. The self-immolative approach adopted for **[HoL^{11}]** and **[HoL^{12}]** did not give the expected results, but modifications to the spacer could lead to better performance. Changing the spacer would enable the use of different enzyme families which would increase the range of possible applications. One possible substrate is shown below, that may act as a probe for protease activity (Fig.4.6):

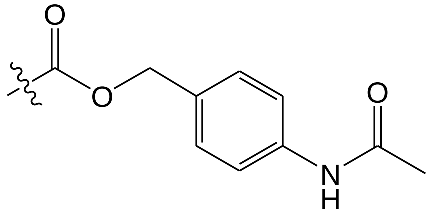

Fig.4.6 Example of self-immolative spacer that can be used for future probes.

Further work could then focus on synthesising new probes with optimised structures and spacers, in order to screen the activity of new enzymes.

References

[1] J. D. Thomas, K. B. Sloan, *Tetrahedron Lett.*, **2007**, *48*, 109.
[2] M. Giardiello, M. P. Lowe, M. Botta, *Chem. Commun.*, **2007**, 4044.
[3] H. Y. Lee, X. Jiang, D. W. Lee, *Org. Lett.*, **2009**, *11*, 2065.
[4] K. Abu Ajaj, M. L. Biniossek, F. Kratz, *Bioconjugate Chem.*, **2009**, *20*, 390.
[5] J. A. Duimstra, F. J. Femia, T. J. Meade, *J. Am. Chem. Soc.*, **2005**, *127*, 12847.
[6] Y. Meyer, J. A. Richard, B. Delest, P. Noack, P. Y. Renard, A. Romieu, *Org. Biomol. Chem.*, *8*, 1777.

Chapter 5

Chitosan conjugates

5.1 Introduction

Low sensitivity is a key issue in all the classical NMR experiments. For ^{19}F MRI, characterised by the absence of endogenous background, the signal intensity of a fluorinated probe is primarily related to the concentration of equivalent fluorine nuclei and to their relaxation rates. Possible strategies to improve the signal to noise ratio are, therefore, to increase the number of fluorine atoms present in the molecule and to reduce their longitudinal relaxation rates. As previously discussed, the introduction of a CF_3 group in the structure of a paramagnetic lanthanide complex, allows the enhancement of the longitudinal and transverse relaxation rates of the fluorine nuclei. With the purpose of combining faster relaxation times with an increased number of fluorine atoms, we set out to prepare a chitosan-based conjugated contrast agent, in which the polymeric chitosan chain functions as a platform for linking numerous lanthanide complexes, each bearing a CF_3 group.

5.2 Synthesis of the conjugate

The requisites of our system were, on the one hand, a macromolecular carrier with repeated monomers, each exhibiting a functional group which could be modified to form a stable linkage with the complexes and, on the other hand, a lanthanide complex that can be linked to the macromolecule. The ideal carrier should contain a functional group, such as an amino group, that allows a stable amide bond to be formed with the lanthanide complex. Several amino groups should be present to allow multiple linkages. The absence of toxicity of the conjugate is also necessary for its *in vivo* application as a contrast agent. A suitable candidate for these requirements is glycol chitosan, a non-toxic compound, well tolerated *in vivo*, composed of repeating glucosamine sugar units, each bearing a primary amino group. Normal chitosan has also been evaluated, but the lower aqueous solubility (it dissolves only in acidic media) has precluded its development. Glycol chitosan, thanks to the additional ethylene glycol groups, presents better solubility over a wider pH range, including neutral physiological values. The lanthanide complex should have an acid group that can form an amide linkage with the chitosan. The complex **[LnL^{1b}]** (synthesis: Chapter 2) contains a *para*-CO_2H group on the aromatic ring, which after suitable activation can be used to form a stable amide linkage. At first, formation of an *N*-hydroxy succinimidyl ester was attempted using NHS in DMSO, with EDC as the coupling agent. This strategy produced small amounts of product, as confirmed by HPLC. Therefore, a different method was employed. Complete conversion of **[LnL^{1b}]** into an active ester form was successfully achieved using TBTU and *N*-methylmorpholine (NMM) in DMF. The active form generated *in situ* was reacted immediately with the amine.

The first example of conjugation was attempted using glucosamine, the monomer of which chitosan is composed. This allowed evaluation of the possibility of forming the amide link with the active ester. The free glucosamine, obtained from the commercially available hydrochloride salt by anion exchange, was dissolved in the minimum amount of water and added in excess to the complex. The reaction went to completion and the clean product was isolated by precipitation (Scheme 5.1). The active ester was obtained under anhydrous conditions and, once formed, the addition of water didn't compromise the subsequent C-N bond forming reaction.

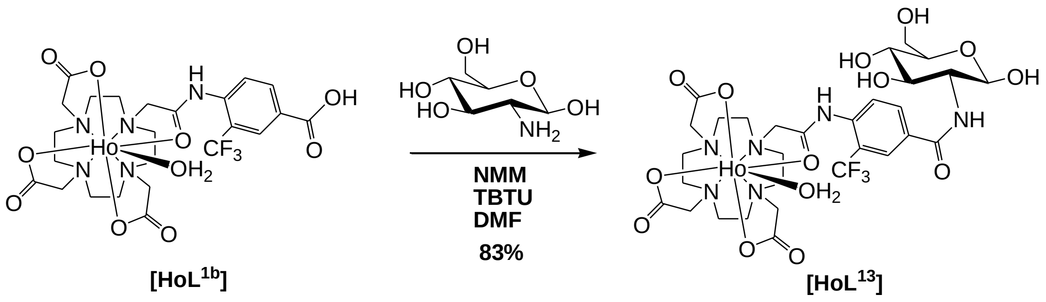

Scheme 5.1 Synthesis of **[HoL^{13}]**.

After this positive result, the conjugation was performed using the glycol chitosan polymer. Glycol chitosan was purchased from Sigma and purified by dialysis before use. After purification, the sample had a molecular weight of about 195,000 D as revealed by GPC analysis; its solubilisation in water required sonication over a period of two hours. The commercial sample was also modified to prepare a lower molecular weight polymer, by acidic digestion with HCl 4 M at 50°C over 24 hours.

After dialysis purification, the sample possessed an average MW of about 6,500 D (vide infra) and exhibited higher water solubility compared to the parent system.

The conjugation was performed on both the polymer samples, using the conditions described for the monomer. Obviously, the different molecular weight implied that different volumes of water were necessary to solubilise the macromolecule (Scheme 5.2). In the case of the larger polymer, the active ester was added dropwise to the viscous aqueous solution, paying particular attention to ensure homogeneous mixing. The enhanced solubility of the lower MW analogue allowed the reaction to be performed with less added water, following the procedure adopted for the glucosamine. The conjugate was obtained in each case following dialysis purification. The conjugation of the smaller polymer was performed using increasing complex concentrations resulting in a parallel increase of the percentage of bound complex. This indicates that the extent of conjugation reflects the quantity of complex used in the reaction, at least in the concentration range that was examined.

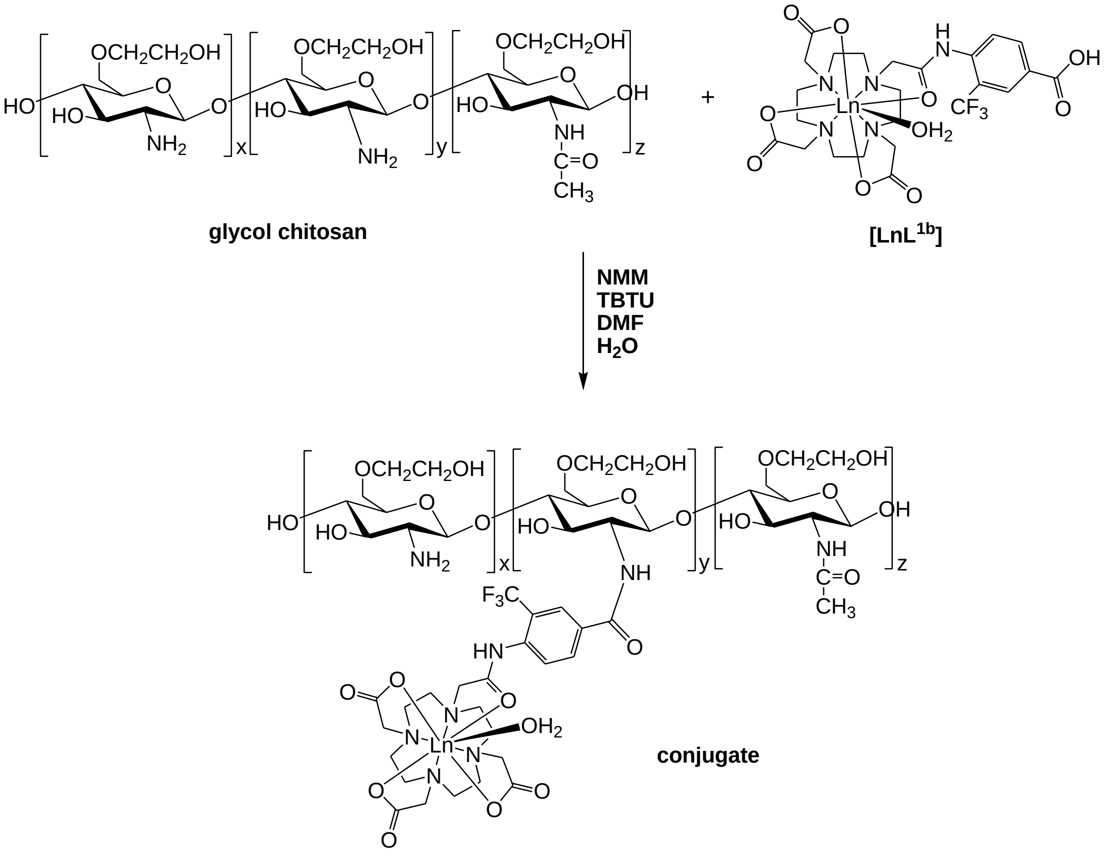

Scheme 5.2 General synthetic scheme for preparation of glycol chitosan complex conjugates.

The resulting materials were characterised by gel permeation chromatography (GPC) analysis to verify the presence of the conjugates. The analysis revealed the increase in the molecular weight of the conjugates, with respect to the unreacted polymer (Table 5.1).

Table 5.1 Gel permeation chromatography (GPC) data for the chitosan samples and their conjugates.

Sample	**M_w [a]**	**M_n [b]**	**PDI [c]**
71 (high MW chitosan)	194,000	50,750	3.8
72 (low MW chitosan)	6,590	2,250	2.9
73 (high MW-Ho conjugate)	278,500	54,650	5.1
74 (low MW-Ho conjugate)	16,200	4,500	3.6
75 (low MW-Gd conjugate)	15,950	4,155	3.8

Mean values obtained from two successive scans. [a] calculated molecular weight averages expressed as the pullulan polysaccaride equivalent molecular weights; [b] number average molecular weights; [c] polydispersity (Mw/Mn).

Elemental analysis was performed on the glycol chitosan samples before and after the conjugation, as variation in the carbon/nitrogen ratio gives indications of structural modifications. For the higher MW chitosan, **71**, the C/N ratio was consistent with ~20% acetylation. For the lower MW precursor, **72**, the analysis revealed a lower ratio indicating the absence of acetylation. This was probably caused by hydrolysis of the amide bonds during the acidic digestion used to prepare the sample.

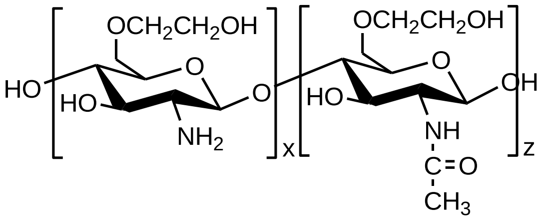

71

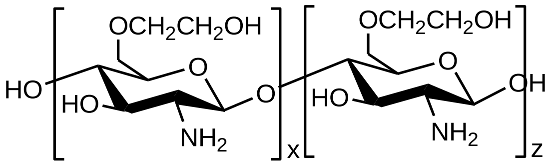

72

For the conjugates, the C/N ratio reflected the addition of the complex molecules and lower ratios were again found when using **72**, confirming the absence of acetylation.

Analysis of the percentage of Gd and Ho in the purified materials was undertaken using the Evans NMR method[1] and ICP-mass spectroscopic analysis. The results are reported below (Table 5.2).

Table 5.2 Metal percentage in the conjugate samples obtained with the Evans NMR method and ICP-MS and calculated percentage of conjugation.

Sample	Evans	ICP-MS	Calculated conjugation
73	/	1.6% Ho	3.6%
74	12.5% Ho	12.5% Ho	9.5%
75	14.9% Gd	14.9% Gd	11.6%

The same amount of metal was found with each methods and corresponded to a degree of conjugation of 3.6% for the higher MW-Ho complex conjugate, **73**, 9.5% for the lower MW-Ho complex conjugate, **74**, and 11.6% lower MW-Gd complex conjugate, **75**. The calculated levels of conjugation agreed with values estimated from the average MW analysis (Table 5.1). These data established the actual formation of covalently linked conjugates.

5.3 NMR studies

The conjugation between glycol chitosan and the lanthanide complexes bearing a CF_3 group was undertaken with the purpose of increasing the signal intensity of the fluorine resonance in ^{19}F MRI. The MR characteristics of the Ho^{3+} and Gd^{3+} conjugates are discussed in this section.

5.3.1 Ho complex conjugates

[HoL^{1b}], with a CO_2H group in the *para* position of the aromatic ring was selected over the *ortho* analogue **[HoL^{4b}]**, because of the presence of one main resonance in the fluorine spectrum, compared to two broader signals for the *ortho* isomer. The selection of the holmium complex ensured fast relaxation (Chapter 3). Upon binding to a macromolecular carrier, broader linewidths for the fluorine NMR resonance of the complex are expected, because of the restricted mobility that the latter experiences. It is important to restrict line-broadening to avoid loss of signal and this has been considered in the design of the contrast agent. A certain degree of mobility is maintained as a result of local rotation of the aromatic ring and of the complex with respect to the macromolecule as shown below (Fig. 5.1).

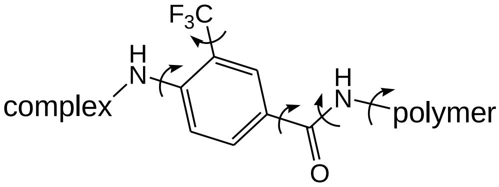

Fig. 5.1 Schematic representation of the possible rotation around the bonds of the linker.

The ^{19}F NMR spectra of dilute solutions of the two Ho-conjugates were recorded in D_2O. The solubility of the higher MW conjugate maintained the characteristics of the parent glycol chitosan, requiring sonication to produce a rather viscous solution. The lower MW polymer conjugate exhibited improved solubility and did not require sonication to dissolve it. In each case, a single peak was observed at δ_F = -56.8 ppm, at the same chemical shift as the parent complex. The linewidth was broader, as expected in each case. For the lower MW conjugate, a better signal to noise ratio was achieved for the same acquisition time compared to the higher MW sample, due to the higher degree of conjugation achieved.

Longitudinal relaxation rates were measured at 188 and 376 MHz and are reported in Table 5.3, together with the values for the complex **[HoL^{13}]**, the simple sugar glucosamine conjugate.

Table 5.3 ^{19}F NMR data for **[HoL^{13}]**, the high MW-Ho conjugate **73** and the lower MW-Ho conjugate **74**.

Sample	**188 MHz**		**376 MHz**	
	T_1 (s)	**$\omega_{1/2}$ (Hz)**	**T_1 (s)**	**$\omega_{1/2}$ (Hz)**
[HoL^{13}]	0.017	55	0.0081	93
73	0.012	100	0.013	262
74	0.018	236	0.010	257

[HoL^{13}] shows sharper signals and a T_1 variation more strongly dependent on the applied magnetic field compared to the conjugate, where the T_1 seems less dependent on the field and the linewidth is broader.

The ^{1}H NMR spectrum was also recorded showing only the resonances of the polymer because of the much higher relative signal intensity compared to those of the complex.

A control experiment was performed with the lower MW chitosan **74** to verify if the values obtained for the conjugate can be attributed to the covalent bonding of the complexes to the carrier and are not simply a consequence of enhanced solution viscosity. The control experiment was carried out by adding glycol chitosan to a solution of **[HoL^{1b}]** in the same proportion contained in the conjugate, measuring the linewidth of the ^{19}F peak at 376 MHz, before and after the addition. This comparison allows the effect of increased viscosity of the solution to be assessed.

The spectra revealed that the addition of the polymer produced only a small increase in the linewidth from 83 Hz to 107 Hz. This variation is much smaller compared to the value of 262 Hz in the case of the conjugate, proving that the effect is primarily related to the presence of the covalently bonded macromolecule.

The ^{19}F NMR spectrum of the holmium conjugate **74** was also recorded at different temperatures, monitoring any change in linewidth that could derive from the increased mobility (*i.e.* reduced viscosity) occurring at higher temperatures. No significant change was observed over the range 278-310 K.

5.3.2 Relaxivity studies with the Gd complex conjugate

The gadolinium analogue was prepared to enable ^{1}H MRI analysis, allowing the tracking of the distribution of the conjugate in an animal model.

The relaxivity of a dilute solution of the Gd-chitosan conjugate **75** in water and of the parent Gd complex **[GdL^{1b}]** was measured at 60 MHz at 37°C. The parent complex has a value of 4.62 $mM^{-1}s^{-1}$, which is typical for a mono-aqua DO3A monoamide complex[2]. In the glycol chitosan conjugate, **75**, the relaxivity per Gd was 11.2 $mM^{-1}s^{-1}$. This enhancement is associated with slower rotation of the Gd complex, which increases the value of the rotational correlation time τ_R, leading to a higher relaxivity. The increased viscosity of the solution, due to the presence of the dissolved polymer, can also be responsible for a greater relaxivity value. To confirm whether the bigger relaxivity value of the conjugate was related only to the viscosity of the solution or to the actual covalently linked macromolecule, a control experiment similar to that for the holmium analogue (section 5.3.1) was performed. A solution containing the Gd complex and the parent small molecular weight glycol chitosan **72** was prepared and its relaxivity measured at 60 MHz at 37°C. The value obtained was 4.79 $mM^{-1}s^{-1}$, which is very similar to that of the parent complex. This proved that the observed increased relaxivity is caused by the presence in solution of the covalently bonded conjugate.

The Gd conjugate can be employed as a conventional contrast agent in proton MRI by virtue of its ability to enhance the rate of relaxation of the bulk water protons. The relaxation behaviour was assessed by Prof. Botta at the Universitá del Piemonte Orientale (Italy) and compared to the behaviour of the parent Gd complex.

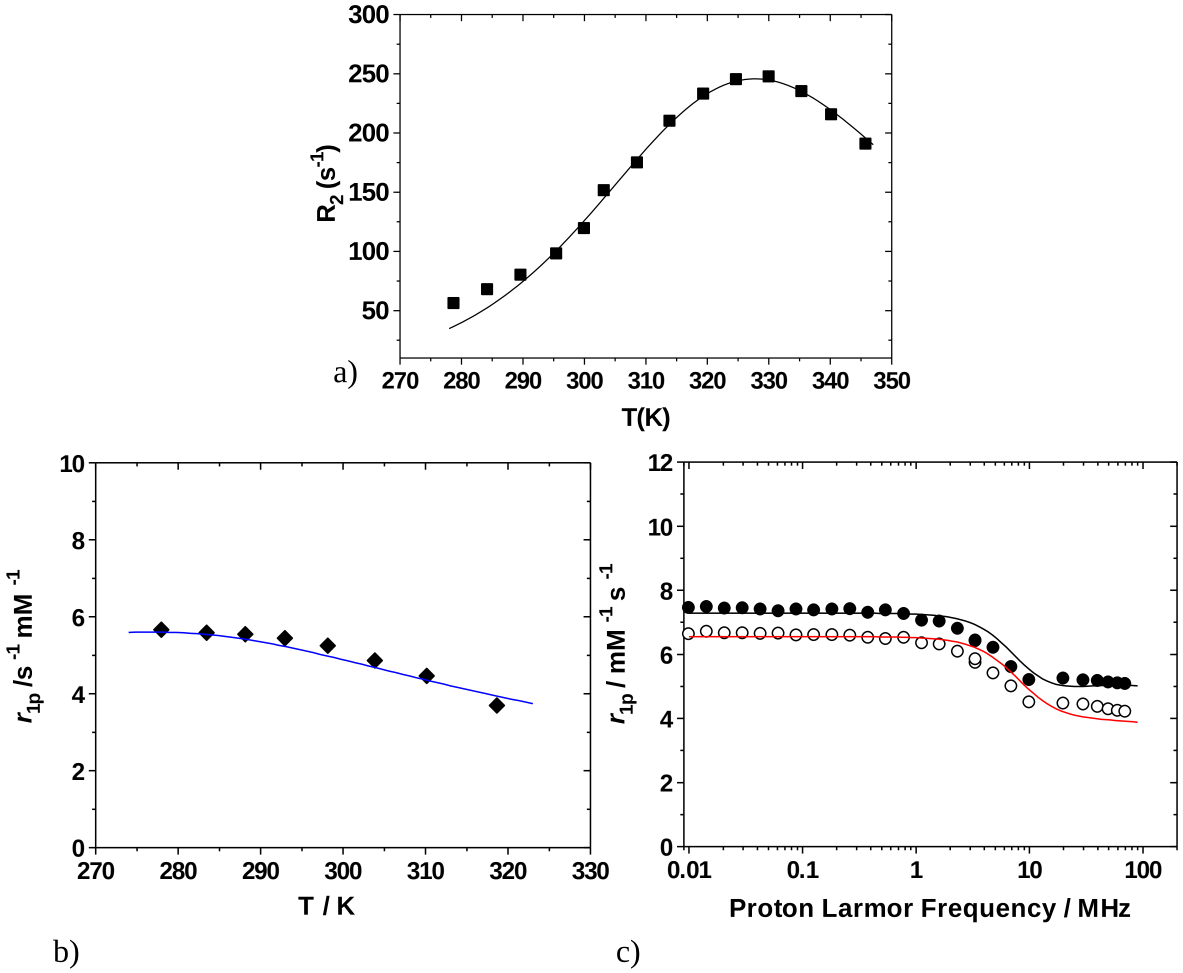

Fig. 5.2 [GdL^{1b}] proton relaxivity studies showing the fit (line) to the measured data. a) ^{17}O R_2 vs temperature profile measured at 11.7 T (500 MHz). b) relaxivity vs temperature profile measured at 20 MHz and pH 7.2. c) $1/T_1$ NMRD profiles at 298 (filled circles) and 310 K (open circles).

Variable temperature ^{17}O NMR measurements for **[GdL^{1b}]** were performed in ^{17}O-enriched water (Fig. 5.2) and the data analysed using the standard Swift-Connick methodology[3] to obtain an estimate of the water exchange lifetime τ_m. The analysis gave a τ_m value of 0.92 μs, which is similar to related monoamide derivatives of Gd-DO3A[2].

The relaxivity profiles as a function of temperature and magnetic field were also measured (Fig. 5.2) allowing information on the water exchange rate and various associated parameters used in the Solomon-Bloembergen-Morgan equations, as explained in Chapter 3. The values of the main parameters that describe the proton relaxation behaviour of the complex are reported (Table 5.4) and are consistent with those expected for such low molecular weight mono-aqua complexes, with two second sphere water molecules[2].

Table 5.4 Relaxation data for **[GdL^{1b}]**.

Parameter [a]	**310 K**
r_{1p} (mM^{-1} s^{-1})	5.2
τ_m (μs)	0.92
τ_R (ps)	83
τ_v (ps)	16
Δ^2 (s^{-2} × 10^{19})	8.8
q	1
q''	2
r'' (Å)	4.4

[a] r_{1p} is the proton relaxivity; τ_M is the water exchange lifetime; τ_R is the rotational correlation time; τ_v is the correlation time for the ZFS modulation; Δ^2 is the mean-square zero field splitting energy; q is the number of inner sphere water molecules; q'' is the number of second sphere water molecules and r'' their distance from Gd.

For the Gd-conjugate **75**, the relaxivity profiles as a function of temperature and magnetic field were also measured (Fig. 5.3). In the case of macromolecular conjugates, the analysis of NMRD profiles requires a different approach, since the presence of a relatively fast local rotation of the complex, compared to the slow motion of the macromolecule, needs to be considered. This is possible by incorporating the description of the rotational dynamics according to the 'model-free' Lipari–Szabo approach into the Solomon-Bloembergen-Morgan equations for the inner sphere relaxation mechanism[4,5]. This model allows the contribution of the global rotation of the whole paramagnetic system (τ_{RG}) to be separated from the contribution of a faster local motion (τ_{RL}) associated with the free rotation of the complex through the pendant arm.

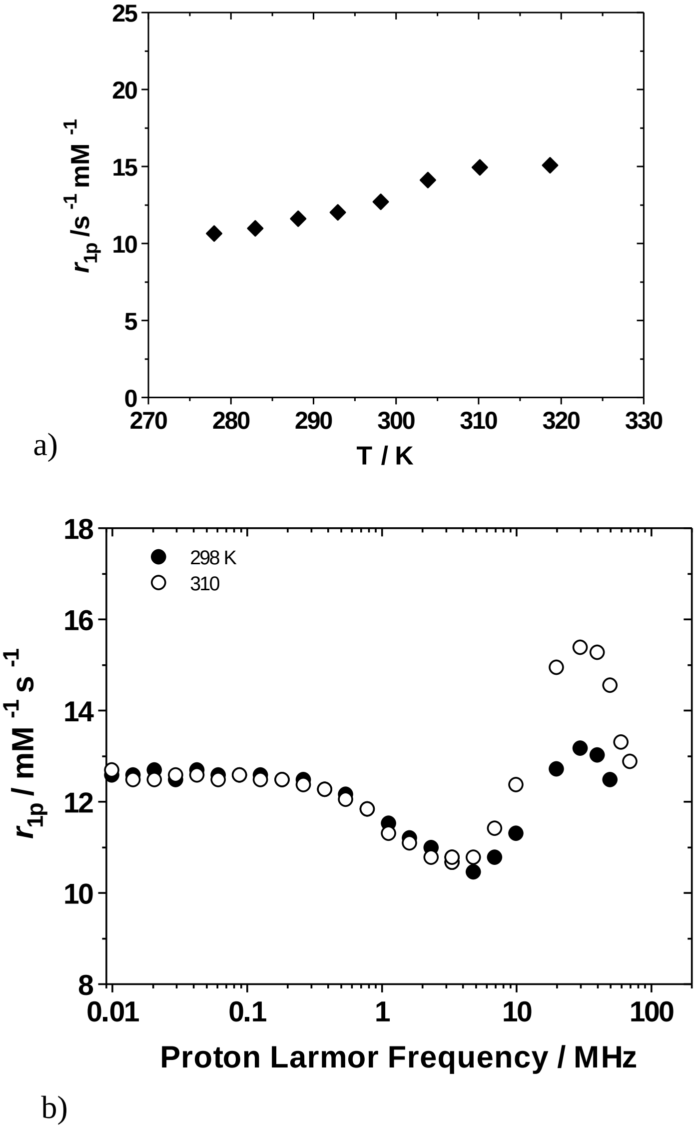

Fig. 5.3 Proton relaxivity studies for the Gd-conjugate **75**. a) relaxivity vs temperature profile measured at 20 MHz. b) 1/T_1 NMRD profiles at 298 (filled circles) and 310 K (open circles).

The correlation of the two types of motions is described by the parameter S^2 whose value ranges between zero (completely independent motion) and one (totally correlated motion). A schematic representation is reported below (Fig. 5.4).

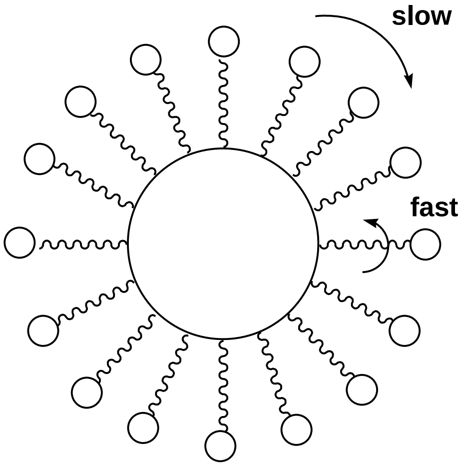

Fig. 5.4 Schematic representation of the slow overall motion of the macromolecule and the fast local motion of the complex.

The fitting of the NMRD profiles with the Lipari-Szabo model is shown in Fig. 5.5 and the resulting parameters are reported in Table 5.5.

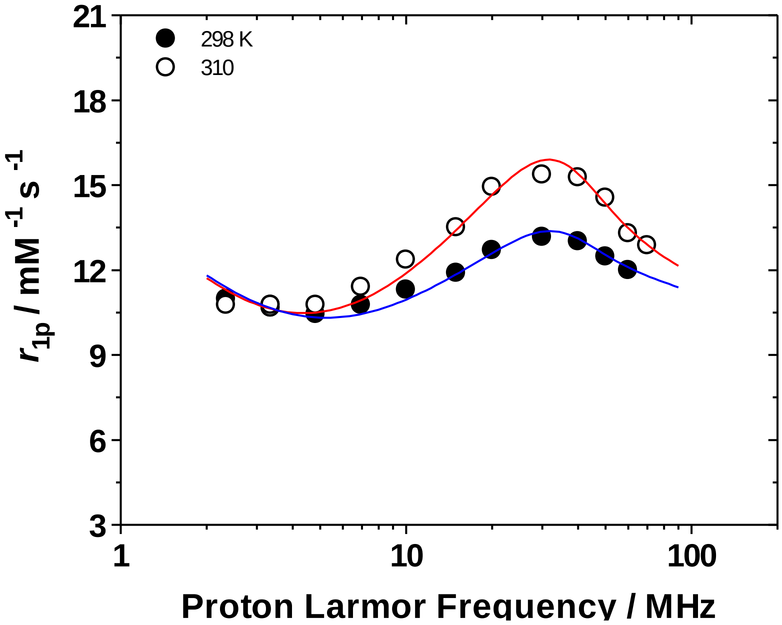

Fig. 5.5 Gd-conjugate NMRD profiles analyzed with the Lipari-Szabo model.

For the macromolecular conjugates, only the high field region was analyzed because of the inadequacy of the SBM model to reproduce the low fields data when the tumbling motion is so long. The parameters Δ^2 and τ_v were treated simply as fitting parameters and do not have a precise physical meaning. The values of q, r, and τ_m were assumed to be identical to those found for the parent Gd complex.

The results are consistent with the presence of a slow tumbling motion of the system, superimposed on fast local rotation of the Gd-chelates. This is underlined by the low value of S^2. Moreover, the relaxivity reaches a maximum value at 30 MHz (typically found at 20 MHz for more 'rigid' systems) of 15.9 $mM^{-1}s^{-1}$ at 310 K. This is probably a consequence of a relatively fast internal motion (0.68 ns) rather than the slow global rotation (30.2 ns). The relatively long residence lifetime of the inner sphere water molecule limits the relaxivity of the slowly tumbling system. Indeed, the relaxivity increases significantly with temperature. A maximum value is reached around 315 K. A simple simulation revealed that the relaxivity would increase to 27 if τ_m was 20 ns at 298 K.

Table 5.5 Relaxation data for the Gd-chitosan conjugate.

75 **(Gd-chitosan conjugate)**	**298 K**	**310 K**
r_{1p} (mM^{-1} s^{-1})	12.7	14.9
τ_m (μs)	0.92	0.74
τ_{RL} (ns)	0.68	0.60
τ_{RG} (ns)	40	30
S^2	0.10	0.18
τ_v (ps)	17.0	16.5
Δ^2 ($s^{-2} \times 10^{19}$)	1.7	1.7
q	1	1
a (Å)	4.0	4.0
D (cm^2 $s^{-1} \times 10^{-5}$)	2.24	3.10

τ_{RG} is the global rotation of the whole paramagnetic system; τ_{RL} the local motion contribution; S^2 the correlation between the global and local motion; a the Gd-H distance for the outer sphere water molecules and D the relative diffusion coefficient.

5.4 MRI studies

In vivo MRI studies of the Gd complex-chitosan conjugate **75** were performed at the Newcastle Magnetic Resonance Centre, using nude mice bearing an HT29 colorectal tumour xenograft as animal model, with the aim of assessing the distribution and the tumour uptake of the conjugate.

A 2.5 mM solution of the Gd complex-chitosan conjugate **75** was administered to four mice by intravenous injection in the tail. Each mouse (~30 g) received 200 μl of the solution corresponding to a dose of 0.017 mmol/Kg. The mice were previously anaesthetised with a mixture of oxygen/1-2% isoflurane.

A Dynamic Contrast Enhanced (DCE) MRI study was performed on a Varian 7 T Unity Inova Pre-Clinical system. A 2 mm slice containing the tumour was selected and the dynamic sequence applied. Five background ^{1}H MR images were collected (30 s), before the intravenous administration of the contrast agent during the sixth image. The remaining 94 were dynamic images, for a total of 100 over a 10 min acquisition period.

In each of the four mice analysed, an almost immediate contrast enhancement (<1 min) was observed after administration of the conjugate, both in the desired tumour area and the bladder (Fig. 5.6). The compound was well tolerated by the animals.

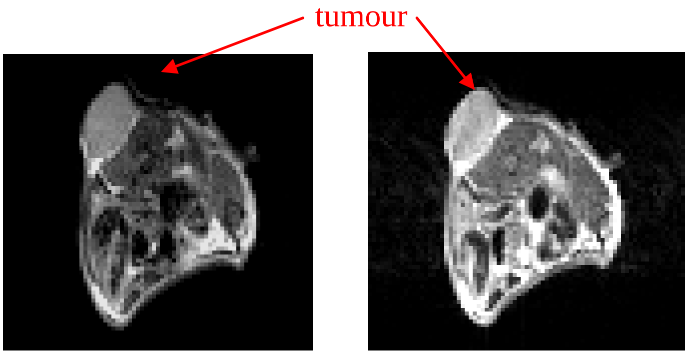

a) pre-injection b) post-injection

Fig. 5.6 ^{1}H MR images before and after administration of Gd-chitosan conjugate **75** (0.017 mmol/Kg dose) in a nude mouse bearing an HT29 colorectal tumour xenograft. a) Background ^{1}H MR image, before injection of the contrast agent (CA). b) Obtained after administration of the CA, showing contrast enhancement (brighter colour) of the tumour area.

The tumour area was analysed to measure the mean signal intensity profile as a function of time (Fig. 5.7). Rapid and selective uptake of the conjugate was observed in the tumour, followed by its slow release (in the 10 min acquisition time). This behaviour is probably related to the EPR (enhanced permeability and retention) that is characteristic of high molecular weight molecules. This leads to their selective accumulation in tumours through the increased fenestration of the blood vessels in the area and subsequent slow clearance from the site. This represents an advantage of the conjugate compared to low molecular weight Gd complexes, which are more rapidly excreted from the tumour and accumulate in the bladder quickly after administration.

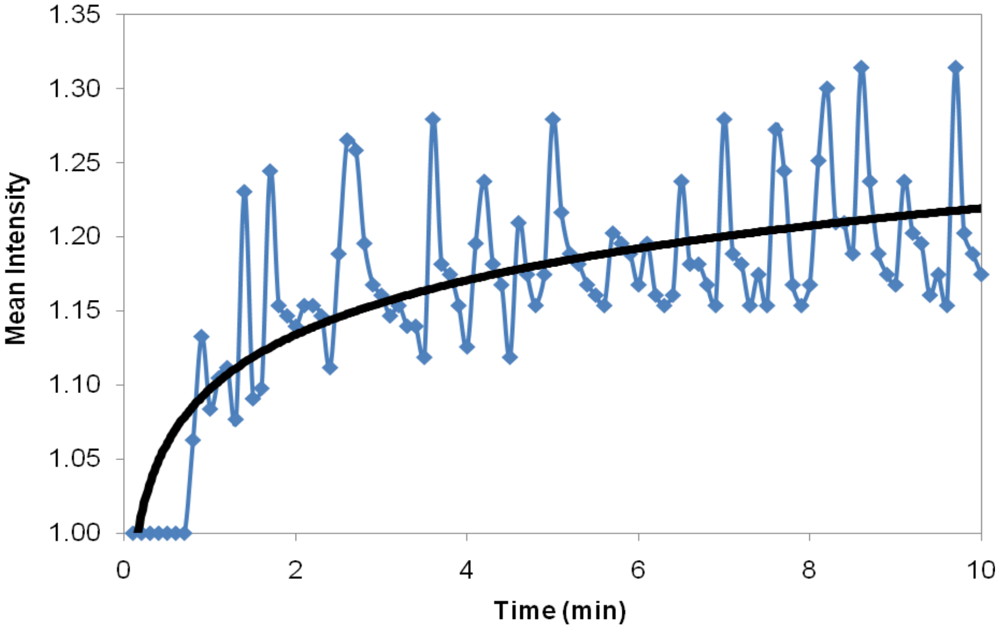

Fig. 5.7 Profile of the mean intensity over 10 min acquisition time of the selected tumour area, showing the increase of the signal intensity after administration of the Gd-conjugate.

The presence of conjugate in the bladder is a sign of renal excretion, which is a desirable characteristic, as it indicates that the conjugate is being eliminated from the system. Future work will include ICP-MS analysis of Gd concentration in the excised organs of the treated mice, that will allow the evaluation of the conjugate biodistribution.

The increase of the mean signal intensity reached the value of 1.22 in the best of the four experiments. The values obtained from the commercially available Gd contrast agents Prohance and Gadovist in analogous experiments were in the range 1.20-1.28. However, the latter were administered in higher doses, *i.e.* 0.1 mmol/kg against 0.017 mmol/kg for the Gd-chitosan, which also possesses a more than 2.5 fold higher relaxivity compared to Prohance and Gadovist.

A ^{19}F MRI dynamic experiment was also performed using the low MW Ho complex-chitosan conjugate **74**, using a dose of 0.034 mmol/kg on the same animal model. A similar dynamic sequence was used to acquire ^{19}F MR images over one hour. Unfortunately, no fluorine signal was detected after administration of the conjugate, most likely due to the rather broad linewidth which led to insufficient signal intensity for observation on the experimental timescale.

5.5 Conclusions

Glycol chitosan conjugates with paramagnetic fluorinated complexes have been prepared and their NMR properties assessed. The lower MW polymer possessed more desirable properties than the higher MW analogue, thanks to improved solubility and a higher rate of conjugation.

The lower MW Gd-glycol chitosan conjugate exhibited higher relaxivity with respect to the complex **[GdL^{1b}]**. *In vivo* experiments in mice allowed evaluation of the biodistribution, showing a rapid uptake of the conjugate in the tumour and subsequent slow clearance. This is an improvement compared to lower MW complexes that are rapidly cleared from the system[6].

The lower MW Gd-glycol chitosan conjugate was clearly visible using ^{19}F MRS *in vitro*, but no signal was observed once administered *in vivo*. As described in chapter 2 and 3, narrower fluorine signals and faster relaxation rates can be achieved using phosphinate complexes. Therefore, future work will focus on the conjugation of the phosphinate analogue of **[LnL^{1b}]** to the lower chitosan precursor **72** employed here. Furthermore, a flexible spacer could also be introduced in order to increase the mobility of the complex and contribute further to the narrowing of the resonances.

References

[1] D. M. Corsi, C. Platas-Iglesias, H. v. Bekkum, J. A. Peters, *Magn. Reson. Chem.*, **2001**, *39*, 723.

[2] P. Caravan, J. J. Ellison, T. J. McMurry, R. B. Lauffer, *Chem. Rev.*, **1999**, *99*, 2293.

[3] T. J. Swift, R. E. Connick, *J. Chem. Phys.*, **1962**, *37*, 307.

[4] G. Lipari, A. Szabo, *J. Am. Chem. Soc.*, **1982**, *104*, 4546.

[5] G. Lipari, A. Szabo, *J. Am. Chem. Soc.*, **1982**, *104*, 4559.

[6] D. A. Fulton, E. M. Elemento, S. Aime, L. Chaabane, M. Botta, D. Parker, *Chem. Commun.*, **2006**, 1064.

Chapter 6

Experimental

6.1 General experimental procedures

Reaction Conditions

All reagents purchased from their respective suppliers were used without further purification. Reactions requiring anhydrous conditions were carried out using Schlenk-line techniques under an atmosphere of dry argon. Anhydrous solvents, when required, were freshly distilled over the appropriate drying agent. Water was purified by the 'Purite$_{\mathrm{STILL}}$plus' system, with a conductivity of $\leq$0.04 μS cm^{-1}.

Purification Procedures

Thin layer chromatography was carried out on silica plates (Merck Art 5554) or neutral alumina plates using UV irradiation (254 nm) or iodine staining as detection. Column chromatography was performed using silica gel (Merck Silica Gel 60, 230–400 mesh) or neutral alumina (Merck Aluminium Oxide 90, activity II-III, 70-230 mesh), pre-soaked in ethyl acetate. Anion exchange chromatography was performed using anion exchange resin DOWEX 1X8 200-400 MESH Cl (Sigma-Aldrich), pre-treated with a solution of 1M HCl or 1M KOH in Purite water, or cation exchange resin DOWEX 50WX4-100 (Sigma-Aldrich) pre-treated with 1M KOH in Purite water.

Dialysis was performed with Dialysis Tubing Cellulose Membrane MWCO 12,000D (Sigma-Aldrich) or Spectra/Por Dialysis Membrane MWCO 1,000D (Spectrum Laboratories, Inc).

Characterisation Techniques: NMR Spectroscopy and Imaging

^{1}H, ^{13}C, ^{19}F and ^{31}P NMR spectra were recorded in commercially-available deuterated solvents on a Varian Mercury-200 (^{1}H at 199.975 MHz, ^{13}C at 50.289 MHz, ^{19}F at 188.179 MHz), Varian Mercury-400 or Bruker Avance-400 (^{1}H at 399.960 MHz, ^{13}C at 100.572 MHz, ^{19}F at 376.338 MHz, ^{31}P at 161.943 MHz), Varian Inova-500 (^{1}H at 499.772 MHz, ^{13}C at 125.671 MHz, ^{19}F at 470.253 MHz) or Varian VNMRS-700 (^{1}H at 699.731 MHz, ^{19}F at 658.407 MHz, ^{31}P at 283.256 MHz) spectrometer. All chemical shifts are given in ppm and coupling constants are in Hz. ^{19}F NMR longitudinal relaxation times (T_1) were measured in dilute D_2O solutions (1 mM) at 295 K using the inversion-recovery technique, without proton decoupling, with chemical shifts reported relative to fluorotrichloromethane.

Water proton T_1 measurements were recorded on a BrukerMinispec mq60 at 60 MHz and 37˚C, and are reported as the mean value of three measurements. In some cases they were measured on a Stelar Spinmaster Spectrometer at 20 MHz and 25˚C using 0.5-2 mM aqueous solutions of the complexes. The proton NMRD profiles were performed at the University of Piemonte Orientale in Alessandria using a fast field-cycling Stelar Spinmaster FFC relaxometer for magnetic fields strengths over the range 0.00024 to 0.5 T (0.01-20 MHz) and a Stelar Spinmaster spectrometer operating at variable fields for data points from 0.47 to 1.7 T (20-70 MHz).

Variable temperature ^{17}O NMR spectra were recorded in Alessandria on a JEOL ECP-400 spectrometer (9.4 T) using aqueous solution of the complexes (20-30 mM) enriched with 3% of ^{17}O isotope. The observed transverse relaxation rates (R_2^{obs}) were calculated from the signal width at half-height ($\omega_{1/2}$): $R_2^{obs} = \pi * \omega_{1/2}$.

MRI *in vivo* studies were performed in the Newcastle Magnetic Resonance Centre using a Varian 7 T Unity Inova Pre-Clinical system equipped with a ^{1}H 39 mm-diameter transmit/receive birdcage coil for proton images and a ^{19}F circular surface coil for fluorine images (12 mm diameter, 281 MHz ^{19}F frequency). Nude mice bearing an HT29 colorectal tumour xenograft were anaesthesised with oxygen/1-2% isoflurane and placed in the coil. A dynamic sequence was used in which 5 background images were collected (30 s) before the endovenous administration of the contrast agent during the 6th image. The remaining 94 images were dynamic images for a total of 100 over a 10 min acquisition period.

Other Experimental Instrumentation and General Procedures

pH measurements were performed using a Jenway 3320 pH meter attached to an Aldrich micro–pH combination electrode, calibrated using pH 4.00 ±0.02, 7.00 ±0.02 and 10.00 ±0.02 buffer solutions by Aldrich. Diluted aqueous solutions of NaOH and HCl (or where required NaOD and DCl in D_2O) were used for pH adjustements. For measurements in D_2O the pD was calculated as pD = pH + 0.41, where pH is the meter reading.

Protonation constants were measured at 295 K and 188 MHz using diluted solutions of the complex (1 mM) in 0.1 M NaCl in H_2O or in solutions of mouse plasma and mouse urine diluted 1:1 with Purite water. A coaxial insert containing D_2O was used to lock the NMR instrument. The resulting curves reporting the ^{19}F NMR chemical shift vs pH were fitted by non-linear least squares iterative analysis using Origin 8.0 software, producing estimates of the pK_a values.

Enzyme activities were obtained at 25 or 37˚C and 188 or 376 MHz using diluted PBS solutions of the complex (1 mM) in H_2O with a constant pH of 7.4. For each experiment, half of the sample without enzyme added was used as a negative control, while to the other half 5 mg of the enzyme was added as a lyophilised powder (15 units/mg, 1 unit hydrolyes 1.0 μmole of ethyl butyrate to butyric acid and ethanol per min at pH 8.0 at 25 °C). A coaxial D_2O insert was used to lock the NMR instrument. The activity was reported as ^{19}F NMR signal intensity vs time.

Reverse phase HPLC traces were recorded at 298 K using a Perkin Elmer system equipped with a Perkin Elmer Series 200 Pump, a Perkin Elmer Series 200 Autosampler and a Perkin Elmer Series 200 Diode array detector (operated at 254 nm). A 4.6 x 150 mm 4μm Phenomenex Synergi Fusion RP 80Å analytical column was used. A gradient elution with a solvent system composed of H_2O + 0.1% HCOOH/MeCN + 0.1% HCOOH was performed for a total run time of 20 min. The details are reported below (Table 6.1):

Table 6.1 Flow rate = 1ml/min; Solvent A = H_2O + 0.1% HCOOH; Solvent B = MeCN + 0.1% HCOOH.

Time (min)	Solvent A (%)	Solvent B (%)	Curvature
0	95	5	0
5	95	5	0
20	0	100	1
25	0	100	0
27	95	5	-3
30	95	5	0

Electrospray mass spectra were recorded on a Fisons VG Platform II, Waters Micromass LCT or Thermo-Finnigan LTQ FT instrument operating in positive or negative ion mode as stated, with methanol as the carrier solvent. Accurate mass spectra were recorded using the Thermo-Finnigan LTQ FT mass spectrometer. GC-MS were acquired on a GSMS Thermo-Finnigan instrument. LC-MS were performed on a Waters system comprising of a 3100 Mass Detector and a 2998 Photodiode array detector.

Gel permeation chromatography was undertaken at Smithers Rapra UK using a Viscotek Model 301 TDA instrument with associated pump, autosampler and refractive index detector (with differential pressure and light scattering). PLaquagel-OH guard plus 2 x PLaquagel-OH Mixed-H, 30 cm, 8 μm columns were used with an eluent composed of 0.5 M $NaNO_3$, 0.01 M NaH_2PO_4 at pH 2 at a flow rate of 1.0 ml/min at 30˚C. The GPC system was calibrated using pullulan polysaccharides and the data were analysed using Malvern/Viscotek 'OmniSec' software.

Melting points were recorded using a Gallenkamp (Sanyo) apparatus and are uncorrected.

Microanalysis measurements were acquired on an Exeter CE-440 Elemental Analyser.

UV/Vis absorbance spectra were recorded on a Perkin Elmer Lambda 900 UV/Vis/NIR spectrometer. Emission Spectra were measured on a ISA Joblin-Yvon Spec Fluorolog-3 luminescence spectrometer, using DataMax v2.20 software, while lifetimes were measured on a Perkin Elmer LS55 luminescence spectrometer using FL Winlab software. Samples were contained in quartz cuvettes with a path length of 1 cm and pure solvent in a matched cell was used as reference. Absorbance of each solution at the excitation wavelength was below 0.3 to avoid inner filter effects. Lifetimes measurements of Tb^{3+} or Eu^{3+} complexes were measured following excitation of the sample by a short light pulse at 233 nm for Tb^{3+} and 397 nm for Eu^{3+}, monitoring the integrated intensity of light (at 542-549 nm for Tb^{3+} and 618 nm for Eu^{3+}, depending on the complex) emitted after a delay time during a fixed gate time (0.1 ms). At least 20 delay times were used to cover more than 3 lifetimes.

The exponential decay curves obtained were fitted with equation 1 using Origin 8.0 software:

$$I = A_0 e^{-kt} \qquad (33)$$

where I is the intensity at time t after the flash, A_0 the pre-exponential factor and k the rate constant for the decay of the excited state. The excited state lifetime, τ, is the inverse of the rate constant, k.

Toxicity studies were performed using two cell lines: CHO (Chinese Hamster Ovary) cells and NIH 3T3, mouse skin fibroblast cells. These cells lines were cultured in an incubator at 37˚C, average 20% humidity and 5% (v/v) CO_2. IC_{50} values were determined using the MTT assay[1], which uses the conversion of MTT to a purple formazan product by the mitochondrial dehydrogenase enzymes of viable cells. The absorbance of the insoluble formazan was measured at 540 nm upon dissolution in DMSO. IC_{50} values were measured as the drug concentration required to reduce by 50% the absorbance of treated cells relative to the untreated cells used as control.

6.2 Synthetic procedures

1. 1,4,7-Tris(*tert*-butoxycarbonylmethyl)-1,4,7,10-tetraazacyclododecane[2]

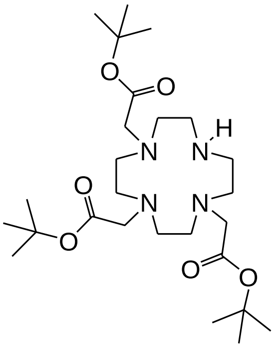

To a solution of 1,4,7,10-tetraazacyclododecane (2.54 g, 14.7 mmol) and $NaHCO_3$ (3.72 g, 44.3 mmol) in dry CH_3CN (75 ml) was added *tert*-butylbromoacetate (6.56 ml, 44.5 mmol) under argon. The reaction was left stirring overnight at room temperature. The mixture was filtered and the solvent evaporated to leave a yellow oil which was purified by recrystallisation from hot toluene to yield a white solid (2.45 g, 32%), m.p. 179-181°C (lit. 178-179°C)[3]. ^1H NMR (700 MHz, $CDCl_3$): δ 1.20 (27H, s, CH_3), 2.50-3.90 (16H, br, CH_2 ring), 3.04 (2H, s, CH_2CO), 3.14 (4H, s, CH_2CO), 9.60 (1H, br, s, NH); ^{13}C NMR (176 MHz, $CDCl_3$): δ 28.20, 28.22 (C-$\underline{C}H_3$), 47.43, 49.18, 51.29 (CH_2 ring), 57.99 ($\underline{C}H_2CO$), 81.48, 81.68 ($\underline{C}$-CH_3), 169.66, 170.51 (COO); ESI/MS$^+$ m/z 515.4 $[M + H]^+$; MS Calcd for $C_{26}H_{51}O_6N_4$ 515.3803. Found 515.3799.

2. Ethyl 4-amino-3-(trifluoromethyl)benzoate

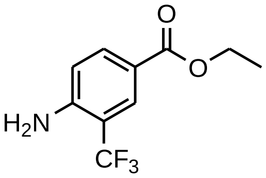

Sulfuric acid (1 ml) was added to a solution of EtOH (5 ml) and H_2O (0.5 ml) at 0°C. 4-Amino-3-(trifluoromethyl)benzonitrile (1.0 g, 5.4 mmol) was added and the mixture was stirred at 110°C for 3 days. The crude was diluted by addition of $CHCl_3$ (20 ml), then extracted with H_2O (10 ml) carefully adjusting the pH to 7 using solid

K_2CO_3 to neutralize the excess acid. The aqueous layer was washed with $CHCl_3$ (3 x 20 ml) and the combined organic extracts dried over K_2CO_3, filtered and solvent removed under reduced pressure to leave a yellow oil which was purified by column chromatography over silica gel, with gradient elution from toluene to toluene/20%CH_2Cl_2, to yield a light yellow solid (646 mg, 52%), m.p. 83-85°C. R_f = 0.2 (Silica, toluene/20%DCM, UV); ^{1}H NMR (700 MHz, $CDCl_3$): δ 1.28 (3H, t, J = 7.0 Hz, $CH_2\underline{CH_3}$), 4.25 (2H, q, J = 7.0 Hz, $\underline{CH_2}CH_3$), 4.88 (2H, br, s, NH_2), 6.67 (1H, d, J = 8.0 Hz, H^5), 7.84 (1H, d, J = 8.0 Hz, H^6), 8.06 (1H, s, H^2); ^{13}C NMR (176 MHz, $CDCl_3$): δ 14.27 ($CH_2\underline{C}H_3$), 60.88 ($\underline{C}H_2CH_3$), 112.48 (q, $^2J_{CF}$ = 31 Hz, $\underline{C}^3$-CF_3), 116.43 (C^5), 119.00 (C^1), 124.78 (q, $^1J_{CF}$ = 272 Hz, CF_3), 129.10 (q, $^3J_{CF}$ = 5 Hz, C^2), 134.26 (C^6), 148.94 (C^4), 166.09 (COO); ^{19}F NMR (188 MHz, $CDCl_3$): δ -63.21 (CF_3); ESI/MS$^-$ m/z 232.1 [M - H]$^-$; MS Calcd for $C_{10}H_9O_2NF_3$ 232.0591. Found 232.0587. Anal Calcd for $C_{10}H_{10}NO_2F_3$ C, 51.51; H, 4.32; N, 6.01%. Found C, 52.01; H, 4.47; N, 6.00%.

3. 2-Chloro-N-(4-(ethoxycarbonyl)-2-trifluoromethylphenyl)-ethanamide

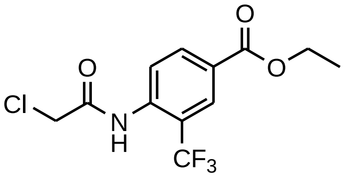

To a stirred solution of ethyl 4-amino-3-(trifluoromethyl)benzoate (594 mg, 2.55 mmol) in CH_2Cl_2 (15 ml) was added dropwise dry triethylamine (420 µl, 3.06 mmol) and chloroacetyl chloride (240 µl, 3.06 mmol) at 0˚C. The reaction mixture was allowed to warm to room temperature and stirred for 6 h. The crude mixture was washed successively with HCl $_{(aq)}$ (pH 2-3, 30 ml), NaOH $_{(aq)}$ (pH 8-9, 30 ml) and H_2O (30 ml). The organic layer was dried over $MgSO_4$, filtered and solvent removed under reduced pressure. The resultant light brown solid was purified by recrystallisation from hexane/diethyl ether to yield light brown needles (647 mg, 82%), m.p. 100-102°C. ^{1}H NMR (500 MHz, $CDCl_3$): δ 1.42 (3H, t, J = 7.0 Hz, $CH_2\underline{CH_3}$), 4.26 (2H, s, CH_2Cl), 4.41 (2H, q, J = 7.0 Hz, $\underline{CH_2}CH_3$), 8.25 (1H, dd, J = 8.5, 1.5 Hz, H^5), 8.33 (1H, d, J = 1.5 Hz, H^3), 8.48 (1H, d, J = 8.5 Hz, H^6), 8.96 (1H, br, s, NH); ^{13}C NMR (125.7 MHz, $CDCl_3$): δ 14.53 ($CH_2\underline{C}H_3$), 43.15 (CH_2Cl), 61.80

($\underline{C}H_2CH_3$), 119.73 (q, $^2J_{CF}$ = 31 Hz, $\underline{C}^2$-CF_3), 122.71 (C^6), 123.71 (q, $^1J_{CF}$ = 273 Hz, CF_3), 127.13 (C^4), 128.09 (q, $^3J_{CF}$ = 5 Hz, C^3), 134.53 (C^5), 138.34 (C^1), 164.54 (CONH), 164.99 (COO); ^{19}F NMR (188 MHz, $CDCl_3$): δ -60.84 (CF_3); ESI/MS$^-$ m/z 308.2 [M - H]$^-$; MS Calcd for $C_{12}H_{10}O_3NF_3Cl$ 308.0307. Found 308.0303. Anal Calcd for $C_{12}H_{11}O_3NF_3Cl$ C, 46.54; H, 3.58; N, 4.52%. Found C, 46.73; H, 3.71; N, 4.32%.

4. 10-[(4-Ethoxycarbonyl-2-trifluoromethyl(phenyl))carbamoylmethyl]-1,4,7-tris(*tert*-butoxycarbonylmethyl)-1,4,7,10-tetraazacyclododecane

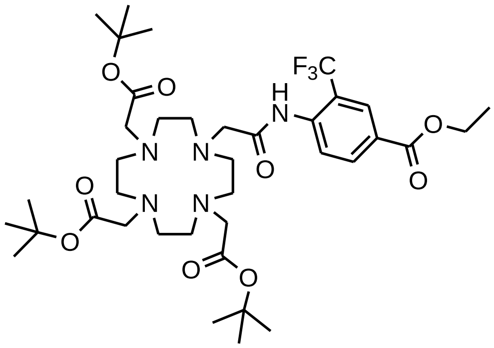

To a solution of 1,4,7-tris(*tert*-butoxycarbonylmethyl)-1,4,7,10-tetraazacyclododecane (500 mg, 0.97 mmol) and 2-chloro-N-(4-(ethoxycarbonyl)-2-trifluoromethylphenyl)-ethanamide (331 mg, 1.07 mmol) in dry CH_3CN (20 ml) under argon, was added K_2CO_3 (161 mg, 1.17 mmol) and KI (5 mg, cat.). The mixture was boiled under reflux for 24 h. After filtration, the residue was washed with CH_2Cl_2 (2 x 30 ml) and solvent removed under reduced pressure to yield a brown oil which was purified by column chromatography over silica gel (CH_2Cl_2 to CH_2Cl_2/10%EtOH). The resultant pale brown oil was purified by recrystallization from hot diethyl ether yielding a white powder (597 mg, 78%), m.p. 185-186°C. R_f = 0.6 (Silica, DCM/5%EtOH, UV); ^{1}H NMR (500 MHz, $CDCl_3$): δ 1.26, 1.37 (27H, br, s, CH_3), 1.33 (3H, t, J = 7.0 Hz, $CH_2\underline{CH_3}$), 1.90-3.80 (24H, br, CH_2 ring and CH_2CO), 4.33 (2H, q, J = 7.0 Hz, $\underline{CH_2}CH_3$), 7.76 (1H, d, J = 8.5 Hz, aromatic H^6), 8.01 (1H, dd, J = 8.5, 1.5 Hz, aromatic H^5), 8.20 (1H, d, J = 1.5 Hz, aromatic H^3), 9.48 (1H, br, s, NH); ^{13}C NMR (125.7 MHz, $CDCl_3$): δ 14.49 ($CH_2\underline{C}H_3$), 27.99, 28.07 (CH_3), 48.52, 52.63 (br, CH_2 ring), 55.74, 55.82, 57.01 ($\underline{C}H_2CO$), 61.64 ($\underline{C}H_2CH_3$), 82.07 ($\underline{C}$-CH_3), 123.35 (q, $^1J_{CF}$ = 274 Hz, CF_3), 124.91 (q, $^2J_{CF}$ = 32 Hz, aromatic <u>C</u>^{2}-CF_3), 127.83 (aromatic C^4), 128.05 (q, $^3J_{CF}$ = 5 Hz, aromatic C^3), 128.29 (aromatic C^6), 133.23 (aromatic C^5), 139.60 (aromatic C^1), 165.26 (COOEt), 172.53, 172.63, 172.75 (C=O); ^{19}F NMR (188 MHz, $CDCl_3$): δ -60.51 (CF_3); ESI/MS$^+$ m/z 810.4 [M + Na]$^+$; MS Calcd for $C_{38}H_{60}N_5O_9F_3Na$ 810.4235. Found 810.4224. The structure was confirmed by single crystal X-ray diffraction (see Appendix B).

5. 10-[(4-Ethoxycarbonyl-2-trifluoromethyl(phenyl)carbamoylmethyl]-1,4,7-tris(carboxymethyl)-1,4,7,10-tetraazacyclododecane, H_3L^{1a}

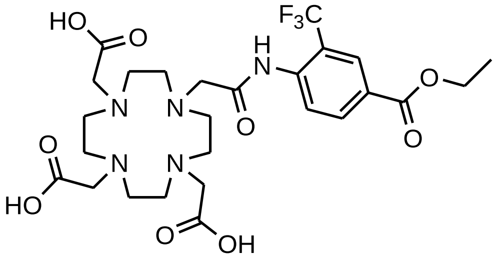

10-[(4-Ethoxycarbonyl-2-trifluoromethyl(phenyl))carbamoylmethyl]-1,4,7-tris(*tert*-butoxycarbonylmethyl)-1,4,7,10-tetraazacyclododecane (410 mg, 0.52 mmol) was dissolved in CH_2Cl_2 (1 ml), followed by the addition of CF_3CO_2H (4 ml). The solution was stirred at room temperature for 24 h. The solvent was removed under reduced pressure and the resulting solid washed with CH_2Cl_2 (5 x 5 ml) removing the solvent each time under reduced pressure (KOH in trap) to give the product as its trifluoroacetate salt (δ_F -76.1 $CF_3CO_2^-$). The residue was dissolved in water (5 ml) and stirred overnight with anion exchange resin (DOWEX 1X8 200-400 MESH Cl, pre-treated with 1M HCl) in Purite H_2O to give the chloride salt. After filtration, the aqueous solution was lyophilised to yield the product (as its dihydrochloride salt) as a light yellow powder (248 mg, 77%), m.p. 210-211°C (dec). ^{1}H NMR (500 MHz, D_2O): δ 1.19 (3H, t, J = 7.0 Hz, $CH_2\underline{CH_3}$), 2.60-4.20 (24H, br, CH_2 ring and CH_2CO), 4.19 (2H, q, J = 7.0 Hz, $\underline{CH_2}CH_3$), 7.63 (1H, d, J = 8.0 Hz, aromatic H^6), 8.01 (1H, d, J = 8.0 Hz, aromatic H^5), 8.10 (1H, s, aromatic H^3); ^{13}C NMR (125.7 MHz, D_2O): δ 13.55 ($CH_2\underline{C}H_3$), 47.00-56.00 (br, CH_2 ring and $\underline{C}H_2CO$), 62.83 ($\underline{C}H_2CH_3$), 123.07 (q, $^1J_{CF}$ = 273 Hz, CF_3), 124.40 (q, $^2J_{CF}$ = 30 Hz, aromatic <u>C</u>^{2}-CF_3), 127.99 (q, $^3J_{CF}$ = 5 Hz, aromatic C^3), 127.60-129.60 (br, aromatic C^4 and C^6), 133.86 (aromatic C^5), 137.57 (aromatic C^1), 166.95 ($\underline{C}$OOEt), 168.00-175.00 (br, C=O); ^{19}F NMR (188 MHz, D_2O): δ -61.54 (CF_3); ESI/MS$^+$ m/z 620.4 $[M + H]^+$, 642.4 $[M + Na]^+$, 658.3 $[M + K]^+$; MS Calcd for $C_{26}H_{37}O_9N_5F_3$ 620.2538. Found 620.2534. HPLC: t_R = 8.4 min.

6. [HoL^1(H_2O)]

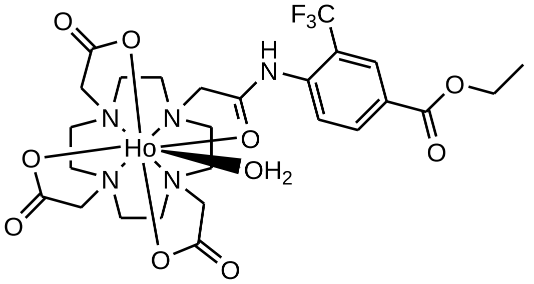

The ligand **L^1** (32.0 mg, 0.052 mmol) and Ho(III)Cl_3 (15.4 mg, 0.057 mmol) were dissolved in water (3 ml) and the pH adjusted to 5.5 using diluted KOH $_{(aq)}$. The reaction was left stirring overnight under reflux. After cooling to room temperature, the solution pH was adjusted to 10 and the mixture centrifuged to remove the precipitated metal hydroxide. The supernatant was adjusted back to pH 6 with diluted HCl $_{(aq)}$ and lyophilised to yield a yellow solid that was extracted into 20%MeOH/CH_2Cl_2 to give a light yellow solid.

The powder obtained was a mixture of the ethyl ester and the hydrolysed acid. The ^{1}H NMR spectral data were obtained on the mixture; the ethyl ester resonances are in a non-shifted region, so the major isomer resonances are expected not to change in both the ester and acid form. ^{1}H NMR (500 MHz, D_2O, pD 8.0): δ major isomer: -247.2, -57.7, 54.7, 88.5, 165.7; minor isomer -223.8, -210.8, -91.9, -78.0, -68.4, -45.9, -36.0, -31.3, -28.3, -23.2, -16.8, -13.1, 83.9, 149.0, 157.3; ^{19}F NMR (188 MHz, D_2O, pD 8.0) δ: ester -54.6 (CF_3, $\omega_{1/2}$ = 120 Hz), acid -56.6 (CF_3, $\omega_{1/2}$ = 46 Hz); ESI/MS$^+$ m/z ester 782.2 $[M + H]^+$, 804.1 $[M + Na]^+$, 820.1 $[M + K]^+$; ESI/MS$^-$ m/z ester 780.1 $[M - H]^-$, acid 752.1 $[M - H]^-$; MS Calcd for ester $C_{26}H_{32}O_9N_5F_3{}^{165}Ho$ 780.1461. Found 780.1465. Calcd for acid $C_{24}H_{28}O_9N_5F_3{}^{165}Ho$ 752.1148. Found 752.1152. HPLC: t_R ester = 8.9 min; LC-MS: t_R ester = 6.7 min, m/z 782.43 $[M + H]^+$, 780.28 $[M - H]^-$.

The ester was obtained separately using the same procedure by carrying out the complexation reaction with the Ln(III) salt at room temperature or by dissolving the mixture of the ester and acid complexes in EtOH/dry HCl for 1 week. The acid was obtained separately by allowing the complex to hydrolyse at pH 10 at room temperature, over a period of 1 week.

7. [TbL^{1}(H$_2$O)] (as a mixture of ethyl ester and its acid): ^{1}H NMR (500 MHz, D_2O, pD 10.0): δ major isomer -407.1, -101.1, -97.2, 85.0, 139.7, 265.6; minor isomer -369.8, -350.1, -238.0, -147.0, -131.5, -114.0, -74.9, -73.2, -71.4, -67.3, -64.1, -50.4, -40.0, -26.0, -23.8, -20.1, 22.5, 36.0, 43.0, 50.0, 64.0, 118.0, 130.0, 238.0, 253.0; ^{19}F NMR (188 MHz, D_2O, pD 10.0): δ ester -35.4 (CF_3, $\omega_{1/2}$ = 235 Hz), acid -45.6 (CF_3, $\omega_{1/2}$ = 207 Hz); ESI/MS^{+} m/z ester 798.2 [M + Na]$^{+}$, acid 769.9 [M + Na]$^{+}$; ESI/MS^{-} m/z ester 774.4 [M - H]$^{-}$, acid 746.4 [M - H]$^{-}$; MS Calcd for ester $C_{26}H_{33}O_9N_5F_3Na^{159}Tb$ 798.1376. Found 798.1375. Calcd for acid $C_{24}H_{28}O_9N_5F_3{}^{159}Tb$ 746.1110. Found 746.1098.

8. [DyL^{1}(H$_2$O)] (as a mixture of ethyl ester and its acid): ^{1}H NMR (500 MHz, D_2O, pD 8.0): δ major isomer -108.6, -100.8, 114.0, 168.1, 318.4; minor isomer -480.7, -210.3, -160.1, -146.2, -103.0, -72.5, -49.2, -39.1, 204.8, 225.1, 280.2; ^{19}F NMR (188 MHz, D_2O, pD 8.0): δ ester -59.7 (CF_3, $\omega_{1/2}$ = 551 Hz), acid -64.0 (CF_3, $\omega_{1/2}$ = 283 Hz); ESI/MS^{+} m/z ester 803.3 [M + Na]$^{+}$, 819.2 [M + K]$^{+}$; ESI/MS^{-} m/z ester 779.5 [M - H]$^{-}$, acid 751.4 [M - H]$^{-}$; MS Calcd for ester $C_{26}H_{32}O_9N_5F_3{}^{162}Dy$ 776.1435. Found 776.1435. Calcd for acid $C_{24}H_{28}O_9N_5F_3{}^{162}Dy$ 748.1114. Found 748.1123.

9. [ErL^{1}(H$_2$O)] (as a mixture of ethyl ester and its acid): ^{1}H NMR (500 MHz, D_2O, pD 5.0): δ major isomer -101.4, -56.4, 11.6, 22.6, 164.5; minor isomer -86.5, -80.6, -70.9, -66.9, -37.0, -33.0, -27.8, 7.2, 9.7, 15.8, 21.3, 28.4, 34.3, 126.2, 132.5, 142.7, 151.9; ^{19}F NMR (188 MHz, D_2O, pD 5.0): δ ester -62.4 (CF_3, $\omega_{1/2}$ = 42 Hz), acid -62.0 (CF_3, $\omega_{1/2}$ = 134 Hz); ESI/MS^{+} m/z ester 823.2 [M + K]$^{+}$, acid 795.2 [M + K]$^{+}$; ESI/MS^{-} m/z ester 783.2 [M - H]$^{-}$, acid 755.3 [M - H]$^{-}$; MS Calcd for ester $C_{26}H_{33}O_9N_5{}^{166}ErF_3K$ 821.1165. Found 821.1164. Calcd for acid $C_{24}H_{29}O_9N_5{}^{166}ErF_3K$ 793.0852. Found 793.0851.

10. [TmL^{1}(H$_2$O)] (as a mixture of ethyl ester and its acid): ^{1}H NMR (500 MHz, D_2O, pD 7.5): δ major isomer: -248.3, -137.2, -116.3, 49.9, 65.0, 387.0; minor isomer -378.4, -215.9, -211.1, -209.1, -205.1, -177.5, -150.2, -143.3, -118.6, -110.8, -89.9, -82.3, -78.9, -70.5, 30.5, 33.6, 36.1, 37.6, 39.4, 57.7, 58.6, 74.5, 313.9, 328.1, 340.5; ^{19}F NMR (188 MHz, D_2O, pD 7.5): δ ester -78.0 (CF_3, $\omega_{1/2}$ = 66 Hz), acid -79.9 (CF_3, $\omega_{1/2}$ = 56 Hz); ESI/MS$^+$ m/z ester 808.3 $[M + Na]^+$, 824.3 $[M + K]^+$, acid 796.3 $[M + K]^+$; ESI/MS$^-$ m/z acid 756.2 $[M - H]^-$; MS Calcd for ester $C_{26}H_{33}O_9N_5F_3{}^{169}TmK$ 824.1204. Found 824.1204. Calcd for acid $C_{24}H_{28}O_9N_5F_3{}^{169}Tm$ 756.1187. Found 756.1180.

11. 10-[(4-Carboxy-2-trifluoromethyl(phenyl)carbamoylmethyl]-1,4,7-tris(carboxymethyl)-1,4,7,10-tetraazacyclododecane, H_4L^{1b}

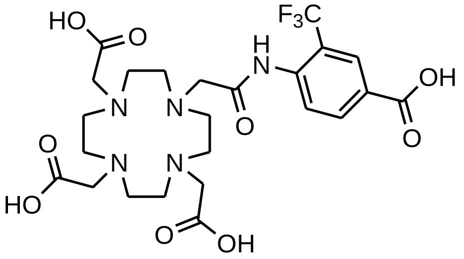

Lithium hydroxide monohydrate (34 mg, 0.81 mmol) was dissolved in water (2 ml) and added to a solution of 10-[(4-ethoxycarbonyl-2-trifluoromethyl(phenyl)carbamoylmethyl]-1,4,7-tris(carboxymethyl)-1,4,7,10-tetraazacyclododecane **H_3L^{1a}** (100 mg, 0.16 mmol) in MeOH (4 ml). The mixture was stirred at room temperature for 48 h. The MeOH was removed under reduced pressure and the pH adjusted to 4 with diluted HCl $_{(aq)}$. The aqueous solution was washed with ethyl acetate (2 x 5 ml) then lyophilised to yield the dihydrochloride salt of the ligand as a white powder which was directly used in complexation reactions without further purification, m.p. >250°C (dec). ^{1}H NMR (500 MHz, D_2O): δ 2.80-3.50 (16H, br, CH_2 ring), 3.38, 3.73, 3.74, 3.77 (2H, br, CH_2CO), 7.49 (1H, d, J = 8.5 Hz, aromatic H^6), 7.80 (1H, dd, J = 8.5, 1.5 Hz, aromatic H^5), 8.11 (1H, d, aromatic H^3); ^{13}C NMR (125.7 MHz, D_2O): δ 48.25, 51.36, 51.68 (br, CH_2 ring), 53.61, 54.46, 56.83 ($\underline{C}H_2CO$), 123.25 (q, $^1J_{CF}$ = 273 Hz, CF_3), 125.54 (q, $^2J_{CF}$ = 31 Hz, aromatic $\underline{C}^2$-CF_3), 127.90 (q, $^3J_{CF}$ = 5 Hz, aromatic C^3), 129.80 (aromatic C^6), 132.82 (aromatic C^4), 133.85 (aromatic C^5), 136.50 (aromatic C^1), 170.36 (C=O), 171.34 (aromatic C=O), 172.05, 174.92 (C=O); ^{19}F NMR (188 MHz, D_2O): δ -61.62 (CF_3); ESI/MS$^+$ m/z 296.6 $[(M + 2H)/2]^{2+}$, 592.2 $[M + H]^+$, 614.2 [M +

Na]$^+$, 630.2 [M + K]$^+$; ESI/MS$^-$ m/z 313.6 [M + Cl - H]$^{2-}$, 628.2 [M + Cl]$^-$; MS Calcd for $C_{24}H_{33}O_9N_5F_3$ 592.2230. Found 592.2240. HPLC: t_R = 5.8 min.

12. [HoL^{1b}(H$_2$O)]

Prepared as described for **[HoL^1(H$_2$O)] (6)** at room temperature.

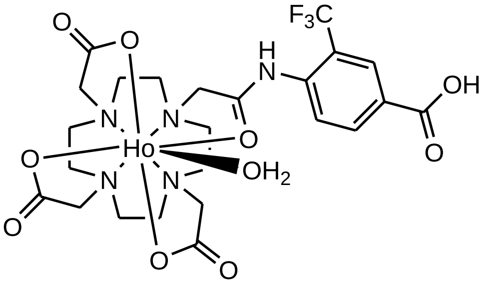

^{1}H NMR (500 MHz, D$_2$O, pD 5.2, partial assignment): δ -256.7, -251.2, -227.6, -223.9, -214.7, -94.0, -79.0, -69.7, -58.4, -46.2, -38.1, -36.0, -31.4, -29.5, -23.2, -13.6, 17.0, 55.9, 86.3, 92.4, 152.7, 159.0; ^{19}F NMR (188 MHz, D$_2$O, pD 5.2) δ: -56.8 (CF$_3$, $\omega_{1/2}$ = 47 Hz), -49.8 (CF$_3$, $\omega_{1/2}$ = 47 Hz); ESI/MS$^+$ m/z 754.1 [M + H]$^+$, 776.1 [M + Na]$^+$, 792.2 [M + K]$^+$; ESI/MS$^-$ m/z 752.1 [M - H]$^-$; MS Calcd for $C_{24}H_{28}O_9N_5F_3{}^{165}Ho$ 752.1142. Found 752.1139. HPLC: t_R = 7.1 min; LC-MS: t_R = 3.1 min, m/z 754.35 [M + H]$^+$.

13. [GdL^{1b}(H$_2$O)] ^{19}F NMR (188 MHz, D$_2$O, pD 5.2) δ: -60.9 (CF$_3$, $\omega_{1/2}$ = 1325 Hz); ESI/MS$^-$ m/z 745.1 [M - H]$^-$; MS Calcd for $C_{24}H_{28}O_9N_5F_3{}^{156}Gd$ 743.1067. Found 743.1061.

14. 2-Chloro-N-(4-nitro-2-trifluoromethylphenyl)-ethanamide

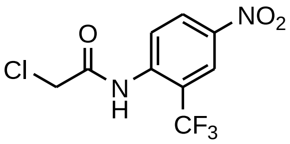

Chloroacetyl chloride (1.95 ml, 24.5 mmol) was added dropwise to a stirred solution of 4-nitro-2-trifluoromethyl aniline (2.01 g, 9.8 mmol), 4-dimethylaminopyridine (10 mg) and triethylamine (1.70 ml, 12.1 mmol) in dry THF (35 ml) at 0˚C. The reaction mixture was allowed to warm to room temperature and stirred for 48 h.

CH_2Cl_2 (30 ml) was added and the organic layer washed with HCl $_{(aq)}$ (pH 2-3, 30 ml), NaOH $_{(aq)}$ (pH 8-9, 30 ml) and H_2O (30 ml) then dried over K_2CO_3. After filtration, the solvent was removed to yield a brown oil that was purified by recrystallization from diethyl ether to yield light brown crystals (1.62 g, 59%), m.p. 62-64°C. ^{1}H NMR (700 MHz, $CDCl_3$): δ 4.27 (2H, s, CH_2Cl), 8.42 (1H, dd, J = 9.0, 2.0 Hz, H^5), 8.52 (1H, d, J = 2.0 Hz, H^3), 8.67 (1H, d, J = 9.0 Hz, H^6), 9.06 (1H, br, s, NH); ^{13}C NMR (176 MHz, $CDCl_3$): δ 43.09 (CH_2Cl), 120.03 (q, $^2J_{CF}$ = 31 Hz, $\underline{C}^2$-CF_3), 122.63 (q, $^3J_{CF}$ = 5 Hz, C^3), 122.91 (q, $^1J_{CF}$ = 274 Hz, CF_3), 123.04 (C^6), 128.56 (C^5), 140.13 (C^1), 143.69 (C^4), 164.68 (CONH); ^{19}F NMR (188 MHz, $CDCl_3$): δ -61.70 (CF_3); ESI/MS$^-$ m/z 281.3 [M - H]$^-$; MS Calcd for $C_9H_5N_2O_3F_3Cl$ 280.9941. Found 280.9835. Anal Calcd for $C_9H_6N_2O_3F_3Cl$ C, 38.20; H, 2.14; N, 9.91%. Found C, 38.30; H, 2.12; N, 9.80%.

15. 10-[(4-Nitro-2-trifluoromethyl(phenyl))carbamoylmethyl]-1,4,7-tris(*tert*-butoxycarbonylmethyl)-1,4,7,10-tetraazacyclododecane

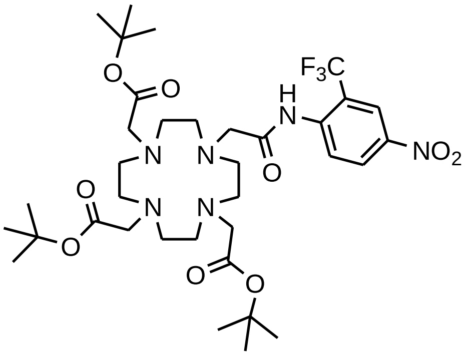

To a solution of 1,4,7-tris(*tert*-butoxycarbonylmethyl)-1,4,7,10-tetraazacyclododecane (330 mg, 0.64 mmol) and 2-chloro-N-(4-nitro-2-trifluoromethylphenyl)-ethanamide (200 mg, 0.71 mmol) in dry CH_3CN (20 ml) under argon, was added K_2CO_3 (106 mg, 0.77 mmol) and KI (5 mg, cat.). The mixture was boiled under reflux for 24 h. After filtration, the residue was washed with CH_2Cl_2 (2 x 30 ml) and solvent removed under reduced pressure to give a brown oil which was purified by column chromatography over silica gel, eluting with a gradient starting from CH_2Cl_2 up to CH_2Cl_2/10%MeOH to give a pale brown oil (402 mg, 83%). R_f = 0.5 (Silica, DCM/5%MeOH, UV); ^{1}H NMR (500 MHz,

$CDCl_3$): δ 1.35, 1.44 (27H, br, s, CH_3), 1.90-4.00 (24H, br, CH_2 ring and CH_2CO), 8.13 (1H, d, J = 9.0 Hz, aromatic H^6), 8.27 (1H, dd, J = 9.0, 2.5 Hz, aromatic H^5), 8.49 (1H, d, J = 2.5 Hz, aromatic H^3); ^{13}C NMR (125.7 MHz, $CDCl_3$): δ 28.13 (CH_3), 48.65, 52.77 (br, CH_2 ring), 55.86, 55.88, 57.66 ($\underline{C}H_2CO$), 82.26 ($\underline{C}$-CH_3), 122.60 (q, $^1J_{CF}$ = 274 Hz, CF_3), 122.76 (q, $^3J_{CF}$ = 5 Hz, aromatic C^3), 125.03 (q, $^2J_{CF}$ = 32 Hz, aromatic $\underline{C}^2$-CF_3), 127.13 (aromatic C^5), 128.37 (aromatic C^6), 141.25 (aromatic C^1), 144.50 (aromatic C^4), 172.83, 172.88 (C=O); ^{19}F NMR (188 MHz, $CDCl_3$): δ -61.17 (CF_3); ESI/MS$^+$ m/z 783.4 [M + Na]$^+$; ESI/MS$^-$ m/z 759.5 [M - H]$^-$; MS Calcd for $C_{35}H_{54}N_6O_9F_3$ 759.3910. Found 759.3900.

16. 10-[(4-Nitro-2-trifluoromethyl(phenyl)carbamoylmethyl]-1,4,7-tris(carboxymethyl)-1,4,7,10-tetraazacyclododecane, H_3L^2

Prepared as described for **H_3L^{1a} (5)**.

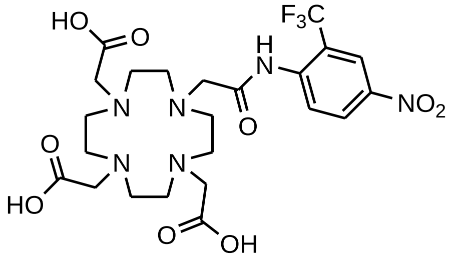

The product was isolated as the dihydrochloride salt as a light yellow powder (113 mg, 47%), m.p. 196-198°C (dec). ^1H NMR (500 MHz, D_2O): δ 2.60-4.30 (24H, br, CH_2 ring and CH_2CO), 7.83 (1H, d, J = 9.0 Hz, aromatic H^6), 8.31 (1H, d, J = 9.0 Hz, aromatic H^5), 8.46 (1H, s, aromatic H^3); ^{13}C NMR (125.7 MHz, D_2O): δ 42.42, 47.83, 48.51, 49.33, 51.78 (br), 52.12, 53.20, 54.68 (br, CH_2 ring and $\underline{C}H_2CO$), 122.48 (q, $^1J_{CF}$ = 274 Hz, CF_3), 122.95 (q, $^3J_{CF}$ = 5 Hz, aromatic C^3), 124.13 (q, $^2J_{CF}$ = 34 Hz, aromatic $\underline{C}^2$-CF_3), 128.02 (aromatic C^5), 129.04 (aromatic C^6), 144.82, 168.90 (br, aromatic C^1, C^4), 169.40 (br), 174.57 (C=O); ^{19}F NMR (188 MHz, D_2O): δ -61.84 (CF_3); ESI/MS$^+$ m/z 615.3 [M + Na]$^+$, 631.2 [M + K]$^+$, 655.0 [M + Cu]$^+$; ESI/MS$^-$ m/z 629.1 [M + Cl]$^-$; MS Calcd for $C_{23}H_{31}O_9N_6F_3K$ 631.1736. Found 631.1739. Calcd for $C_{23}H_{31}O_9N_6F_3Cu$ 655.1395. Found 655.1403. HPLC: t_R = 7.1 min; LC-MS: t_R = 4.8 min, m/z 593.31 [M + H]$^+$.

17. [HoL^2(H$_2$O)]

Prepared as described for **[HoL^1(H$_2$O)] (6)**.

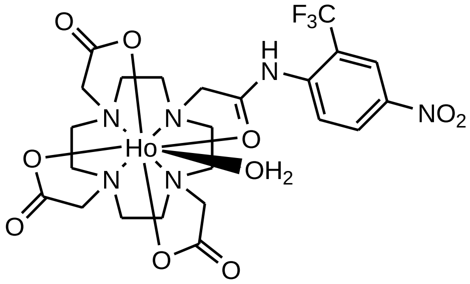

^{1}H NMR (500 MHz, D$_2$O, pD5.2): δ -256.2, -249.7, -224.2, -218.9, -210.2, -96.4, -80.0, -69.7, -58.1, -45.4, -40.1, -33.2, -28.0, -20.5, -16.2, 55.6, 88.7, 94.0, 147.1, 156.4, 166.9; ^{19}F NMR (188 MHz, D$_2$O, pD 5.2): δ (exists as mixture of isomers) -57.7 (CF$_3$, $\omega_{1/2}$ = 51 Hz, major isomer 88%); ESI/MS$^+$ m/z 777.0 [M + Na]$^+$, 793.0 [M + K]$^+$; MS Calcd for $C_{23}H_{28}O_9N_6F_3{}^{165}HoNa$ 777.1065. Found 777.1067. MS Calcd for $C_{23}H_{28}O_9N_6F_3{}^{165}HoK$ 793.0805. Found 793.0816. HPLC: t_R = 7.5 min.

18. [TbL^2(H$_2$O)] ^{1}H NMR (500 MHz, D$_2$O, pD 5.2): δ -409.0 (1H, br), -365.9 (1H, br), -363.7 (1H, br), -342.7 (1H, br), -151.4 (1H), -133.6 (1H), -114.1 (1H), -99.4 (1H), -96.5, -74.6 (1H), -64.4 (1H), -60.7 (2H), -46.2 (1H), -30.5 (1H), 30.1 (1H), 36.4, 84.0, 121.4 (1H), 133.2 (1H), 232.9 (1H, br), 241.4 (2H, br), 246.0 (1H, br); ^{19}F NMR (188 MHz, D$_2$O, pD 5.2): δ -50.2 (CF$_3$, $\omega_{1/2}$ = 73 Hz); ESI/MS$^+$ m/z 749.3 [M + H]$^+$, 771.3 [M + Na]$^+$, 787.3 [M + K]$^+$; ESI/MS$^-$ m/z 747.3 [M - H]$^-$; MS Calcd for $C_{23}H_{28}O_9N_6F_3{}^{159}TbK$ 787.0755. Found 787.0758.

19. [DyL^2(H$_2$O)] ^{1}H NMR (500 MHz, D$_2$O, pD 5.2): δ -479.2, -440.5, -422.2, -392.1, -217.6, -165.3, -149.3, -117.4, -108.5, -103.1, -100.9, -87.5, -69.8, -48.4, -43.9, -33.5, -30.3, -5.0, 112.7, 166.4, 211.8, 231.2, 268.8, 316.9, 357.1; ^{19}F NMR (188 MHz, D$_2$O, pD 5.2): δ (exists as mixture of isomers) -65.5 (CF$_3$, $\omega_{1/2}$ = 74 Hz, major isomer 70%); ESI/MS$^+$ m/z 776.0 [M + Na]$^+$; MS Calcd for $C_{23}H_{28}O_9N_6F_3{}^{164}DyNa$ 776.1054. Found 776.1064.

20. [ErL^2(H$_2$O)] ^{1}H NMR (500 MHz, D$_2$O, pD 5.2): δ -99.1 (1H, br), -84.2 (1H, br), -80.3 (2H, br), -78.4 (2H, br), -71.0 (1H, br), -66.9 (1H), -56.6 (1H), -55.0 (1H), -35.9 (1H), -31.1 (1H), -25.8 (1H, br), 10.0 (1H), 14.3 (1H), 20.8 (1H), 22.0 (1H), 23.2 (1H), 24.1 (1H), 33.6 (1H), 35.0 (1H), 120.4 (1H, br), 127.7 (1H, br), 138.2 (1H, br), 148.4 (1H, br), 160.1 (1H, br); ^{19}F NMR (188 MHz, D$_2$O, pD 5.2): δ -64.7

(CF_3, $\omega_{1/2}$ = 63 Hz); ESI/MS$^+$ m/z 778.3 [M + Na]$^+$, 796.2 [M + K]$^+$; ESI/MS$^-$ m/z 756.3 [M - H]$^-$; MS Calcd for $C_{23}H_{28}O_9N_6{}^{166}ErF_3K$ 794.0805. Found 794.0816.

21. [TmL^2(H$_2$O)] ^{1}H NMR (500 MHz, D_2O, pD 5.3): δ -203.0 (2H), -196.1 (1H), -194.4 (1H), -149.5 (1H), -141.9 (1H), -117.0 (1H), -109.7 (1H), -81.9 (1H), -76.1 (1H), -73.0 (1H), -63.2 (1H), 31.4 (1H), 34.1 (2H), 36.9 (1H), 38.4 (1H), 46.2 (1H), 50.2 (1H), 57.2 (1H), 58.0 (1H), 74.5 (1H), 302.7 (2H), 315.6 (1H), 331.0 (1H); ^{19}F NMR (188 MHz, D_2O, pD 5.4): δ -77.5 (CF_3, $\omega_{1/2}$ = 45 Hz); ESI/MS$^+$ m/z 759.1 [M + H]$^+$, 781.1 [M + Na]$^+$, 797.1 [M + K]$^+$; ESI/MS$^-$ m/z 757.2 [M - H]$^-$; MS Calcd for $C_{23}H_{28}O_9N_6F_3K^{169}Tm$ 797.0844. Found 797.0849.

22. 2-Chloro-N-(4-(cyano)-2-trifluoromethylphenyl)-ethanamide

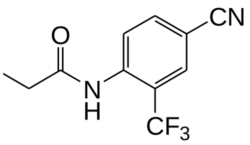

To a stirred solution of 4-amino-3-(trifluoromethyl)benzonitrile (2.01 g, 10.8 mmol), and 4-dimethylaminopyridine (10 mg) in dry THF (35 ml) were added dropwise dry triethylamine (1.87 ml, 13.5 mmol) and chloroacetyl chloride (2.15 ml, 26.9 mmol) at 0˚C. The reaction mixture was allowed to warm to room temperature and stirred overnight. The crude was washed successively with HCl $_{(aq)}$ (pH 2-3, 20 ml), NaOH $_{(aq)}$ (pH 8-9, 20 ml) and water (20 ml). The organic layer was dried over $MgSO_4$, filtered and solvent removed under reduced pressure to yield a yellow oil. Recrystallisation from ethyl acetate/hexane yielded an off-white solid (2.94 g, 99%), m.p. 113-114°C. ^{1}H NMR (700 MHz, $CDCl_3$): δ 4.25 (2H, s, CH_2Cl), 7.86 (1H, dd, J = 8.5, 1.5 Hz, H^5), 7.93 (1H, s, H^3), 8.60 (1H, d, J = 8.5 Hz, H^6), 8.99 (1H, br, s, NH); ^{13}C NMR (176 MHz, $CDCl_3$): δ 43.06 (CH_2Cl), 108.84 (C^4), 117.33 (CN), 120.43 (q, $^2J_{CF}$ = 31 Hz, $\underline{C}^2$-CF_3), 123.32 (C^6), 122.97 (q, $^1J_{CF}$ = 274 Hz, CF_3), 130.57 (q, $^3J_{CF}$ = 5 Hz, C^3), 137.00 (C^5), 138.53 (C^1), 164.63 (CONH); ^{19}F NMR (188 MHz, $CDCl_3$): δ -61.77 (CF_3); ESI/MS$^-$ m/z 261.1 [M - H]$^-$; MS Calcd for $C_{10}H_5N_2OF_3Cl$ 261.0048. Found 261.0045. Anal Calcd for $C_{10}H_6N_2OF_3Cl$ C, 45.73; H, 2.30; N, 10.67%. Found C, 45.41; H, 2.47; N, 10.72%.

23. 10-[(4-Cyano-2-trifluoromethyl(phenyl))carbamoylmethyl]-1,4,7-tris(*tert*-butoxycarbonylmethyl)-1,4,7,10-tetraazacyclododecane

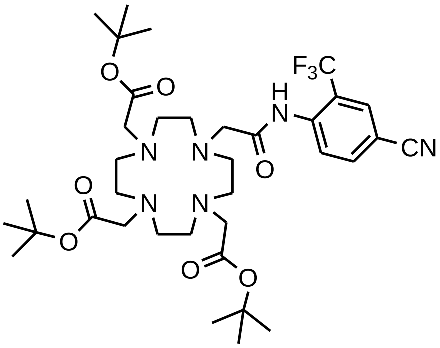

To a solution of 1,4,7-tris(*tert*-butoxycarbonylmethyl)-1,4,7,10-tetraazacyclododecane (205 mg, 0.40 mmol) and 2-chloro-N-(4-(cyano)-2-trifluoromethylphenyl)-ethanamide (115 mg, 0.44 mmol) in dry CH_3CN (10 ml) under argon, was added K_2CO_3 (66 mg, 0.48 mmol) and KI (5 mg, cat.). The mixture was boiled under reflux for 24 h. After filtration, the residue was treated with CH_2Cl_2 (2 x 30 ml), the organic extracts were combined and the solvent removed under reduced pressure to leave a brown oil which was purified by column chromatography over silica gel eluting from CH_2Cl_2 to 5%MeOH/CH_2Cl_2. Recrystallisation from diethyl ether yielded a white amorphous solid (110 mg, 37%), m.p. >250°C (dec). R_f = 0.5 (Silica, DCM/5%MeOH, UV); ^{1}H NMR (700 MHz, $CDCl_3$): δ 1.1-1.5 (27H, br, CH_3), 1.80-3.90 (24H, br, CH_2 ring and CH_2CO), 7.67 (1H, d, J = 9.0 Hz, aromatic H^5), 7.85 (1H, s, aromatic H^3), 7.98 (1H, d, J = 9.0 Hz, aromatic H^6), 9.23 (1H, br, s, NH); ^{13}C NMR (176 MHz, $CDCl_3$): δ 28.09 (CH_3), 48.77, 52.77 (br, CH_2 ring), 55.86, 57.52 ($\underline{C}H_2CO$), 82.19 ($\underline{C}$-CH_3), 109.52 (aromatic C^4), 117.57 (CN), 122.62 (q, $^1J_{CF}$ = 274 Hz, CF_3), 125.76 (q, $^2J_{CF}$ = 33 Hz, $\underline{C}^2$-CF_3), 128.85 (aromatic C^6), 130.73 (q, $^3J_{CF}$ = 5 Hz, C^3), 135.58 (aromatic C^5), 139.62 (aromatic C^1), 172.76, 172.79 (CO); ^{19}F NMR (188 MHz, $CDCl_3$) δ -61.16 (CF_3); ESI/MS$^+$ m/z 740.9 $[M + H]^+$, 762.9 $[M + Na]^+$; MS Calcd for $C_{36}H_{55}N_6O_7F_3Na$ 763.3977. Found 763.3973.

24. 10-[(4-Cyano-2-trifluoromethyl(phenyl)carbamoylmethyl]-1,4,7-tris(carboxymethyl)-1,4,7,10-tetraazacyclododecane, $\mathbf{H_3L^3}$

Prepared as described for $\mathbf{H_3L^{1a}}$ **(5)**.

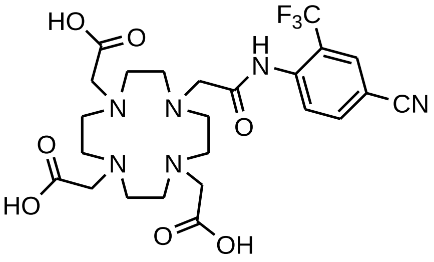

The product was isolated as the dihydrochloride salt as a light yellow powder (71 mg, 84%), m.p. 204-206°C (dec.). ^{1}H NMR (700 MHz, D_2O): δ 2.70-4.10 (24H, br, CH_2 ring and CH_2CO), 7.75 (1H, d, J = 8.5 Hz, aromatic H^5), 7.88 (1H, d, J = 8.5 Hz, aromatic H^6), 8.05 (1H, s, aromatic H^3); ^{13}C NMR (176 MHz, D_2O): δ 47.00-56.00 (br, CH_2 ring and $\underline{C}H_2CO$), 109.84 (aromatic C^4), 118.27 (CN), 122.62 (q, $^1J_{CF}$ = 273 Hz, CF_3), 124.90 (q, $^2J_{CF}$ = 30 Hz, $\underline{C}^2$-CF_3), 129.43 (q, $^3J_{CF}$ = 5 Hz, C^3), 131.50 (aromatic C^6), 137.01 (aromatic C^5), 138.01 (aromatic C^1), 168.15 (br, CO); ^{19}F NMR (188 MHz, D_2O): δ -61.93 (CF_3); ESI/MS$^+$ m/z 573.3 $[M + H]^+$, 595.3 $[M + Na]^+$; MS Calcd for $C_{24}H_{32}O_7N_6F_3$ 573.2279. Found 573.2283. HPLC: t_R = 6.9 min.

25. $\mathbf{[HoL^3(H_2O)]}$

Prepared as described for $\mathbf{[HoL^1(H_2O)]}$ **(6)**.

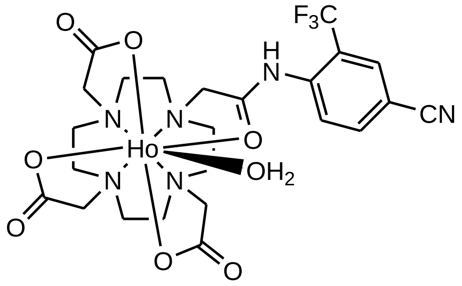

^{1}H NMR (500 MHz, D_2O pD 5.3): δ -252.4, -245.9, -222.2, -216.8, -208.7, -94.2, -78.5, -69.0, -58.0, -45.1, -39.4, -33.9, -28.1, -21.3, -16.9, 14.2, 54.5, 86.7, 91.8, 146.1, 153.1, 164.7; ^{19}F NMR (188 MHz, D_2O, pD 5.4): δ -55.4 ($CF_{3,}$ $\omega_{1/2}$ = 45 Hz);

ESI/MS$^+$ m/z 735.1 [M + H]$^+$, 757.1 [M + Na]$^+$; MS Calcd for $C_{24}H_{28}O_7N_6F_3{}^{165}HoNa$ 757.1167. Found 757.1173. HPLC: t_R = 7.5 min.

26. [TbL^3(H$_2$O)] ^{1}H NMR (500 MHz, D_2O, pD 5.2): δ -411.9, -407.8, -368.3, -346.3, -151.1, -133.4, -114.8, -101.1, -100.0, -97.3, -74.2, -64.6, -61.9, -55.1, -46.5, -29.4, -5.1, 31.6, 38.2, 85.3, 122.1, 134.0, 140.0, 234.6, 240.5, 245.6, 265.6; ^{19}F NMR (188 MHz, D_2O, pD 5): δ -50.1 (CF_3, $\omega_{1/2}$ = 63 Hz); ESI/MS$^+$ m/z 751.2 [M + Na]$^+$, 767.1 [M + K]$^+$; ESI/MS$^-$ m/z 727.2 [M - H]$^-$; MS Calcd for $C_{24}H_{28}O_7N_6F_3Na{}^{159}Tb$ 751.1117. Found 751.1120.

27. [ErL^3(H$_2$O)] ^{1}H NMR (500 MHz, D_2O, pD 5.3): δ -100.3, -85.0, -79.5, -71.2, -67.0, -57.0, -55.8, -35.8, -31.3, -26.5, 9.6, 11.0, 15.0, 21.1, 21.1, 22.3, 24.0, 31.6, 35.2, 122.6, 129.3, 140.0, 150.0, 162.5; ^{19}F NMR (188 MHz, D_2O, pD 5.4): δ -64.1 (CF_3, $\omega_{1/2}$ = 39 Hz); ESI/MS$^+$ m/z 758.1 [M + Na]$^+$, 776.2 [M + K]$^+$; ESI/MS$^-$ m/z 735.3 [M - H]$^-$; MS Calcd for $C_{24}H_{28}O_7N_6{}^{166}ErF_3Na$ 758.1167. Found 758.1164.

28. [TmL^3(H$_2$O)] ^{1}H NMR (500 MHz, D_2O, pD 5.4): δ -243.2, -207.4, -204.9, -200.9, -197.8, -196.4, -149.8, -142.3, -133.3, -117.5, -113.3, -110.2, -86.0, -83.3, -79.0, -77.0, -74.0, -64.7, 1.5, 2.0, 3.3, 6.1, 6.3, 7.9, 8.3, 31.7, 32.8, 34.4, 34.8, 36.0, 38.6, 46.7, 47.8, 49.1, 57.4, 58.0, 63.8, 74.5, 304.8, 309.3, 317.8, 332.8, 375.8; ^{19}F NMR (188 MHz, D_2O, pD 5.4): δ -78.2 (CF_3, $\omega_{1/2}$ = 36 Hz); ESI/MS$^+$ m/z 739.1 [M + H]$^+$, 761.1 [M + Na]$^+$; MS Calcd for $C_{24}H_{28}O_7N_6F_3Na{}^{169}Tm$ 761.1206. Found 761.1203.

29. Ethyl 2-amino-3-(trifluoromethyl)benzoate

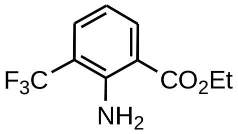

Sulfuric acid (2 ml, 18 M) was added dropwise to a solution of 2-amino-3-(trifluoromethyl)benzoic acid (2.0 g, 9.75 mmol) in EtOH (30 ml). The mixture was left stirring at 105°C overnight. The crude mixture was diluted by addition of $CHCl_3$ (20 ml), then extracted with H_2O (10 ml) carefully adjusting the pH to 7 using solid K_2CO_3 to neutralize the excess acid. The aqueous layer was extracted with $CHCl_3$ (3 x 20 ml) and the combined organic extracts were dried over K_2CO_3, filtered and solvent removed under reduced pressure to give a pale yellow solid (2.02 g, 89%), m.p. 72-73°C. ^{1}H NMR (700 MHz, $CDCl_3$): δ 1.36 (3H, t, J = 7.0 Hz, $CH_2\underline{CH_3}$), 4.31 (2H, q, J = 7.0 Hz, $\underline{CH_2}CH_3$), 6.45 (2H, br, s, NH_2), 6.63 (1H, t, J = 8.0 Hz, H^5), 7.55 (1H, dd, J = 8.0, 1.5 Hz, H^4), 8.05 (1H, dd, J = 8.0, 1.5 Hz, H^6); ^{13}C NMR (176 MHz, $CDCl_3$): δ 14.36 ($CH_2\underline{C}H_3$), 60.99 ($\underline{C}H_2CH_3$), 112.66 (C^1), 114.77 (q, $^2J_{CF}$ = 29 Hz, $\underline{C}^3$-CF_3), 114.79 (C^5), 124.89 (q, $^1J_{CF}$ = 273 Hz, CF_3), 131.88 (q, $^3J_{CF}$ = 5 Hz, C^4), 135.65 (C^6), 148.34 (C^2), 167.79 (C=O); ^{19}F NMR (188 MHz, $CDCl_3$): δ -63.98 (CF_3); ESI/MS$^+$ m/z 234.1 $[M + H]^+$; MS Calcd for $C_{10}H_{11}O_2NF_3$ 234.0742. Found 234.0739. Anal Calcd for $C_{10}H_{10}NO_2F_3$ C, 51.51; H, 4.32; N, 6.01%. Found C, 51.64; H, 4.26; N, 5.76%. GC-MS: t_R = 12.2 min, m/z 233.1 $[M]^+$.

30. 2-Chloro-N-(6-(ethoxycarbonyl)-2-trifluoromethylphenyl)-ethanamide

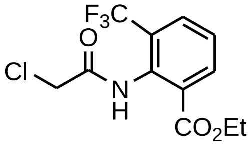

To a stirring solution of ethyl 2-amino-3-(trifluoromethyl)benzoate (1.36 g, 5.9 mmol) in CH_2Cl_2 (10 ml) were added dropwise dry triethylamine (2.43 ml, 17.5 mmol) and chloroacetyl chloride (1.40 ml, 17.5 mmol) at 0˚C. The reaction mixture was allowed to warm to room temperature and stirred overnight. The crude was washed successively with HCl $_{(aq)}$ (pH 2-3, 20 ml), NaOH $_{(aq)}$ (pH 8-9, 20 ml) and water (20 ml). The organic layer was dried over $MgSO_4$, filtered and solvent removed under reduced pressure to leave a pale brown oil which was filtered through a layer of silica gel, washing with diethyl ether. Removal of solvent under reduced pressure afforded a pale yellow solid (1.65 g, 91%), m.p. 79-81°C. ^{1}H NMR (700 MHz, $CDCl_3$): δ 1.33 (3H, t, J = 7.0 Hz, $CH_2\underline{CH_3}$), 4.16 (2H, s, CH_2Cl), 4.31 (2H, q, J = 7.0 Hz, $\underline{CH_2}CH_3$), 7.43 (1H, t, J = 8.0 Hz, H^4), 7.80 (1H, d, J = 7.0 Hz, H^3), 8.05 (1H, d, J = 7.0 Hz, H^5), 8.68 (1H, br, s, NH); ^{13}C NMR (176 MHz, $CDCl_3$): δ 14.05 ($CH_2\underline{C}H_3$), 42.62 (CH_2Cl), 61.82 ($\underline{C}H_2CH_3$), 123.11 (q, $^1J_{CF}$ = 273 Hz, CF_3), 127.38 (C^4), 130.16 (q, $^3J_{CF}$ = 5 Hz, C^3), 130.29 (C^6), 133.30 (C^1), 134.45 (q, $^2J_{CF}$ = 29 Hz, $\underline{C}^2$-CF_3), 134.54 (C^5), 165.22 (COO), 165.75 (NHCO); ^{19}F NMR (188 MHz, $CDCl_3$): δ -61.58 (CF_3); ESI/MS$^+$ m/z 310.1 $[M + H]^+$, 332.1 $[M + Na]^+$;

ESI/MS$^-$ m/z 308.2 [M - H]$^-$; Found 310.0447. MS Calcd for $C_{12}H_{12}NO_3F_3Cl$ 310.0452. Found 310.0447. Anal Calcd for $C_{12}H_{11}NO_3F_3Cl$ C, 46.54; H, 3.58; N, 4.52%. Found C, 46.44; H, 3.66; N, 4.43%.

31. 10-[(6-Ethoxycarbonyl-2-trifluoromethyl(phenyl))carbamoylmethyl]-1,4,7-tris(*tert*-butoxycarbonylmethyl)-1,4,7,10-tetraazacyclododecane

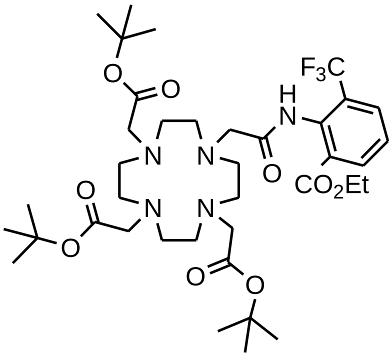

To a solution of 1,4,7-tris(*tert*-butoxycarbonylmethyl)-1,4,7,10-tetraazacyclododecane (200 mg, 0.39 mmol) and 2-chloro-N-(6-(ethoxycarbonyl)-2-trifluoromethylphenyl)-ethanamide (132 mg, 0.43 mmol) in dry CH_3CN (10 ml) under argon, was added K_2CO_3 (64 mg, 0.47 mmol) and KI (5 mg, cat.). The mixture was boiled under reflux for 24 h. After filtration, the residue was washed with CH_2Cl_2 (2 x 30 ml) and solvent removed under reduced pressure to leave a brown oil which was purified by column chromatography over silica gel with gradient elution from CH_2Cl_2 to 5%EtOH/CH_2Cl_2. A pale brown oil was afforded (196 mg, 64%). $R_f = 0.3$ (Silica, DCM/5%EtOH, UV and I_2); ^{1}H NMR (700 MHz, $CDCl_3$): δ 1.00-1.60 (27H, br, CH_3), 1.21 (3H, t, J = 7.0 Hz, $CH_2\underline{CH_3}$), 1.80-3.50 (22H, br, CH_2 ring and CH_2CO), 3.69 (2H, q, J = 7.0 Hz, $\underline{CH_2}CH_3$), 4.36 (2H, br, s, CH_2CO), 7.47 (1H, t, J = 8.0 Hz, aromatic H^4), 7.81 (1H, d, J = 8.0 Hz, aromatic H^3), 8.16 (1H, d, J = 8.0 Hz, aromatic H^5), 8.41 (1H, s, NH); ^{13}C NMR (176 MHz, $CDCl_3$): δ 18.62 ($CH_2\underline{C}H_3$), 27.89 (br), 28.07 (CH_3), 49.10, 52.70, 55.63 (br, CH_2 ring), 55.98, 57.42 ($\underline{C}H_2CO$), 58.58 ($\underline{C}H_2CH_3$), 61.86 ($\underline{C}H_2CO$), 81.82 (br), 81.96 ($\underline{C}$-CH_3), 123.19 (q, $^1J_{CF}$ = 274 Hz, CF_3), 127.43 (aromatic C^4), 129.95 (q, $^2J_{CF}$ = 29 Hz, aromatic $\underline{C}^2$-CF_3), 130.38 (aromatic C^6), 130.59 (q, $^3J_{CF}$ = 5 Hz, aromatic C^3), 134.50 (aromatic C^5), 135.47 (aromatic C^1), 164.61 ($\underline{C}$OOEt), 170.77, 172.64 (br), 172.83 ($CH_2\underline{C}OO$ and NHCO); ^{19}F NMR (188 MHz, $CDCl_3$): δ -60.83 (CF_3);

ESI/MS$^+$ m/z 788.4 [M + H]$^+$, 810.4 [M + Na]$^+$; MS Calcd for $C_{38}H_{60}N_5O_9F_3Na$ 810.4235. Found 810.4235.

32. 10-[(6-Ethoxycarbonyl-2-trifluoromethyl(phenyl)carbamoylmethyl]-1,4,7-tris(carboxymethyl)-1,4,7,10-tetraazacyclododecane, H_3L^{4a}

Prepared as described for **H_3L^{1a} (5)**.

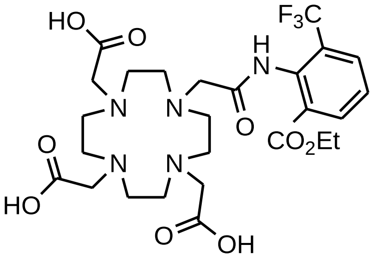

The product was isolated as the dihydrochloride salt as a white powder (120 mg, 81%), m.p. 235-236°C (dec). ^{1}H NMR (700 MHz, D_2O): δ 1.22 (3H, t, J = 7.0 Hz, $CH_2\underline{CH_3}$), 2.80-4.10 (24H, br, CH_2 ring and CH_2CO), 4.22 (2H, q, J = 7.0 Hz, $\underline{CH_2}CH_3$), 7.54 (1H, t, J = 7.5 Hz, aromatic H^4), 7.90 (1H, d, J = 7.5 Hz, aromatic H^3), 8.12 (1H, d, J = 7.5 Hz, aromatic H^5); ^{13}C NMR (176 MHz, D_2O): δ 13.61 ($CH_2\underline{C}H_3$), 46.00-56.00 (br, CH_2 ring and $\underline{C}H_2CO$), 63.06 ($\underline{C}H_2CH_3$), 123.16 (q, $^1J_{CF}$ = 272 Hz, CF_3), 128.94 (q, $^2J_{CF}$ = 30 Hz, aromatic $\underline{C}^2$-CF_3), 129.27 (aromatic C^4), 130.42 (aromatic C^6), 131.20 (q, $^3J_{CF}$ = 4 Hz, aromatic C^3), 132.80 (aromatic C^1), 135.16 (aromatic C^5), 166.49 ($\underline{C}OOEt$), 168.00-174.00 (br, C=O); ^{19}F NMR (188 MHz, D_2O): δ -61.57 (CF_3); ESI/MS$^+$ m/z 620.1 [M + H]$^+$, 642.0 [M + Na]$^+$; MS Calcd for $C_{26}H_{37}O_9N_5F_3$ 620.2538. Found 620.2538. HPLC: t_R = 7.2 min.

33. $[HoL^{4a}(H_2O)]$

Prepared as described for **$[HoL^1(H_2O)]$ (6)** at room temperature.

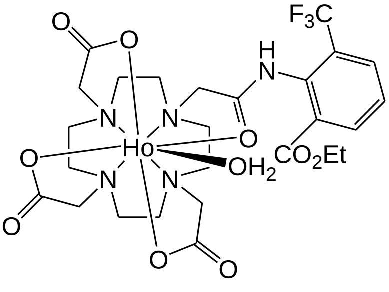

^{1}H NMR (500 MHz, D_2O, pD 5.3, two isomers 1:1): δ -267.3, -257.0, -246.6, -227.3, -224.5, -206.7, -187.9, -160.3, -146.1, -133.7, -119.0, -100.0, -98.4, -84.9, -82.7, -73.4, -58.5, -57.0, -41.9, -36.5, -33.2, -29.9, -28.0, -23.0, -18.9, -15.8, -15.0, -4.2, -2.3, 7.0, 8.6, 10.7, 14.2, 18.8, 54.7, 91.0, 100.6, 145.8, 151.3, 157.1, 164.8; ^{19}F NMR (188 MHz, D_2O, pD 5.4, two isomers 1:1): δ -80.8 (CF_3, $\omega_{1/2}$ = 262 Hz), -46.8 (CF_3, $\omega_{1/2}$ = 260 Hz); ESI/MS$^+$ m/z 782.2 $[M + H]^+$, 804.2 $[M + Na]^+$, 820.1 $[M + K]^+$; ESI/MS$^-$ m/z 780.2 $[M - H]^-$; MS Calcd for $C_{26}H_{32}O_9N_5F_3{}^{165}Ho$ 780.1461. Found 780.1458.

34. [TbL^{4a}(H$_2$O)] ^{1}H NMR (500 MHz, D_2O, pD 5.4, two isomers 1:1): δ -417.3, -413.4, -404.9, -373.9, -341.5, -330.3, -267.4, -251.5, -200.9, -187.2, -183.1, -156.0, -154.7, -142.2, -134.9, -121.2, -102.0, -100.8, -96.9, -94.4, -72.4, -69.6, -66.8, -65.4, -61.1, -38.7, -30.3, -27.0, -22.2, -14.8, -10.3, -9.5, 10.8, 14.1, 16.9, 21.0, 21.6, 24.0, 28.5, 42.2, 84.5, 125.0, 128.4, 138.7, 142.2, 147.7, 187.6, 234.3, 254.7, 258.6, 264.0; ^{19}F NMR (188 MHz, D_2O, pD 5.4, two isomers 1:1): δ -89.0 (CF_3, $\omega_{1/2}$ = 125 Hz), -39.3 (CF_3, $\omega_{1/2}$ = 89 Hz); ESI/MS$^+$ m/z 797.7 $[M + Na]^+$, 813.6 $[M + K]^+$; MS Calcd for $C_{26}H_{33}O_9N_5F_3Na{}^{159}Tb$ 798.1376. Found 798.1379. HPLC: t_R = 8.1 min.

35. [ErL^{4a}(H$_2$O)] ^{1}H NMR (500 MHz, D_2O, pD 5.3, two isomers 1:1): δ -100.3, -76.1, -70.9, -59.5, -55.8, -35.8, -34.8, -30.8, -28.2, -26.1, -5.6, -5.0, -3.4, 7.6, 7.8, 11.5, 14.3, 16.2, 17.2, 21.0, 22.8, 25.8, 27.3, 36.2, 37.4, 125.0, 134.4, 145.9, 153.6, 162.4; ^{19}F NMR (188 MHz, D_2O, pD 5.3, two isomers 1:1): δ -69.9 (CF_3, $\omega_{1/2}$ = 85 Hz), -49.7 (CF_3, $\omega_{1/2}$ = 104 Hz); ESI/MS$^+$ m/z 807.2 $[M + Na]^+$, 823.2 $[M + K]^+$; ESI/MS$^-$ m/z 783.2 $[M - H]^-$; MS Calcd for $C_{26}H_{32}O_9N_5{}^{166}ErF_3$ 779.1450. Found 779.1445.

36. [TmL^{4a}(H$_2$O)] ^{1}H NMR (500 MHz, D_2O, pD 5.3, two isomers 1:1): δ -244.3 (1H), -212.1 (2H), -207.2 (2H), -205.9 (1H), -199.4 (1H), -159.3 (1H), -156.8 (1H), -151.1 (1H), -143.6 (1H), -134.0 (1H), -125.3 (1H), -123.5 (1H), -113.7 (1H), -113.3 (1H), -112.5 (1H), -90.8 (1H), -87.8 (1H), -80.1 (1H), -78.1 (1H), -74.0 (1H), -73.6 (1H), -63.9 (1H), -57.8 (1H), -21.8 (1H), -17.5 (1H), -15.2 (3H), 1.1 (1H), 2.0 (1H), 11.4 (2H), 14.3 (1H), 19.0 (2H), 31.8 (3H), 34.3 (3H), 35.2 (1H), 36.2 (1H), 37.7 (1H), 42.7 (1H), 44.3 (1H), 49.5 (1H), 50.1 (1H), 51.4 (1H), 58.2 (1H), 59.0 (1H), 62.3 (1H), 64.3 (1H), 64.7 (1H), 78.2 (1H), 80.1 (1H), 309.7 (1H), 313.3 (1H), 331.8 (1H), 342.2 (1H), 345.7 (1H), 378.1 (1H); ^{19}F NMR (188 MHz, D_2O, pD 5.3, two isomers 1:1): δ -91.6 (CF_3, $\omega_{1/2}$ = 74 Hz), -38.0 (CF_3, $\omega_{1/2}$ = 93 Hz); ESI/MS$^+$ m/z

807.7 [M + Na]$^+$, 823.6 [M + K]$^+$; MS Calcd for $C_{26}H_{33}O_9N_5F_3K^{169}Tm$ 824.1204. Found 824.1210.

37. [EuL^{4a}(H$_2$O)] ^{1}H NMR (500 MHz, D$_2$O, pD 5.2, two isomers 1:1): δ -18.6, -16.6, -15.8, -15.6, -15.0, -14.8, -14.4, -14.1, -13.6, -12.8, -10.8, -10.3, -9.8, -8.7, -8.4, -8.1, -7.6, -6.8, -6.4, -5.6, -4.5, -3.6, -3.0, -2.4, -1.1, -0.2, 0.1, 1.7, 2.7, 7.2, 7.9, 8.8, 9.3, 10.5, 11.5, 28.3, 29.6, 31.2, 34.3; ^{19}F NMR (188 MHz, D$_2$O, pD 5.2, two isomers 1:1): δ -63.8 (CF$_3$, $\omega_{1/2}$ = 104 Hz), -60.2 (CF$_3$, $\omega_{1/2}$ = 145 Hz); ^{19}F NMR (658.4 MHz, D$_2$O, pD 5.2,): major pair of isomers 1:1: δ -62.0 (CF$_3$, $\omega_{1/2}$ = 124 Hz), -58.6 (CF$_3$, $\omega_{1/2}$ = 140 Hz); minor pair of isomers 1:1: δ -59.9 (CF$_3$, $\omega_{1/2}$ = 605 Hz), -59.4 (CF$_3$, $\omega_{1/2}$ = 528 Hz); ESI/MS$^+$ m/z 770.3 [M + H]$^+$, 792.3 [M + Na]$^+$, 808.3 [M + K]$^+$; ESI/MS$^-$ m/z 768.3 [M - H]$^-$; MS Calcd for $C_{26}H_{33}O_9N_5{}^{151}EuF_3Na$ 790.1321. Found 790.1320.

38. [GdL^{4a}(H$_2$O)] ^{19}F NMR (188 MHz, D$_2$O, pD 5.4, two isomers 1:1): δ -60.1 (CF$_3$, mean $\omega_{1/2}$ = 1130 Hz); ESI/MS$^+$ m/z 797.2 [M + Na]$^+$, 813.2 [M + K]$^+$; MS Calcd for $C_{26}H_{33}O_9N_5F_3{}^{158}GdNa$ 797.1364. Found 797.1366.

39. 10-[(6-Carboxy-2trifluoromethyl(phenyl)carbamoylmethyl]-1,4,7-tris(carboxymethyl)-1,4,7,10-tetraazacyclododecane, H$_4$L^{4b}

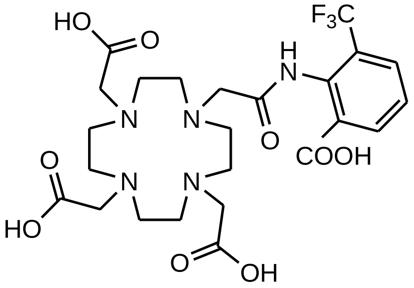

10-[(6-Ethoxycarbonyl-2-trifluoromethyl(phenyl)carbamoylmethyl]-1,4,7-tris(carboxymethyl)-1,4,7,10-tetraazacyclododecane **H$_3$L^{4a}** (10.2 mg, 0.016 mmol) was stirred for 48 h at 50ºC in water (1 ml) at pH 12 (diluted KOH $_{(aq)}$). The pH was adjusted back to 7 (diluted HCl$_{(aq)}$) and the solution treated with a strong acid cation exchange resin (Dowex 50W/H+). After filtration the solution was lyophilized to yield the dihydrochloride salt as a white solid (9.5 mg, 98%), m.p. 210-211°C (dec). ^{1}H NMR (700 MHz, D$_2$O): δ 2.98, 3.03, 3.11, 3.18, 3.27, 3.39 (20H, br, CH$_2$ ring and CH_2CO), 3.77 (4H, br, CH_2CO), 7.47 (1H, t, J = 7.5 Hz, aromatic H^4), 7.68 (1H, d, J = 7.5 Hz, aromatic H^5), 7.72 (1H, d, J = 7.5 Hz, aromatic H^3); ^{13}C NMR (176 MHz, D_2O): δ 48.14, 48.50, 51.68 (br, CH_2 ring), 52.07, 54.68, 55.48, 57.13 (br, $\underline{C}H_2CO$), 123.63 (q, $^1J_{CF}$ = 273 Hz, CF_3), 127.53 (q, $^3J_{CF}$ = 4 Hz, aromatic C^3), 128.06 (q, $^2J_{CF}$ = 30 Hz, aromatic C^2-CF_3), 128.90 (aromatic C^4), 130.10 (aromatic C^1), 132.32 (aromatic C^5), 140.62 (aromatic C^6), 170.46, 172.51, 177.17 (C=O), 173.96 (aromatic C=O); ^{19}F NMR (188 MHz, D_2O): δ -61.39 (CF_3); ESI/MS$^+$ m/z 592.3 $[M + H]^+$, 614.3 $[M + Na]^+$, 630.2 $[M + K]^+$; ESI/MS$^-$ m/z 590.3 $[M - H]^-$; Calcd for $C_{24}H_{31}O_9N_5F_3$ 590.2079. Found 590.2071.

40. [HoL^{4b}(H$_2$O)]

Prepared as described for **[HoL^1(H$_2$O)] (6)** at room temperature.

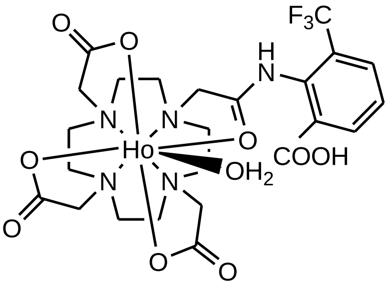

^{1}H NMR (500 MHz, D_2O, pD 5.2, two isomers 1:3): δ -258.2, -247.8, -228.9, -223.6, -209.8, -102.3, -97.9, -84.8, -69.2, -57.6, -53.4, -42.5, -31.5, -22.7, -18.3, -14.2, -2.8, 7.8, 55.1, 85.1, 89.1, 94.2, 103.2, 152.0, 164.1; ^{19}F NMR (188 MHz, D_2O, pD 5.4, two isomers 1:3): δ -79.3 (CF_3, $\omega_{1/2}$ = 530 Hz), -46.4 (CF_3, $\omega_{1/2}$ = 377 Hz); ESI/MS$^+$ m/z 776.2 $[M + Na]^+$; ESI/MS$^-$ m/z 752.1 $[M - H]^-$; Calcd for $C_{24}H_{28}O_9N_5F_3{}^{165}Ho$ 752.1137. Found 752.1137. HPLC: t_R = 7.4 min.

41. [TbL^{4b}(H$_2$O)] ^{1}H NMR (500 MHz, D_2O, pD 5.2, two isomers 3:1): δ -415.1, -406.1, -383.8, -375.0, -366.9, -350.7, -345.2, -158.9, -155.7, -144.1, -137.9, -120.2, -106.3, -101.1, -99.0, -97.3, -94.1, -71.2, -65.6, -53.0, -40.7, -38.3, -24.0, 28.0, 84.6, 124.7, 139.3, 142.1, 146.8, 248.5, 264.5; ^{19}F NMR (188 MHz, D_2O, pD 5.4, two isomers 3:1): δ -89.8 (CF_3, $\omega_{1/2}$ = 311 Hz), -42.1 (CF_3, $\omega_{1/2}$ = 536 Hz); ESI/MS$^+$ m/z 770.2 $[M + Na]^+$, 786.2 $[M + K]^+$; ESI/MS$^-$ m/z 746.2 $[M - H]^-$; MS Calcd for $C_{24}H_{29}O_9N_5F_3K{}^{159}Tb$ 786.0803. Found 786.0798.

42. [ErL^{4b}(H$_2$O)] ^{1}H NMR (500 MHz, D_2O, pD 5.3, two isomers 3:1): δ -101.0, -83.6, -71.2, -59.5, -56.2, -37.6, -34.4, -29.7, -2.4, 11.5, 13.0, 16.0, 20.0, 22.6, 24.6, 36.0, 39.0, 123.5, 133.0, 144.7, 152.3, 157.2, 163.7; ^{19}F NMR (188 MHz, D_2O, pD 5.4, two isomers 3:1): δ -66.6 (CF_3, $\omega_{1/2}$ = 263 Hz), -45.8 (CF_3, $\omega_{1/2}$ = 542 Hz); ESI/MS$^+$ m/z 779.2 $[M + Na]^+$, 795.1 $[M + K]^+$; ESI/MS$^-$ m/z 755.2 $[M - H]^-$; Calcd for $C_{24}H_{28}O_9N_5{}^{166}ErF_3$ 753.1137. Found 753.1135.

43. [TmL^{4b}(H$_2$O)] ^{1}H NMR (500 MHz, D_2O, pD 5.3, two isomers 3:1): δ -246.1 (1H), -213.7 (1H), -209.4 (1H), -203.6 (3H), -201.6 (3H), -152.7 (3H), -147.0 (1H), -144.6 (2H), -135.6 (1H), -127.6 (1H), -120.0 (2H), -115.0 (1H), -111.2 (1H), -107.8 (2H), -101.7 (1H), -85.6 (2H), -84.3 (1H), -78.3 (2H), -71.0 (3H), -54.9 (3H), -9.1, -7.7, -7.1, -5.7, -5.0, -4.3, 16.7 (2H), 18.5 (1H), 31.5 (6H), 33.8 (2H), 35.4 (2H), 38.4 (1H), 39.7 (1H), 41.9 (2H), 49.8 (4H), 55.3 (3H), 63.1 (1H), 64.7 (1H), 68.0 (1H), 78.1 (2H), 84.3 (1H), 302.0 (5H), 316.4 (1H), 321.4 (2H), 334.5 (2H), 340.2 (1H), 347.9 (1H), 381.5 (1H); ^{19}F NMR (188 MHz, D_2O, pD 5.3, 2 isomers 3:1): δ -89.6 (CF_3, $\omega_{1/2}$ = 410 Hz), -37.0 (CF_3, $\omega_{1/2}$ = 556 Hz); ESI/MS$^+$ m/z 780.1 $[M + Na]^+$, 796.1 $[M + K]^+$; ESI/MS$^-$ m/z 756.2 $[M - H]^-$; Calcd for $C_{24}H_{29}O_9N_5F_3K^{169}Tm$ 796.0891. Found 796.0900.

44. [EuL^{4b}(H$_2$O)] ^{1}H NMR (500 MHz, D_2O, pD 5.2, two isomers 3:1): δ -18.5, -16.6, -16.4, -15.4, -15.0, -14.1, -13.6, -13.4, -13.1, -11.5, -9.8, -8.7, -8.3, -7.4, -6.8, -5.2, -4.4, -3.7, -2.8, -1.1, -0.8, 1.8, 8.5, 29.1, 31.4, 34.3, 34.4; ^{19}F NMR (188 MHz, D_2O, pD 5.2, two isomers 3:1): δ -61.5 (br, 2xCF_3, $\omega_{1/2}$ = 432 Hz); ^{19}F NMR (658.4 MHz, D_2O, pD 5.2, two isomers): δ -61.7 (CF_3, $\omega_{1/2}$ = 562 Hz), -60.1 (CF_3, $\omega_{1/2}$ = 2618 Hz); ESI/MS$^+$ m/z 764.2 $[M + Na]^+$, 780.2 $[M + K]^+$; ESI/MS$^-$ m/z 740.3 $[M - H]^-$; Calcd for $C_{24}H_{28}O_9N_5{}^{151}EuF_3$ 738.1043. Found 738.1043.

45. [GdL^{4b}(H$_2$O)] ^{19}F NMR (188 MHz, D_2O, pD 5.4, two isomers 3:1): δ -59.2 (CF_3, mean $\omega_{1/2}$ = 1500 Hz); ESI/MS$^+$ m/z 768.3 $[M + Na]^+$, 785.2 $[M + K]^+$; ESI/MS$^-$ m/z 745.3 $[M - H]^-$; Calcd for $C_{24}H_{28}O_9N_5F_3{}^{156}Gd$ 741.1053. Found 741.1048.

46. 2-Chloro-N-(6-(cyano)-2-trifluoromethylphenyl)-ethanamide

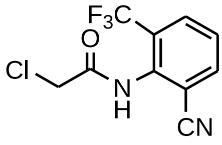

To a stirred solution of 2-amino-3-(trifluoromethyl)benzonitrile (1.00 g, 5.4 mmol) in dry DMF (35 ml) was added sodium hydride (60% dispersion in mineral oil) in portions (0.54 g, 13.4 mmol) under argon at 0˚C, accompanied by vigorous gas development, then chloroacetyl chloride (1.71 ml, 21.5 mmol) dropwise. The reaction mixture was allowed to warm to room temperature and stirred for 48 h. The reaction was quenched with water (5 ml) and the solution volume reduced. To the crude solution was added CH_2Cl_2 (30 ml) and the mixture was washed successively with HCl $_{(aq)}$ (pH 2-3, 20 ml), NaOH $_{(aq)}$ (pH 8-9, 20 ml) and water (20 ml). The organic layer was dried over K_2CO_3, filtered and solvent removed under reduced pressure to leave a black oil which was purified over silica gel in CH_2Cl_2 to yield a light yellow solid (0.98 g, 69%), m.p. 116-117°C. $R_f = 0.2$ (Silica, CH_2Cl_2, UV); ^{1}H NMR (700 MHz, $CDCl_3$): δ 4.23 (2H, s, CH_2Cl), 7.54 (1H, t, J = 8.0 Hz, H^4), 7.87 (1H, d, J = 8.0 Hz, H^5), 7.89 (1H, d, J = 8.0 Hz, H^3), 8.56 (1H, br, s, NH); ^{13}C NMR (176 MHz, $CDCl_3$): δ 42.57 (CH_2Cl), 115.31 (CN), 115.43 (C^6), 122.60 (q, $^1J_{CF}$ = 274 Hz, CF_3), 128.34 (q, $^2J_{CF}$ = 31 Hz, $\underline{C}^2$-CF_3), 128.58 (C^4), 130.97 (q, $^3J_{CF}$ = 5 Hz, C^3), 136.71 (C^1), 136.99 (C^5), 165.56 (NHCO); ^{19}F NMR (188 MHz, $CDCl_3$): δ -62.17 (CF_3); ESI/MS$^+$ m/z 263.1 $[M + H]^+$, 285.1 $[M + Na]^+$; MS Calcd for $C_{10}H_6N_2OF_3ClNa$ 285.0013. Found 285.0014. Anal Calcd for $C_{10}H_6N_2OF_3Cl$ C, 45.73; H, 2.30; N, 10.67%. Found C, 45.74; H, 2.27; N, 10.47%.

47. 10-[(6-Cyano-2-trifluoromethyl(phenyl))carbamoylmethyl]-1,4,7-tris(*tert*-butoxycarbonylmethyl)-1,4,7,10-tetraazacyclododecane

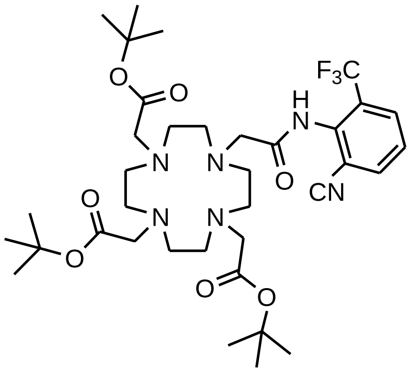

To a solution of 1,4,7-tris(*tert*-butoxycarbonylmethyl)-1,4,7,10-tetraazacyclododecane (500 mg, 0.97 mmol) and 2-chloro-N-(6-(cyano)-2-trifluoromethylphenyl)-ethanamide (281 mg, 1.07 mmol) in dry CH_3CN (20 ml) under argon, was added K_2CO_3 (161 mg, 1.17 mmol) and KI (5 mg, cat.). The mixture was boiled under reflux for 24 h. After filtration, the residue was treated with CH_2Cl_2 (2 x 30 ml), the extracts were combined and solvent removed under reduced pressure to leave a brown oil which was purified by column chromatography over silica gel eluting from CH_2Cl_2 to 5%MeOH/CH_2Cl_2. Recrystallisation from hot toluene gave a white amorphous solid (612 mg, 85%), m.p. 262-263°C. R_f = 0.4 (Silica, DCM/5%MeOH, UV); ^{1}H NMR (500 MHz, $CDCl_3$): δ 1.0-1.5 (27H, br, CH_3), 1.80-3.80 (24H, br, CH_2 ring and CH_2CO), 7.56 (1H, t, J = 8.0 Hz, aromatic H^4), 7.77 (1H, d, J = 8.0 Hz, aromatic H^5), 7.84 (1H, d, J = 8.0 Hz, aromatic H^3), 9.58 (1H, s, NH); ^{13}C NMR (125.7 MHz, $CDCl_3$): δ 27.95, 28.04 (br, CH_3), 48.60, 52.84 (br, CH_2 ring), 55.77, 55.81, 57.02 ($\underline{C}H_2CO$), 81.97 ($\underline{C}$-CH_3), 116.49 (CN), 116.79 (aromatic C^6), 122.36 (q, $^1J_{CF}$ = 274 Hz, CF_3), 128.36 (aromatic C^4), 130.01 (q, $^2J_{CF}$ = 31 Hz, $\underline{C}^2$-CF_3), 130.95 (q, $^3J_{CF}$ = 5 Hz, aromatic C^3), 136.08 (aromatic C^5), 138.33 (aromatic C^1), 172.70, 172.77 (CO); ^{19}F NMR (188 MHz, $CDCl_3$) δ -60.79 (CF_3); ESI/MS$^+$ m/z 741.4 $[M + H]^+$, 763.4 $[M + Na]^+$; ESI/MS$^-$ m/z 739.6 $[M - H]^-$; MS Calcd for $C_{36}H_{56}N_6O_7F_3$ 741.4157. Found 741.4153.

48. 10-[(6-Cyano-2-trifluoromethyl(phenyl)carbamoylmethyl]-1,4,7-tris(carboxymethyl)-1,4,7,10-tetraazacyclododecane, H_3L^5

Prepared as described for **H_3L^{1a} (5)**.

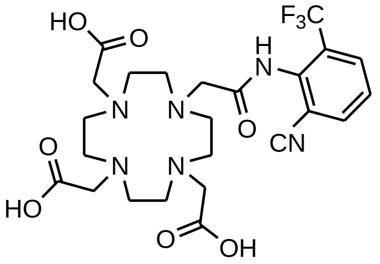

The product was isolated as the dihydrochloride salt as a white powder (215 mg, 98%), m.p. 249-251°C. ^{1}H NMR (700 MHz, D_2O): δ 2.70-4.30 (24H, br, CH_2 ring and CH_2CO), 7.59 (1H, t, J = 8.0 Hz, aromatic H^4), 7.96 (1H, d, J = 8.0 Hz, aromatic H^5), 7.98 (1H, d, J = 8.0 Hz, aromatic H^3); ^{13}C NMR (125.7 MHz, D_2O): δ 46.00-56.00 (CH_2 ring and $\underline{C}H_2CO$), 114.40 (CN), 122.44 (q, $^1J_{CF}$ = 273 Hz, CF_3), 128.29 (q, $^2J_{CF}$ = 31 Hz, $\underline{C}^2$-CF_3), 129.20 (aromatic C^6), 129.46 (aromatic C^4), 132.05 (q, $^3J_{CF}$ = 5 Hz, aromatic C^3), 132.49 (aromatic C^1), 137.17 (aromatic C^5), 168.39 (br), 171.69, 174.02 (br, C=O); ^{19}F NMR (188 MHz, D_2O): δ -61.96 (CF_3); ESI/MS$^+$ m/z 573.3 $[M + H]^+$, 595.3 $[M + Na]^+$; ESI/MS$^-$ m/z 571.3 $[M - H]^-$; MS Calcd for $C_{24}H_{32}O_7N_6F_3$ 573.2279. Found 573.2284. HPLC: t_R = 6.3 min; LC-MS: t_R = 3.6 min, m/z 573.29 $[M + H]^+$.

49. $[HoL^5(H_2O)]$

Prepared as described for **$[HoL^1(H_2O)]$ (6)**.

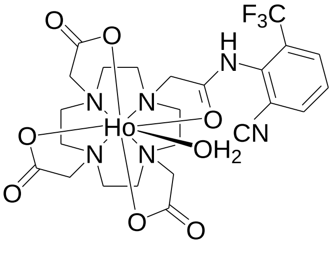

^{1}H NMR (500 MHz, D_2O, pD 5.0, two isomers 1:1): δ -260.0, -256.1, -247.0, -222.6, -217.0, -203.5, -163.5, -132.3, -120.1, -104.0, -86.3, -74.6, -57.0, -41.4, -32.2,

-30.2, -25.1, -23.3, -15.0, -10.9, 7.6, 54.9, 82.8, 88.5, 96.1, 106.3, 143.5, 157.2, 160.8, 165.9, 173.3; ^{19}F NMR (188 MHz, D_2O, pD 5.4): δ two major isomers 1:1 -78.1 (CF_3, $\omega_{1/2}$ = 419 Hz), -48.8 (CF_3, $\omega_{1/2}$ = 745 Hz), two minor isomers -61.0 (CF_3, $\omega_{1/2}$ = 93 Hz); ESI/MS$^+$ m/z 735.2 [M + H]$^+$, 757.2 [M + Na]$^+$, 773.2 [M + K]$^+$; ESI/MS$^-$ m/z 733.3 [M - H]$^-$; MS Calcd for $C_{24}H_{27}O_7N_6F_3{}^{165}Ho$ 733.1202. Found 733.1193.

50. [TbL^5(H$_2$O)] ^{1}H NMR (500 MHz, D_2O, pD 5.1, two isomers 1:1): δ -421.1, -413.7, -406.8, -372.2, -367.6, -344.8, -337.8, -286.0, -276.6, -219.1, -194.2, -185.3, -162.0, -141.1, -121.9, -101.0, -98.2, -97.0, -93.8, -85.2, -83.2, -69.4, -67.1, -65.0, -63.3, -59.5, -54.0, -52.1, -45.2, -39.4, -37.0, -32.3, -26.1, -11.7, -10.0, -2.7, 30.1, 85.2, 100.3, 128.0, 134.4, 139.7, 146.0, 155.1, 232.4, 244.5, 264.9; ^{19}F NMR (188 MHz, D_2O, pD 5.4): δ two major isomers 1:1 -84.6 (CF_3, $\omega_{1/2}$ = 505 Hz), -40.6 (CF_3, $\omega_{1/2}$ = 670 Hz), two minor isomers -57.4 (CF_3, $\omega_{1/2}$ = 82 Hz); ESI/MS$^+$ m/z 751.3 [M + Na]$^+$, 767.3 [M + K]$^+$; ESI/MS$^-$ m/z 727.4 [M - H]$^-$; MS Calcd for $C_{24}H_{27}O_7N_6F_3{}^{159}Tb$ 727.1152. Found 727.1148.

51. [DyL^5(H$_2$O)] ^{1}H NMR (500 MHz, D_2O, pD 5.1, two isomers 1:1): δ -455.0, -450.2, -429.9, -425.1, -400.6, -380.2, -359.6, -270.2, -240.5, -225.5, -179.6, -164.7, -150.5, -130.1, -110.2, -100.1, -90.4, -84.7, -60.3, -50.5, -20.3, -14.9, 10.1, 49.6, 215.2, 240.0, 265.3, 279.8, 330.2; ^{19}F NMR (188 MHz, D_2O, pD 5.4): δ two major isomers 1:1 -109.9 (CF_3, $\omega_{1/2}$ = 515 Hz), -59.3 (CF_3, $\omega_{1/2}$ = 465 Hz), two minor isomers -78.0 (CF_3, $\omega_{1/2}$ = 98 Hz); ESI/MS$^-$ m/z 731.9 [M - H]$^-$; MS Calcd for $C_{24}H_{27}O_7N_6F_3{}^{162}Dy$ 728.1151. Found 728.1153. HPLC: t_R = 6.6, 8.8 min; LC-MS: t_R = 3.4 min, m/z 733.06 [M + H]$^+$, 731.03 [M - H]$^-$, t_R = 6.4 min, m/z 732.01 [M + H]$^+$, 731.97 [M - H]$^-$.

52. [ErL^5(H$_2$O)] ^{1}H NMR (500 MHz, D_2O, pD 5.2, two isomers 1:1): δ -100.3, -87.3, -82.2, -78.1, -73.1, -60.5, -55.8, -47.4, -44.0, -37.4, -32.4, -26.5, -24.3, -19.7, -16.0, -13.5, -5.1, -3.5, -1.3, 12.0, 14.3, 14.8, 21.1, 22.3, 26.2, 28.0, 38.7, 45.0, 56.5, 74.8, 89.9, 120.9, 128.7, 142.8, 151.7, 155.0, 162.6; ^{19}F NMR (188 MHz, D_2O, pD 5.4): δ two major isomers 1:1 -67.6 (CF_3, $\omega_{1/2}$ = 453 Hz), -49.6 (CF_3, $\omega_{1/2}$ = 423 Hz), two minor isomers -58.2 (CF_3, $\omega_{1/2}$ = 94 Hz); ESI/MS$^+$ m/z 758.3 [M + Na]$^+$, 776.3 [M + K]$^+$; ESI/MS$^-$ m/z 735.4 [M - H]$^-$; MS Calcd for $C_{24}H_{27}O_7N_6{}^{166}ErF_3$ 734.1202. Found 734.1202.

53. [TmL^5(H$_2$O)] ^{1}H NMR (500 MHz, D_2O, pD 5.1, two isomers 1:1): δ -244.8, -216.0, -207.3, -205.1, -202.3, -198.3, -190.9, -180.1, -177.5, -158.1, -153.3, -146.8, -140.0, -134.6, -126.2, -118.1, -114.1, -83.7, -81.9, -77.4, -74.3, -66.8, -52.3, -48.3, -20.2, -13.1, 12.0, 18.8, 20.2, 29.1, 32.3, 33.9, 43.0, 45.1, 46.5, 49.2, 50.0, 56.4, 64.3, 81.1, 84.3, 104.0, 115.0, 177.7, 222.3, 271.7, 300.6, 309.5, 318.5, 325.2, 335.9, 340.3, 379.0; ^{19}F NMR (188 MHz, D_2O, pD 5.4): δ two major isomers 1:1 -88.1 (CF_3, $\omega_{1/2}$ = 419 Hz), -39.0 (CF_3, $\omega_{1/2}$ = 444 Hz), two minor isomers -63.7 (CF_3, $\omega_{1/2}$ = 99 Hz); ESI/MS$^+$ m/z 739.3 $[M + H]^+$, 761.3 $[M + Na]^+$, 777.2 $[M + K]^+$; ESI/MS$^-$ m/z 737.3 $[M - H]^-$; MS Calcd for $C_{24}H_{27}O_7N_6F_3{}^{169}Tm$ 737.1241. Found 737.1235. LC-MS: t_R = 3.34 min, m/z 739.39 $[M + H]^+$, t_R = 6.54 min, m/z 739.35 $[M + H]^+$, 737.22 $[M - H]^-$.

54. [GdL^5(H$_2$O)] ^{19}F NMR (188 MHz, D_2O, pD 5.4, two isomers 1:1): δ -60.4 (CF_3, $\omega_{1/2}$ = 899 Hz), -58.6 (CF_3, $\omega_{1/2}$ = 832 Hz); ESI/MS$^+$ m/z 364.6 $[(M + 2H)/2]^{2+}$, 728.1 $[M + H]^+$, 748.1 $[M + Na]^+$, 766.1 $[M + K]^+$; ESI/MS$^-$ m/z 726.1 $[M - H]^-$; Calcd for $C_{24}H_{27}O_7N_6F_3{}^{158}Gd$ 726.1140. Found 726.1145.

55. [YL^5(H$_2$O)] ^{1}H NMR (500 MHz, D_2O, pD 5.1, two isomers 1:1): δ 1.28, 1.32, 2.11, 2.38, 2.41, 2.53, 2.56, 2.66, 2.76, 2.81, 2.97, 3.12, 3.14, 3.17, 3.19 , 3.34, 3.41, 3.46, 3.49, 3.74, 3.83, 3.87, 4.04, 4.08, 7.4 (t, J = 8.0 Hz), 7.7 (t, J = 8.0 Hz), 8.0 (t, J = 7.0 Hz), 8.2 (d, J = 8.0 Hz); ^{19}F NMR (188 MHz, D_2O, pD 5.4): δ two major isomers 1:1 -61.6 (CF_3, $\omega_{1/2}$ = 34 Hz), two minor isomers -59.8 (CF_3, $\omega_{1/2}$ = 7 Hz); ESI/MS$^+$ m/z 659.3 $[M + H]^+$, 681.3 $[M + Na]^+$, 697.3 $[M + K]^+$; ESI/MS$^-$ m/z 657.3 $[M - H]^-$; MS Calcd for $C_{24}H_{27}O_7N_6F_3{}^{89}Y$ 657.0957. Found 657.0952.

56. 1-[(6-Cyano-2-trifluoromethyl(phenyl))carbamoylmethyl]-1,4,7,10-tetraazacyclododecane[4]

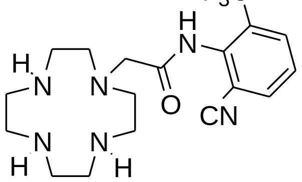

To a solution of 1,4,7,10-tetraazacyclododecane (1.312 g, 7.62 mmol) in dry CH_3CN (10 ml) was added K_2CO_3 (0.105 g, 0.76 mmol) and 2-chloro-N-(6-(cyano)-2-trifluoromethylphenyl)-ethanamide (0.200 g, 0.76 mmol) under argon. The reaction was left stirring at 55°C overnight. The crude mixture was dried under reduced pressure, dissolved in CH_2Cl_2 (20 ml) and extracted with water (2 x 20 ml). The aqueous layer was washed with $CHCl_3$ (3 x 20 ml), the organic layer was then evaporated and the residue redissolved in water then extracted with CH_2Cl_2 yielding, after solvent removal, a pale yellow oil (0.160 g, 53%). ^{1}H NMR (700 MHz, $CDCl_3$): δ 2.61, 2.62, 2.71 (16H, br, CH_2 ring), 3.35 (2H, s, CH_2CO), 7.46 (1H, t, J = 7.5 Hz, aromatic H^4), 7.82 (1H, d, J = 7.5 Hz, aromatic H^5), 7.85 (1H, d, J = 7.5 Hz, aromatic H^3); ^{13}C NMR (176 MHz, $CDCl_3$): δ 45.84, 46.27, 46.99, 47.26, 53.95 (CH_2 ring), 59.03 ($\underline{C}H_2CO$), 116.02 (aromatic C^6), 116.47 (CN), 122.74 (q, $^1J_{CF}$ = 274 Hz, CF_3), 127.98 (aromatic C^4), 129.72 (q, $^2J_{CF}$ = 30 Hz, $\underline{C}^2$-CF_3), 131.17 (q, $^3J_{CF}$ = 5 Hz, aromatic C^3), 136.71 (aromatic C^5), 139.63 (aromatic C^1), 172.50 (CO); ^{19}F NMR (188 MHz, $CDCl_3$): δ -61.21 (CF_3); ESI/MS$^+$ m/z 200.3 $[(M + 2H)/2]^{2+}$, 399.3 $[M + H]^+$; ESI/MS$^-$ m/z 397.3 $[M - H]^-$; MS Calcd for $C_{18}H_{26}N_6OF_3$ 399.2115. Found 399.2116.

57. Triethyl 10-[(6-cyano-2-trifluoromethyl(phenyl))carbamoylmethyl]-1,4,7,10-tetraazacyclododecane-1,4,7-triyltrimethylenetri(methyl-phosphinate)[5]

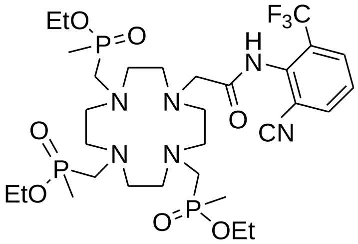

To a refluxing solution, over 4 Å molecular sieves under argon, of 1-[(6-cyano-2-trifluoromethyl(phenyl))carbamoylmethyl]-1,4,7,10-tetraazacyclododecane (160 mg, 0.40 mmol) in dry THF (30 ml) was added paraformaldehyde (54 mg, 1.81 mmol) then diethoxymethylphosphine (0.28 ml, 1.81 mmol). The reaction was left stirring at 85°C overnight. Solvent was evaporated and the residue purified by column chromatography over alumina, eluting with a gradient starting from CH_2Cl_2 up to CH_2Cl_2/5%MeOH to yield a pale yellow oil (59 mg, 19%). R_f = 0.5 (Alumina, DCM/5%MeOH, UV, I_2); ^{1}H NMR (700 MHz, $CDCl_3$): δ 1.15-1.40 (9H, br, m, $CH_2\underline{CH_3}$), 1.40-1.60 (9H, br, m, $^2J_{HP}$ = 14.0 Hz, PCH_3), 2.50-3.30 (24H, br, CH_2 ring, CH_2P and CH_2CO), 4.02 (6H, m, $\underline{CH_2}CH_3$), 7.48 (1H, t, J = 7.5 Hz, aromatic H^4), 7.85 (1H, d, J = 7.5 Hz, aromatic H^5), 7.88 (1H, d, J = 7.5 Hz, aromatic H^3); ^{13}C NMR (176 MHz, $CDCl_3$): δ 14.00 (br, m, $^1J_{CP}$ = 89 Hz, PCH_3), 16.89 (t, $^3J_{CP}$ = 5 Hz, $CH_2\underline{C}H_3$), 53.40 (m, $^1J_{CP}$ = 95 Hz, CH_2P), 54.10-55.40 (CH_2 ring and $\underline{C}H_2CO$), 60.40 (m, $\underline{C}H_2CH_3$), 116.01 (aromatic C^6), 116.16 (CN), 122.76 (q, $^1J_{CF}$ = 276 Hz, CF_3), 127.66 (aromatic C^4), 129.13 (q, $^2J_{CF}$ = 30 Hz, $\underline{C}^2$-CF_3), 130.89 (q, $^3J_{CF}$ = 5 Hz, aromatic C^3), 136.66 (aromatic C^5), 139.03 (aromatic C^1), 168.00 (CO); ^{19}F NMR (376.4 MHz, $CDCl_3$): δ -61.20, -61.24 (CF_3); ^{31}P NMR (162 MHz, $CDCl_3$): 51.4-52.9 (3P); ESI/MS$^+$ m/z 380.2 [(M + 2H)/2]$^{2+}$, 759.3 [M + H]$^+$; ESI/MS$^-$ m/z 757.3 [M - H]$^-$; MS Calcd for $C_{30}H_{53}N_6O_7F_3P_3$ 759.3135. Found 759.3148.

58. 10-[(6-Cyano-2-trifluoromethyl(phenyl))carbamoylmethyl]-1,4,7,10-tetraazacyclododecane-1,4,7-triyltrimethylenetri(methyl-phosphinic acid) H_3L^6

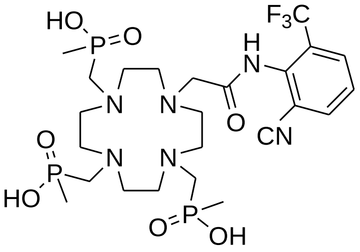

Triethyl 10-[(6-cyano-2-trifluoromethyl(phenyl))carbamoylmethyl]-1,4,7,10-tetraazacyclododecane-1,4,7-triyltrimethylenetri(methyl-phosphinate) (18 mg, 23.7 μmol) was stirred in a solution of KOD (2 ml, 0.1M) for 1 week at room temperature. The pH was then adjusted to 7 with dilute $HCl_{(aq)}$ and the solution lyophilised to yield the dihydrochloride salt as a light yellow solid that was used directly for complexation reactions, m.p. 229-230°C (dec). ^{1}H NMR (700 MHz, D_2O): δ 1.00-1.30 (9H, br, m, PCH_3), 2.50-3.60 (24H, br, CH_2 ring, CH_2P and CH_2CO), 7.63 (1H, t, J = 7.5 Hz, aromatic H^4), 8.01 (2H, t, J = 7.0 Hz, aromatic $H^{5,3}$); ^{13}C NMR (176 MHz, D_2O): δ 16.00 (br, PCH_3), 50.00-54.50 (CH_2 ring, CH_2P and $\underline{C}H_2CO$), 114.89 (aromatic C^6), 116.65 (CN), 123.15 (q, $^1J_{CF}$ = 275 Hz, CF_3), 128.98 (q, $^2J_{CF}$ = 30 Hz, $\underline{C}^2$-CF_3), 129.70 (aromatic C^4), 132.21 (q, $^3J_{CF}$ = 5 Hz, aromatic C^3), 137.22 (aromatic C^1), 137.51 (aromatic C^5), 171.30 (CO); ^{19}F NMR (658.4 MHz, D_2O): δ -61.61 (CF_3); ^{31}P NMR (283.3 MHz, D_2O): 20.6-40.0 (br, 3P); ESI/MS$^+$ m/z 357.6 [(M + K + H)/2]$^{2+}$, 714.2 [M + K]$^+$; ESI/MS$^-$ m/z 674.2 [M - H]$^-$; MS Calcd for $C_{24}H_{39}N_6O_7F_3P_3$ 673.2045. Found 673.2045. LC-MS: t_R = 4.5 min, m/z 677.31 [M + H]$^+$.

59. [HoL^6]

Prepared as described for **[HoL^1(H_2O)] (6)** at 50°C and purified by dialysis (cut off 1,000D).

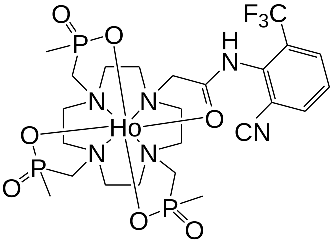

^{1}H NMR (500 MHz, D_2O, pD 5.4): δ -276.1 (br), -272.1 (br), -210.1 (br), -157.8 (br), -146.3 (br), -119.0, -113.5, -96.0 (br), -86.9 (br), -58.3, -53.1, -39.8, -35.3, -28.3, -17.9, -11.6, -9.1, -7.2, -4.5, 17.2, 32.8, 48.9, 55.4, 64.6 (br), 71.7 (br), 89.7 (br), 101.5 (br), 111.7 (br), 130.8 (br), 138.9 (br), 232.5 (br); ^{19}F NMR (188 MHz, D_2O, pD 5.4): δ -106.4 (CF_3, $\omega_{1/2}$ = 83 Hz), -62.4 (CF_3, $\omega_{1/2}$ = 99 Hz), -61.6 (CF_3, $\omega_{1/2}$ = 101 Hz); ESI/MS$^+$ m/z 419.6 [(M + 2H)/2]$^{2+}$, 838.1 [M + H]$^+$; MS Calcd for $C_{24}H_{38}O_7N_6F_3P_3{}^{165}Ho$ 837.1270. Found 837.1294. LC-MS: t_R = 5.1 min, m/z 419.80 [(M + 2H)/2]$^{2+}$, 838.08 [M + H]$^+$, 836.03 [M - H]$^-$.

60. [TbL^6] ^{1}H NMR (500 MHz, D_2O, pD 5.0): δ -405.1 (br), -339.2 (br), -261.2 (br), -252.5 (br), -180.7, -170.7 (br), -150.8, -93.6, -91.3, -89.0, -83.4, -78.4, -53.3, -42.5, -39.3, -37.7, -26.3, -15.0, 17.0, 31.9, 38.8, 45.9, 75.0, 86.9, 89.0, 101.5, 142.5 (br), 149.2 (br), 156.0 (br); ^{19}F NMR (188 MHz, D_2O, pD 5.0): δ -98.5 (CF_3, $\omega_{1/2}$ = 77 Hz), -62.7 (CF_3, $\omega_{1/2}$ = 160 Hz), -60.1 (CF_3, $\omega_{1/2}$ = 190 Hz), -52.1 (CF_3, $\omega_{1/2}$ = 149 Hz); ESI/MS$^-$ m/z 831.2 [M - H]$^-$; MS Calcd for $C_{24}H_{37}O_7N_6F_3P_3{}^{159}Tb$ 830.1142. Found 830.1156. LC-MS: t_R = 4.99 min, m/z 417.12 [(M + 2H)/2]$^{2+}$, 833.24 [M + H]$^+$, 831.21 [M - H]$^-$.

61. [TmL^6] ^{1}H NMR (500 MHz, D_2O, pD 5.0): δ -356.9 (br), -350.7 (br), -344.2 (br), -327.8 (br), -286.7 (br), -228.0 (br), -223.0 (br), -214.3 (br), -184.5, -182.3, -163.5, -158.8, -123.6, -92.2, -82.9, -75.4, -68.5, -63.8, -46.9, -44.4, -31.8, -19.9, -32.0, -20.1, 15.2, 21.6, 24.0, 33.0, 44.8, 46.5, 47.4, 65.1, 93.6, 134.4, 136.7, 140.8, 147.6, 165.0 (br), 173.0 (br); ^{19}F NMR (188 MHz, D_2O, pD 5.0): δ -106.4 (CF_3, $\omega_{1/2}$ = 61 Hz), -62.3 (CF_3, $\omega_{1/2}$ = 127 Hz), -60.1 (CF_3, $\omega_{1/2}$ = 131 Hz), -1.3 (CF_3, $\omega_{1/2}$ = 73 Hz); ESI/MS$^-$ m/z 841.2 [M - H]$^-$; MS Calcd for $C_{24}H_{37}O_7N_6F_3P_3{}^{169}Tm$ 840.1231. Found 840.1227. LC-MS: t_R = 4.9 min, m/z 422.12 [(M + 2H)/2]$^{2+}$, 843.27 [M + H]$^+$, 841.22 [M - H]$^-$.

62. 1,4,7,10-Tetra[N-(4-(ethoxycarbonyl)-2-trifluoromethyl(phenyl))-ethanamide]-1,4,7,10-tetraazacyclododecane, L^7

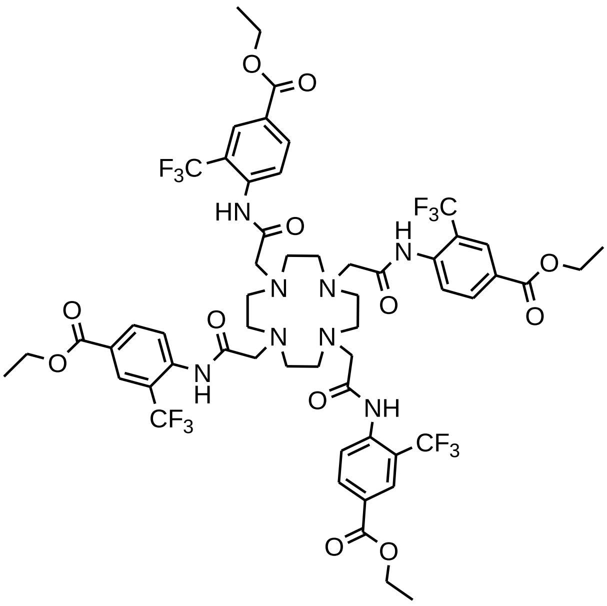

To a solution of 1,4,7,10-tetraazacyclododecane (20.6 mg, 0.12 mmol) and 2-chloro-N-(4-(ethoxycarbonyl)-2-trifluoromethylphenyl)-ethanamide (185.5 mg, 0.60 mmol) in dry CH_3CN (5 ml) under argon, was added K_2CO_3 (82.6 mg, 0.60 mmol) and KI (5 mg, cat.). The mixture was boiled under reflux for 24 h. After filtration, the residue was treated with CH_2Cl_2 (2 x 10 ml), the extracts combined and solvent removed under reduced pressure to leave a brown oil which was subsequently purified by column chromatography over silica gel, eluting from CH_2Cl_2 to 10%MeOH/CH_2Cl_2 and then from CH_2Cl_2 to 8%EtOH/CH_2Cl_2 to give a yellow oil

(13.3 mg, 9%). R_f = 0.3 (Silica, DCM/6%MeOH, UV); ^{1}H NMR (700 MHz, $CDCl_3$): δ 1.36 (12H, t, J = 7.0 Hz, $CH_2\underline{CH_3}$), 1.74, 2.15, 3.01, 3.32, 1.60-3.80 (24H, br, CH_2 ring and CH_2CO), 4.34 (8H, q, J = 7.0 Hz, $\underline{CH_2}CH_3$), 7.83 (4H, d, J = 8.5 Hz, aromatic H^5), 7.95 (4H, d, J = 8.5 Hz, aromatic H^6), 8.00 (4H, s, NH), 8.16 (4H, s, aromatic H^3); ^{13}C NMR (176 MHz, $CDCl_3$): δ 14.39 ($CH_2\underline{C}H_3$), 51.24, 57.59, 60.70, 47.00-54.00 (br, CH_2 ring and CH_2CO), 61.66 ($\underline{C}H_2CH_3$), 121.72 (q, $^2J_{CF}$ = 29 Hz, aromatic $\underline{C}^2$-CF_3), 123.58 (q, $^1J_{CF}$ = 273 Hz, CF_3), 125.96 (aromatic C^6), 127.45 (aromatic C^4), 127.81 (q, $^3J_{CF}$ = 5 Hz, aromatic C^3), 133.80 (aromatic C^5), 138.31 (aromatic C^1), 164.81 ($\underline{C}OOEt$), 171.26 (CONH); ^{19}F NMR (188 MHz, $CDCl_3$): δ -60.99 (CF_3); ESI/MS$^+$ m/z 633.5 $[(M + 2H)/2]^{2+}$, 1265.4 $[M + H]^+$, 1287.4 $[M + Na]^+$; MS Calcd for $C_{56}H_{61}N_8O_{12}F_{12}$ 1265.421. Found 1265.419.

63. $[HoL^7(H_2O)]Cl_3$

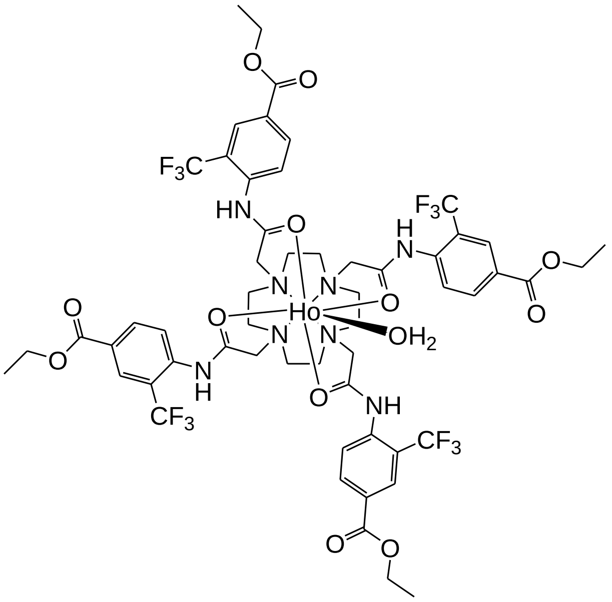

A solution of the ligand $\mathbf{L^7}$ (13.3 mg, 0.011 mmol) and $Ho(OTf)_3$ (7.1 mg, 0.012 mmol) in dry acetonitrile (1.5 ml) was stirred at 75°C overnight under argon. The solution was added dropwise to stirring dry diethyl ether (15 ml). The resulting precipitate was removed by centrifugation (20 min). The solid was redissolved in the minimum amount of acetonitrile and the procedure repeated once more. The yellow solid resulted was treated with anion exchange resin (DOWEX 1X8 200-400 MESH Cl, pre-treated with 1M HCl) in CH_3CN/H_2O to obtain the chloride salt. ^{1}H NMR

(500 MHz, CD_3OD, pD 5.3): δ -51.2 (br), -2.0, 0.8, 1.9, 11.6, 33.8 (br), 40.9 (br); ^{19}F NMR (188 MHz, CD_3OD/D_2O 80:20, pD 5.4): δ -62.16 (CF_3, $\omega_{1/2}$ = 272 Hz); ESI/MS$^+$ m/z 714.4 [(M + 2H)/2]$^{2+}$, 1427.0 [M + H]$^+$; ESI/MS$^-$ m/z 1425 [M - H]$^-$; MS Calcd for $C_{56}H_{59}O_{12}N_8F_{12}{}^{165}Ho$ 714.1677. Found 714.1676.

64. [HoL^8(H_2O)]

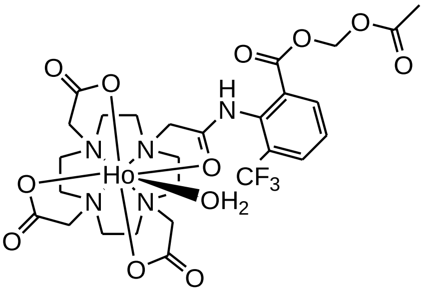

To a solution of **[HoL^{4b}]** (13 mg, 17 μmol) in dry DMSO (0.6 ml) was added K_2CO_3 (7 mg, 52 μmol) and the mixture was left stirring for 30 min at room temperature under argon. Bromomethyl acetate (5 μl, 52 μmol) was then added and the reaction stirred overnight. The crude product was precipitated by dropping onto stirred dry diethyl ether (15 ml) and the solvent removed by centrifugation (10 min). The product was triturated with MeCN, isolated by centrifugation, then taken up into water and lyophilised to yield the product as a pale brown solid. ^1H NMR (500 MHz, D_2O, pD 5.3): δ -264.9, -258.6, -248.2, -230.0, -223.3, -217.6, -210.0, -203.3, -107.5, -103.9, -98.2, -89.7, -85.5, -69.4, -65.9, -57.3, -52.9, -50.6, -45.6, -42.9, -33.3, -24.2, -22.8, -12.3, -11.2, -3.3, 10.9, 11.8, 12.5, 13.3, 15.7, 17.2, 55.2, 88.0, 103.7, 141.0, 149.4, 159.6, 165.5; ^{19}F NMR (376 MHz, D_2O, pD 6.0): δ -49.1 (CF_3, $\omega_{1/2}$ = 183 Hz, 50%), -56.9, -96.1; ESI/MS$^+$ m/z 826.2 [M + H]$^+$, 848.1 [M + Na]$^+$; MS Calcd for $C_{27}H_{34}O_{11}N_5F_3{}^{165}Ho$ 826.1510. Found 826.1502. LC-MS: t_R = 5.3 min, m/z 826.35 [M + H]$^+$, 824.19 [M - H]$^-$.

65. [HoL^9(H$_2$O)]

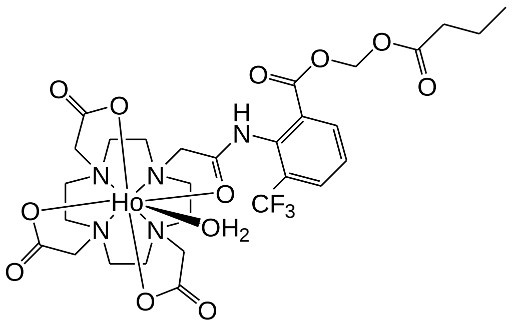

To a solution of **[HoL^{4b}]** (10 mg, 13.3 μmol) in dry DMSO (0.5 ml) was added K_2CO_3 (6 mg, 39.8 μmol) and the mixture was left stirring for 30 min at room temperature under argon. Chloromethylbutyrate (5 μl, 39.8 μmol) was added and the reaction stirred overnight. A crude material was precipitated by dropping the solution slowly onto stirred dry diethyl ether (15 ml) and the solvent removed by centrifugation (10 min). The product was triturated with MeCN, isolated by centrifugation, then taken up into water and lyophilised to yield the product as a light yellow powder. ^{1}H NMR (500 MHz, D_2O, pD 5.2): δ -265.9, -248.8, -229.4, -224.5, -218.0, -204.2, -107.6, -103.9, -89.3, -69.5, -66.2, -58.0, -54.1, -51.3, -45.1, -43.0, -33.4, -30.2, -25.8, -23.4, -19.3, -15.2, -12.0, -10.0, 7.5, 10.8, 11.7, 12.4, 13.2, 15.8, 17.0, 55.1, 88.5, 103.6, 142.2, 150.0, 160.0, 166.5; ^{19}F NMR (376 MHz, D_2O, pD 6.0): δ -49.4 (CF_3, $\omega_{1/2}$ = 190 Hz, 46%), -53.1, -56.8, -96.4; ESI/MS$^+$ m/z 428.1 $[(M + 2H)/2]^{2+}$, 855.2 $[M + H]^+$, 877.2 $[M + Na]^+$; MS Calcd for $C_{29}H_{37}O_{11}N_5F_3{}^{165}Ho$ 853.1745. Found 853.1780. LC-MS: t_R = 7.1 min, m/z 855.16 $[M + H]^+$, 853.02 $[M - H]^-$.

66. Chloromethyl ethyl carbonate[6]

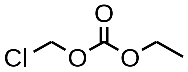

To a solution of EtOH (70 μl) in CH_2Cl_2 (6 ml) was added pyridine (125 μl, 1.55 mmol) then chloromethyl chloroformate (137 μl, 1.55 mmol) dropwise at 0˚C. The mixture was left stirring for 4 h, then the crude product was washed with HCl $_{(aq)}$ (pH 2-3, 10 ml), NaOH $_{(aq)}$ (pH 8-9, 10 ml) and H_2O (10 ml) then dried over $MgSO_4$.

After filtration the solvent was carefully removed to yield a colourless liquid (140 mg, 65%). ^{1}H NMR (400 MHz, $CDCl_3$): δ 1.27 (3H, t, J = 7.0 Hz, $CH_2\underline{CH_3}$), 4.22 (2H, q, J = 7.0 Hz, $\underline{CH_2}CH_3$), 5.67 (2H, s, CH_2Cl); ^{13}C NMR (100.6 MHz, $CDCl_3$): δ 14.02 ($CH_2\underline{C}H_3$), 65.17 ($\underline{C}H_2CH_3$), 72.09 (CH_2Cl), 153.27 (C=O).

67. Reaction between [HoL^{4b}] and chloromethyl ethyl carbonate, [HoL^{10}(H_2O)]

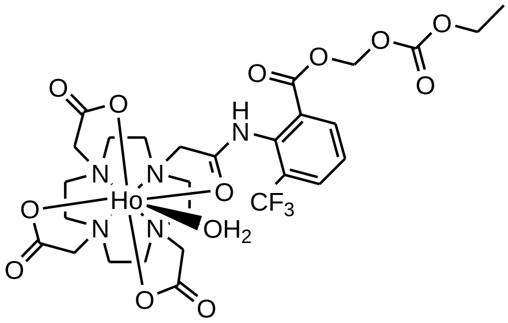

To a solution of **[HoL^{4b}]** (10 mg, 13.3 μmol) in dry DMSO-d_6 (0.6 ml) was added K_2CO_3 (6 mg, 39.8 μmol) and the mixture was left stirring for 30 min at room temperature under argon. Chloromethyl ethyl carbonate (10 μl, 7.23 μmol) was then added and the reaction stirred overnight. ^{19}F NMR (376 MHz, DMSO-d_6): δ -61.3 (CF_3, $\omega_{1/2}$ = 281 Hz, 88%); ESI/MS^{+} m/z 855.6 [M + H]$^{+}$, 894.6 [M + K]$^{+}$; ESI/MS^{-} m/z 854.8 [M - H]$^{-}$; Calcd for $C_{28}H_{34}O_{12}N_5F_3{}^{165}Ho$ 854.1459. Found 854.1448.

68. [HoL^{11}(H_2O)]

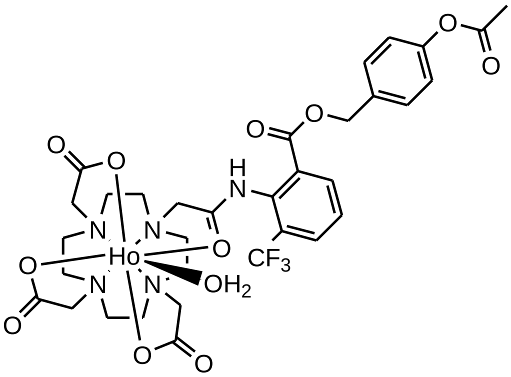

To a solution of **[HoL^{4b}]** (10 mg, 13.3 μmol) in dry DMSO (0.5 ml) was added K_2CO_3 (6 mg, 39.8 μmol) and the mixture was left stirring for 30 min at room temperature under argon. 4-(Chloromethyl)phenylacetate (6 μl, 39.8 μmol) was then added and the reaction stirred overnight. The crude was precipitated by dropping onto stirred dry diethyl ether (15 ml) and the solvent removed by centrifugation (10 min). The product was triturated with MeCN, isolated by centrifugation, then taken up into water and lyophilised to yield the product as a light yellow powder. ^{1}H NMR (500 MHz, D_2O, pD 5.2): δ -260.2, -247.8, -239.0, -228.5, -217.8, -93.7, -82.2, -64.1, -57.5, -50.4, -47.4, -40.0, -37.3, -31.7, -22.6, -13.2, -8.5, -5.2, -3.4, 1.9, 2.1, 2.3, 7.1, 7.4, 14.0, 14.2, 14.5, 18.4, 55.0, 81.1, 88.8, 94.2, 144.0, 151.9, 165.9; ^{19}F NMR (376 MHz, D_2O, pD 6.0): δ -44.2 (CF_3, $\omega_{1/2}$ = 183 Hz, 60%), -42.0, -45.6, -46.8; ESI/MS$^+$ m/z 903.2 $[M + H]^+$, 927.2 $[M + Na]^+$, 941.1 $[M + K]^+$; MS Calcd for $C_{33}H_{38}O_{11}N_5F_3{}^{165}Ho$ 902.1818. Found 902.1815. HPLC: t_R = 9.4 min; LC-MS: t_R = 6.9 min, m/z 903.34 $[M + H]^+$.

69. [HoL^{12}(H$_2$O)]

Prepared as described for **[HoL^{11}(H$_2$O)] (68)**.

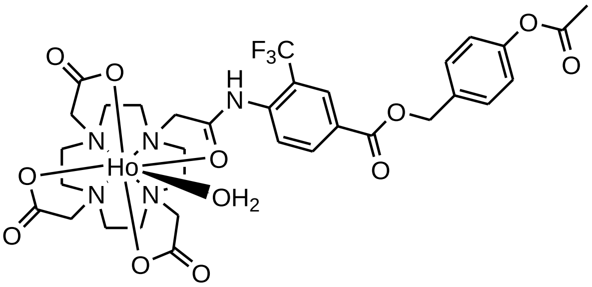

^{1}H NMR (500 MHz, D_2O, pD 5.2): δ -255.1 (br), -245.4 (br), -226.1 (br), -221.3 (br), -216.0 (br), -91.3, -87.0, -77.7, -75.5, -66.3, -58.4, -55.1, -50.2, -48.0, -43.5, -33.0, -31.3, -28.9, -12.1, -11.0, -2.3, 9.3, 9.7, 10.9, 13.1, 15.2, 16.0, 16.6, 20.0, 21.3, 24.2, 25.4, 27.2, 57.6, 83.0 (br), 91.6 (br), 152.2 (br), 160.0 (br), 168.2 (br); ^{19}F NMR (376 MHz, D_2O, pD 6.0): δ -51.1 (CF_3, $\omega_{1/2}$ = 95 Hz, 40%), -49.2, -49.7, -52.2, -57.2; ESI/MS$^-$ m/z 900.9 $[M - H]^-$. LC-MS: t_R = 7.2 min, m/z 902.42 $[M + H]^+$, 900.38 $[M - H]^-$.

70. [HoL^{13}(H$_2$O)]Glucosamide

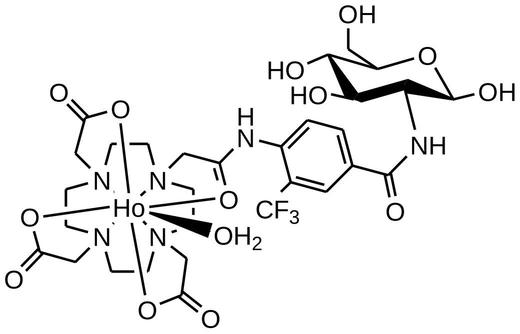

To a stirring suspension of **[HoL^{1b}]** (20 mg, 26.5 μmol) in dry DMF (0.7 ml) under argon was added N-methylmorpholine (4 μl, 39.8 μmol) and after 30 min TBTU (13 mg, 39.8 μmol). The solution was left stirring for 30 min at room temperature. Glucosamine hydrochloride was treated with anion exchange resin (DOWEX 1X8 200-400 MESH, pre-treated with 1M KOH) in water to liberate the free amine, filtered then dried. The free glucosamine (9 mg, 39.8 μmol) was dissolved in the minimum amount of water (4 drops) then added to the reaction mixture, which was left stirring at 40°C for 2 days. The DMF volume was reduced under reduced pressure and the crude precipitated by dropping onto stirred dry diethyl ether (15 ml) and the product isolated by centrifugation (10 min). The product was triturated with MeCN, isolated by centrifugation then taken up into water and lyophilised to yield the product as a pale brown solid (20 mg, 83%). ^{1}H NMR (500 MHz, D_2O, pD 5.1): δ -253.8, -248.1, -224.8, -221.2, -212.0, -93.1, -78.4, -69.1, -58.2, -45.7, -35.1, -32.3, -30.3, -22.7, -14.6, 17.0, 24.0, 85.7, 91.4, 151.5, 159.0, 167.0; ^{19}F NMR (188 MHz, D_2O, pD 5.4): δ -56.8 (CF_3, $\omega_{1/2}$ = 55 Hz, 92%); ESI/MS$^+$ m/z 915.7 [M + H]$^+$, 937.7 [M + Na]$^+$, 953.2 [M + K]$^+$; ESI/MS$^-$ m/z 913.2 [M - H]$^-$; MS Calcd for $C_{30}H_{41}O_{13}N_6F_3{}^{165}Ho$ 915.1987. Found 915.1984. HPLC: t_R = 5.0, 5.4 min; LC-MS: t_R = 1.7 min, 915.27 [M + H]$^+$, t_R = 2.2 min, m/z 915.30 [M + H]$^+$.

71. Preparation of glycol chitosan (MW~194,000)[7]

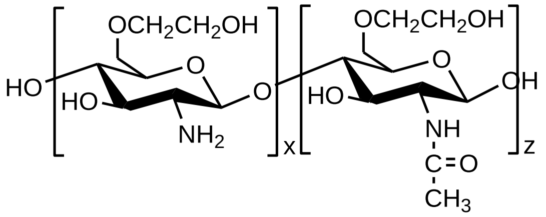

Glycol chitosan (500 mg, purchased from Sigma) was dissolved in water (50 ml) by sonication for 10 min and centrifuged. The higher molecular weight polymer remained as a gel whilst the supernatant solution was removed and dialysed (cut off filter 12,000D) against Purite water for 2 days. The solution was lyophilized to give a white cotton-like solid (370 mg). Anal Found C, 42.64; H, 6.61; N, 5.66%. For GPC analysis see Table 6.2.

72. Preparation of glycol chitosan (MW~6,590)[8]

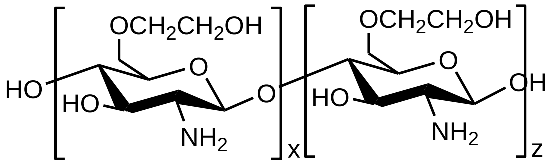

Glycol chitosan (1 g, purchased from Sigma) was dissolved in a solution of HCl 4M (75 ml), insoluble material was manually removed from the solution. The solution was left stirring at 50˚C for 24 h then dialysed (cut off 12,000D) against Purite water until the pH of the tube contents reached neutral (2 days). Lyophilisation yielded a light brown powder (560 mg). Anal Found C, 37.84; H, 6.92; N, 5.57%. For GPC analysis see Table 6.2.

73. Glycol chitosan Ho complex conjugate (MW~278,500)

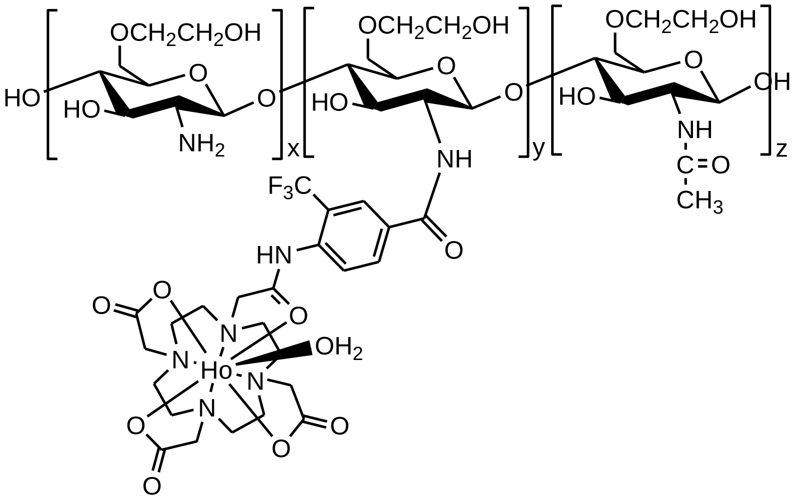

To a stirred suspension of **[HoL^{1b}]** (65 mg, 86.3 μmol) in dry DMF (0.7 ml) under argon was added N-methylmorpholine (14 μl, 129.0 μmol) and after 30 min TBTU (42 mg, 129.0 μmol). The solution was left stirring for 30 min at room temperature, then added dropwise to a solution of glycol chitosan (MW~194,000) **71** (200 mg in 3 ml of water dissolved by sonication for 2 h) with vigorous shaking. The viscous solution was left stirring overnight at 40˚C. The crude product was precipitated in isopropanol twice and then redissolved in water to be dialysed against Purite water over 2 days (cut off 1,000D). The solution was lyophilised to yield a white light powder. ^{1}H NMR (400 MHz, D_2O): only glycol chitosan visible δ 1.89 (br, CH_3CO), 2.65 (br, CHNH), 3.20-4.00 (br, CH and CH2), 4.4 (br, OCHO); ^{19}F NMR (188 MHz, D_2O): δ -56.8 (CF_3, $\omega_{1/2}$ = 262 Hz); Ho% = 1.60; Anal Found C, 39.68; H, 5.99; N, 5.66%. For GPC analysis see Table 6.2.

74. Glycol chitosan Ho complex conjugate (MW~16,200)

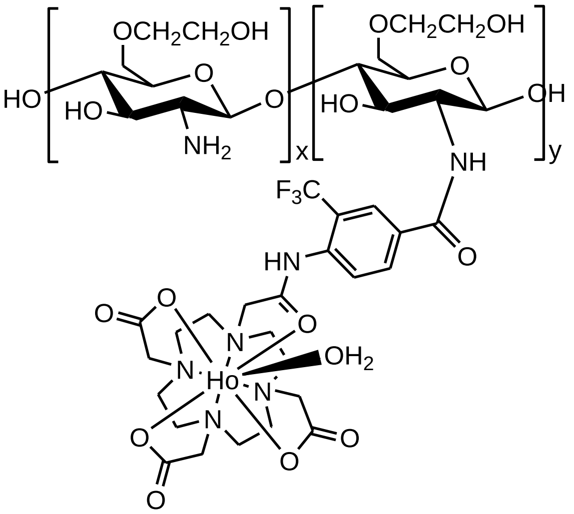

To a stirring suspension of **[HoL^{1b}]** (260 mg, 345 μmol) in dry DMF (2.2 ml) under argon was added N-methylmorpholine (57 μl, 518.0 μmol) and after 30 min TBTU (166 mg, 518.0 μmol). The solution was left stirring for 30 min at room temperature then a solution of glycol chitosan (MW~6,590) **72** (40 mg in 0.4 ml of water) was added dropwise. The mixture was left stirring overnight at 40˚C. The crude was diluted with water and dialysed against Purite water over 2 days (cut off 1,000D). The solution was lyophilised to yield a light brown solid. ^{19}F NMR (376.3 MHz, D_2O): δ -56.8 (CF_3, $\omega_{1/2}$ = 257 Hz); Ho% = 12.5; Anal Found C, 37.65; H, 4.93; N, 7.53%. For GPC analysis see Table 6.2.

75. Glycol chitosan Gd complex conjugate (MW~15,950)

Prepared as described for **74**.

Gd% = 14.9; Anal Found C, 34.84; H, 4.64; N, 6.98%. For GPC analysis see Table 6.2.

Table 6.2 Gel permeation chromatography (GPC) data for the chitosan samples and their conjugates.

Sample	**M_w [a]**	**M_n [b]**	**PDI [c]**
71	194,000	50,750	3.8
72	6,590	2,250	2.9
73	278,500	54,650	5.1
74	16,200	4,500	3.6
75	15,950	4,155	3.8

Mean values obtained from two successive scans. [a] calculated molecular weight averages expressed as the pullulan polysaccaride equivalent molecular weights; [b] number average molecular weights; [c] polydispersity (Mw/Mn).

References

[1] J. Carmichael, W. G. Degraff, A. F. Gazdar, J.D. Minna, J. B. Mitchell, *Cancer Res.*, **1987**, *47*, 936.

[2] O. Reany, T. Gunnlaugsson, D. Parker, *J. Chem. Soc.-Perkin Trans. 2,* **2000**, 1819.

[3] M. Woods, PhD thesis, University of Durham (Durham), **1998**.

[4] J. P. L. Cox, A. S. Craig, I. M. Helps, K. J. Jankowski, D. Parker, M. A. W. Eaton, A. T. Millican, K. Millar, N. R. A. Beeley, B. A. Boyce, *J. Chem. Soc.-Perkin Trans. 1*, **1990**, 2567.

[5] S. Aime, M. Botta, R. S. Dickins, C. L. Maupin, D. Parker, J. P. Riehl, J. A. G. Williams, *J. Chem. Soc.-Dalton Trans.*, **1998**, 881.

[6] J. D. Thomas, K. B. Sloan, *Tetrahedron Lett.*, **2007**, *48*, 109.

[7] K. Kim, S. Kwon, J. H. Park, H. Chung, S. Y. Jeong, I. C. Kwon, *Biomacromolecules,* **2005**, *6*, 1154.

[8] W. Wang, A. M. McConaghy, L. Tetley, I. F. Uchegbu, *Langmuir,* **2001**, *17*, 631.

Appendix A:

Notable complex ^{1}H NMR spectra

Full ^{1}H NMR spectra of **[LnL^{1a}]** and **[LnL^{1b}]** are shown below. It is visible the presence of two isomers in 1:1 ratio for **[LnL^{1a}]** and 3:1 ratio for **[LnL^{1b}]**, as illustrated for the ^{19}F NMR spectra.

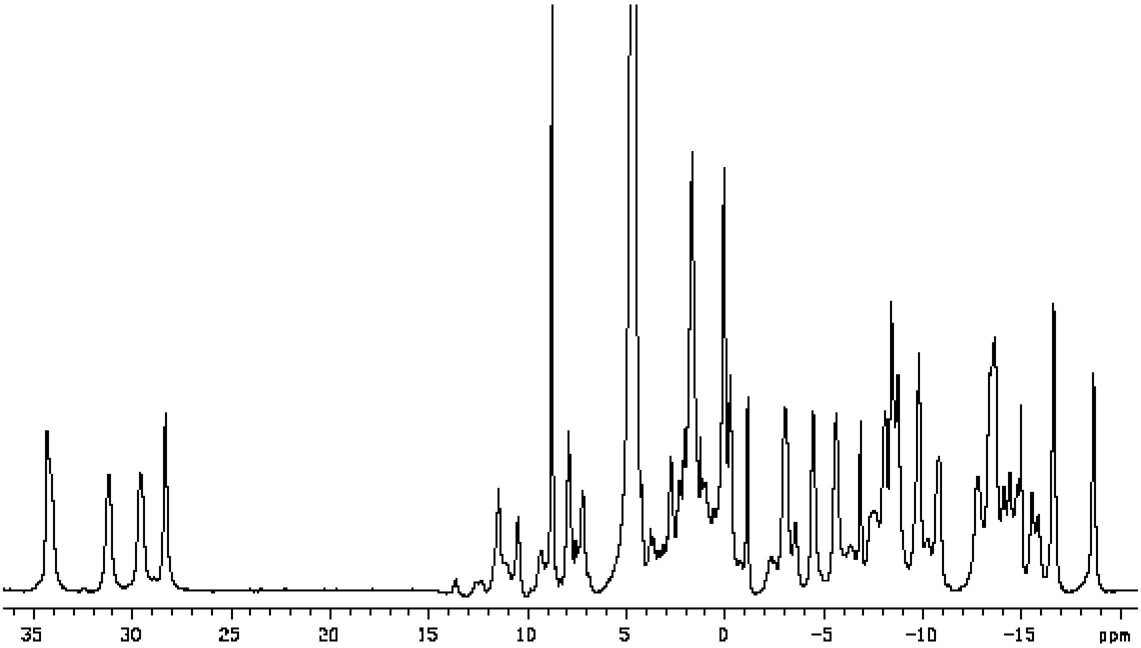

Fig. A.1 [EuL^{4a}] (D_2O, 500 MHz, 295 K).

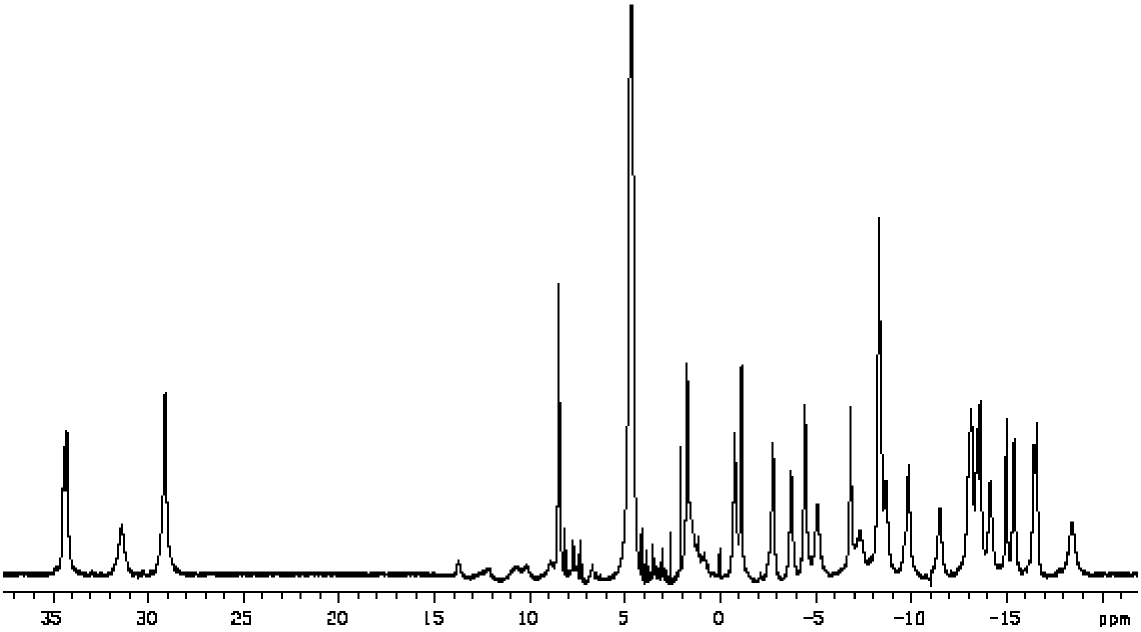

Fig. A.2 [EuL^{4b}] (D_2O, 500 MHz, 295 K).

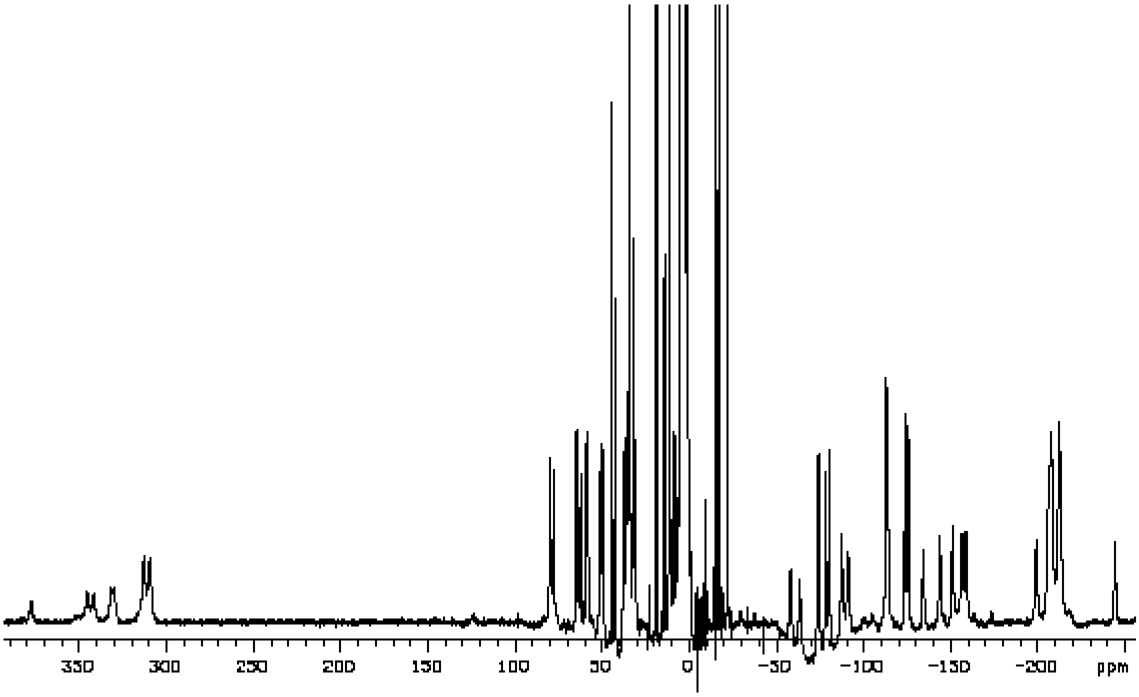

Fig. A.3 [TmL^{4a}] (D$_2$O, 500 MHz, 295 K).

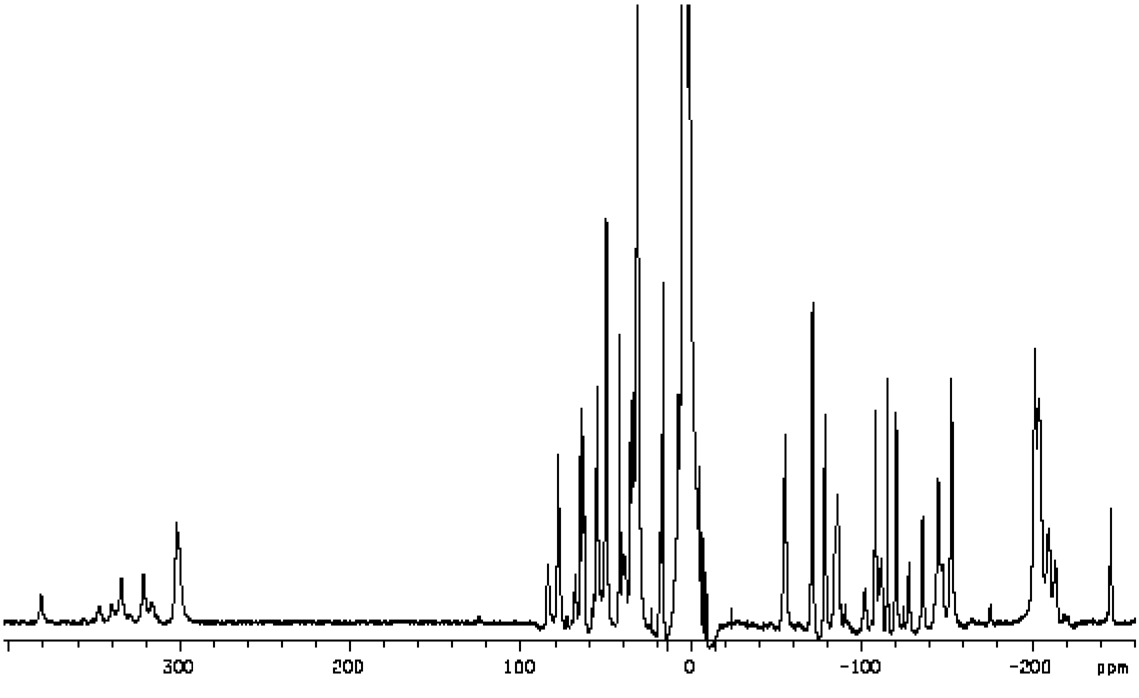

Fig. A.4 [TmL^{4b}] (D$_2$O, 500 MHz, 295 K).

Appendix B:

Crystal data: single crystal X-ray analysis

The data for 10-[(4-Ethoxycarbonyl-2-trifluoromethyl(phenyl))carbamoylmethyl]-1,4,7-tris(*tert*-butoxycarbonylmethyl)-1,4,7,10-tetraazacyclododecane (**4**) are reported below.

Empirical formula	$C_{38}H_{60}N_5O_9F_3Na^+\ Br^- \cdot 1/2\ C_4H_{10}O$
Formula weight	927.87
T (K)	120 (2)
Crystal system	Tetragonal
Space group	P4/n (no. 85)
a, b, c (Å)	27.1772(10), 27.1772(10), 12.4222(4)
α, β, γ (deg)	90.00, 90.00, 90.00
Volume (Å^3)	9175.0(6)
Z	8
ρ_{calc} (mg mm^{-3})	1.343
μ (mm^{-1})	0.975
F(000)	3912
Crystal size (mm^3)	0.45 × 0.4 × 0.24
Theta range for data collection	1.50 to 30.00°
Index ranges	$-38 \le h \le 38$, $-38 \le k \le 37$, $-17 \le l \le 17$
Reflections collected	119016
Independent reflections	13394[R(int) = 0.0879]
Data/restraints/parameters	13394/0/569
Goodness-of-fit on F^2	0.973
Final R indexes [I>2σ (I)]	$R_1 = 0.0372$, $wR_2 = 0.0952$
Final R indexes [all data]	$R_1 = 0.0561$, $wR_2 = 0.1007$
Largest diff. peak/hole/e (Å^{-3})	0.530/-0.377

Appendix C:

Notable structures

Notable structures discussed in this thesis are included for reference use.

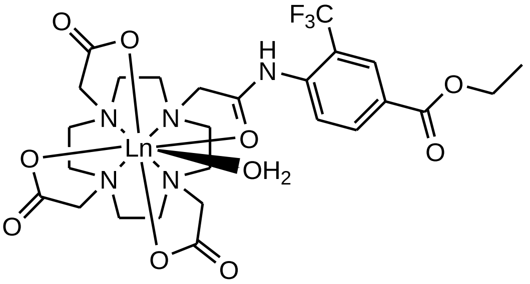

[LnL^{1a}]

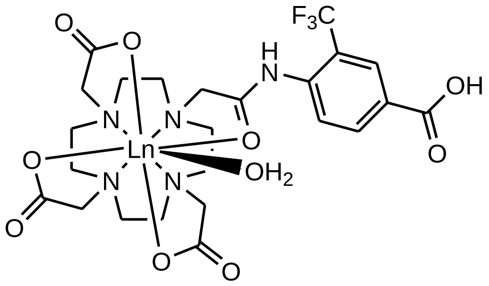

[LnL^{1b}]

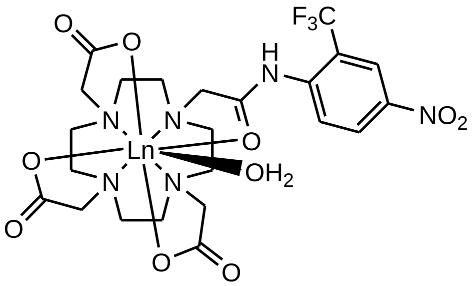

[LnL^{2}]

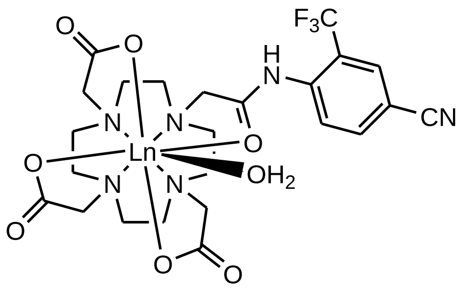

[LnL^{3}]

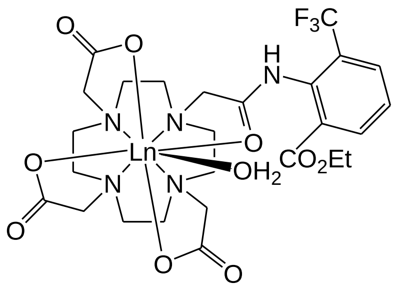

[LnL^{4a}]

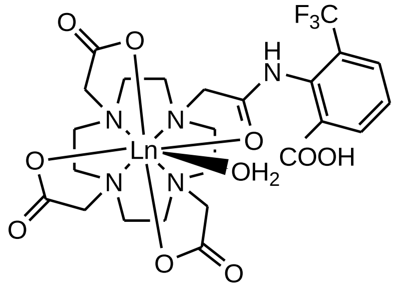

[LnL^{4b}]

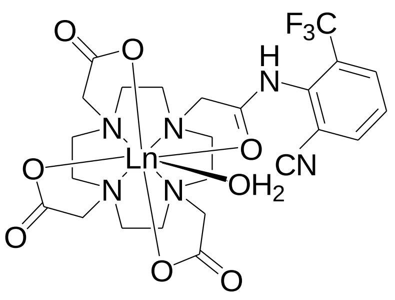

[LnL^{5}]

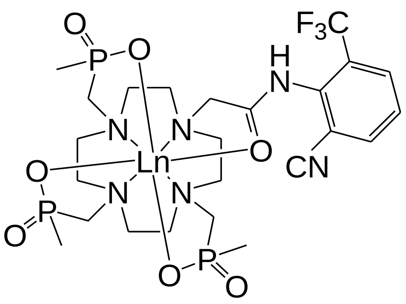

[LnL^{6}]

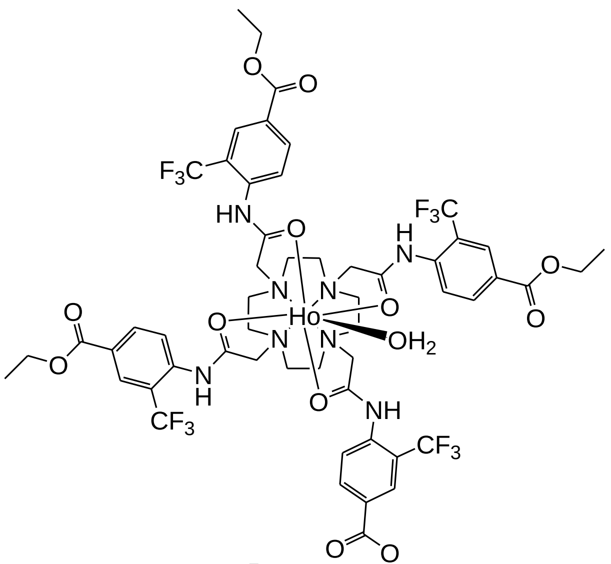

[HoL^{7}]

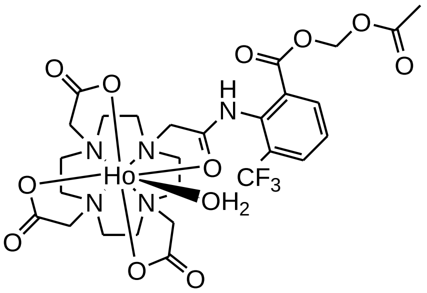

[HoL^{8}]

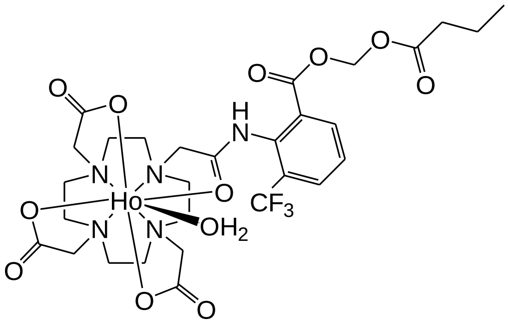

[HoL^{9}]

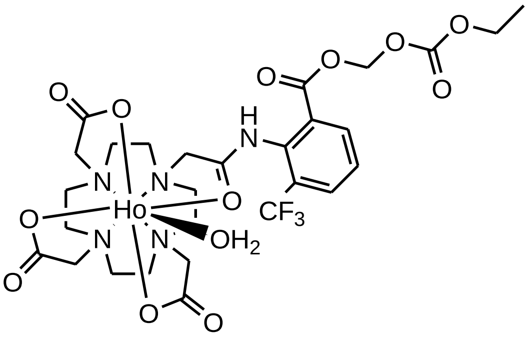

[HoL^{10}]

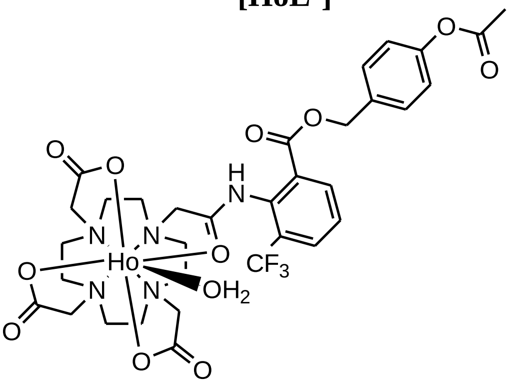

[HoL^{11}]

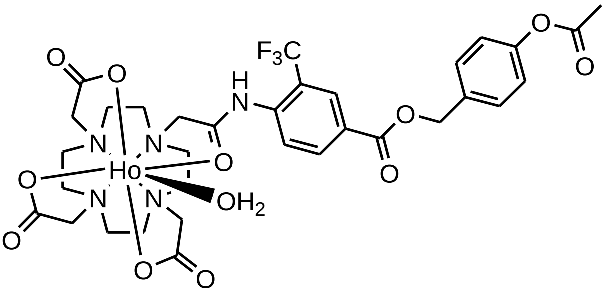

[HoL^{12}]

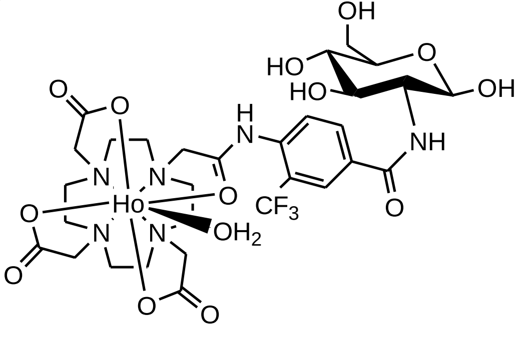

[HoL^{13}]

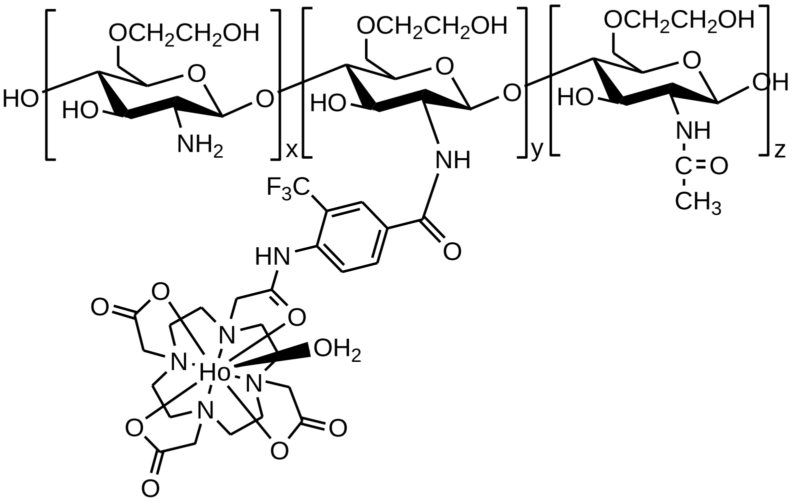

High MW glycol chitosan Ho complex conjugate

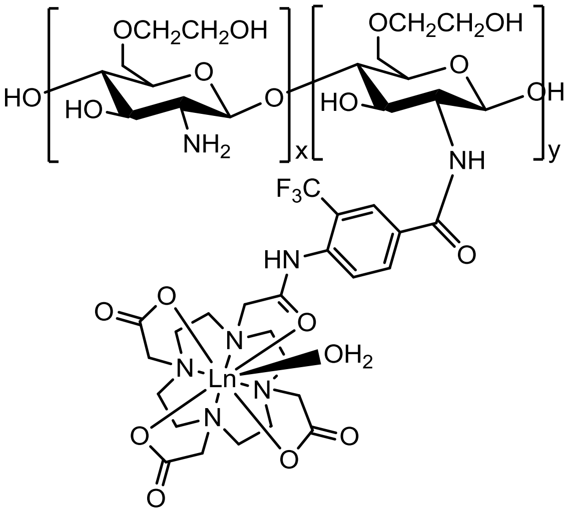

Low MW glycol chitosan Ln complex conjugate (Ln = Ho 74, Ln = Gd 75)